Modelling refrigerant distribution in minichannel evaporators

Brix, Wiebke

Publication date:
2010

Document Version
Publisher's PDF, also known as Version of record

Modelling refrigerant distribution in minichannel evaporators

PhD Thesis

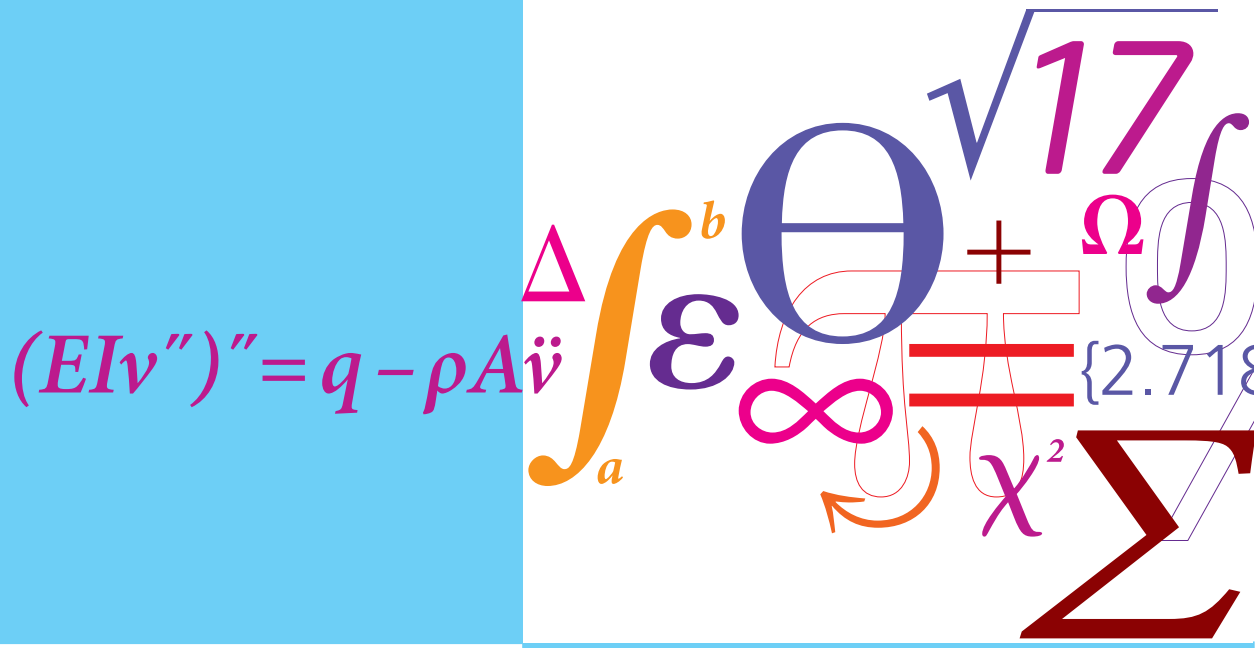

Wiebke Brix
DCAMM Special Report no. S114
May 2010

DTU Mechanical Engineering
Department of Mechanical Engineering

PhD Thesis

Modelling refrigerant distribution in minichannel evaporators

Wiebke Brix

Supervisor: Brian Elmegaard

Department og Mechanical Engineering
Technical University of Denmark, DTU

May 2010

Modelling refrigerant distribution in minichannel evaporators

ISBN: I978-87-90416-27-0

Preface

This thesis is submitted in candidacy for the PhD degree at the Technical University of Denmark, DTU. The work has been carried out from June 2006 to May 2010 at the Department of Mechanical Engineering, Section of Thermal Energy Systems under supervision of Associate Prof. Brian Elmegaard and co-supervision of Prof. Henrik Carlsen, Associate Prof. Martin O. L. Hansen and Arne Jacobsen. The project has been financed by DTU.

I would like to thank my principal supervisor Brian Elmegaard for a countless number of inspiring discussions and for many good questions, which always helped me progressing with my work. I would also like to thank my co-supervisors for good discussions, especially during the start-up period of my project.

Furthermore, I would like to acknowledge Prof. Pega Hrnjak and his group at the Air Conditioning and Refrigeration Center for their hospitality during my stay at the University of Illinois at Urbana-Champaign in Fall 2007.

I would also like to thank Morten Skovrup and Mette Havgaard Vorre for a pleasant working environment and many helpful discussions in the 'IPU office', and I especially thank Morten helping me getting started with WinDali. Thanks also to my fellow PhD-students and all other colleagues at TES, always being open for questions and making a nice working environment.

Last, but not least, thanks to Troels for always supporting me and for showing interest in my work and to our son Lasse for plenty of pleasant distractions.

Wiebke Brix

Abstract

This thesis is concerned with numerical modelling of flow distribution in a minichannel evaporator for air-conditioning. The study investigates the impact of non-uniform airflow and non-uniform distribution of the liquid and vapour phases in the inlet manifold on the refrigerant mass flow distribution and on the cooling capacity of the evaporator. A one dimensional, steady state model of a minichannel evaporator is used for the study.

An evaporator consisting of two multiport minichannels in parallel is used as a test case and two different refrigerants, R134a and R744 (CO_2), are applied in the numerical experiments using the test case evaporator.

The results show that the reduction in cooling capacity due to non-uniform airflow and non-uniform liquid and vapour distribution is generally larger when using R134a than when using CO_2 as refrigerant. Comparing the capacity reductions with reductions of the area covered by refrigerant in a two-phase condition shows that the capacity decreases significantly more than the two-phase area when imposing a non-uniform airflow. On the other hand the reductions in capacity and in two-phase area are almost equal when imposing a non-uniform distribution of the liquid and vapour in the inlet manifold.

Combining non-uniform airflow and non-uniform liquid and vapour distribution shows that a non-uniform airflow distribution to some degree can be compensated by a suitable liquid and vapour distribution. Controlling the superheat out of the individual channels to be equal, results in a cooling capacity very close to the optimum.

A sensitivity study considering parameter changes shows that the course of the pressure gradient in the channel is significant, considering the magnitude of the capacity reductions due to non-uniform liquid and vapour distribution and non-uniform airflow. It is found that a large pressure gradient in the first part of the channel is beneficial.

Resumé

Denne afhandling omhandler numerisk modellering af strømningsfordelinger i en minikanalfordamper til luftkonditionering. Det undersøges, hvorledes en ujævn fordeling af luftstrømningen og en ujævn fordeling af væske og damp i indløbsmanifolden påvirker kølemiddelfordelingen i de parallelle kanaler. Endvidere undersøges, hvordan de ujævne fordelinger påvirker fordamperens kølekapacitet. Fordampermodellen er en endimensionel model, der antager stationær strømning.

Som testcase anvendes en fordamper bestående af to parallelle multiport minikanaler, og der anvendes to forskellige kølemidler, R134a og R744 (CO_2), i simuleringerne.

Generelt viser resultaterne at reduktionen af kølekapaciteten pga. ujævn luftstrømning eller ujævn fordeling af væske og damp er større for R134a end for CO_2. En sammenligning af reduktionen af kølekapaciteten med reduktionen af det areal, der er i berøring med kølemiddel i to-fase tilstand viser, at kølekapaciteten reduceres betydelig mere end to-fase arealet, såfremt en ujævn luftstrømning er årsagen til kapacitetsreduktionen. Derimod reduceres kølekapaciteten og to-fasearealet i næsten samme grad, når en ujævn fordeling af væske og damp i indløbsmanifolden er årsagen til kapacitetsreduktionen.

Kombineres ujævn luftstrømning og ujævn fordeling af væske og damp, ses at en ujævn luftstrømning til en hvis grad kan kompenseres ved en passende ujævn fordeling af væske og damp. Styres overhedningen i de enkelte kanaler til at være ens, opnås en kølekapacitet, der er meget tæt på optimum.

Et studie af følsomheden overfor parametervariationer viser, at forløbet af trykgradienten i kanalerne har væsentlig betydning for hvor store kapacitetsreduktionerne pga. ujævne fordelinger af væske og damp i indløbsmanifolden og af luftstrømmen vil være. En høj gradient i den første del af kanalerne viser sig at være hensigtsmæssig.

List of publications

Journal papers:

Paper I:
Brix, W., M. R. Kærn, and B. Elmegaard (2009). Modelling refrigerant distribution in microchannel evaporators. *International Journal of Refrigeration 32*(7), 1736–1743.

Paper II:
Brix, W., M. R. Kærn, and B. Elmegaard (2010). Modelling distribution of evaporating CO_2 in parallel minichannels. *International Journal of Refrigeration 33*(6), 1086–1094.

Peer reviewed conference contributions:

Paper III:
Brix, W., A. Jakobsen, B. D. Rasmussen, and H. Carlsen (2007). Analysis of airflow distribution in refrigeration system. In *International Congress of Refrigeration*. ICR07-B2-581.

Paper IV:
Brix, W. and B. Elmegaard (2008). Distribution of evaporating CO_2 in parallel microchannels. In 8^{th} *IIR Gustav Lorentzen Conference on Natural Working Fluids*.

Paper V:
Brix, W. and B. Elmegaard (2009). Comparison of two different modelling tools for steady state simulation of an evaporator. In *SIMS50 - Modelling and Simulation of Energy Technology*.

Invited conference contributions:

Paper VI:
Brix,W. (2008). Modelling of refrigerant distribution in microchannel evaporators. In *Danske Køledage 2008*.

Paper VII:
Brix,W. (2010). Modelling refrigerant distribution in a minichannel evaporator using CO_2 and R134a. In *Danske Køledage 2010*.

Contents

Nomenclature

Roman

A	area (m^2)
C	heat capacity rate (J $s^{-1}K^{-1}$)
c_p	specific heat (J $kg^{-1}K^{-1}$)
D	diameter (m)
F	enhancement factor
f	friction factor (-)
f	maldistribution parameter (-)
G	mass flux (kg $s^{-1}m^{-2}$)
g	gravitational acceleration (m s^{-2})
h	enthalpy (J/kg)
h	heat transfer coefficient (W $m^{-2}K^{-1}$)
i	enthalpy of moist air (J/kg)
k	thermal conductivity (W $m^{-1}K^{-1}$)
L	channel length (m)
$\dot{m}$	mass flow rate (kg s^{-1})
NTU	number of transfer units
P	perimeter (m)
p	pressure (bar)
Pr	Prandtl number
$\dot{Q}$	heat transfer rate (W)
q''	heat flux (W m^{-2})

r	latent heat of vaporization (J/kg)
R	relative residual
Re	Reynolds number
RH	relative humidity
S	suppression factor
T	temperature (°C)
U	air velocity (m s^{-1})
u	velocity (m s^{-1})
UA	overall heat transfer coefficient (W K^{-1})
w	humidity ratio (kg/kg)
x	quality
z	axial coordinate (m)

Greek

ϵ	effectiveness
η_0	surface efficiency
μ	dynamic viscosity (kg $m^{-1}s^{-1}$)
ρ	density (kg m^{-3})
σ	surface tension (N/m)
τ	shear stress (N m^{-2})
θ	angle of inclination (°)

Subscripts

0	at reference temperature 0°C
1,2	referring to channel number
a	air side
ac	acceleration
acc	accurate
conv	convective boiling
dew	dew point
dry	dry wall condition
fr	friction
g	gas
gr	gravitaion

h	hydraulic diameter
in	inlet
l	liquid
lat	latent
max	maximum
mean	mean value
min	minimum
NB	nucleate boiling
out	outlet
r	refrigerant side
rat	ratio
s	saturation
sh	superheat
SP	single phase
sen	sensitive
TP	two-phase
th	threshold
tot	total
U	maldistribution of air velocity
v	vapour
w	wall
$1+w$	property of mixture per kg dry air
x	maldistribution of inlet quality

Chapter 1

Introduction

In recent years compact refrigeration systems with low refrigerant charges have become more and more popular. For many applications, especially for mobile or unitary applications, compactness and weight is an important design issue. Increasing compactness is usually accompanied by material savings that lead to cost reductions. Low refrigerant charges help reducing the system weight, and are furthermore interesting due to safety and legislative issues (Kandlikar, 2007; Palm, 2007).

The most commonly used refrigerants today are HFC-type refrigerants. These refrigerants do not deplete the ozone layer, but still they are greenhouse gases, typically having a global warming potential more than 1000 times larger than CO_2 (McMullan, 2002). In Europe the use of HFC-type refrigerants is subject to legislative restrictions in order to reduce their use. In Denmark levies are imposed on HFC-type refrigerants and since 2007 it is forbidden to build new systems containing a refrigerant charge of more than 10 kg HFC-type refrigerant. All of this encourages the development of minimum charge systems.

One solution in the design of compact, minimum charge systems is to use minichannel heat exchangers. These aluminium braced heat exchangers have channel sizes in the range of 1 mm, and the internal volume is much smaller than in a conventional fin and tube coil.

Also during the last two decades CO_2 has had a revival as a refrigerant, because of its favourable environmental properties. However, using CO_2 as a refrigerant requires high working pressures, which means that the heat exchangers have to be able to handle the high pressures. Minichannel heat exchangers are a popular choice for the design of compact and environmentally friendly refrigerant systems using CO_2 as refrigerant.

1.1 Minichannel heat exchangers

A typical minichannel heat exchanger employs flat extruded aluminium tubes with several small, rectangular or circular passages. These passages usually have a hydraulic diameter in a range of 0.5-2.5 mm. The smallest sizes below 1 mm are primarily used for condensers, while passage sizes of 1-2.5 mm are also used for evaporators. However, when using CO_2 as refrigerant smaller sized channels are used for evaporators as well.

Minichannel heat exchangers are typically used as refrigerant-to-air heat exchangers and on the air side folded, louvred fins connect the minichannel tubes. In order to reduce pressure drop in the small refrigerant passages, a minichannel heat exchanger typically consists of several parallel tubes that are connected by manifolds. The length of the tubes and the number of tubes in parallel depend on the refrigerant and on the operating conditions. Figure 1.1 shows pictures of parts of minichannel heat exchangers.

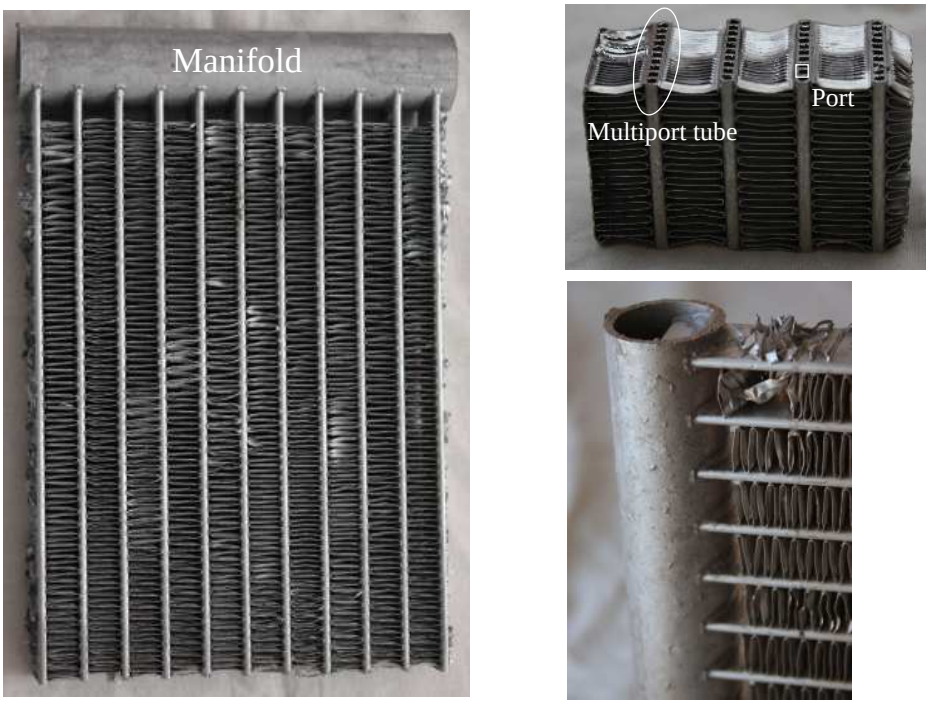

***Figure 1.1**: Pictures showing parts of minichannel heat exchangers. The distance between two multiport tubes is typically around 1 cm.*

1.1.1 Micro- vs. minichannel

In the literature these heat exchangers are sometimes called microchannel heat exchangers. The classification of the channel sizes that define whether a channel is a macro-, mini- or a microchannel is ambiguous, and the term microchannel is often used for channels of the same sizes as the channels described above. Different criteria have been proposed in the literature to classify the different types. Some are based on flow phenomena and others on applications. Furthermore some researchers discuss all three kinds of channels, while others only consider one transition between macro- and microchannels. Kandlikar and Grande (2003) propose a threshold of 3 mm between macro- and minichannels and 0.20 mm between mini- and microchannels. Kew and Cornwell (1997) define only one threshold based on the confinement of a bubble in the channel. According to their definition a channel is a microchannel, when the channel diameter is below a critical value depending on fluid properties, given by

$$D_{\mathrm{th}} = \left(\frac{4\sigma}{g\left(\rho_l - \rho_g\right)} \right)^{1/2}, \tag{1.1}$$

where σ is surface tension, g is gravitational acceleration and ρ_l and ρ_g are liquid and vapour densities. Figure 1.2 from Thome (2006), compares the transition thresholds defined by Kandlikar and Grande and Kew and Cornwell for CO_2 and water as a function of reduced pressures. It is seen, that the threshold defined by Kew and Cornwell can differ by more than a factor of two, even for the same fluid.

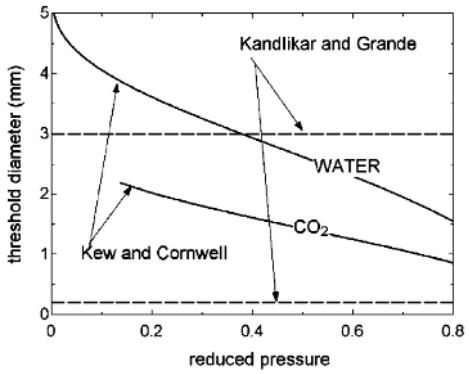

***Figure 1.2**: Different thresholds between macro-, mini- and microchannels. Figure from Thome (2006).*

In the present study we follow the classification proposed by Kandlikar and Grande (2003). According to their definition the channels typically used for

the heat exchangers considered in the present study fall into the minichannel category.

1.2 The maldistribution problem

One of the main challenges in minichannel heat exchangers is to ensure a uniform refrigerant distribution. Especially for the evaporator the distribution of the flow into the parallel channels is a challenge (Kandlikar, 2007; Kim et al., 2004), since the refrigerant is usually in a two-phase condition at the inlet to the evaporator. The design of the distribution manifold plays an important role in how the liquid and vapour distribute in the manifold. Especially if the liquid is not uniformly distributed and some channels receive mainly vapour, the heat exchanger area is not utilised optimally, which affects the evaporator capacity.

One way to illustrate the refrigerant distribution in minichannel evaporators in practice, is to use infrared pictures of an evaporator that show the distribution of the superheated area. Figure 1.3 from Elbel and Hrnjak (2004) shows a minichannel evaporator with clearly uneven distribution of the superheated area. Uneven superheated zones might result in capacity reductions of the evaporator. If large superheat is found in some regions, while liquid refrigerant exits the evaporator in other regions, mixing in the manifold determines the evaporator outlet conditions. The liquid that is evaporated by the mixing does not contribute optimally to the cooling capacity. Therefore reductions in the cooling capacity are expected if the superheat is not distributed uniformly.

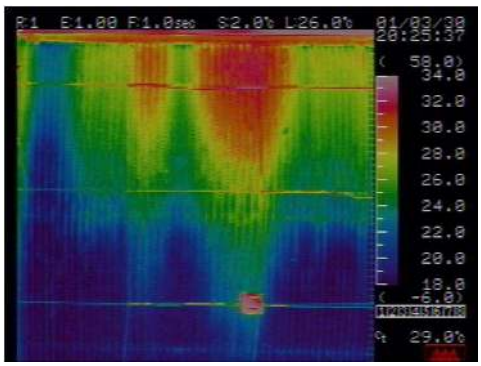

***Figure 1.3**: Unevenly distributed superheat in a minichannel evaporator. Figure from Elbel and Hrnjak (2004).*

Furthermore the distribution of the airflow may influence the evaporator

performance. If the heat load is higher on some of the parallel channels the refrigerant evaporates faster in these channels. The superheated regions will thus be non-uniformly distributed in case of non-uniform airflow. Faster evaporation in some of the channels also affects the pressure gradient in the channels such that the refrigerant mass flow distribution might be affected too by the airflow distribution.

1.2.1 Literature review

Maldistribution in heat exchangers has been a topic of interest for many years. Mueller and Chiou (1988) discuss different types of maldistribution and their causes for both single-phase and two-phase heat exchangers. They categorise the main causes of maldistribution into four categories, being:

- mechanical causes due to header design
- self-induced maldistribution due to the heat transfer process itself
- two-phase flow distribution; gas-liquid separation and two-phase flow instabilities
- fouling and/or corrosion

Causes of maldistribution are performance deteriorations and material damage due to high thermal stresses and large temperature differences.

Kitto and Robertson (1989) point out that maldistribution is especially critical in heat exchangers with two-phase flow inlet conditions, and that there is a continued need for research in this area. Furthermore it is stated that airflow maldistribution in air cooled heat exchangers can be a problem, especially if the non-uniform airflow leads to maldistribution of the refrigerant.

The effect of airflow maldistribution on the evaporator performance has also been considered by Domanski (1991). This study presents a simulation model, which is used to model a finned tube evaporator. The modelled evaporator is exposed to different airflow distributions and the resulting refrigerant distribution into the different circuits is calculated by the model. It is shown that non-uniform airflow distribution affects the refrigerant distribution. For increasing maldistribution of the airflow the evaporator capacity decreases, and this capacity reduction is associated with the uneven refrigerant superheat at the outlet of the different circuits. The model is verified against an experimental study by Chwalowski et al. (1989), which also considers the effects of non-uniform airflow on the performance of an evaporator coil.

Kirby et al. (1998) performed experiments on the evaporator of a 5 kW window air conditioner. The results show that the effects of airflow non-uniformity are small under a wide range of working conditions. It is furthermore found that no significant maldistribution of the refrigerant is induced by the non-uniform airflow. It is concluded that effective circuiting strategies are important in evaporator design in order to eliminate effects of non-uniform airflow on the refrigerant distribution in finned tube evaporators.

Payne and Domanski (2003) experimentally and numerically studied three different R22 finned tube evaporators, each having three parallel circuits. The three circuits were not interlaced, such that the air velocity flowing across one circuit was not necessarily the same as across one of the other circuits. The evaporator was placed in a system with a variable speed compressor such that the refrigerant mass flow rate could be controlled. Furthermore each circuit was connected to its own expansion device such that the superheat out of the individual circuits could be controlled. It is shown that capacity reductions due to airflow maldistribution could be recovered within a few percent if the superheat out of each circuit was controlled to be equal. The more non-uniform the airflow was, the larger was the benefit of controlling the individual superheat.

Considering minichannel heat exchangers a number of studies have been performed, where the majority focuses on the manifolds. Phase separation in manifolds and the distribution of liquid and vapour depending on manifold diameter, inlet quality, mass flow rate and heat load have been studied using refrigerant R134a and CO_2 in Vist and Pettersen (2004; 2003). The results showed severe maldistribution of the liquid and vapour phases. The manifolds were horizontally oriented. For upwards evaporating refrigerant flow the liquid tended to flow into the tubes far away from the manifold inlet, while for downwards evaporation the liquid distributed much easier into the tubes close to the manifold inlet. Hwang et al. (2007) presented a similar study using R410a as refrigerant and concluded that the liquid distribution could be improved when locating the inlet to the manifold in the middle of the manifold instead of at the end. However, a fully uniform distribution could not be achieved by changing the location of the inlet.

Hrnjak (2004) discusses a few solutions that could either help to avoid phase separation or benefit from it by designing devices, which can distribute liquid and vapour separately. It is however pointed out, the presented solutions are not directly suitable for minichannel heat exchangers. Webb et al. (2005) studied the patent literature and found that many different solutions exist that should help to provide a uniform distribution of liquid and vapour in minichannel heat exchangers. These solutions include both installed objects such as weirs, inserts or throttle plates and special distributor devices, which

locally feed the fluid into the branch tubes. The shortcomings of most of these solutions are that they were empirically designed for certain fluids and operating conditions.

Another solution to avoid maldistribution due to phase separation is proposed in Elbel and Hrnjak (2004). The study presents a system using flash gas removal such that only liquid enters the evaporator, while the gas bypasses the evaporator. The system was compared to a similar system using direct expansion. Infrared pictures of the evaporator showed clearly more uniformly distributed superheat for the system with flash gas removal. The system performance was also better when using flash gas bypass.

Kulkarni et al. (2004) discuss maldistribution in minichannel heat exchangers occurring due to pressure drop in the manifold. A simulation model was used to investigate how refrigerant maldistribution occurring due to pressure drop in the manifold affects the cooling capacity. If the pressure drop in the manifold is large compared to the pressure drop in the tubes, maldistribution of refrigerant will occur. It was concluded that if the manifold pressure drop was limited to approximately 10% of the in tube pressure drop, the capacity was reduced by less that 5%.

Recently, Kim et al. (2009a; 2009b) presented a numerical study of the effects of void fraction maldistribution, feeder tube blockages and airflow non-uniformity on the performance of a five circuit, finned tube evaporator using R410A as refrigerant. The above mentioned non-uniformities were imposed such that the evaporator was divided into two sections. Two and three circuits thus worked under the same conditions, respectively. Significant reductions in cooling capacity and COP were found for airflow non-uniformity and refrigerant maldistribution due to both maldistribution of the inlet void fraction and feeder tube blockages. It was furthermore shown that the losses in cooling capacity and COP could be mostly recovered by controlling the individual superheat of the different passes.

As can be seen from the above presented literature, many different aspects of the maldistribution phenomena have been studied. Most of these studies have been performed on the basis of understanding the phenomena that govern the refrigerant distribution. Since still not all aspects considering maldistribution are fully understood, the basis for this thesis is precisely to contribute to the understanding of these phenomena.

1.3 Thesis statement

Non-uniform distribution of the liquid and vapour in the inlet manifold of a minichannel evaporator as well as non-uniform airflow distribution affect the performance of the evaporator in a refrigeration system. One solution to eliminate the effects of maldistribution of the liquid or maldistribution of the airflow is to increase the size of the heat exchanger. However, this is not compatible with the goals of increasing compactness and decreasing refrigerant charge that are two of the main design issues in todays development of refrigeration systems.

In order to design minichannel evaporators that are less vulnerable to maldistribution, we first of all need to understand the mechanisms that determine the effects of maldistribution. The objective of the present study is to gain understanding of the effects of two different maldistribution phenomena (i): Non-uniform distribution of the liquid and vapour in the inlet manifold and (ii): Non-uniform airflow distribution. The following questions are sought to be answered:

- How do the effects of non-uniform distribution of the liquid and vapour in the inlet manifold compare to the effects of airflow non-uniformity?
- Which parameters are determining the performance reductions due to maldistribution?
- Can we predict the impacts of a non-uniform distribution of liquid and vapour and non-uniform airflow?
- Which measures can help reducing problems occurring due to maldistribution of the liquid and vapour or the airflow?

1.3.1 Method

In order to answer the above questions, a numerical study is performed. A test case is defined based on a real system and the influence of non-uniform liquid and vapour distribution and non-uniform airflow on the evaporator performance is investigated by numerical simulation. Taking the test case evaporator as a reference, a sensitivity study is carried out in order to determine which parameters are decisive for the effects of maldistribution.

1.3.2 General delimitations

In the present study the evaporator is tested under 'stand alone' conditions, and not as a part of a total refrigeration system. The test case parameters

are chosen such that the inlet condition of the refrigerant is kept constant and the outlet condition is fixed by a constant superheat. The total mass flow rate of refrigerant on the other hand can vary as a response when imposing non-uniform liquid and vapour distribution or non-uniform airflow. In a real system with a compressor running at constant speed, a change in both mass flow rate, suction pressure and evaporator inlet quality would be expected as a response to the non-uniform liquid and vapour distribution or non-uniform airflow.

Furthermore, the present study focuses on the evaporation process, and the maldistribution occurring only due to pressure changes in the evaporator itself. The manifold geometry as well as pressure drop in the manifold are not considered, although these can also cause maldistribution of the refrigerant.

Lastly, the study is based on the assumption of steady state. Any problems related to dynamics are hence not taken into consideration.

1.4 Thesis outline

The thesis is organized as follows:

Chapter 2 describes the evaporator model, which is used for the numerical studies in this thesis. The main assumptions on which the model is build are discussed and the model equations are presented.

Chapter 3 presents the results that are obtained using a test case evaporator. The evaporator is exposed to both non-uniform distribution of the liquid and vapour in the manifold and non-uniform airflow and a combination of the two. The effects of maldistribution on the distribution of the refrigerant mass flow rate and on the cooling capacity are considered.

Chapter 4 presents a sensitivity study. By performing several parameter variations it is investigated which parameters are important for the effects of maldistribution. As part of the sensitivity study a modified version of the model is considered, which accounts for moist air.

Chapter 5 summarizes the main conclusions and gives an outlook for further work.

Chapter 2

The evaporator model

This chapter describes the evaporator model that is used to investigate the effects of airflow non-uniformity and maldistribution of the inlet quality on the evaporator performance. First the one-dimensional single channel model is presented. Next the parallel channel model is considered. A test evaporator is defined and the model is validated. At last two different modelling tools are compared.

2.1 The one-dimensional channel model

In order to build the evaporator model, a discretized model of a single minichannel tube is created. First, we consider the refrigerant flow inside one port of the minichannel. Since there is only one main flow direction it is assumed that the flow can be considered one-dimensional. Figure 2.1 shows a sketch of a channel where the flow is partly in two-phase and partly in single phase condition.

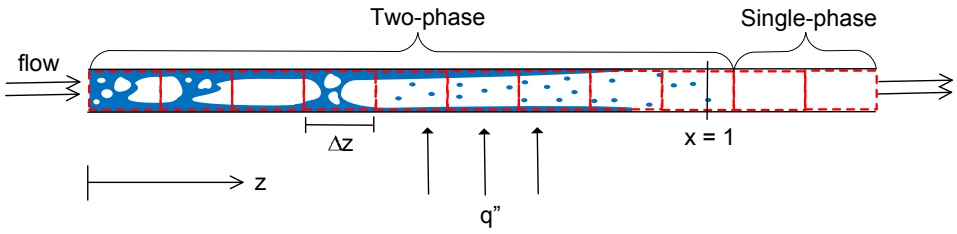

***Figure 2.1**: Evaporator channel discretised into several control volumes of length Δz.*

In order to model the flow in the channel two main assumptions are made.

Firstly, only steady state flow is considered and secondly, the two-phase flow is considered to be homogeneous. It is thus assumed that the liquid and vapour phases are well mixed and travelling at the same velocity. Furthermore thermodynamic equilibrium between the two phases is assumed.

The assumption of homogeneous two-phase flow simplifies the general equations for two-phase flow significantly, and several studies have shown, that this assumption is adequate for two-phase flow in minichannels. Revellin et al. (2006) investigated void fractions of evaporating R134a in a 0.5 mm channel, and found that the measured void fractions compared reasonably well with homogeneous values. Thome (2007, chap.20) shows that measured void fraction data from studies by Triplett et al. (1999), Serizawa et al. (2002) and Chung and Kawaji (2004) are well predicted by the homogeneous model.

In the following the governing equations ensuring conservation of mass, momentum and energy are considered. In order to solve the governing equations the finite volume method is applied. The channel is thus discretised into a number of volumes and the equations are integrated over each volume.

When integrating and solving the equations, different conditions may apply depending on whether the flow is in two-phase or single phase condition. Knowing the inlet conditions of a control volume the volume is declared a two-phase volume or a single phase volume. In the transition between two-phase flow and single phase flow there is one control volume, for which the flow is in two-phase condition at the inlet and in single-phase condition at the outlet. This control volume is in the calculations considered as a two-phase volume, receiving some special treatment, however.

2.1.1 Conservation of mass

Considering a small control volume of a channel, having a constant cross sectional area, A, and a length Δz, as shown in figure 2.2, the mass balance for a steady state flow yields

$$(\bar{\rho}\, A\, \bar{u}) - \left[(\bar{\rho}\, A\, \bar{u}) + \frac{d}{dz}(\bar{\rho}\, A\, \bar{u})\, \Delta z\right] = 0 \tag{2.1}$$

In the limit of $\Delta z \to 0$ we obtain the differential mass conservation equation

$$\frac{d}{dz}(\bar{\rho}\, A\, \bar{u}) = 0, \tag{2.2}$$

where $\bar{\rho}$ is the homogeneous density and $\bar{u}$ is the mean velocity of the flow. Integration of the continuity equation over a finite volume of the length Δz merely tells that

$$\dot{m}_{\text{out}} = \dot{m}_{\text{in}}, \tag{2.3}$$

where the subscripts 'in' and 'out' denote the conditions at the inlet and outlet boundaries of a control volume.

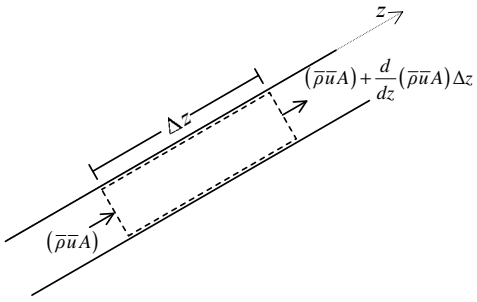

***Figure 2.2**: Control volume for the mass balance.*

2.1.2 Conservation of momentum

In figure 2.3 the forces acting on the fluid in a control volume of length Δz are shown. Momentum changes occur due to the acting of pressure forces, wall friction and gravitational forces.

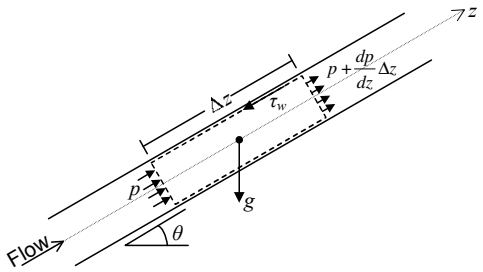

***Figure 2.3**: Forces acting on the control volume.*

The momentum balance is obtained by applying Newton's law of motion to the control volume

$$\int_{\Delta z} \frac{d}{dz}\left(\dot{m}\bar{u}\right) dz \;=\; -\int_A \frac{dp}{dz}\Delta z \; dA - \int_P \tau_w \Delta z \; dP - \int_A \rho g \sin\theta \, \Delta z \; dA$$

$$\Downarrow$$

$$-\frac{dp}{dz} \;=\; \frac{1}{A}\tau_w P \;+\; \bar{\rho}\, g \, \sin\theta \;+\; G\frac{d}{dz}\left(\bar{u}\right), \tag{2.4}$$

where τ_w is the mean wall stress for the homogeneous flow acting on the perimeter, P, and G is the total mass flux. The three terms on the right

hand of equation (2.4) side are three contributions to the overall pressure drop: a frictional, a gravitational and a contribution due to acceleration of the flow. The total pressure drop can hence be expressed as a combination of these three contributions

$$\left(-\frac{dp}{dz}\right) = \left(\frac{dp}{dz}\right)_{\text{fr}} + \left(\frac{dp}{dz}\right)_{\text{gr}} + \left(\frac{dp}{dz}\right)_{\text{ac}}. \tag{2.5}$$

where the three terms according to equation (2.4) are

$$\left(\frac{dp}{dz}\right)_{\text{ac}} = G\frac{d}{dz}\left(\bar{u}\right) \tag{2.6}$$

$$\left(\frac{dp}{dz}\right)_{\text{gr}} = \bar{\rho}\, g\, \sin\theta \tag{2.7}$$

$$\left(\frac{dp}{dz}\right)_{\text{fr}} = \frac{1}{A}\,\tau_w P. \tag{2.8}$$

In the following each of these contributions is considered separately.

Pressure drop due to acceleration

Whenever liquid is evaporated, the flow accelerates due to the changes in density. Applying the continuity equation, the acceleration term, equation (2.6), can be rewritten as

$$\int_{\Delta z}\left(\frac{dp}{dz}\right)_{\text{ac}} dz = G^2 \int_{\Delta z}\frac{d}{dz}\left[\frac{1}{\bar{\rho}}\right] dz. \tag{2.9}$$

Performing the integration yields

$$\Delta p_{\text{ac}} = G^2\left(\frac{1}{\bar{\rho}_{\text{out}}} - \frac{1}{\bar{\rho}_{\text{in}}}\right) \tag{2.10}$$

For single-phase flow the density changes are very small, and in this case the pressure drop due to acceleration is neglected in the calculations. For two-phase flow the homogeneous mean density can be written in terms of equilibrium quality and the single-phase vapour and liquid densities (Collier and Thome, 1994, chap.2)

$$\frac{1}{\bar{\rho}} = \frac{x}{\rho_g} + \frac{1-x}{\rho_l}. \tag{2.11}$$

Inserting this into equation (2.10) and collecting the terms, the pressure drop due to acceleration yields

$$\Delta p_{\text{ac}} = G^2\left(x_{\text{out}} - x_{\text{in}}\right)\left(\frac{\rho_l - \rho_g}{\rho_g\,\rho_l}\right), \tag{2.12}$$

where ρ_l and ρ_g are considered constant within a control volume. These densities are evaluated at the centre of the control volume, where the pressure is found as the mean between the inlet and outlet pressures.

Gravitational pressure drop

The gravitational contribution to the overall pressure drop is

$$\int_{\Delta z} \left(\frac{dp}{dz}\right)_{\text{gr}} dz = \int_{\Delta z} \bar{\rho}\, g\ \sin\theta dz \tag{2.13}$$

For single-phase flow this integral is straightforward, since it is assumed that the single-phase density is constant over the volume, again evaluated at the centre of the control volume.

For two-phase flow equation (2.11) is inserted into equation (2.13)

$$\int_{\Delta z} \left(\frac{dp}{dz}\right)_{\text{gr}} dz \quad = \quad g\ \sin\theta \int_{\Delta z} \left(\frac{x}{\rho_g} + \frac{1-x}{\rho_l}\right)^{-1} dz \tag{2.14}$$

Since x is a function of z, this integral can only be solved if the connection between these two variables is known. Assuming constant heat flux over the control volume, implies that the quality depends linearly on z and the variation of x within a volume of length Δz can be expressed as

$$x = x_{\text{in}} + \frac{x_{\text{out}} - x_{\text{in}}}{\Delta z} z. \tag{2.15}$$

Inserting this into equation (2.14) and solving the integral leads to the gravitational pressure drop over the control volume

$$\Delta p_{\text{gr}} \quad = \quad \frac{g \sin\theta\ \Delta z}{\left(\frac{1}{\rho_g} - \frac{1}{\rho_l}\right)(x_{\text{out}} - x_{\text{in}})} \ln\left(\frac{\frac{1}{\rho_l} + \left(\frac{1}{\rho_g} - \frac{1}{\rho_l}\right) x_{\text{out}}}{\frac{1}{\rho_l} + \left(\frac{1}{\rho_g} - \frac{1}{\rho_l}\right) x_{\text{in}}}\right) \tag{2.16}$$

Frictional pressure drop

Even with the simplifications of the homogeneous equilibrium model the frictional pressure gradient cannot be integrated as easily as the two previously considered terms, since the wall shear stress is unknown.

For single-phase flow, the wall shear stress is commonly expressed in terms of a friction factor, such that

$$\tau_w = f\left(\frac{\rho u^2}{2}\right), \tag{2.17}$$

where f is a dimensionless friction factor. Inserting this into equation (2.8) yields

$$\left(\frac{dp}{dz}\right)_{\text{fr}} \quad = \quad \frac{1}{A}\tau_w\ P = \frac{f\,P}{A}\left(\frac{\bar{\rho}\bar{u}^2}{2}\right). \tag{2.18}$$

Integrating the frictional pressure gradient over a control volume of length Δz yields the frictional contribution to the pressure drop in this control volume

$$\Delta p_{\mathrm{fr}} = \frac{f\,P}{A}\left(\frac{\bar{\rho}\bar{u}^2}{2}\right)\Delta z. \tag{2.19}$$

For laminar flow in a circular channel it can be analytically shown that $f = 16/\mathrm{Re}$ (Fox and McDonald, 1998, chap.8), while for turbulent flow an empirical correlation has to be applied. For turbulent flow the Blasuis correlation for smooth tubes (Fox and McDonald, 1998, chap.8) is applied to calculate the single-phase friction factor in this model

$$f = 0.0791\left(\frac{G\,D_h}{\mu}\right)^{-1/4}, \tag{2.20}$$

The Blasius correlation was developed for conventional channel sizes, however several studies have shown, that the correlation predicts well for single-phase flow in minichannels too (Celata et al., 2009; Caney et al., 2007).

For two-phase flow many different types of correlations exist to model the frictional pressure drop. For the present evaporator model, the Müller-Steinhagen and Heck (1986) correlation is chosen to model the frictional pressure gradient. Revellin et al. (2006) compared a wide range of pressure drop correlations, developed for both small channels and conventional channels, against experimental data of evaporating R134a in small channels. It was found that the Müller-Steinhagen and Heck (1986) correlation best predicted the data. For calculating frictional pressure drop of evaporating CO_2 in minichannels, many different correlations have been proposed in the literature, where the Müller-Steinhagen and Heck (1986) correlation is one of them. In chapter 4 the sensitivity of the results on the choice of correlation is investigated.

Adding the three contributions gives us the total pressure drop over one control volume

$$\Delta p = \Delta p_{\mathrm{ac}} + \Delta p_{\mathrm{gr}} + \Delta p_{\mathrm{fr}}, \tag{2.21}$$

where the three terms on the right hand side are given by equations (2.12), (2.16) and (2.19). In order to perform the calculation the inlet state and exit quality (or enthalpy) have to be known. The exit quality is an output from the heat transfer calculations, which are considered in the following.

2.1.3 Conservation of energy

Figure 2.4 shows a control volume for the heat transfer calculations. The heat transfer to each of the ports in the minichannel is considered equal.

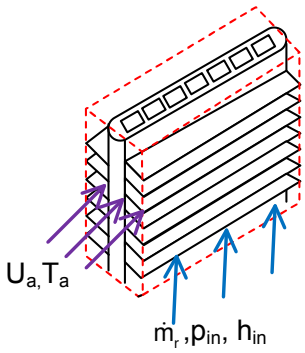

***Figure 2.4**: Control volume for heat transfer calculations.*

Applying the first law of thermodynamics to the refrigerant side of the control volume, still assuming steady state flow and furthermore neglecting changes in kinetic and potential energy, yields

$$\dot{Q} = \dot{m}_r \left(h_{\text{out}} - h_{\text{in}} \right), \tag{2.22}$$

$\dot{Q}$ is the total heat transfer rate to the volume, i.e. the cooling capacity of the volume, and $\dot{m}_r$ is the total mass flow rate of refrigerant flowing in all ports. Assuming $\dot{Q}$ to be known, this equation defines the refrigerant outlet enthalpy, which is needed in the pressure drop calculations. Conversion between the outlet enthalpy and quality is done using the definition of quality, such that

$$\Delta x = \frac{\Delta h}{r}, \tag{2.23}$$

where r is the latent heat of vaporization.

Another energy balance can be formulated for the airside of the evaporator, where the air is considered to be dry

$$\dot{Q} = \dot{m}_a \, c_{p,a} \left(T_{a,\text{in}} - T_{a,\text{out}} \right). \tag{2.24}$$

Since the air outlet temperature is unknown, an additional equation is needed in order to solve the equations. This equation is given by applying the effectiveness-NTU method (Incropera and DeWitt, 2002, chap.11). The heat transfer between the air and the refrigerant is calculated using a heat exchanger effectiveness

$$\dot{Q} = \epsilon \, C_{\min} \left(T_{a,\text{in}} - T_{r,\text{in}} \right), \tag{2.25}$$

where $C_{\min}$ is the minimum heat capacity rate, given by

$$C_{\min} = \min \left\{ \left(\dot{m}_r \, c_{p,r} \right), \left(\dot{m}_a \, c_{p,a} \right) \right\}. \tag{2.26}$$

Usually the airside heat capacity rate will be the smallest of the two. The effectiveness, ϵ, defined as the ratio of the actually transferred heat to the maximum possible heat transfer rate, is a function of the heat capacity ratio and the number of transfer units, NTU. The heat capacity ratio and the NTU are defined as

$$C_{\text{rat}} = C_{\min}/C_{\max} \quad \text{and} \quad \text{NTU} = \frac{\text{UA}}{C_{\min}}, \tag{2.27}$$

where UA is the overall heat transfer coefficient.

How the effectiveness relates to the heat capacity ratio and the number of transfer units depends on the geometry and whether phase changes occur or not. For an evaporator control volume with two phase flow, the capacity ratio is close to zero and the effectiveness is defined as (Incropera and DeWitt, 2002, chap.11)

$$\epsilon = 1 - \exp\left(-\text{NTU}\right) \tag{2.28}$$

For single-phase refrigerant the relation for cross flow and both fluids unmixed is applied (Incropera and DeWitt, 2002, chap.11)

$$\epsilon = 1 - \exp\left[\left(\frac{1}{C_{\text{rat}}}\right)\ \text{NTU}^{0.22}\left(\exp\left(-C_{\text{rat}}\ \text{NTU}^{0.78}\right) - 1\right)\right] \tag{2.29}$$

In order to calculate NTU the overall heat transfer coefficient, UA, must be calculated. This is defined as

$$\frac{1}{\text{UA}} = \frac{1}{\eta_0\, h_a\, A_a} + \frac{1}{h_r\, A_r}, \tag{2.30}$$

where the conduction resistance of the wall and potential fouling has been neglected. The surface efficiency of the finned air side surface is calculated using a fin efficiency for straight rectangular fins (Incropera and DeWitt, 2002, chap2).

Local heat transfer coefficients

The air and refrigerant side local heat transfer coefficients are found from empirical correlations. The air side heat transfer coefficient is calculated from a correlation for louvred fins proposed by Kim and Bullard (2002), where

$$h_a = f\left(U_a, T_a,\ \text{geometry}, T_w\right). \tag{2.31}$$

However, h_a is only a very weak function of the surface temperature, which actually only enters for evaluating fluid properties at the film temperature.

For a test evaporator outlined in table 2.1 the air side heat transfer coefficient varies less than 0.5% when varying the surface temperature from 5-40°C. In the calculation of the air side heat transfer coefficient a constant surface temperature is therefore assumed.

For two-phase flow the refrigerant side heat transfer coefficient is calculated from a correlation proposed by Bertsch et al. (2009), which was developed for boiling in small channels based on a large database of experimental results using many different refrigerants. The correlation follows the basic form of the classical Chen correlation for boiling in conventional channels (Chen, 1966), where the two-phase heat transfer coefficient has two contributions

$$h_{\mathrm{TP}} = h_{\mathrm{NB}} \cdot S + h_{\mathrm{conv}} \cdot F, \tag{2.32}$$

where S is a suppression factor accounting for the supression of the nucleate boiling heat transfer coefficient at higher qualities, and F is an enhancement factor that is one for pure liquid and pure gas and otherwise greater than one, accounting for the increased convective heat transfer in two-phase flow compared to single-phase flow. Applying the Bertsch et al. (2009) correlation, the heat transfer coefficient is a function of the following variables

$$h_{\mathrm{TP}} = f\left(x, p, G, D_h, \text{ channel length}, q"\right), \tag{2.33}$$

where the pressure and quality are evaluated at the control volume centre, found as the mean between the inlet and outlet conditions.

For single-phase flow the refrigerant side heat transfer coefficient is calculated applying the Gnielinski (1976) correlation,

$$h_{\mathrm{SP}} = \frac{k}{D_h} \frac{\left(\frac{f}{8}\right)\left(\mathrm{Re} - 1000\right)\mathrm{Pr}}{1 + 12.7\left(\frac{f}{8}\right)\left(\mathrm{Pr}^{2/3} - 1\right)} \tag{2.34}$$

$$\tag{2.35}$$

$$\tag{2.36}$$

where k is the thermal conductivity of the gas and with the friction factor, f, calculated as

$$f = \left(0.790 \ln\left(\mathrm{Re}\right) - 1.64\right)^{-2} \tag{2.37}$$

The transition between the two-phase heat transfer coefficient and the single-phase heat transfer coefficient is not smooth, when the above equations are applied. In fact, the heat transfer coefficient calculated from the two-phase correlation gets lower than the single-phase heat transfer coefficient at high qualities. In reality a smooth transition would be expected, and numerically a smooth transition is also preferable, therefore a transition function

is applied when the quality comes close to 1. The heat transfer coefficient is calculated as a weighted mean of the two-phase heat transfer coefficient and the single-phase heat transfer coefficient at saturated conditions

$$h_{\mathrm{TP}} = (1-W)\, h_{\mathrm{TP,Bertsch}} + W\, h_{\mathrm{SP},x=1} \tag{2.38}$$

$$\text{where} \qquad W = \frac{1}{2}\left(\tanh\left(\frac{x-0.9}{0.03}\right)+1\right) \tag{2.39}$$

For $x > 0.98$ the two-phase heat transfer coefficient, $h_{\mathrm{TP,Bertsch}}$, is kept constant at the value calculated for $x = 0.98$. This is done because the heat transfer coefficient gets close to zero in this region, and the single-phase heat transfer coefficient is the dominating term anyway, when calculating h_{TP}.

By solving these equations the outlet conditions of the refrigerant and air side (where air side pressure drop is neglected) as well as the cooling capacity of the control volume are found. The refrigerant outlet state of one volume is then used as inlet state for the following control volume. The total cooling capacity of the channels is found by summation of contributions from the different volumes.

2.1.4 Handling the transition volume

If the refrigerant at the outlet of the channel is superheated there will be one control volume, in which the refrigerant condition changes from two-phase to single-phase. In general this volume is considered as a two-phase volume, i.e. the equations for two-phase conditions are applied. However, the refrigerant flow might be in single-phase condition at the centre, and is for sure at the outlet, and this generates problems in the calculations.

In order to calculate the frictional pressure gradient $x_{\mathrm{out}} = 1$ is used. It is assumed that the error associated with this assumption is small. For calculating the two other contributions, no special arrangements are made. Since the quality is calculated solely based on the enthalpies, there is no problem if x_{out} is larger than one. Likewise the difference $(x_{\mathrm{out}} - x_{\mathrm{in}})$ is not affected by the fact that x_{out} is larger than one.

Calculating the refrigerant side heat transfer coefficient does not give any problems if $x > 1$, the value calculated from the correlation is calculated at $x = 0.98$ in this case, as mentioned above. The only difference regarding the heat transfer calculations for this volume is that the temperatures at the outlet, and if necessary also at the centre, are evaluated from the enthalpy and pressure, instead of just from the pressure.

2.2 Modelling parallel channels

In order to model two minichannels in parallel, the single channel models are connected through manifolds. Since the focus in this study is on the evaporator channels, and not on the manifolds, these are modelled in a very simple way. The two main assumptions made on the manifold level are:

- No pressure drop in the manifold.
- No heat transfer in the manifold.

The inlet manifold thus simply divides the mass flow rate, while the outlet manifold mixes the two flows from the single channel models. Since no pressure loss is assumed in the manifolds the pressure drop over each minichannel has to be equal

$$\Delta p_1 = \Delta p_2. \tag{2.40}$$

This equation connects the channels together with conservation of mass

$$\dot{m}_{\mathrm{mf}} = \dot{m}_1 + \dot{m}_2, \tag{2.41}$$

where the distribution of the mass flow rate in the different channels is determined by the requirement of equal pressure drop over the channels.

The distribution of the liquid and vapour into the different channels is not determined by the model, this has to be given as an input. However, an energy balance over the manifold ensures that the total mass flow rates of liquid and vapour are conserved such that

$$\dot{m}_{\mathrm{mf}}\, x_{\mathrm{mf}} = \dot{m}_1\, x_1 + \dot{m}_2\, x_2. \tag{2.42}$$

During investigation of non-uniform airflow, the quality at the inlet of both channels is the same. When investigating the effects of a non-uniform distribution of the liquid and vapour, the quality into one of the channels is decreased while the quality into the other channel is found from equation (2.42).

At the outlet manifold an energy balance is used to calculate the state out of the evaporator after mixing of the two flows

$$\dot{m}_{\mathrm{mf}}\, h_{\mathrm{mf,out}} = \dot{m}_1\, h_1 + \dot{m}_2\, h_2. \tag{2.43}$$

Figure 2.5 shows an overview over the model inputs and outputs. It is seen that the total mass flow rate is not given as an input to the model, instead the total, mixed superheat out of the evaporator is given. In a refrigeration system controlled by a thermostatic expansion valve the superheat will

usually be the parameter that determines the mass flow rates of refrigerant through the valve. Both the total mass flow rate and the distribution of the mass flow rate are thus calculated from the model. The pressure drop across any tube depends on the mass flow rate, inlet quality and heat load, thus almost all model equations depend on each other. This is illustrated in the model flowchart shown in figure 2.6. The flowchart shows the top layer of the model, while the governing equations for each control volume are solved in the box indicated as procedure HX_volume.

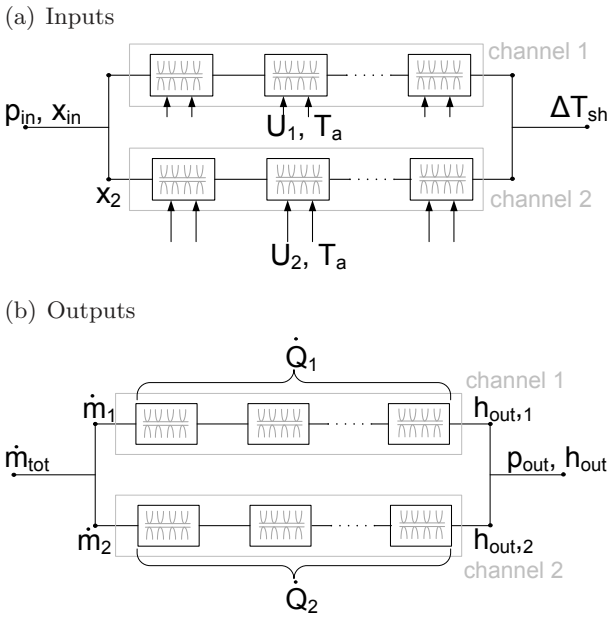

***Figure 2.5**: Schematic overview with (a) inputs and (b) outputs to the model.*

2.3 Modelling tools

In order to solve the model equations, the model is implemented using two different modelling tools. Both modelling tools are implemented in equation solvers, and both tools are designed for solving models of thermodynamic processes.

2.3.1 Engineering Equation Solver

Engineering Equation Solver (EES, 2007), is developed for numerically solving systems of algebraic equations, but it is also possible to solve differential equations. Using EES the model is written as mathematical equations

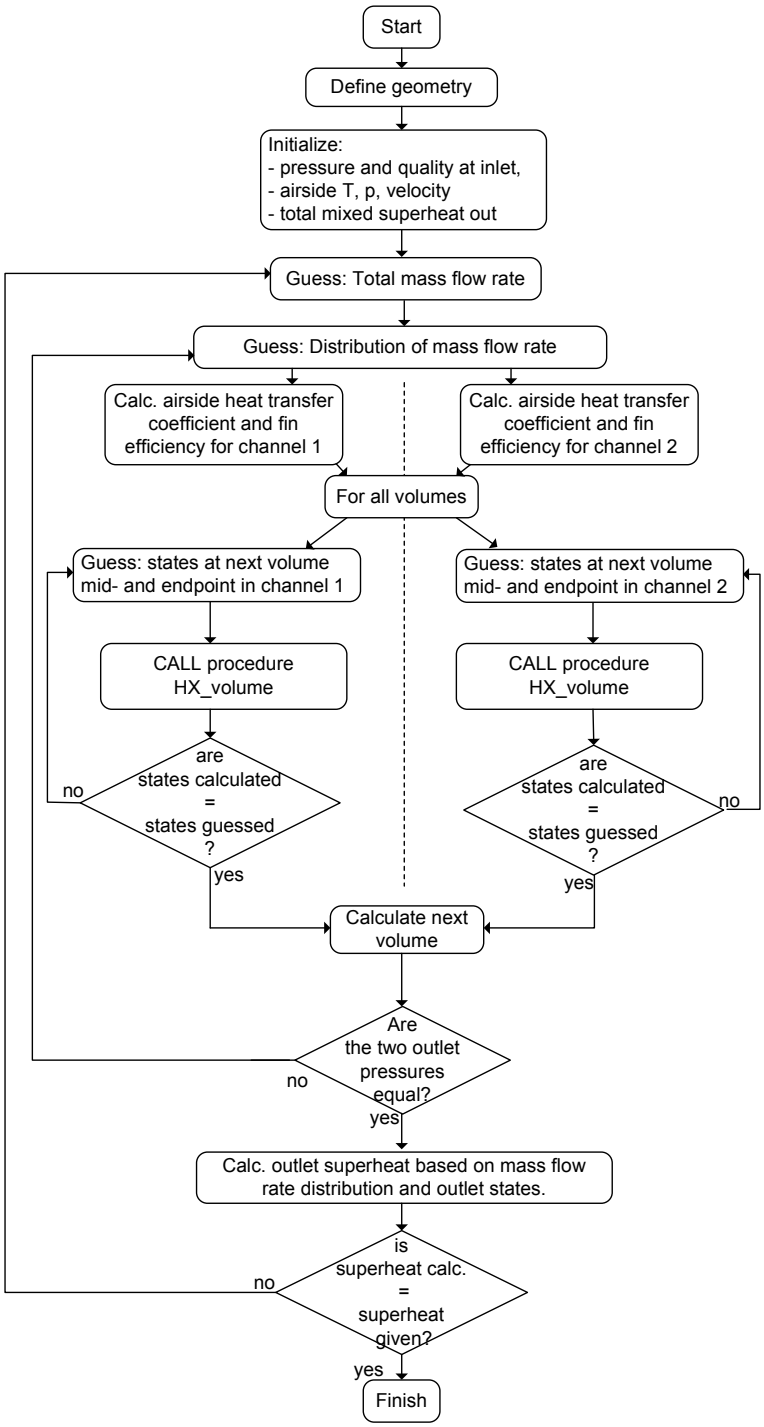

***Figure 2.6**: Flowchart of the model equations. The pressure drop and heat transfer calculations are performed inside the procedure HX_volume.*

in a very free form where the equations may be arranged in according to the user's preferences. Pascal-like functions and procedures may be implemented. For the numerical solution the equations are blocked, and each block is solved using a Newton-Raphson method. Convergence of the solution is reached as soon as the relative residuals are smaller than a specified value. Thermodynamic and thermophysical properties of a large number of fluids can be found using built in functions that call equations of state.

2.3.2 WinDali

WinDali (Skovrup, 2005) is a modelling and simulation software that solves systems of ordinary differential equations (ODE's) or algebraic equations (AE's). The software comprises of two parts, a model editor, which is an extended version of the Free Pascal Editor (Skovrup, 2005), and a simulation program that reads the compiled model and solves the equations. All static equations that are part of the iterations need to be formulated as residual equations. The algebraic equations are solved using a modified Newton iteration scheme. Otherwise, the software has the same main properties as EES, i.e. functions with thermodynamic properties are a built-in part, and it is possible to include procedures and functions.

2.4 The test evaporator

In order to investigate the influence of non-uniform airflow and inlet qualities on the evaporator performance, a test case is defined. For simplicity reasons the test case evaporator consists of only two minichannels in parallel. Although calculations are performed for only two minichannels, the results could represent an evaporator with many more parallel channels, where e.g. the velocity of the air is constant over each half but varying between the two halves. In that case the two channels represent a worst case scenario considering non-uniform distribution of the airflow. Considering non-uniform distribution of liquid and vapour in the inlet manifold the two channels can be representative for more channels to some extend. However, the distribution of liquid and vapour can vary significantly more if the evaporator has more than two channels, why in this case the investigation of two channels does not necessarily represent a worst case.

The channels are oriented vertically with the refrigerant flowing in the upwards direction. The parameters chosen for the test case evaporator are based on a real evaporator for a small air-conditioning system. The parameters describing the modelled evaporator geometry as well as the flow parameters for the test case are summarized in table 2.1. As seen from the

table two different refrigerants, R134a and CO_2 are applied. The real evaporator, on which the test case evaporator is based is working with R134a, and in practice a CO_2 evaporator would be designed differently. However, using CO_2 in the test evaporator provides interesting results, and in the numerical experiment the practical problems are not present.

Evaporator geometry	
Tube length	0.47 m
Number of ports in one tube	11
Cross section of one port	0.8 x 1.2 mm
Flow depth	16 mm
Gap between two microchannels	8 mm
Fin pitch	727 m^{-1}
Fin thickness	0.13 mm
Tube width	1.2 mm
Louvre length	6.0 mm
Louvre pitch	1.0 mm
Louvre angle	20 deg
Airflow parameters	
Air temperature	35 °C
Air velocity	1.6 m/s
Refrigerant parameters	
Refrigerants	CO_2, R134a
Evaporation temperature	7.4 °C
Quality at manifold inlet	0.3
Total superheat	6 K

***Table 2.1**: Parameters defining the test case.*

2.5 Model accuracy

2.5.1 Accuracy considering discretisation

In order to determine an adequate discretisation of the channel, solutions are found for a single minichannel of the test evaporator with different discretisations, using CO_2 as refrigerant. Three variables are chosen to calculate the errors connected to the discetisation: the cooling capacity of the channel, the mass flow rate and the pressure drop. Solutions are found using 12, 24, 47 and 94 volumes. Since we have no analytical solution for comparison, the solutions are compared to a numerical solution found using a even more fine-graded discretisation - using 188 control volumes. For each of the solutions the three variables mentioned above are compared to the

fine solution and the relative error is calculated as

$$\text{rel.error} = \frac{\dot{Q} - \dot{Q}_{\text{fine}}}{\dot{Q}_{\text{fine}}}, \tag{2.44}$$

for the cooling capacity, and likewise for the two other variables. Figure 2.7 shows the relative error of the three variables as a function of the number of volumes on a logarithmic scale. It is seen that the relative error decreases with decreasing volume size, which indicates that the solution converges. For all further calculations a discretisation of the channel into 47 volumes has been chosen, where the relative error due to discretization is in the order of 0.01%.

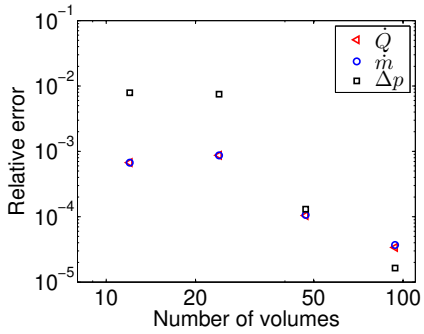

***Figure 2.7**: Relative error of the cooling capacity, the mass flow rate and the pressure drop as a function of the number of volumes for discretisation of one channel.*

2.5.2 Accuracy considering relative residuals

For both modelling tools a stop criterion for the Newton-Raphson iterations needs to be given. For both EES and WinDali this criterion is given by setting the maximum allowable relative residual. The accuracy of the solution increases with decreased residuals, but so does the solution time, therefore a suitable stop criterion has to be found.

Using the test evaporator and solving the model for one minichannel tube with CO_2 as refrigerant solutions are found for different stopping criteria. A relative error of the solution at a given stopping criterion is found by comparing the solutions to a more accurate solution:

$$\text{Error} = \max\left(\left|\frac{y - y_{\text{acc}}}{y_{\text{acc}}}\right|\right), \tag{2.45}$$

where y is a solution vector containing all static variables found by iteration, and y_{acc} is assumed to be the accurate solution. Since no analytical solution

is available, y_{acc} is a numerical solution with a very small relative residual requirement, $R = 10^{-8}$ is used for this solution.

In table 2.2 errors are summarized for the solution of the uniformly distributed case. For the Newton method quadratic convergence would be expected, such that for each iteration step, the number of correct digits is roughly doubled. This behavior is seen for the WinDali solutions. An extra iteration is performed when setting the maximum relative residual from 10^{-3} to 10^{-4}, while for the following solutions no extra iteration is needed to fulfill the residual requirement. Using EES the behavior is different, here the solution converges more slowly. A stop criterion of 10^{-4} is chosen for both modelling tools.

R	10^{-3}	10^{-4}	10^{-5}	10^{-6}
Error, EES	9.1e-3	2.7e-4	6.4e-5	6.8e-6
Error, WinDali	2.1e-3	3.9e-7	3.9e-7	3.9e-7

***Table 2.2**: Error for different stop criteria.*

2.6 Model verification

The minichannel evaporator model is verified against results obtained using the modelling software CoilDesigner (Jiang et al., 2006). This software is a state-of-the-art modelling tool used for commercial heat exchanger design. Since the software is not able to calculate refrigerant maldistribtution in parallel channels, only the single channel model is considered. Again the test case evaporator defined in section 2.1 is used.

In CoilDesigner a minichannel geometry is chosen and all geometry parameters are chosen to match the test case. For calculating the heat transfer and pressure drop correlations need to be selected. On the air side and for single-phase refrigerant, the same correlations are used for the CoilDesigner model and the present model. For the two-phase heat transfer coefficient the Bertsch et al. (2009) correlation is not available in CoilDesigner and neither is the Müller-Steinhagen and Heck (1986) correlation for the frictional pressure drop. Correlations presented by Jung and Radermacher (Jiang et al., 2006) for both the heat transfer coefficient and the frictional pressure drop are therefore applied in the CoilDesigner model.

The single channel model presented above is compared to the results given by the CoilDesigner software and shows good agreement. In table 2.3 some key parameters are summarized. The differences in the calculated cooling capacities and mass flow rates are around 5% for CO_2 and around 8% for R134a. Since different correlations were used to achieve the results, these differences are considered insignificant.

	CO_2		R134a	
	Model	CoilDesigner	Model	CoilDesigner
Heat transfer rate [W]	141.7	149.1	136.6	148.1
Mass flow rate [g/s]	0.90	0.95	0.98	1.06

Table 2.3: *Comparing key parameters calculated by the present model and the simulation software CoilDesigner.*

Figures 2.8 and 2.9 show the air outlet temperature and the refrigerant temperature, as well as the pressure and refrigerant side heat transfer coefficient along the channel. It is seen that the pressure development along the channel is more or less the same for this model and the CoilDesinger results. However, the refrigerant side heat transfer coefficient shows some deviations. The correlation applied in the present model, accounts for dryout by suppressing the nucleate boiling at high qualities. This is not the case in the CoilDesinger results, where the heat transfer coefficient stays high until single-phase gas is reached. The different development of the refrigerant side heat transfer coefficient is also responsible for the differences in the air outlet temperatures seen in figures 2.8(a) and 2.9(a), where the air outlet temperature starts to increase, even though the refrigerant is still in two-phase condition. We believe that the present model is more in accordance with reality as it accounts for dryout. We find that the model is verified.

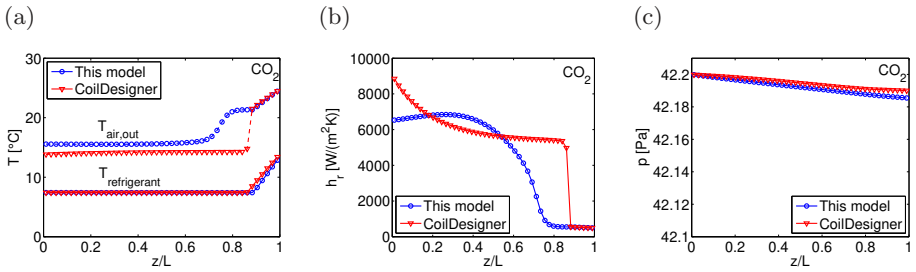

Figure 2.8: *Comparing modelling results with CO_2 as refrigerant to results obtained using the simulation software CoilDesigner.*

2.7 Comparison of the two modelling tools

The two modelling tools, EES and WinDali are compared by solving the model with both of the tools. The geometry of the evaporator used for this test is the same as the test evaporator presented in table 2.1. However, the total superheat out of the evaporator is set to 0 K (saturated vapour) when

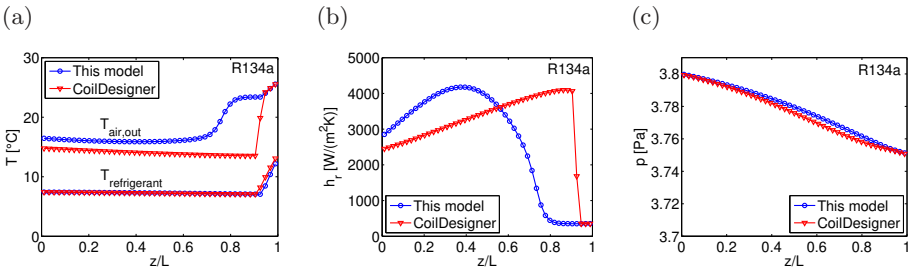

***Figure 2.9**: Comparing modelling results with R134a as refrigerant to results obtained using the simulation software CoilDesigner.*

using CO_2 as refrigerant. All other flow parameters are the same as for the test evaporator. Furthermore, different correlations are used to calculate the two-phase refrigerant heat transfer coefficient than the one stated in section 2.1. With R134a as refrigerant a correlation presented by Zhang et al. (2004) was used, while when using CO_2 as refrigerant a correlation presented by Choi et al. (2007) was used. However, this does not have any influence on the results comparing the two modelling tools. Besides here, the two tools have been compared in Brix and Elmegaard (2009).

Figure 2.10 shows the local heat flux and the pressure along a single minichannel for R134a and CO_2. It is seen, that the solutions using EES and WinDali do not totally coincide for neither of the refrigerants. These discrepancies occur because of differences in the thermophysical property functions. However, the solutions are considered sufficiently identical to compare the two tools.

When solving the parallel channel case, the most significant difference between the two modelling tools is the solution time. Applying a non-uniform airflow distribution different solutions for two minichannels in parallel are found, and figure 2.11 shows the time used for solutions. All calculations were performed on the same personal computer, an Intel(R) Core(TM) 2 CPU, U7600@1.2 GHz and 2 GB of RAM. It was furthermore tested that the solution times were repeatable. At $f_U = 1$ the airflow is uniformly distributed and the solution to this case is used as initial guess for all other solutions. For the equal distribution case WinDali solves the model 25 times faster than EES for R134a and 40 times faster for CO_2. Changing the airflow distribution with increasing steps results in longer solution times. For all other airflow distributions than uniform, WinDali solves the equations more than 100 times faster than EES, in the order of 1-2 minutes, where EES needs 2-3 hours.

When running the model both tools showed difficulties when performing large parameter variations without adjusting the initial guesses, and no dif-

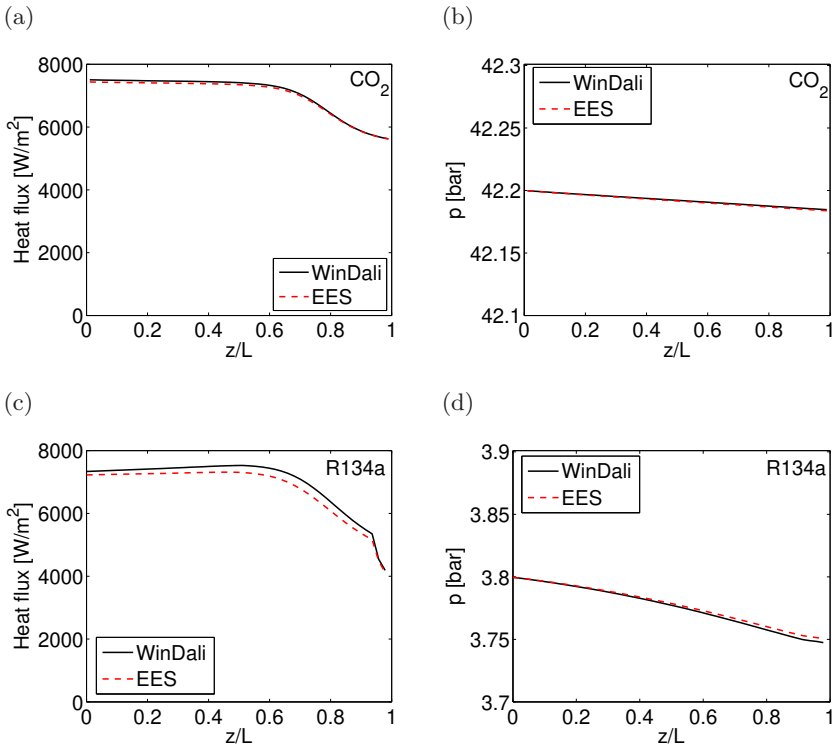

***Figure 2.10**: Comparison of the local heat flux and pressure in the channel using EES and WinDali as modelling tool.*

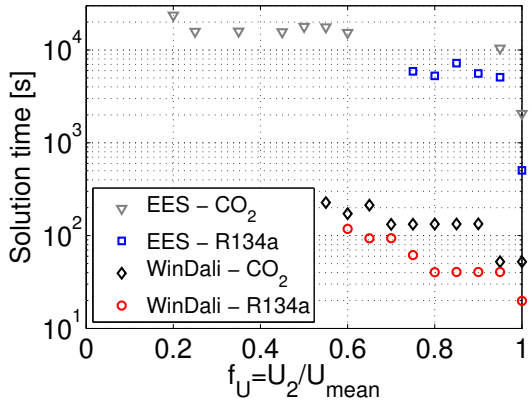

***Figure 2.11**: Time used to reach the solution when the solution of the uniform distribution case ($f_U = 1$) is used as guess values.*

ference between the two tools was found in this regard. Generally, WinDali thus has some considerable advantages to EES, since it is much faster. However, on the implementation side EES has advantages. Implementation of small models in EES is extremely easy and fast and it is also straightforward to build up a larger model gradually, extending the model bit by bit. Using WinDali the model structure is more locked.

When implementing the evaporator model discussed above, EES was used for prototyping. For this purpose EES is an excellent tool. The final model was then transferred to WinDali.

2.8 Summary

In this chapter a description of the evaporator model is given. The main assumptions are:

- The system is in steady state.
- The refrigerant flow is one-dimensional.
- The refrigerant flow is homogeneous and vapour and liquid are in thermodynamic equilibrium.
- Heat conduction in the flow direction and between different tubes is negligible.
- The air is dry.
- The manifolds are adiabatic and there is no pressure drop in the manifolds.

Firstly, the model of a single minichannel is considered. The governing equations are solved using the finite volume method. For calculation of the frictional pressure drop and the local heat transfer coefficients empirical correlations are applied and an overview of the chosen correlations is shown in table 2.4. In order to connect several single channels in parallel, continuity and energy conservation equations are solved on the manifolds.

The final model is tested concerning accuracy in order to determine an adequate discretisation and stopping criterion for the iterations. Furthermore the model is verified against results obtained using the simulation software CoilDesigner. At last two different modelling tools for solving the model are compared.

Air side	
Heat transfer coefficient	Kim and Bullard (2002)
Two-phase region	
Heat transfer coefficient	Bertsch et al. (2009)
Frictional pressure drop	Müller-Steinhagen and Heck (1986)
single-phase region	
Heat transfer coefficient	Gnielinski (1976)
Frictional pressure drop	Blasius (Fox and McDonald, 1998)

***Table 2.4**: Summary of correlations used to calculate heat transfer coefficients and pressure drop.*

Chapter 3

Distribution studies for two channels in parallel

This chapter presents the main results found by modelling two channels in parallel. First, the impact of the distribution of liquid and vapour in the inlet manifold on the refrigerant distribution and cooling capacity is considered. Second, airflow non-uniformity is addressed, and at last a combination of non-uniform airflow and non-uniform distribution of liquid and vapour is considered. Parts of the results are also discussed in Brix et al. (2009), Brix and Elmegaard (2008) and Brix et al. (2010).

3.1 Distribution of liquid and vapour in the inlet manifold

When entering the evaporator the mixture of liquid and vapour coming from the expansion valve has to be distributed into the parallel minichannels of the evaporator. A uniform distribution of especially the liquid is preferable, since the heat exchanger area is not utilized ideally if some channels receive only vapour. However, the distribution of liquid and vapour depends on the geometry and the flow conditions in the manifold, and very often a uniform distribution of the liquid cannot be achieved. For this reason it is interesting to study how strongly a non-uniform distribution of the liquid and vapour in the manifold affects the performance of the evaporator. In figure 3.1 a sketch of the two channels is shown.

As mentioned in the description of the model, the manifold is not modelled in detail, and the distribution of liquid and vapour is thus simply given as an input. In order to quantify the degree of maldistribution a distribution

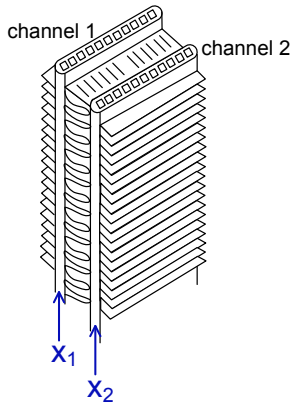

***Figure 3.1**: Sketch of the two channels.*

parameter, f_x, is defined as

$$f_x = \frac{x_2}{x_{\mathrm{mf}}}, \quad 0 \leq f_x \leq 1. \tag{3.1}$$

Here x_2 is the quality into channel 2. For increased maldistribution the quality into channel 2 is decreased, while the manifold inlet quality, x_{mf}, is kept constant. For uniform distribution of the inlet quality $f_x = 1$, while for $f_x = 0$ only liquid is fed into channel 2 and the remaining mixture of liquid and vapour enters channel 1.

In figure 3.2 the local UA-values and the local heat flux along the channels is shown for CO_2 and R134a. The local UA-values depend on the air- and refrigerant side areas and are calculated for each control volume. For each of the three distributions of liquid and vapour imposed, $f_x = 1$, $f_x = 0.5$ and $f_x = 0$, three curves are shown. Two curves show the local UA-values or heat flux in each channel. The third, which is provided with markers, shows the mean local value. The solid line with circular markers shows UA-values or heat flux for a uniform distribution of liquid and vapour. In this case there is no maldistribution and the three lines coincide.

As long as the refrigerant flow in the channels is not approaching dryout, the local UA-values and the heat flux are relatively constant. When approaching fully evaporated flow, the refrigerant side heat transfer coefficient begins to decrease until it reaches the single-phase heat transfer coefficient. This results in a decrease of the overall heat transfer coefficient. Meanwhile, the temperature difference between the refrigerant and the air decreases as the refrigerant is superheated, which results in the continued decrease of the heat flux in the superheated zone that is seen in figures 3.2(b) and 3.2(d). Additional graphs showing the refrigerant temperature, enthalpy, pressure and heat transfer coefficients are shown in appendix A.2.

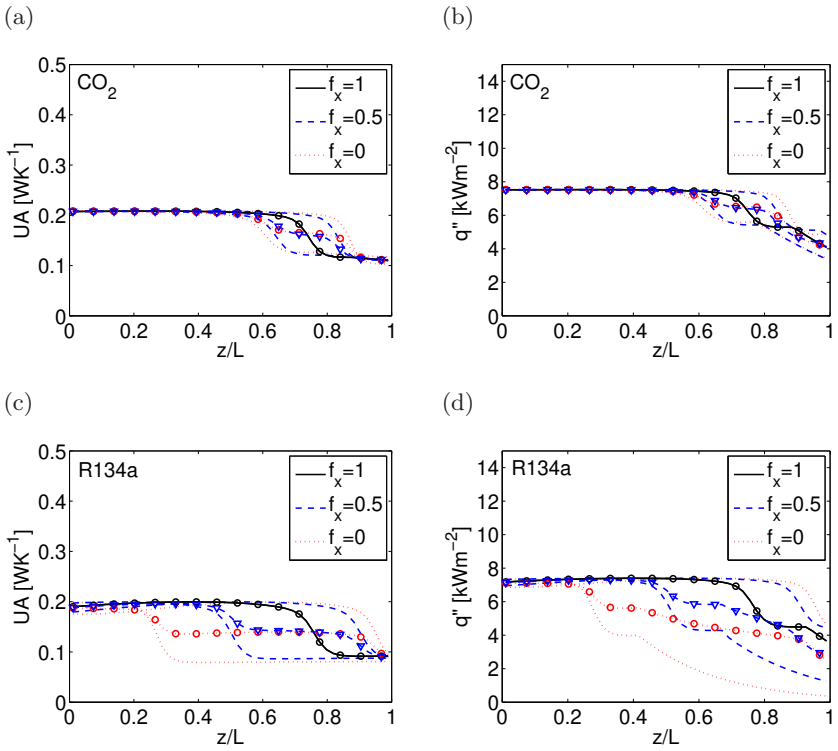

***Figure 3.2**: Local UA-values and local heat flux in the channels for (a+b) CO_2 and (c+d) R134a for different inlet quality distributions. The curves without markers show the local values in each channel, while the curves provided with markers show a local mean of the two channels.*

Imposing non-uniform distribution of liquid and vapour corresponding to a value of $f_x = 0.5$ or $f_x = 0$, does not change the heat flux significantly as long as the refrigerant is in a two-phase condition. However, the refrigerant flow in channel 1, which has a higher quality at the inlet, will reach dryout earlier than in the uniform distributed case, while the refrigerant in channel 2 stays in two-phase condition further down the channel.

A comparison of the graphs for CO_2 and R134a shows some significant differences. For CO_2 the total area of the evaporator containing two-phase flow is more or less constant when imposing a non-uniform liquid and vapour distribution. For R134a the refrigerant in channel 1, receiving less liquid, evaporates very fast such that the area with two-phase flow decreases for increased maldistribution of liquid and vapour. Consequently, the mean heat flux is lower for increased maldistribution of the liquid and vapour when using R134a and a capacity reduction is expected.

Another difference between the two refrigerants is the difference between

the two-phase and the single-phase refrigerant side heat transfer coefficient. This difference is smaller for CO_2, which results in a smaller difference in UA-values between two-phase and single-phase.

The different behaviour of CO_2 and R134a seen in figure 3.2 can be explained by a different distribution of the mass flow rate into the two channels when imposing a non-uniform distribution of the liquid and vapour. Figure 3.3 shows the mass flow rate in each of the channels as well as the total mass flow rate as a function of f_x for the two refrigerants.

For CO_2 the mass flow rate in channel 1 increases and the mass flow rate in channel 2 decreases for increased maldistribution of the liquid and vapour, while the total mass flow rate stays more or less constant. For R134a the total mass flow rate decreases in order to keep the superheat out of the evaporator at the specified value. The distribution of the mass flow rate is such that channel 2 actually receives slightly more refrigerant than channel 1.

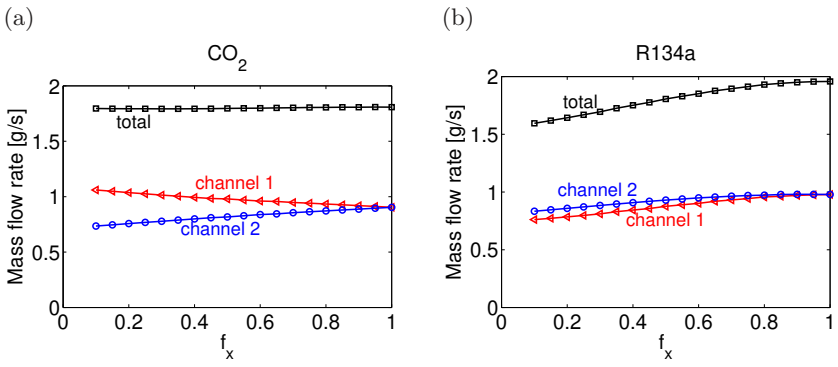

***Figure 3.3**: Distribution of the mass flow rate into the two channels as a function of the liquid and vapour distribution.*

Now the question arises, how comes that the distribution of the mass flow rate is so different for the two refrigerants? The answer lies in the different development of the pressure gradient and hence pressure drop. Figure 3.4 shows the three contributions to the pressure gradient as well as the total pressure gradient along a single channel for CO_2 and R134a. Using R134a the frictional contribution to the pressure gradient is clearly the most dominant. For CO_2, which has a higher density and lower viscosity, the frictional contribution is much lower, while the gravitational contribution is considerably higher than for R134a, especially in the part of the channel where most of the refrigerant is in liquid condition.

In figure 3.5 the solid lines show the pressure drop in a single minichannel as a function of the inlet quality for different mass flow rates. Furthermore triangular and circular markers show the pressure drop that is calculated for

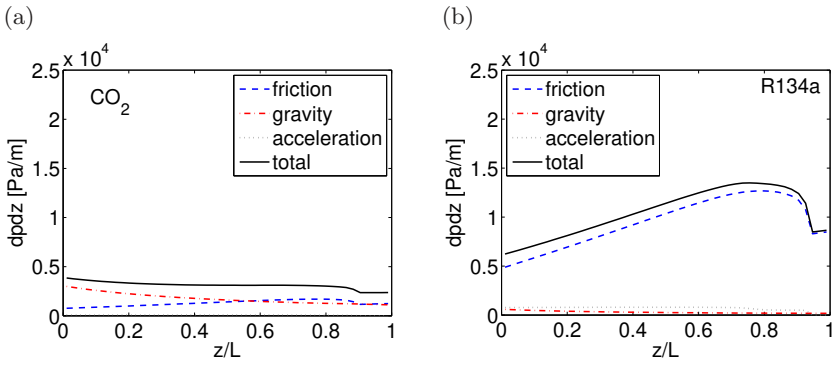

***Figure 3.4**: Pressure gradient contributions along a single channel.*

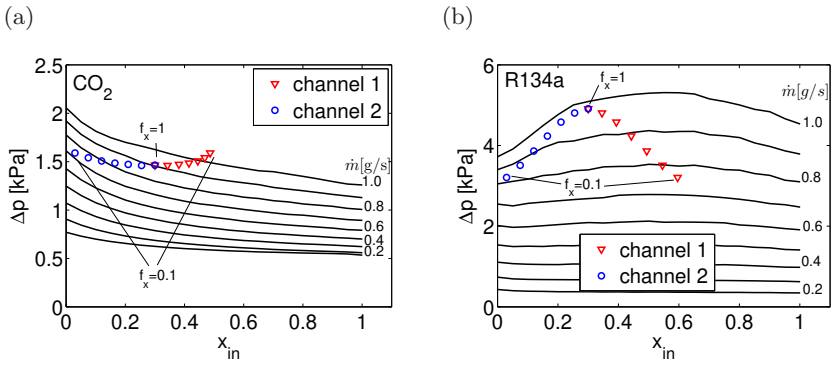

***Figure 3.5**: Pressure drop in a single minichannel as a function of the inlet quality for different mass flow rates. The triangular and circular markers show the pressure drop that is calculated for different distributions of the liquid and vapour in channel 1 and 2 respectively.*

different liquid distributions in channel 1 and 2, respectively. The markers set at $x_{\text{in}} = 0.3$ coincide and show the case for uniform distribution of the liquid and vapour. Moving away from this point shows the pressure drop for decreasing f_x. The solid lines show that for CO_2 the pressure drop in a single channel increases when decreasing the inlet quality. This is due to the large gravitational pressure gradient at low qualities. For R134a the pressure drop is more or less constant for low mass flow rates, while at larger mass flow rates the pressure drop increases as the inlet quality is increased, until at some point such a large part of the channel is containing single-phase gas that pressure drop decreases again.

Considering the parallel channels, figure 3.5 shows that for CO_2 the pressure drop increases with increased maldistribution of liquid and vapour, while it decreases for R134a. Furthermore, it shows that for CO_2 the mass flow

rate will increase in channel 1 and decrease in channel 2, as it was seen in figure 3.3(a). Considering R134a, it is seen that the mass flow rate has to decrease in both channels and more in channel 1 than in channel 2 when the pressure drop decreases.

Looking at the solid lines in figure 3.5, it is seen that for a given inlet quality, only one mass flow rate corresponds to one value of the pressure drop. It thus seems that the Ledinegg instability would not cause problems in this case. Traditionally the Ledinegg instability is investigated by considering the pressure drop as a function of the mass flux. Graphs, showing in the traditional way that the Ledinegg instability is not a problem for the present case, are shown in appendix A.3.

Figure 3.6 shows the cooling capacity of each of the parallel channels and the total cooling capacity as a function of the liquid and vapour distribution. As expected, the cooling capacity of the evaporator using CO_2 does not change significantly when imposing a non-uniform distribution of the liquid and vapour. Using R134a the cooling capacity of the channel receiving mostly gas decreases significantly, while the extra liquid in channel 2 only increases the cooling capacity of this channel moderately, such that the total cooling capacity decreases considerably.

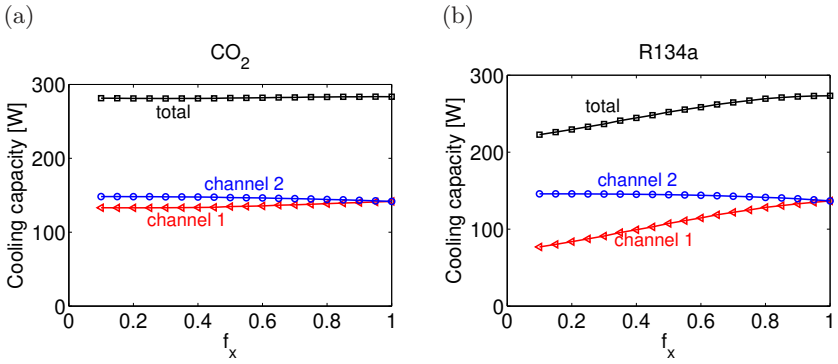

***Figure 3.6**: Cooling capacity as a function of the liquid and vapour distribution.*

The superheat out of the individual channels is shown in figure 3.7, where it is seen that for R134a, the refrigerant in channel 2 is not fully evaporated for $f_x < 0.8$, while the superheat out of channel 1 is quickly increasing, approaching the air temperature. The superheat from this channel is then used to evaporate the leftover liquid from channel 2. Using CO_2 the superheat changes only moderately, and the refrigerant is always fully evaporated at the outlet of the channels.

Figure 3.8 compares the reduction of the mass flow rate, the cooling capacity and the area of the evaporator that is in contact with two-phase flow (the

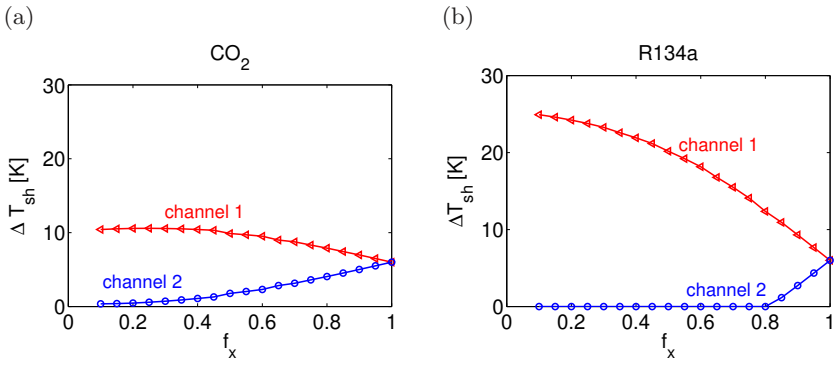

***Figure 3.7**: Superheat out of the individual channels as a function of the liquid and vapour distribution.*

two-phase area) as a function of the liquid and vapour distribution. For both refrigerants the curves showing the cooling capacity and the mass flow rate coincide. It is furthermore noticed that the capacity decreases more or less the same rate as the two-phase area. For R134a the two-phase area is reduced by 22% at $f_x = 0.1$, while the cooling capacity is reduced by 19%. The cooling capacity is hence reduced a little less than the two-phase area.

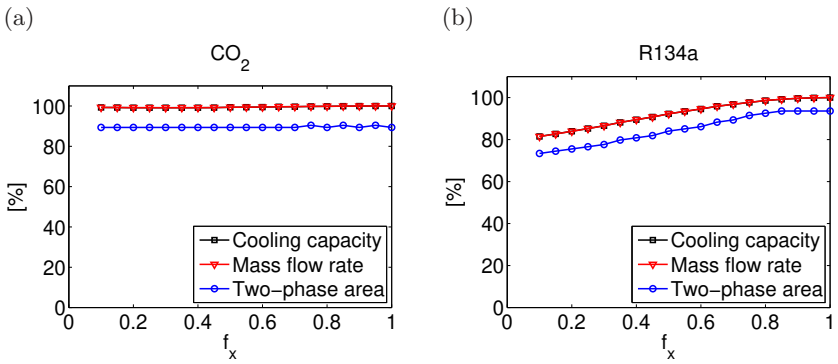

***Figure 3.8**: Comparison of the reduction in cooling capacity, mass flow rate and two-phase area as a function of the liquid and vapour distribution. The curves for cooling capacity and mass flow rate coincide.*

To conclude on these investigations of the impact of liquid and vapour distribution on the refrigerant mass flow rate distribution and on the capacity of the evaporator, we have seen that using the conventional refrigerant R134a the capacity of the evaporator decreases by up to around 20% due to non-uniform distribution of the liquid and vapour in the inlet manifold. This

decrease of the cooling capacity is close to, but a little smaller than the reduction of the two-phase area, and it is therefore believed that the decrease in capacity is primarily a direct result of the decrease of the two-phase area. Using the natural refrigerant CO_2 the two-phase area does not decrease with increased maldistribution of the liquid and vapour and neither does the capacity of the evaporator.

3.2 Non-uniform airflow

Apart from the liquid distribution, also the distribution of the air velocity on the outside of the channels influences the refrigerant distribution in the parallel channels. Keeping the airflow rate constant and varying the velocities over the different channels, changes the heat load on the channels, which results in different pressure gradients inside the channel, and hence influences the mass flow rate distribution and the capacity. A sketch of the two channels is shown in figure 3.9.

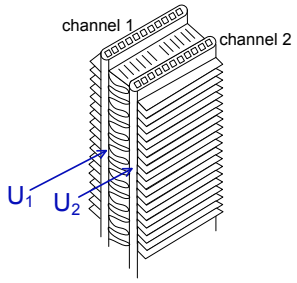

***Figure 3.9**: Sketch of the two channels.*

When investigating the impact of the airflow distribution on the cooling capacity of the evaporator, the airflow is imposed such that each channel receives a uniform air velocity. The total airflow rate is kept constant, while the velocity on each channel is varied. The velocities are varied such that the velocity increases for channel 1 and decreases for channel 2. A non-dimensional parameter, f_U, which quantifies the degree of non-uniformity of the airflow, is defined as:

$$f_U = \frac{U_2}{U_{\text{mean}}},\ 0 \leq f_U \leq 1, \tag{3.2}$$

where $f_U = 1$ for equal air velocities on both channels, while for $f_U = 0$ there is no airflow at channel 2, and all air flows by channel 1. While performing the investigations on the impact of the airflow distribution, the distribution of liquid and vapour is considered to be uniform.

In figure 3.10 local UA-values and the local heat flux are shown along the channel direction for three different airflow distributions.

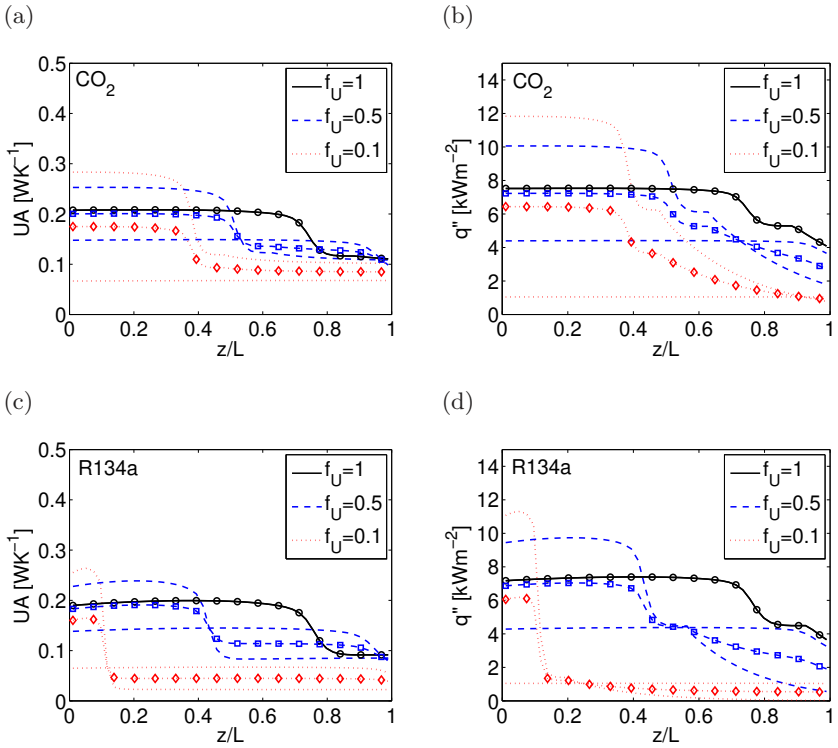

***Figure 3.10**: Local UA-values and local heat flux in the channel for (a+b) CO_2 and (c+d) R134a for different airflow distributions. The curves without markers show the local values in each channel, while the curves with markers show a local mean of the two channels.*

For each of the three airflow distributions imposed, $f_U = 1$, $f_U = 0.5$ and $f_U = 0.1$, three curves are shown for each graph in figure 3.10. Two curves show the local values in each channel and the third, which is provided with markers shows the mean local values. The solid curve with circular markers shows local values in the minichannels for a uniform airflow. In this case there is no maldistribution and the three curves coincide.

For $f_U = 0.5$ channel 1 is exposed to a higher air velocity than channel 2. In channel 1 the air side heat transfer coefficient will be higher than for the uniform airflow case, which results in a higher local UA-value and hence a higher heat flux. However, in this channel the refrigerant is fully evaporated much earlier than in the uniform airflow case. In the part of the channel containing single-phase gas, the local UA-values are considerably lower. Regarding the heat flux, the temperature difference between the

air and refrigerant decreases in this part of the channel, which results in a decreasing heat flux. Channel 2, which receives the low air velocity has lower UA-values than in the uniform airflow case, due to the lower air side heat transfer coefficient. In this channel dryout is not reached before the very end of the channel, and the UA-values and the heat flux are thus relatively constant throughout this channel. Additional graphs showing the refrigerant temperature, enthalpy, pressure and heat transfer coefficients in the channel are shown in appendix A.2.

From the dashed curve with square markers, showing the mean heat flux of the two channels at $f_U = 0.5$, it is noted that as long as there is two-phase flow in both channels the mean heat flux is only slightly lower than for the uniform airflow case. However, for the part of the channel, where dryout has been reached in channel 1 the mean heat flux is considerably lower. For $f_U = 0.1$, the same behaviour is seen as for $f_U = 0.5$, but it is even more pronounced. In this case the mean heat flux is lower than in the uniform airflow case also when there is two-phase refrigerant flow in both channels. This indicates that as long as all channels contain two-phase refrigerant only a severe non-uniformity of the airflow will impact the cooling capacity of the evaporator.

This result is in good agreement with the results presented in Brix et al. (2007), where the effect of airflow maldistribution on the cooling capacity and COP of a refrigeration system with a liquid overfeed minichannel evaporator was investigated. In the model used for the study, the refrigerant side contributions to the UA-values were neglected, and it was found that for small degrees of maldistribution, corresponding to $f_U > 0.5$, the reductions of the cooling capacity were below 5%, while for $f_U = 0$ the cooling capacity was reduced by around 20%.

Figure 3.11 shows the distribution of the mass flow rate in each of the two channels as well as the total mass flow rate as a function of airflow distribution. For both refrigerants the total mass flow rate decreases with increasing airflow non-uniformity. For R134a, the mass flow rate is more or less the same into both of the channels. Why this is the case can easily be seen from figure 3.12(b). The figure shows the pressure drop in a single minichannel as a function of the air velocity for different mass flow rates. The triangular and circular markers show the pressure drop that is calculated for different airflow distributions in channel 1 and 2, respectively. It is seen that above a certain air velocity, depending on the mass flow rate in the channel, the pressure drop in the channel is independent of the air velocity on the outside. For a given pressure drop in the channel, the mass flow rate will thus be the same, regardless the air velocity on the outside.

For CO_2 on the other hand, the pressure drop in a single channel does depend on the air velocity on the outside, as seen in figure 3.12(a). Using

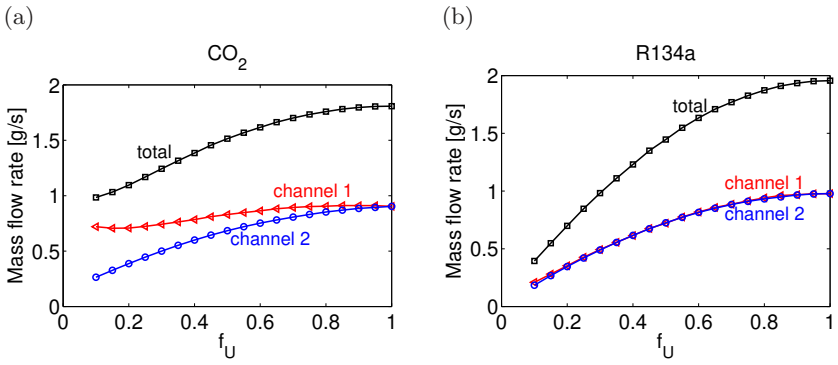

***Figure 3.11**: Distribution of the refrigerant mass flow rate as a function of the airflow distribution.*

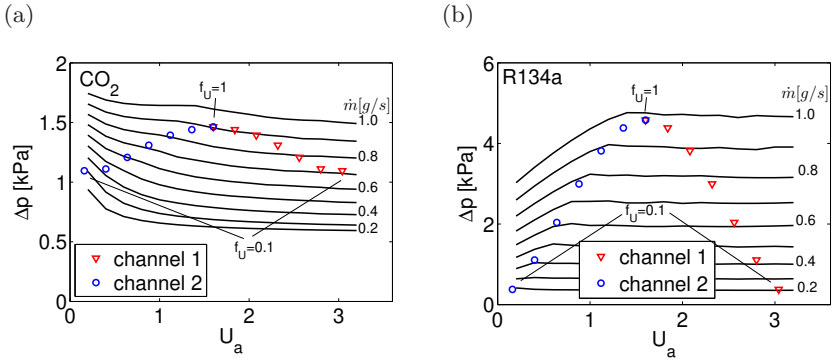

***Figure 3.12**: Pressure drop in a single minichannel as a function of the air velocity for different mass flow rates. The triangular and circular markers show the pressure drop that is calculated for different airflow distributions in channel 1 and channel 2, respectively.*

this refrigerant the mass flow rate decreases only slightly in channel 1 and much more in channel 2. Looking at the impact of the airflow distribution on the cooling capacity for CO_2, shown in figure 3.13(a), it is seen that the cooling capacity of channel 1 is slightly increasing for f_U decreasing to 0.65 and decreasing slightly for lower values of f_U, although the airside heat transfer coefficient increases in this channel for increasing maldistribution. Nevertheless, the decreasing mass flow rate and the increasing single-phase zone prevents the cooling capacity to increase. In channel 2 the cooling capacity decreases steadily as the air velocity on this channel is decreased.

Using R134a as refrigerant the cooling capacity of channel 1 is slightly increasing for f_U decreasing to 0.8 and decreasing for lower values of f_U, due to the reduced mass flow rate. In channel 2 the cooling capacity decreases as

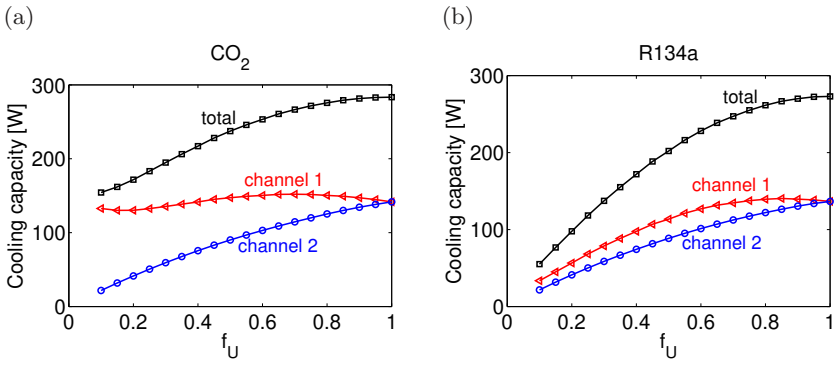

Figure 3.13: *Cooling capacity of the individual channels and the total cooling capacity of the evaporator as a function of the airflow distribution.*

for CO_2. For small degrees of non-uniformity of the airflow, the total cooling capacity is not affected much. However, for larger degrees of maldistributed airflow, the cooling capacity of the evaporator decreases significantly. It is furthermore worth noting, that in the extreme case ($f_U = 0.1$), the capacity of the evaporator with R134a is reduced more than twice as much as the evaporator with CO_2 compared to the case with uniform airflow.

Looking at the superheat out of the individual channels, shown in figure 3.14, it is seen that the refrigerant out of channel 2 is not fully evaporated if $f_U < 0.85$ for R134a and if $f_U < 0.75$ for CO_2. At the outlet of channel 1 the refrigerant temperature is stabilized a little below air temperature when using CO_2, while it approaches the air temperature for R134a for increased non-uniformity of the airflow.

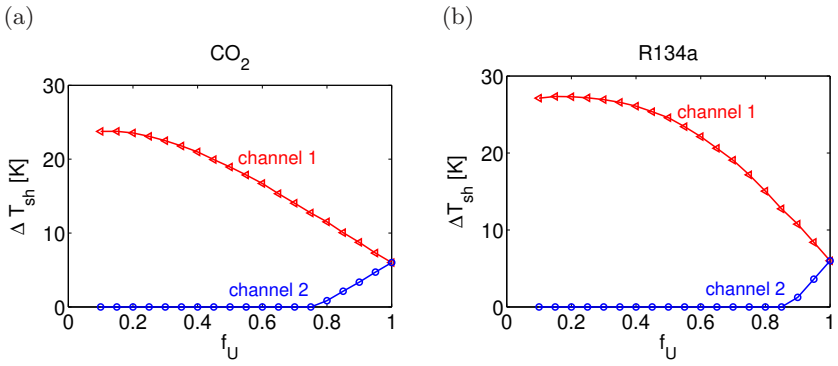

Figure 3.14: *The superheat out of the individual channels as a function of the airflow distribution.*

Figure 3.15 compares the reduction of the cooling capacity, the total mass

flow rate and the area of the evaporator containing two phase flow. The curves showing the cooling capacity and the mass flow rate coincide, and these actually decrease faster than the two-phase area.

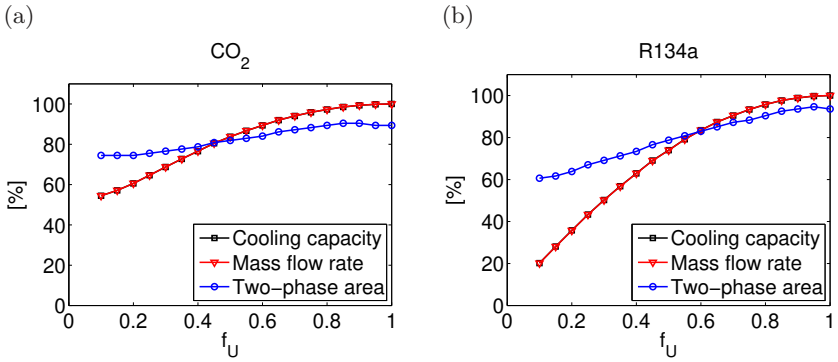

***Figure 3.15**: Comparison of the reductions in mass flow rate, cooling capacity and the area of the evaporator containing two-phase flow.*

Although the two distribution parameters f_U and f_x cannot be compared directly, it is interesting to compare the findings of the liquid and vapour distribution and the distribution of the airflow. First of all, the capacity was affected much more by the airflow distribution than by the distribution of liquid and vapour in the extreme cases. Furthermore, it was found that where the capacity decreased at the same rate as the two-phase area for varying liquid and vapour distribution, the capacity decreased more than twice as much as the two-phase area for varying airflow distribution.

3.3 Combining non-uniform distributions of liquid and vapour and airflow

One thing is to vary the distribution of the liquid and vapour and the airflow distribution only separately, but in a real system most likely both of the considered sources of maldistribution will be present at the same time. Therefore, an investigation of combined non-uniform distribution of the liquid in the manifold and the airflow airflow is performed.

For this purpose the airflow distribution parameter, f_U, is varied between 0 and 2, such that both of the channels are exposed to both increased and decreased air velocities. Figure 3.16(a) and figure 3.17(a) show the relative total cooling capacity as a function of the airflow distribution for different distributions of the liquid and vapour, for R134a and CO_2, respectively. The capacity is set to 100% for uniform distribution of both the airflow and

the liquid and vapour in the manifold. Furthermore the superheat out of the individual channels is shown in figures 3.16(b) and 3.17(b).

Considering the evaporator using R134a, it clearly seen that for a given distribution of liquid and vapour an optimum airflow distribution exists and vice versa. Having uniform airflow the optimum liquid and vapour distribution is also uniform. However, for a non-uniform airflow distribution an optimum capacity can be obtained at a certain, non-uniform distribution of the liquid and vapour. As it could be expected it is desirable to have a larger fraction of the liquid going into the channel, that is exposed to a higher air velocity. The optimum cooling capacity is slightly decreasing with increasing airflow non-uniformity, which means that most, but not all of the capacity can be recovered by distributing the liquid and vapour suitably.

Comparing graphs (a) and (b) in figure 3.16 it is seen that the optimum cooling capacity is attained in the region where the refrigerant is fully evaporated out of both channels, but where the superheat out of channel 2 is lower than in channel 1. In practice it would probably be difficult to control the system to reach the exact optimum. It could, however, be possible to control the distribution of liquid such that the superheat out of the channels is equal. At this point the capacity is still very close to the optimum, since the curve is very flat in the region around the optimum.

Considering CO_2 as refrigerant, for which the distribution of liquid and vapour has only minor influence on the capacity, the graphs look slightly different, shown in figure 3.17. Also in this case an optimum cooling capacity can be reached by a suitable distribution of liquid and vapour. However, the optimum is not far from the curve having uniform liquid and vapour distribution. For CO_2 the largest airflow maldistribution that can be compensated to the optimum by controlling the distribution of liquid and vapour is $f_U = 1.1$. At this point only liquid enters channel 2. For larger degrees of airflow non-uniformity, the capacity decreases regardless the distribution of liquid and vapour. For R134 this point of a maximum airflow distribution that can be compensated to the optimum capacity by controlling the distribution of liquid and vapour is found at a considerably higher degree of airflow non-uniformity up to $f_U = 1.55$.

Concluding on this, we see that in general the capacity reductions due to airflow non-uniformity are smaller for CO_2 than for R134a. However, for R134a most of the capacity reduction can be recovered by suitably distributing the liquid and vapour in the inlet manifold. Controlling the individual superheat to be equal, a distribution close to the optimum is attained. For small degrees of non-uniform airflow capacity recovery is also possible for CO_2, while it is not possible to compensate for larger degrees of airflow non-uniformity.

(a)

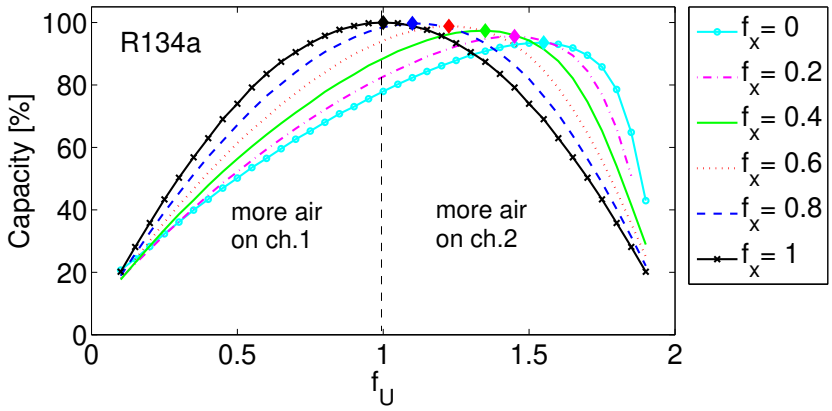

(b)

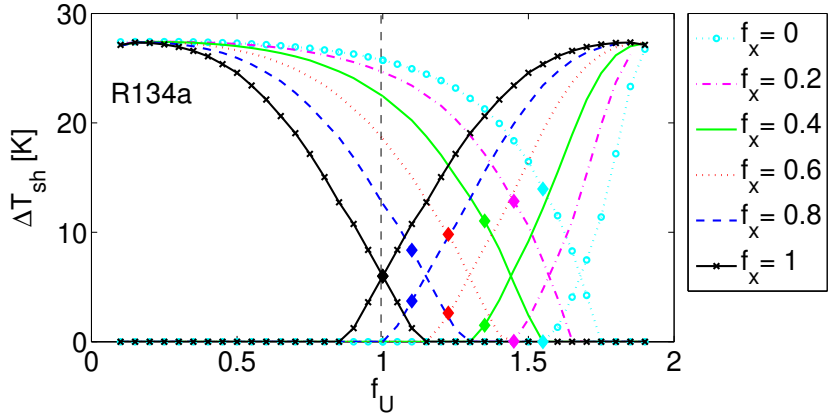

Figure 3.16: *(a) The cooling capacity for simultaneous variation of the airflow and liquid distribution using R134a as refrigerant. At uniform distribution of both liquid and vapour and airflow the capacity is 100%. (b) The superheat out of the individual evaporator channels.*

(a)

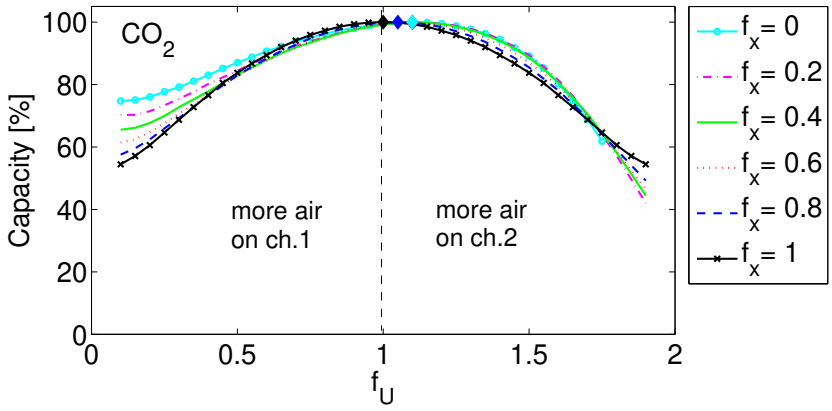

(b)

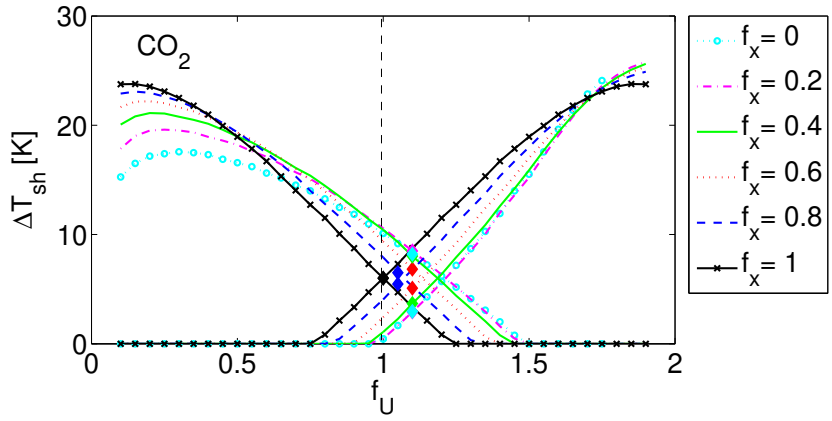

***Figure 3.17**: (a) The cooling capacity for simultaneous variation of the airflow distribution and distribution of liquid and vapour using CO_2 as refrigerant. At uniform distribution of both the liquid and vapour and the airflow the capacity is 100%. (b) The superheat out of the individual evaporator channels.*

As an example, having an airflow distribution corresponding to $f_U = 1.6$, using R134a as refrigerant the cooling capacity is only 63% of the uniform airflow capacity if the liquid and vapour phases are distributed uniformly. By imposing the optimal liquid and vapour distribution the capacity can be recovered to 92% of the uniform distribution capacity. Using CO_2 the maximum capacity that can be reached is 80% of the uniform distribution capacity.

3.4 Verification of results

The most appropriate way to validate the results would be to compare the simulation results to experimental results performed using a heat exchanger corresponding to the test case evaporator. However, directly applicable test results have not been possible to find in the literature. The results are therefore compared to results obtained in similar studies.

Vist (2003) studied two-phase flow distribution in heat exchanger manifolds experimentally. The manifolds studied were a typical manifolds used for minichannel heat exchangers. However, ten water cooled, 'single port' tubes having a diameter of 4mm were connected to the manifold. Two different refrigerants, R134a and CO_2 were studied. In order to investigate the impact of different distribution patterns on the performance of the evaporator a simulation model was used. Both uniform and totally separated distributions of the liquid and vapour were considered.

Contrary to the results presented in the present study, the mass flow rate of refrigerant was kept constant in the simulations, while the evaporator superheat varied for the different distributions of liquid and vapour. Comparing the two refrigerants, it was shown that the the capacity reductions were in general around twice as large for R134a as for CO_2. For R134a the largest capacity reductions were 35% and 18% for CO_2.

Although the test conditions were not quite the same, these results correspond to the results presented in this study in that the evaporator using R134a is more affected by maldistribution of the liquid and vapour than an evaporator using CO_2.

Vestergaard (2009) presented results of a study of the impact of the liquid and vapour distribution on the evaporator performance for a minichannel heat exchanger. A transparent header permitted to study the distribution of liquid and vapour in the manifold. The minichannels were oriented vertically with upwards flow direction and R134a was used as refrigerant. The airflow on the outside of the evaporator was uniform. In an initial case the liquid and vapour phases were strongly maldistributed and the performance of the evaporator was 78% of the theoretical capacity. In the present study, a

capacity of 80% was predicted by the model if severe maldistribution of the liquid and vapour phases is considered.

Payne and Domanski (2003) showed that by controlling the individual superheat of each circuit in a three circuit finned tube evaporator, capacity reductions due to a non-uniform airflow could be recovered within 2%. The benefit of controlling the individual superheat increased with increasing maldistribution of the airflow.

Kim et al. (2009a) studied the impact of the distribution of liquid and vapour and the distribution of the airflow on the evaporator of a 10.55 kW residential R410a heat pump. The evaporator was a five circuit finned tube evaporator, where the circuits were equal three and two. The study was performed by numerical modelling of the heat pump. Contrary to the present study, where the saturation temperature at the evaporator inlet is held constant, the saturation pressure in the evaporator varied with the maldistribution. Considering the distribution of liquid and vapour, the cooling capacity was reduced to 90%, when increasing the void fraction into three of the circuits by 5%. This increase in void fraction corresponds to $f_x = 0.53$. In the present study the capacity is reduced to 93% when $f_x = 0.53$ and R134a is used as refrigerant. Considering a non-uniform airflow with an airflow distribution corresponding to $f_U = 0.57$ the capacity of the evaporator studied by Kim et al. (2009a) was 85% of the uniform airflow capacity. For R134a our results show a capacity of 82% of the uniform airflow capacity at this airflow distribtion. The study of Kim et al. (2009a) furthermore shows, that no big differences were found if refrigerants R134a or R22 are used in stead of R410a.

3.5 Summary

In this chapter distribution studies with two parallel channels are presented. First the impact of the liquid and vapour distribution in the inlet manifold on the evaporator performance are investigated. The main findings are:

- The cooling capacity is not affected by a non-uniform distribution of the liquid and vapour for CO_2.
- The cooling capacity decreases by up to 20% for R134a at extreme maldistribution of the liquid and vapour.
- The difference between the two refrigerants occurs due to different pressure drop characteristics.
- Decreases in the cooling capacity are almost equal to decreases in the two-phase area. The cooling capacity is decreased a little less than the two-phase area.

Next the impact of the airflow distribution on the evaporator performance is considered. The main findings of this study are:

- The cooling capacity is strongly affected by airflow non-uniformity.
- Capacity reductions are more than twice as large for R134a than for CO_2.
- Decreases in the cooling capacity are significantly larger than decreases in the two-phase area.

Furthermore, combining the non-uniform airflow and non-uniform distribution of the liquid and vapour showed that:

- A non-uniform airflow distribution can be compensated by a suitable distribution of the liquid and vapour in the inlet manifold.
- If the superheat out of the individual channels is controlled to be equal, the cooling capacity is close to the optimum.
- R134a has a higher potential for capacity recovery than CO_2.

At last, some of the results are compared to results presented in the literature, and it is found that the results are in good agreement with other results.

Chapter 4

Sensitivity studies

In this chapter three aspects of sensitivity of the evaporator model are investigated. Firstly, this chapter investigates the sensitivity of the model with respect to the correlations chosen when building the model. Next, the sensitivity with respect to parameter changes is considered, and lastly the model is modified such that it can simulate dehumidifying conditions. The aim of the sensitivity study is to investigate which parameters most significantly influence the capacity reductions due to non-uniform distribution of liquid and vapour in the inlet manifold and non-uniform airflow distribution.

4.1 Significance of the choice of correlations

In the model empirical correlations are used to model frictional pressure drop and heat transfer coefficients. These correlations are typically developed using a database of experimental data. The correlations are developed to fit for certain ranges of flow parameters and geometries. However, even when applied for fully matching conditions the uncertainties of the correlations are high. Especially for two-phase flow correlations an uncertainty of up to 30% has to be expected.

A large number of different correlations exist to model frictional pressure drop and heat transfer coefficients, and it can be difficult to determine which correlation is the best to model a specific case. In the literature different recommendations that are based on comparison of experimental data with different correlations can be found. However, it might be hard to find experiments, that match well with the test case defined in section 2.4.

In order to tell whether the choice of correlation is significant regarding the results obtained when using the model in the distribution studies, we apply different correlations for the two-phase frictional pressure drop and

the two-phase heat transfer coefficient. Since correlations for single-phase flow usually have higher accuracy than correlations for two-phase flow, we will focus on the correlations applied in the region with two-phase flow in the present study.

The study is carried out using CO_2 as refrigerant. This refrigerant is atypical in that its properties such as density and viscosity differ from most conventional refrigerants and that the working pressure is very high. It is therefore not evident that standard correlations give accurate results.

The test case evaporator presented in chapter 2 is used for the study, with one difference though - the superheat is set to 0 K instead of the 6 K used elsewhere. However, later in this chapter it is shown that the value of the superheat does not influence the results significantly.

4.1.1 The pressure drop correlation

A review of the literature on advice for the choice of pressure drop correlation suitable for evaporating CO_2 in minichannels, shows different recommendations. Pettersen (2004) was one of the first to study flow boiling of CO_2 in small channels, and the Lombardi and Carsana (1992) correlation was recommended to model frictional pressure drop. Park and Hrnjak (2007) recommended the Müller-Steinhagen and Heck (1986) correlation for evaporating CO_2 in a conventional channel. Thome and Ribatski (2005) also showed good results for this correlation for CO_2 in mini- and microchannels. The Friedel (1979) correlation showed the best results in the study by Thome and Ribatski (2005) and is also recommended by Park and Hrnjak (2009). However, Pamitran et al. (2008) did not find good results for this correlation, and recommend instead a homogeneous model using an expression for the two-phase viscosity proposed by Dukler et al. (1964).

The above mentioned recommendations are nearly all based on experimental data covering only higher mass fluxes than the mass fluxes in the present study. One exception is the study by Park and Hrnjak (2007) in a conventionally sized channel recommending the Müller-Steinhagen and Heck (1986) correlation. Therefore, the Müller-Steinhagen and Heck (1986) correlation was chosen in the baseline model. However, all of the mentioned correlations were developed covering low mass fluxes. Since no evident superior correlation could be found from the literature review, the three other correlations are applied for comparison, in order to see whether the choice of correlation is crucial for the modelling results.

Figures 4.1 and 4.2 show results obtained imposing non-uniform inlet qualities and non-uniform airflow, respectively, using the following four correlations for calculating the frictional pressure drop:

- Müller-Steinhagen and Heck (1986)
- Lombardi and Carsana (1992)
- Friedel (1979)
- Homogeneous flow with two-phase viscosity after Dukler et al. (1964)

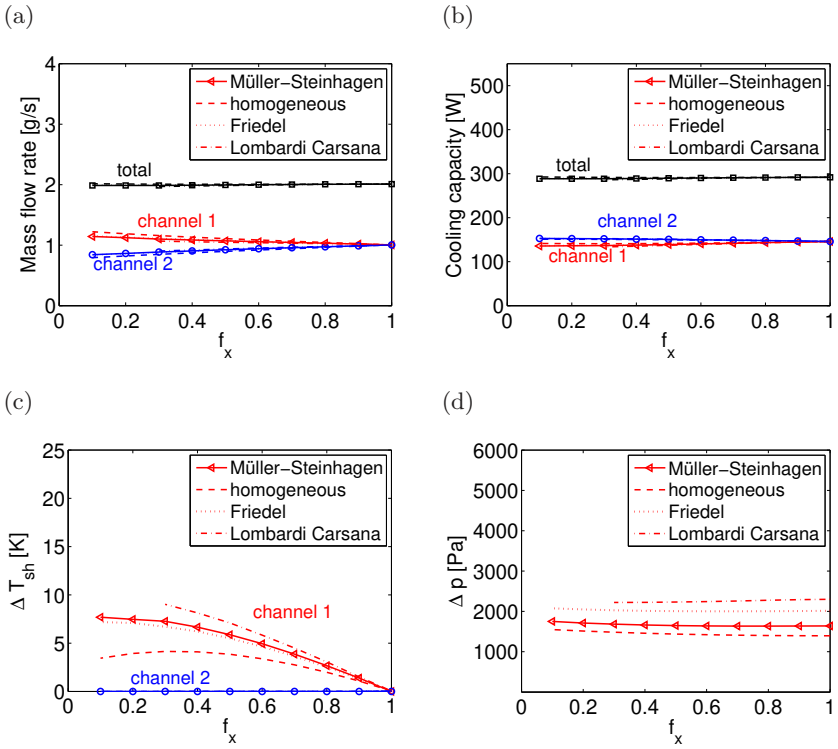

***Figure 4.1**: Selected parameters as a function of inlet quality distribution. CO_2 is used as refrigerant. Results are found using four different pressure drop correlations.*

From the figures it is seen that the distribution of mass flow rate and the cooling capacities are insignificantly dependent on the choice of pressure drop correlation. In figures 4.1(d) and 4.2(d) it is seen that the total pressure drop over the minichannel shows significant dependency on the choice of correlation. Using the Lombardi and Carsana (1992) correlation the pressure drop is found to be more than 60% higher than using the homogeneous model. From this study we cannot know, which of the correlations predicts the pressure drop most accurately, and in future work it would be interesting to identify, which correlation gives the most correct results.

It could be argued, that the total pressure drop over the evaporator could affect the results more significantly, if the whole refrigeration system was

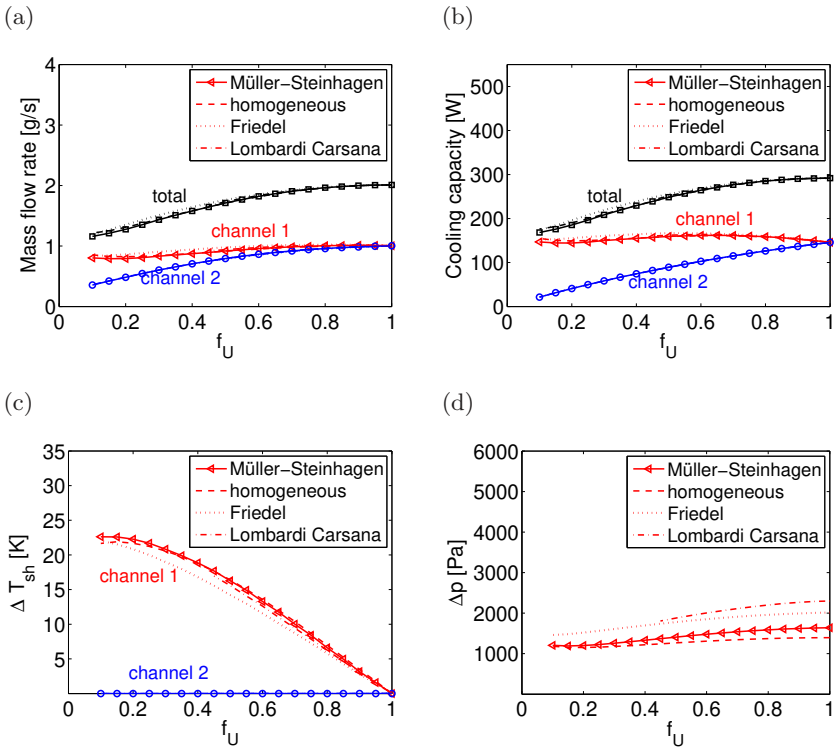

***Figure 4.2**: Selected parameters as a function of airflow distribution. CO_2 is used as refrigerant. Results are found using four different pressure drop correlations.*

considered. The larger the pressure drop in the evaporator, the higher is the load on the compressor. However, the total pressure in the CO_2 system is very high, and the pressure ratio over the compressor will not change significantly, when using one correlation instead of the other. It would thus be expected that the isentropic efficiency is not significantly affected by the differences in pressure drop given by the different correlations. Furthermore, the difference in the absolute pressure at the evaporator outlet is still small considering the different correlations, such that it is expected that the inlet density is not strongly affected by the choice of correlation, leading to a mass flow rate that is more or less independent on the choice of correlation.

4.1.2 The heat transfer coefficient correlation

Considering two-phase heat transfer coefficients, the following correlations have been tested:

- Bertsch et al. (2009)

- Choi et al. (2007), with a smooth transition to the single phase heat transfer coefficient for $x > 0.7$
- A constant two-phase heat transfer coefficient.

In the baseline model the Bertsch et al. (2009) correlation was applied for calculating the two-phase heat transfer coefficient. This correlation covers a wide range of refrigerants, including CO_2 and furthermore it covers mass fluxes down to 20 kg m^{-2} s^{-1} and vapour qualities from 0 to 1. The Choi et al. (2007) correlation, which has been applied for comparison, was developed for CO_2, but it does not cover the low mass fluxes used in this numerical experiment, and furthermore it only applies for qualities below 0.7.

As seen in figure 4.3 the calculated cooling capacity is almost independent on the choice of correlation. The same applies for the other outputs, which are shown in appendix A.4.

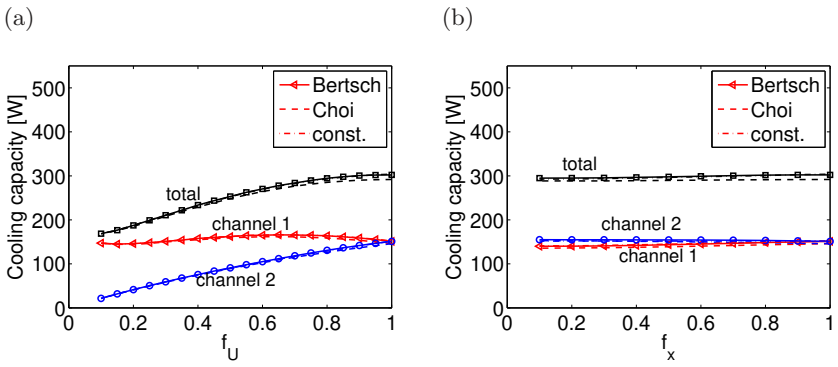

***Figure 4.3**: Cooling capacity as a function of f_U and f_x calculated using different correlation for two-phase heat transfer.*

4.2 Significance of parameter variations

In order to investigate which parameters are determining the capacity reductions that occur as a result of non-uniform distribution of liquid and vapour or non-uniform airflow, parameter variations are carried out using the test case evaporator. In the following a number of different parameters are considered and varied one at a time. In each case, the total capacity of course depends on the set of parameters chosen. However, we here focus on the capacity reductions due to a non-uniform distribution of liquid and vapour or a non-uniform airflow and not on the effect of the parameter changes on

the total capacity. Therefore, for each parameter variations the capacity is set to 100% when the liquid and vapour phases are distributed uniformly and the airflow is distributed uniformly, and the capacity reductions are investigated according to this reference.

4.2.1 Varying the channel orientation

Based on the conditions given in the test case, the pressure gradient in the evaporator develops differently for CO_2 than for the conventional refrigerant R134a. Due to the low viscosity and the high density of CO_2 the ratio between frictional and gravitational pressure drop contributions is very different from that of R134a for the tested conditions. This was illustrated in figure 3.4, page 37. With these differences in mind, it is natural to study the effects of the channel orientation.

Figure 4.4 shows the cooling capacity as a function of the distribution of liquid and vapour for CO_2 and R134a and for different channel orientations. For R134a the channel orientation does not affect the deterioration curve of the cooling capacity, while this is different for CO_2. Here a considerably larger reduction of the cooling capacity is found in the horizontal channel compared to the vertical channel. In the horizontal channel the frictional pressure gradient is dominating the total pressure gradient, just as in the case using R134a, and in this case the capacity reduction in the CO_2 evaporator corresponds more or less to the capacity reduction of the R134a evaporator. Exactly the same is seen for non-uniform airflow, shown in figure 4.5. The large gravitational contribution to the pressure drop thus seems to affect the distribution of the mass flow rate favourable, when imposing non-uniform airflow or non-uniform inlet qualities. Consequently, a smaller capacity reduction is found for the vertical channels.

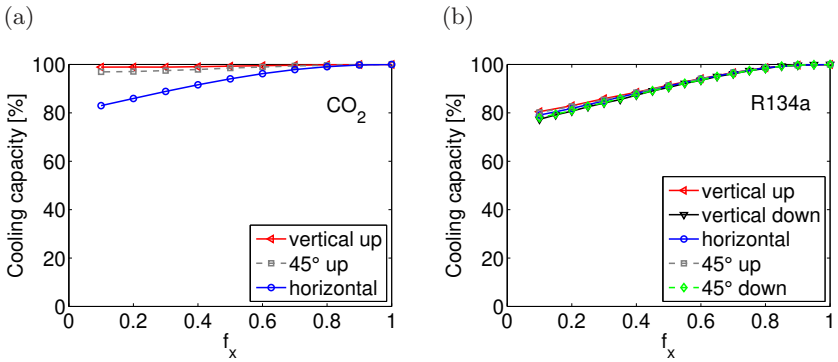

Figure 4.4: *Cooling capacity vs. inlet quality distribution for (a) CO_2 and (b) R134a.*

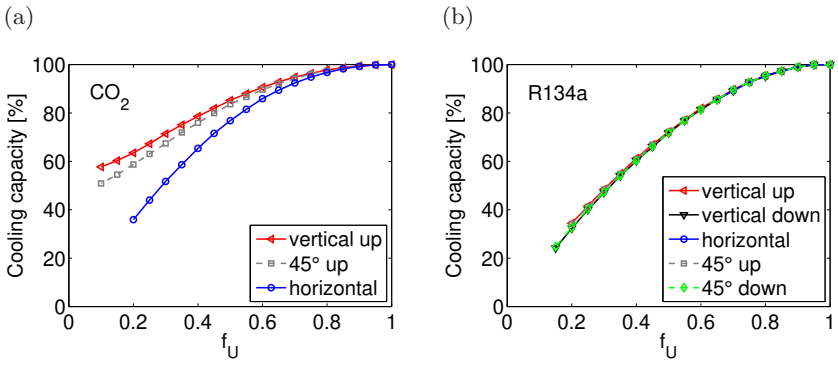

***Figure 4.5**: Cooling capacity vs. airflow distribution for (a) CO_2 and (b) R134a.*

4.2.2 Varying the outlet superheat

The superheat out of the test case evaporator is set to 6 K. Figure 4.6 shows the impact of a non-uniform distribution of liquid and vapour on the cooling capacity for three different values of superheat: 0 K (saturated vapour), 6 K and 12 K. It is seen that the reduction in capacity is not significantly affected by changing the outlet superheat. We thus conclude that the outlet superheat is not a significant parameter, considering the effects of non-uniform distribution of liquid and vapour on the evaporator performance.

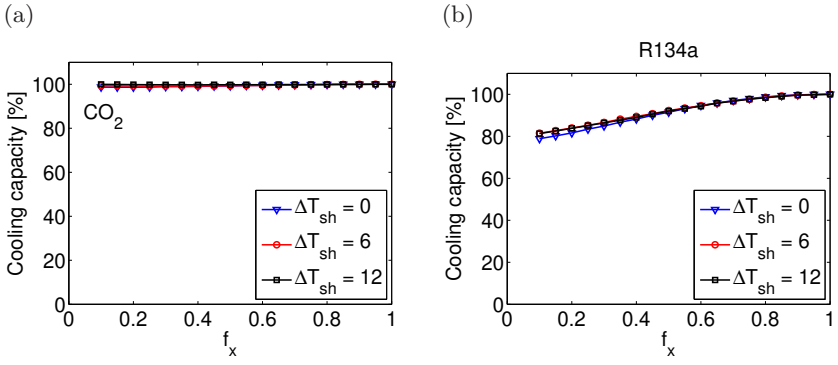

***Figure 4.6**: Impact of non-uniform distribution of liquid and vapour on the cooling capacity for different values of the outlet superheat. For $\Delta T_{\mathrm{sh}} = 0$ K saturated vapour exits the evaporator.*

Figure 4.7 shows the impact of non-uniform airflow on the cooling capacity for the three values of superheat. It is seen that also for a non-uniform

airflow the capacity reductions are not significantly affected by the variations of the outlet superheat.

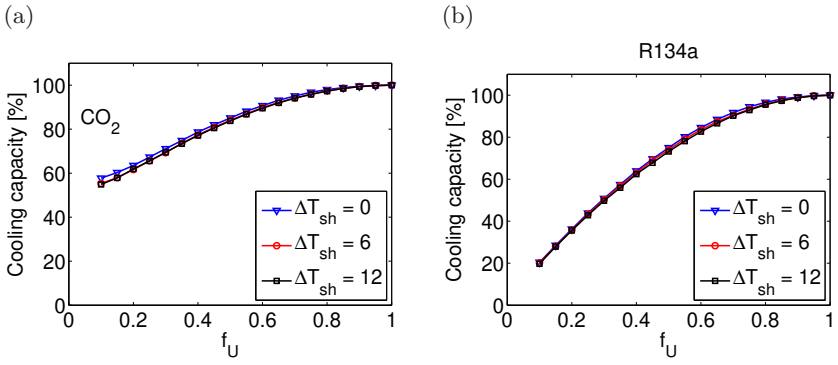

***Figure 4.7**: Impact of non-uniform airflow on the cooling capacity for different values of the outlet superheat. For $\Delta T_{\mathrm{sh}} = 0$ K saturated vapour exits the evaporator.*

It has not been investigated how the capacity reductions would be affected if the refrigerant was not fully evaporated at the outlet of the evaporator. However, it would be expected that the capacity was reduced less when decreasing the outlet quality, since a non-uniform distribution of liquid and vapour or a non-uniform airflow up to some degree would not decrease the two-phase area of the evaporator.

4.2.3 Varying the airflow rate

When changing the airflow rate first of all the air side heat transfer coefficient is affected. The airflow rate is given by a mean air velocity, which for the test case is 1.6 m/s. Figure 4.8 shows the impact of the distribution of liquid and vapour on the evaporator capacity for three different mean velocities of the airflow: 1.3 m/s, 1.6 m/s and 1.9 m/s. Decreasing the air velocity to 1.3 m/s results in a reduction of the airside heat transfer coefficient by 10% compared to the test case. On the other hand the airside heat transfer coefficient is increased by 9% when changing the mean air velocity to 1.9 m/s. From figure 4.8 it is seen that the capacity reductions are not significantly affected by changing the air velocity.

In figure 4.9 the effect of a non-uniform airflow on the capacity is shown for the three different air velocities. It is seen that for R134a, the capacity reductions are not significantly affected by changing the mean air velocity. For CO_2 on the other hand, the capacity reductions at severely non-uniform airflow are larger for increased mean air velocity.

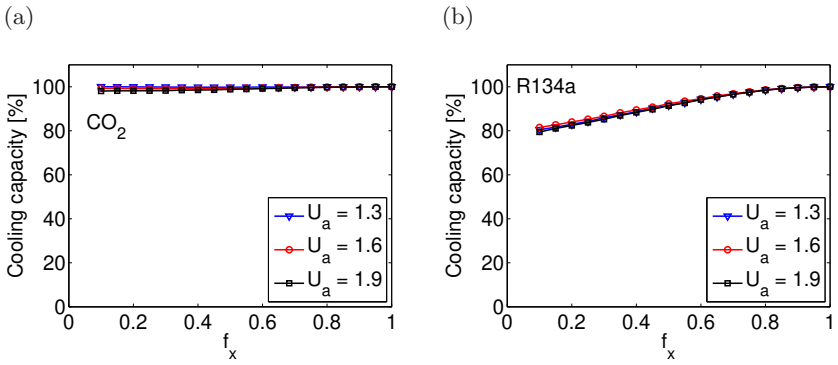

***Figure 4.8**: Impact of non-uniform distribution of liquid and vapour on the evaporator capacity for different values of the mean air velocity.*

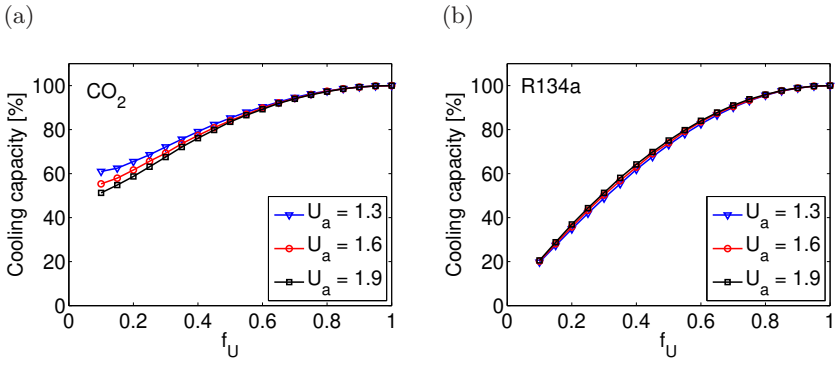

***Figure 4.9**: Impact of non-uniform airflow on the evaporator capacity for different values of mean air velocity.*

Figure 4.10 shows the area of the evaporator containing two-phase flow for CO_2 and R134a as a function of the airflow distribution for the three different mean air velocities. It is seen that the two-phase area is not affected

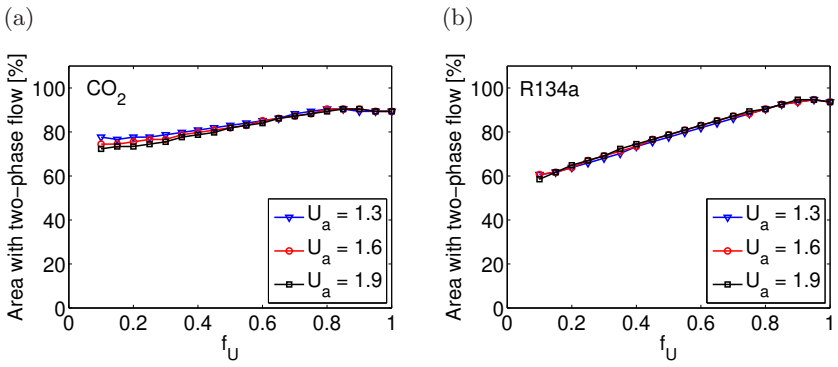

***Figure 4.10**: Impact of non-uniform airflow on the two-phase area for different values of mean air velocity.*

by changing the mean air velocity when using R134a as refrigerant, while for CO_2 the two-phase area is reduced slightly more for increasing mean air velocity when imposing non-uniform airflow. However, just as the results in chapter 3 showed, the decrease in capacity is larger than the decrease of the two-phase area for increasing non-uniformity of the airflow.

The fact that CO_2 is less affected by non-uniform airflow for lower airflow rates can be explained from the differences in the distribution of the mass flow rate and in the reduction rates of the mass flow rate. Figure 4.11 shows the pressure drop as a function of the air velocity on a single tube for different refrigerant mass flow rates. The triangular and circular markers indicate the pressure drop in channel 1 and 2, respectively, for varying f_U and for the three different airflow rates. It is seen that for R134a the pressure drop in the two channels is independent of the air velocity on the individual channel for the three cases. This results in an almost uniform distribution of the refrigerant mass flow rate between the two channels regardless the non-uniformity of the airflow for all cases.

For CO_2 the pressure drop in a single channel decreases with increasing air velocity (the black solid curves), which results in a non-uniform distribution of the mass flow rate when imposing a non-uniform distribution of the airflow. This decrease of the pressure drop is steepest at low air velocities and low refrigerant mass fluxes, changing to an almost flat curve for high air velocities. Therefore, the distribution of the mass flow rate is different for varying airflow rates.

Imposing a mean air velocity of 1.9 m/s results in a decrease of the mass

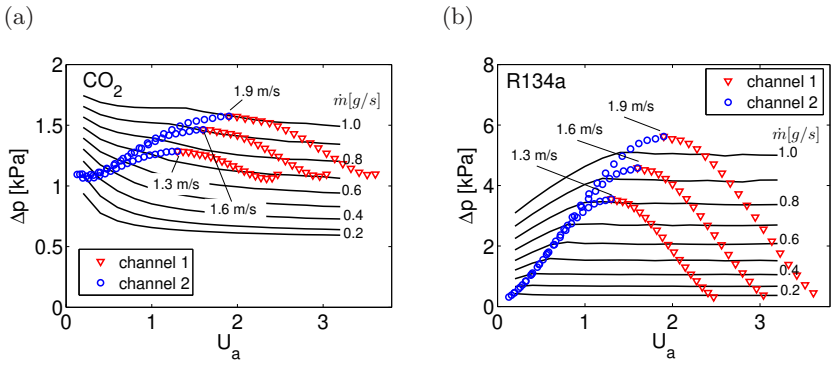

***Figure 4.11**: The black curves show the pressure drop as a function of the air velocity on a single tube for different refrigerant mass flow rates. The triangular and circular markers indicate the pressure drop in channel 1 and 2, respectively, for varying f_U, and for the three different airflow rates.*

flow rate in both channels when increasing non-uniformity of the airflow. However, the reduction is larger in channel 2 than in channel 1. Imposing an airflow rate corresponding to a mean air velocity of 1.3 m/s, also results in a decrease of the mass flow rate in channel 2. However, the mass flow rate of refrigerant in channel 1 decreases much less despite the decreasing pressure drop, such that the reduction of the total mass flow rate is comparably smaller at the lower airflow rate. The decrease in pressure drop with increasing air velocity found especially at low air velocities is thus beneficial for the mass flow rate distribution. The beneficial distribution results in less excess liquid in channel 2, such that the total mass flow rate does not need to decrease as much, in order to reach the specified superheat out of the manifold. All in all this results in a smaller reduction of the cooling capacity for the lower airflow rate.

4.2.4 Varying the manifold inlet quality

Changing the manifold inlet quality affects both the refrigerant side heat transfer coefficients and the pressure gradients. When considering the distribution of liquid and vapour it also changes the potential for a non-uniform distribution of liquid and vapour. If pure liquid enters the manifold there is no possibility for a non-uniform distribution of liquid and vapour. Intuitively, it can be expected that a total separation of the two phases will affect the evaporator performance increasingly when increasing the inlet quality. Figure 4.12, showing the effect of non-uniform distribution of liquid and vapour on the cooling capacity for different values of manifold inlet quality, supports this. Three different inlet qualities to the manifold have been

tested: $x_{mf} = 0.1$, $x_{mf} = 0.3$ and $x_{mf} = 0.5$. It is seen that for both CO_2 and for R134a the capacity reductions due to non-uniform distribution of liquid and vapour are largest in the case where $x_{mf} = 0.5$. However, for $x_{mf} = 0.3$

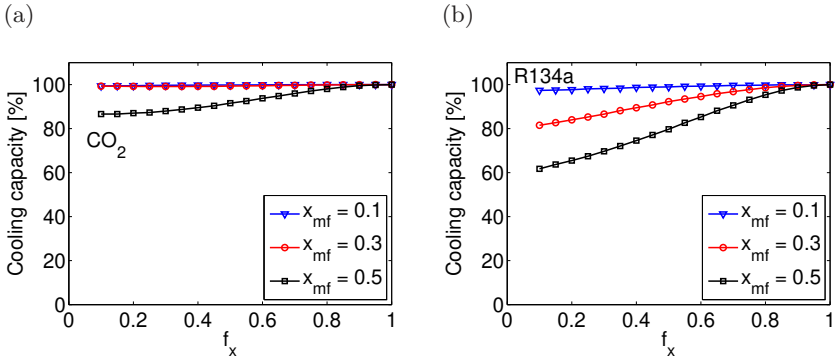

Figure 4.12: *Impact of non-uniform distribution of liquid and vapour on the cooling capacity for different values of manifold inlet quality.*

the capacity is unaffected by the distribution of liquid and vapour when using CO_2, while the capacity decreases with increasing non-uniformity of the liquid and vapour distribution for R134a. Considering the two-phase area of the evaporator shown in figure 4.13, it is found that the two-phase area decreases slightly more than the capacity in those cases, where a reduction of the capacity is found. These results are thus also in agreement with the results shown previously.

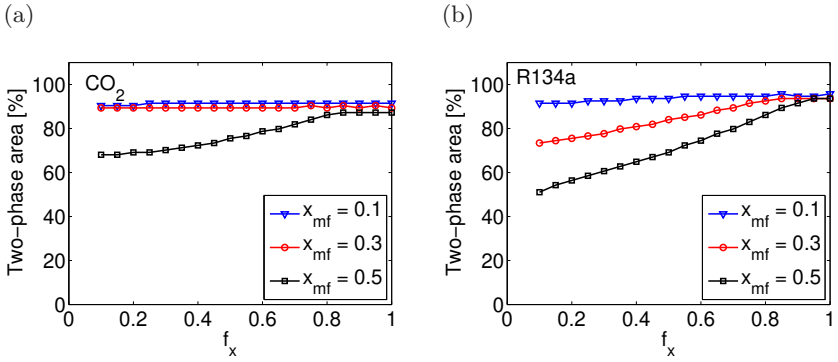

Figure 4.13: *Impact of non-uniform distribution of liquid and vapour on the percentage of the refrigerant side evaporator area that is in contact with two-phase refrigerant for different values of manifold inlet quality.*

In order to understand why CO_2 is unaffected by the distribution of liquid and vapour for higher manifold inlet qualities than R134a, we first consider

the connection between the pressure drop and inlet quality in a single channel for different mass flow rates, shown in figure 4.14. Considering graph (a) with CO_2 and moving from $f_x = 1$ to $f_x = 0.1$ we see that for $x_{\mathrm{mf}} = 0.1$ and $x_{\mathrm{mf}} = 0.3$ the mass flow increases in channel 1 and decreases in channel 2. For $x_{\mathrm{mf}} = 0.5$ the mass flow rate in channel 1 stays almost constant, while the mass flow rate in channel 2 decreases, such that the total mass flow rate is decreased in this case. The fact that the curves showing the pressure drop as a function of the inlet quality have a negative slope is again beneficial for the distribution of the mass flow rate, and it is the large gravitational pressure drop for the liquid that is responsible for this shape of the curves. Considering R134a it is seen that the mass flow rate is almost constant in

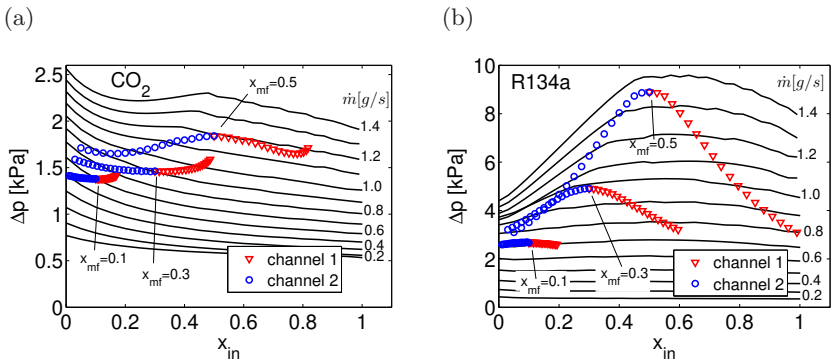

***Figure 4.14**: The black curves show the pressure drop as a function of the inlet quality of a single tube for different refrigerant mass flow rates. The triangular and circular markers indicate the pressure drop in channel 1 and 2, respectively, for varying f_x, and for the three different manifold inlet qualities.*

both channels for $x_{\mathrm{mf}} = 0.1$, while the mass flow rate decreases in both channels for the two larger values of the inlet quality, resulting in a capacity reduction.

It is interesting to see, at which manifold inlet quality the capacity starts to decrease if almost full separation of the liquid and vapour phases is assumed. Figure 4.15 shows the capacity of each of the channels and the total capacity as a function of the manifold inlet quality having a distribution of liquid and vapour of $f_x = 0.1$. The capacity is shown relative to the capacity that would have been obtained at uniform distribution of liquid and vapour at the given inlet quality. Furthermore, the superheat out of the individual channels is shown as a function of the manifold inlet quality in graphs (c) and (d). From the graphs it is seen that as long as the refrigerant in channel 2 is fully evaporated at the outlet, which it is for manifold inlet qualities of up to 0.3 for CO_2 and 0.1 for R134a, the capacity is not affected by the non-uniform distribution of the liquid and vapour.

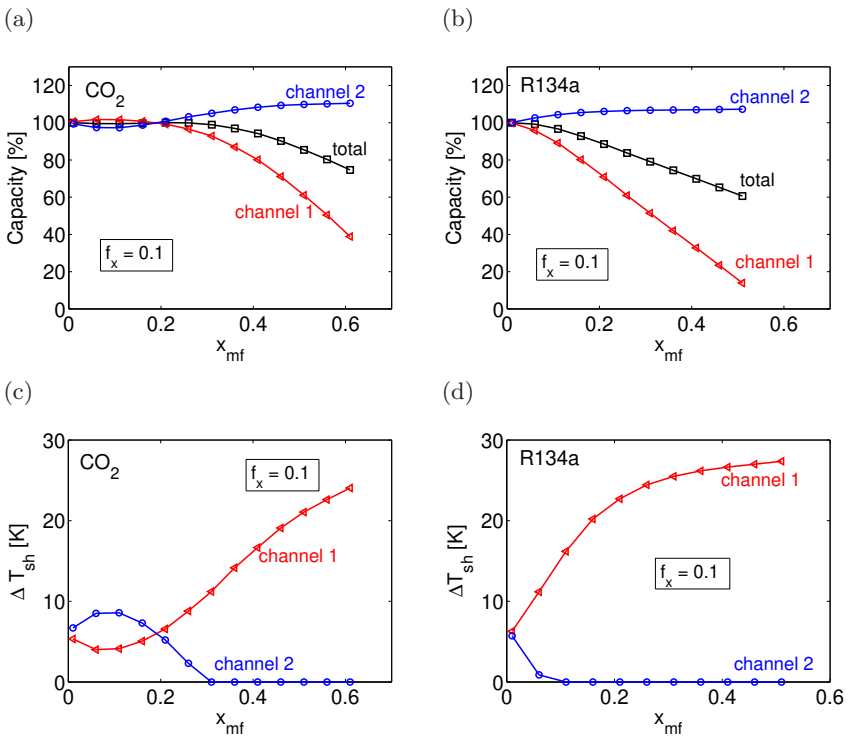

***Figure 4.15**: Graphs (a) and (b) show the capacity of each channel and the total capacity as a function of the manifold inlet quality having a distribution of liquid and vapour corresponding to $f_x = 0.1$ for CO_2 and R134a, respectively. The capacity is calculated relative to the capacity that would have been obtained for uniform distribution of liquid and vapour at the given manifold inlet quality. Graphs (c) and (d) show the corresponding superheat out of the individual channels.*

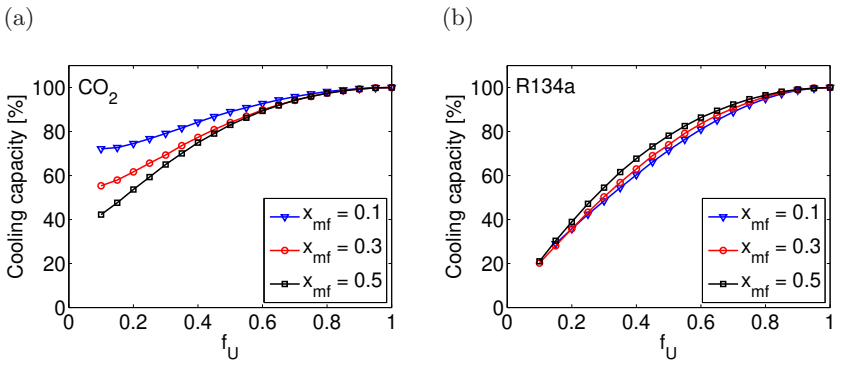

***Figure 4.16**: Impact of non-uniform airflow on the evaporator performance for different values of manifold inlet quality.*

Considering the impact of non-uniform airflow on the cooling capacity for different manifold inlet qualities, figure 4.16 shows that the manifold inlet quality affects the capacity reduction for CO_2 much more than for R134a. For CO_2 the capacity reductions due to non-uniform airflow are largest for higher values of the manifold inlet quality. Comparing to the results obtained above this is not surprising, since the contribution of the gravitational pressure drop, which is responsible for the expedient mass flow rate distribution, is largest at low inlet qualities. For R134a the capacity reductions are not much affected by the manifold inlet quality. Actually, it is seen that for airflow distributions not close to uniform and not close to the extreme, the capacity reductions are lower for high manifold inlet quality.

4.2.5 Varying the temperature difference

The temperature difference that drives the heat transfer between the air and the refrigerant may be changed by varying either the air inlet temperature or the evaporation temperature. In order to investigate how changes of these temperatures affect the capacity reductions, simulations are performed changing the evaporation temperature at the inlet 7K up and down, while keeping the air inlet temperature constant, and changing the air inlet temperature 7K up and down, while keeping the evaporation temperature at test case conditions. Figure 4.17 compares the impact of non-uniform distribution of liquid and vapour on the cooling capacity for the test case evaporator with the capacities found at the different air inlet temperatures and evaporation temperatures. It is seen that a change in the temperature difference does not impact the capacity reductions significantly.

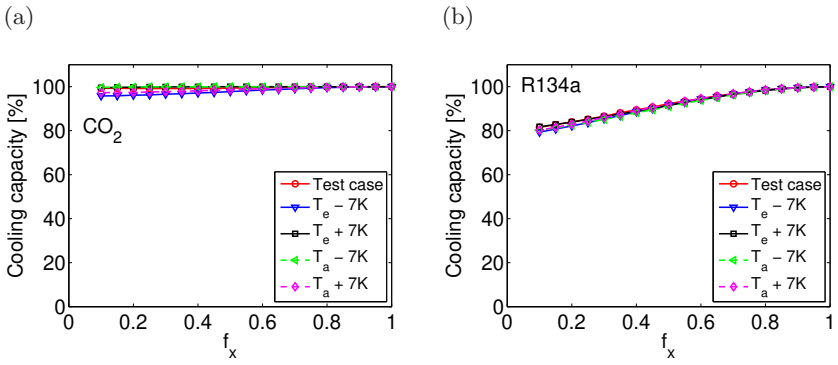

***Figure 4.17**: Impact of non-uniform distribution of liquid and vapour on the cooling capacity for different air inlet temperatures and different evaporation temperatures. The temperature is changed with reference to the test case.*

Figure 4.18 shows the impact of a non-uniform airflow distribution on the

cooling capacity for the different air inlet temperatures and evaporation temperatures mentioned above. It is seen that if using R134a as refrigerant the capacity reductions are not affected by the temperature changes. For

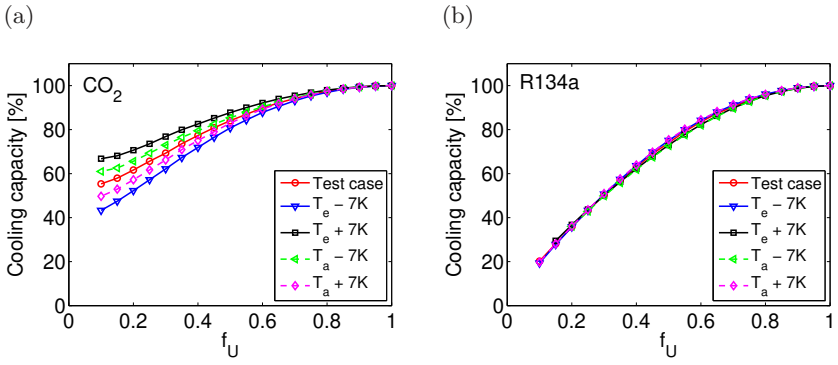

***Figure 4.18**: Impact of non-uniform airflow distribution on the cooling capacity for different air inlet temperatures and different evaporation temperatures. The temperature is changed with reference to the test case.*

CO_2, however, the capacity reduction at severe non-uniformity of the airflow changes significantly when changing the temperature difference. Decreasing the temperature difference between the inlet air and the refrigerant, results in smaller capacity reductions, while increasing the temperature difference leads to an increase of the capacity reductions at a given non-uniform airflow distribution. Furthermore, it is seen that the capacity reductions are affected more by changing the evaporation temperature than by changing the air temperature equivalently. However, to explain why this is the case, we need to consider the changes of the mass flux that are a result of changing the respective temperatures, while keeping all other parameters constant. In table 4.1 the mass flux at uniform airflow distribution is shown for each of the temperatures used in the above simulations. The temperature dif-

	T [°C]	G [kg/(m^{2}s)]
	0.7	100
T_e	7.4	85
	14.4	69
	28	109
$T_{a,\text{in}}$	35	85
	42	62

***Table 4.1**: Mass flux in the evaporator channels using CO_2 at different temperatures.*

ference between refrigerant and air is decreased by either increasing the evaporation temperature or decreasing the air temperature. From table 4.1 it is seen that a lower mass flux is needed to obtain the specified superheat when increasing the evaporation temperature, while a higher mass flux of refrigerant is needed when air temperature is decreased to 28°C. When increasing the mass flux, the frictional pressure drop contribution increases of the order $\sim G^2$, while the gravitational contribution is independent of the mass flux. When decreasing the temperature difference between air and refrigerant, the frictional pressure gradient is hence much more dominating in the case where the evaporation temperature is increased compared to the case where the air temperature is lowered. Again the results indicate that the ratio between the frictional and the gravitational pressure drop is an important factor determining how much the capacity is affected by a non-uniform airflow.

4.2.6 Varying the port dimension

Changing the port dimension affects the hydraulic diameter and the refrigerant mass flux. Since the refrigerant mass flux for the test case is already in the low end of what would be expected in a real evaporator, the port dimension are only varied to smaller ports, decreasing the port height and port length each by 10% and 20%.

Figure 4.19 shows the capacity reductions due to non-uniform distribution of liquid and vapour for three different port sizes. It is seen that for both refrigerants the capacity reductions at severe non-uniformity of the liquid and and vapour distribution are slightly increased when decreasing the port dimension. Considering the impact of a non-uniform airflow, figure 4.20 shows the reductions in capacity of the test case compared to the two other port dimensions. For R134a the capacity reductions are not affected by changing the port dimension, while for CO_2 the capacity reductions at considerable non-uniformity of the airflow are increased when using smaller channels. These results relate well to the results presented above, since both the increase in the mass flux and the decrease of the hydraulic diameter results in an increase of the frictional pressure drop, while the gravitational contribution remains unaffected.

4.2.7 Varying the channel length

Figures 4.21 and 4.22 show the impact of non-uniform distribution of liquid and vapour and non-uniform airflow on the cooling capacity for three different channel length. Channels 10 cm longer and 10 cm shorter than the test case evaporator are used in the simulations. Changing the channel

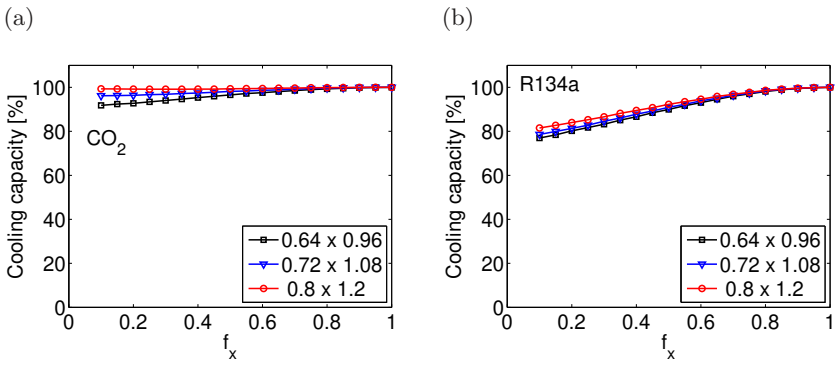

***Figure 4.19**: Impact of non-uniform distribution of liquid and vapour on the cooling capacity for different port dimensions.*

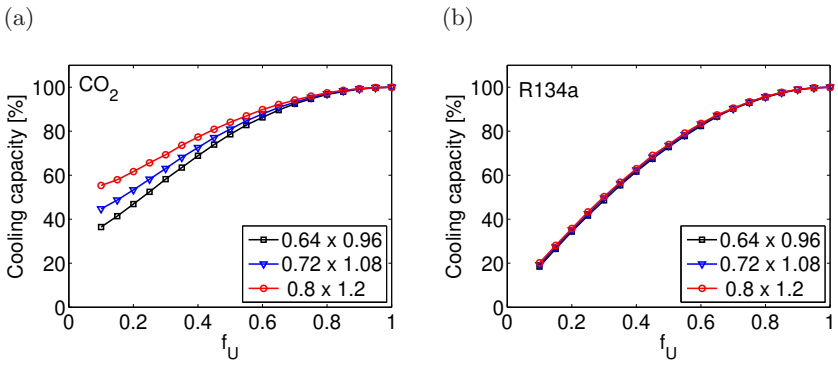

***Figure 4.20**: Impact of non-uniform airflow distribution on the cooling capacity for different port dimensions.*

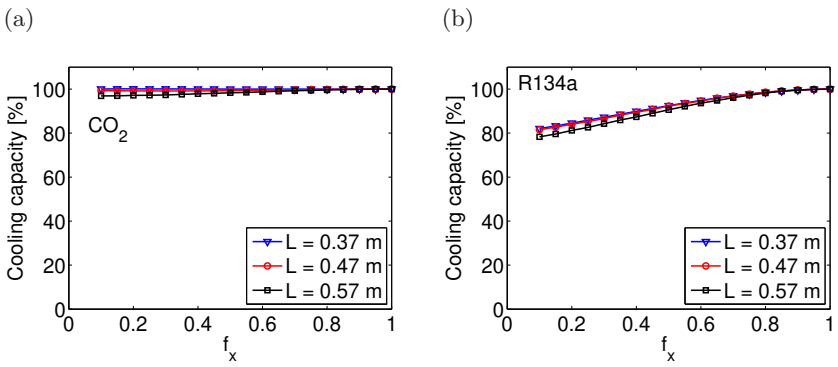

***Figure 4.21**: Impact of non-uniform distribution of liquid and vapour on the cooling capacity for different channel length.*

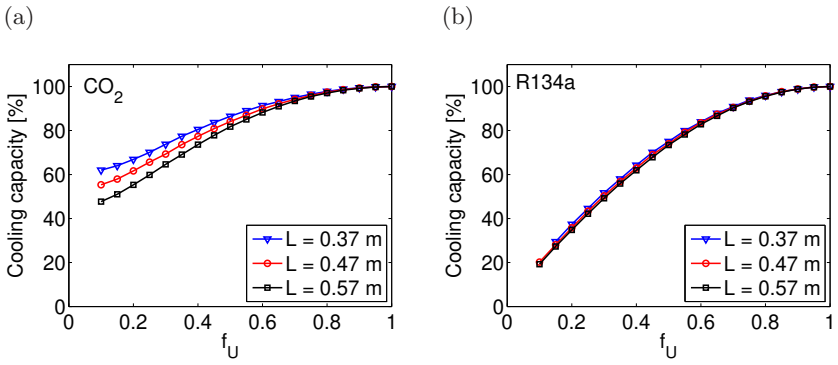

Figure 4.22: *Impact of non-uniform airflow distribution on the cooling capacity for different channel length.*

length mainly affects the mass flow rate needed to obtain the specified superheat. For channels longer than the test case channels, the heat transfer area is increased such that a higher mass flow rate can be evaporated and vice versa. The effects of changing the channel length is seen to be very similar to changing the port dimensions.

4.2.8 Manipulating the gravitational pressure gradient for R134a

The results of the sensitivity study indicate that the gravitational pressure drop is an important factor considering the magnitude of the capacity reductions. All other parameters investigated only showed an impact on the capacity reductions, if the specific parameter change also affected the significance of the gravitational pressure drop contribution, which was the case for several parameters when using CO_2 as refrigerant. For R134a the gravitational pressure drop contribution is very small compared to the contribution of the frictional pressure drop, and for this refrigerant the reductions in capacity found when applying a non-uniform distribution of liquid and vapour or a non-uniform airflow did not change for most of the parameter changes. Therefore, it is interesting to investigate what would happen if the gravitational pressure drop would be increased for this refrigerant. In practice this is not possible, since the gravitational pressure gradient is determined by the refrigerant properties, but theoretically it is an interesting experiment. Figure 4.23 compares the capacity as a function of the distribution of liquid and vapour (graph a) and as a function of the airflow distribution (graph b) for the test case with the capacity found when multiplying the gravitational pressure gradient by a factor of ten. The figure shows that the cooling capacity is reduced significantly less for both non-uniform dis-

tribution of liquid and vapour and non-uniform airflow in the case where the gravitational pressure gradient has been increased artificially.

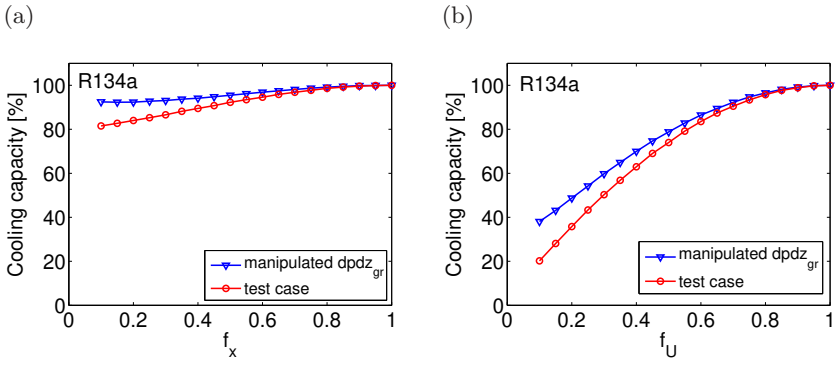

***Figure 4.23**: Comparison of the cooling capacity of the test case with the cooling capacity found multiplying the gravitational pressure gradient by a factor of ten. The cooling capacity is shown as a function of the distribution of liquid and vapour (a) and as a function of the airflow distribution (b).*

Figure 4.24 shows the mass flow rate in each channel as well as the total mass flow rate as a function of the distribution of liquid and vapour (graph a) and as a function of the airflow distribution (graph b). The figure compares the

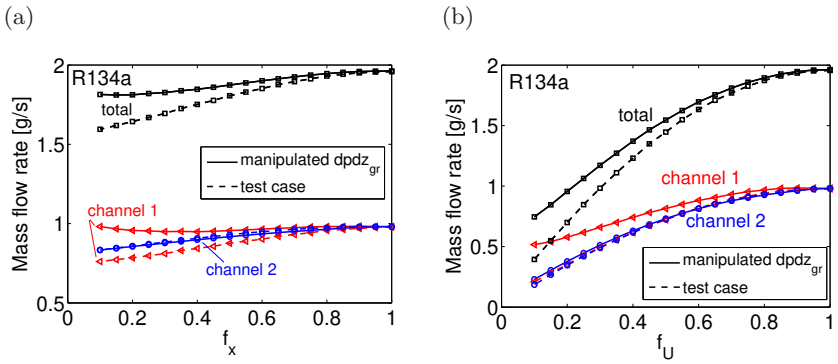

***Figure 4.24**: The mass flow rate, total and in each of the channels is shown as a function of (a) distribution of liquid and vapour and (b) as a function of the airflow distribution for test case conditions and for a manipulated case, where the gravitational pressure gradient increased by a factor of ten.*

test case results with the solutions found when the gravitational pressure gradient is multiplied by a factor of ten. It is seen that the total mass flow rate is reduced less in the case of the manipulated gravitational pressure gradient, mainly because the mass flow rate in channel 1 is reduced less.

Both for non-uniform distribution of liquid and vapour and for non-uniform airflow the refrigerant in channel 1 is evaporated faster than in channel 2. A larger mass flow rate in this channel, decreases the superheat out of this channel and is therefore beneficial.

4.3 Significance of moist air

All previously presented results were obtained assuming dry air in the evaporator. In order to investigate the impact of moist air on the capacity reductions, the model has to be modified such that the combined heat and mass transfer is taken into account for those parts of the evaporator where water condenses on the evaporator surface.

4.3.1 Model modifications

In order to solve the energy balance equations when moist air is cooled in the evaporator it is necessary to determine whether the surface temperature of the evaporator is below the dew point temperature of the air. Providing the relative humidity of the air as an additional input to the model, the dew point temperature of the incoming air can be calculated using the Antoine equation (Danig and Holm, 1998)

$$T_{\text{dew}} = \frac{B}{\ln p_{v,s} - A} - C - 273.25 \quad [^{\circ}\text{C}], \tag{4.1}$$

with

$$A = 23.5771, \quad B = -4042.9, \quad C = -37.58,$$

where $p_{v,s}$ is the partial pressure of the water vapour at saturation (at the given air temperature).

The surface temperature, however, is an output of the energy balance equations. In order to determine a surface temperature that can be used to determine if there is condensation on the surface or not, the balance equations are solved assuming non-dehumidifying conditions. In this case there will be no condensation of moisture and the model is very similar to the dry air model presented in chapter 2. The only modification compared to the model previously presented is the air side energy balance, which is now calculated from

$$\dot{Q} = \dot{m}_a \, c_{1+w} \, (T_{a,\text{in}} - T_{a,\text{out}}), \tag{4.2}$$

where the mass flow rate, $\dot{m}_a$ is the mass flow rate of dry air and c_{1+w} is the mixture c_p of humid air calculated per unit mass of dry air

$$c_{1+w} = c_{p,a} + w \, c_{p,v}, \tag{4.3}$$

where w is the humidity ratio. It is assumed that c_{1+w} is constant in a control volume.

The temperature of the dry surface is assumed to be constant for one control volume and is calculated on the refrigerant side using

$$T_{w,\mathrm{dry}} = \frac{\dot{Q}_{\mathrm{dry}}}{h_r \cdot A_r} + \frac{T_{r,\mathrm{in}} + T_{r,\mathrm{out}}}{2}. \tag{4.4}$$

It is assumed that the surface temperature on the refrigerant side equals the surface temperature on the air side, which is in accordance with equation (2.30), used to calculate UA-value of the evaporator, where any conduction resistance has been neglected. The main reason for calculating the surface temperature on the refrigerant side is that the model showed to be numerically more stable if it was calculated on this side.

If the calculated dry surface temperature is below the dew point temperature, moisture will condense on the surface and this has to be included in the equations. In this case the total heat transferred to the refrigerant compounds of the sensible heat, which is energy transfer due to the temperature different and the latent heat, which is energy transfer due mass transfer. The energy balance of the humid air flow in a control volume yields

$$\dot{Q} = \dot{m}_a \left(i_{\mathrm{in}} - i_{\mathrm{out}}\right). \tag{4.5}$$

According to the definition of enthalpy of humid air this equations can be written as

$$\dot{Q} = \dot{Q}_{\mathrm{sen}} + \dot{Q}_{\mathrm{lat}} = \dot{m}_a \left[c_{1+w} \left(T_{a,\mathrm{in}} - T_{a,\mathrm{out}}\right) + r_0 \left(w_{\mathrm{in}} - w_{\mathrm{out}}\right)\right], \tag{4.6}$$

where the first term in the brackets on the right hand side is the specific sensible heat and the second term is the specific latent heat.

The sensible heat transfer between the air and the heat exchanger surface is calculated as

$$\dot{Q}_{\mathrm{sen}} = h_a \, A_a \, \Delta T, \tag{4.7}$$

where $\Delta T = T_{a,\mathrm{mean}} - T_w$. In order to calculate the latent heat transfer rate it is convenient to define a latent heat transfer coefficient, h_{lat} (Knudsen, 2004) such that

$$\dot{Q}_{\mathrm{lat}} = h_{\mathrm{lat}} \, A_a \, \Delta T. \tag{4.8}$$

The total heat transfer rate is hence given by

$$\dot{Q} = \left(h_a + h_{\mathrm{lat}}\right) A_a \, \Delta T = h_{\mathrm{tot}} \, A_a \, \Delta T. \tag{4.9}$$

With the sensible and the latent heat transfer rate related to the same temperature difference the ratio between the total heat transfer rate and the sensible heat transfer rate is found as

$$\frac{\dot{Q}}{\dot{Q}_{\text{sen}}} = \frac{h_{\text{tot}}}{h_a} = \frac{\Delta i}{\Delta i - r_0 \Delta w} = \frac{\frac{\Delta i}{\Delta w}}{\frac{\Delta i}{\Delta w} - r_0} \tag{4.10}$$

such that

$$h_{\text{tot}} = h_a \left(\frac{\frac{\Delta i}{\Delta w}}{\frac{\Delta i}{\Delta w} - r_0} \right). \tag{4.11}$$

The heat transfer rate in an air cooler working under dehumidifying conditions can thus be calculated in the same way as the dry air cooler, just replacing h_a with h_{tot}. However, in order to calculate the h_{tot} the gradient, $\frac{di}{dw}$ has to be known. Assuming the Lewis number to be one, it can be shown that the process direction of air dehumidifying on a surface is linear, going from the inlet state of the air towards the state of the air at the surface, which is saturated air at the surface temperature (Knudsen, 2004). The total heat transfer coefficient can thus be calculated as

$$h_{\text{tot}} = h_a \left(\frac{\frac{i_{\text{in}} - i_w}{w_{\text{in}} - w_w}}{\frac{i_{\text{in}} - i_w}{w_{\text{in}} - w_w} - r_0} \right). \tag{4.12}$$

It is assumed that the sensible heat transfer coefficient under wet conditions is the same as under dry conditions. In reality the sensible heat transfer coefficient will change slightly due to water film on the surface.

In the evaporator model, h_{tot} is used for calculating the overall heat transfer coefficient, which is used for determining the NTU, if the dry surface temperature of the control volume is below the dew point temperature.

4.3.2 Variation of the relative humidity

By varying the relative humidity the effective air side heat transfer coefficient is increased for the areas of the evaporator, which have a low surface temperature. This leads to an improved heat transfer primarily in the areas of the evaporator, where the refrigerant is in a two-phase state, while the heat transfer is comparably smaller in areas where the refrigerant is superheated. If the relative humidity is 30%, the sensible air side heat transfer coefficient is multiplied by around 1.3 in order to obtain the total air side heat transfer coefficient. Setting the relative humidity to 60%, this factor is around 2.3.

Figure 4.25 shows the cooling capacity as a function of the liquid and vapour distribution at the channel inlets for three different values of the air relative

humidity: dry air, 30% and 60%. For all cases the cooling capacity is set to 100% at uniform distribution of the liquid and vapour. It is seen that for both refrigerants the reductions of the cooling capacity are not affected much by changing the relative humidity of the air. However, a small increase of the capacity reductions is found when increasing moisture content of the air. The absolute cooling capacity of the evaporator is higher for increased relative humidity, due to the latent heat transfer contribution, which is seen in figure 4.26, and the refrigerant mass flow rate increases correspondingly. It is therefore likely that the changes in the capacity reductions for different relative humidities are again mainly a result of changes in the dominance of different pressure drop contributions.

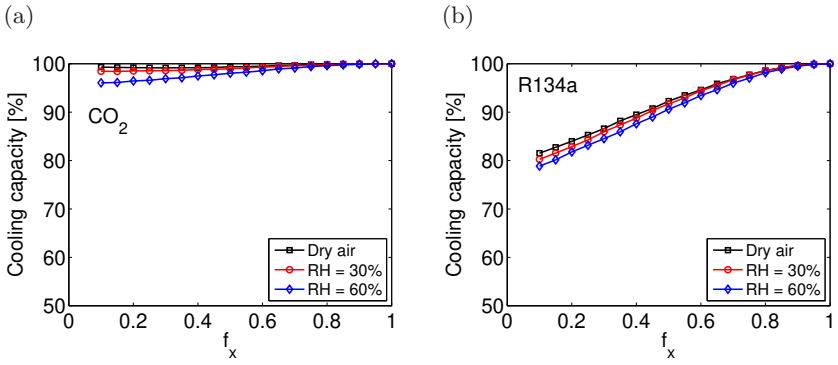

***Figure 4.25**: The cooling capacity as a function of the distribution of liquid and vapour at the inlet for different values of the air relative humidity.*

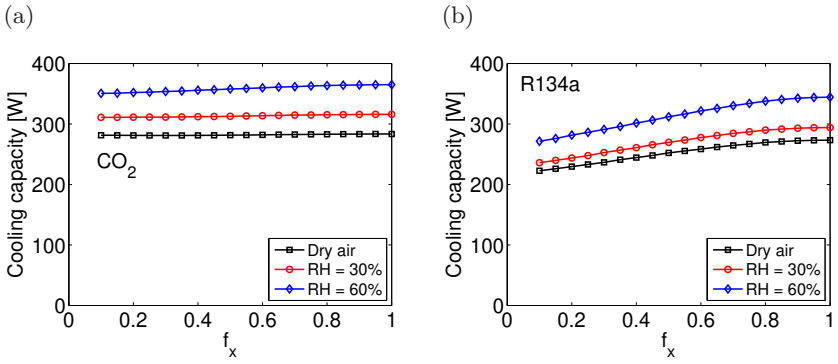

***Figure 4.26**: The cooling capacity as a function of the distribution of liquid and vapour at the inlet for different values of the air relative humidity.*

Considering a non-uniform airflow distribution, figure 4.27 shows that the cooling capacity decreases slightly with increasing relative humidity for both

refrigerants. When using R134a the model had numerical difficulties solving for low values of f_U. Therefore the curves for RH = 30% and RH = 60% stop before the curve for dry air.

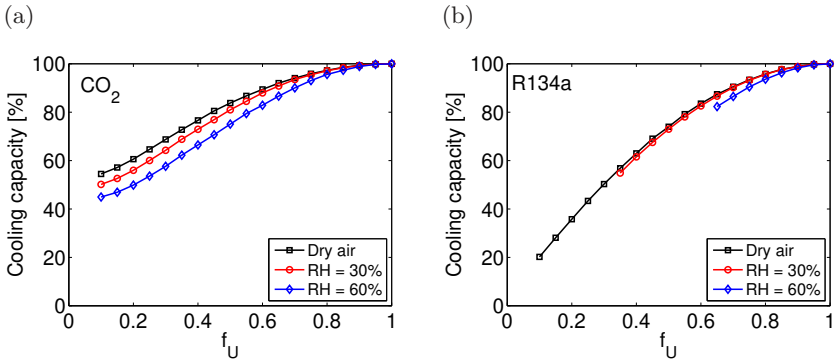

***Figure 4.27**: The cooling capacity as a function of the airflow distribution at the inlet for different values of the air relative humidity.*

4.4 Discussion and summary

The results presented in this chapter indicate, that the development of the pressure gradient in the channel is significant, considering the magnitude of the capacity reductions due to non-uniform distribution of liquid and vapour and non-uniform airflow. The study considering the choice of correlations shows that amongst the tested correlations no significant differences in the results considering capacity reductions can be found. However, considering the correlations for the two-phase frictional pressure drop, the shape of the curve showing the frictional pressure gradient along the channel is similar for all correlations.

The sensitivity study regarding parameter changes and moist air shows that parameter variations, which affect the gravitational pressure gradient impact most significantly on the capacity reductions. It is found that a significant contribution of the gravitational pressure gradient to the total pressure gradient is beneficial, in that the capacity is less sensitive to both non-uniform distribution of liquid and vapour and non-uniform airflow. However, changes of the gravitational pressure gradient simply lead to a change in the total pressure gradient, and it is thus the shape of the curve showing the total pressure gradient along the channel that is the important factor. Increasing the gravitational pressure gradient significantly, primarily results in an increase of the total pressure gradient in the first part of the channel, where most of the refrigerant is liquid. It is thus ex-

pected that an increase of the total pressure gradient in the first part of the channel, e.g. by varying the channel dimensions, would lead to similar results.

In practice, it would probably be more realistic to change the channel dimensions along the channel in order to change the course of the total pressure gradient, than letting the gravitational pressure gradient be as dominating as we did in these numerical experiments. In order to prevent maldistribtuion of the refrigerant due to the pressure drop in the manifolds a certain pressure drop is necessary. However, an increased pressure drop also means a higher load on the compressor, so a trade-off has to be made.

Chapter 5

Conclusions

Using minichannel heat exchangers in refrigeration systems significantly reduces the refrigerant charge and increases compactness of the system. Both of these issues are currently among the main targets within research and development of refrigeration systems. Minichannel heat exchangers have been successfully applied as condensers for a number of years. However, using minichannel heat exchangers as evaporators still brings up challenges. One of these challenges is refrigerant maldistribution and capacity reductions due to a non-uniform heat load and a non-uniform distribution of the liquid and vapour phases in the inlet manifold.

Evaporator model and test case

This thesis presents an evaporator model that is used to investigate the impact of non-uniform airflow and non-uniform distribution of the liquid and vapour phases in the inlet manifold on the refrigerant mass flow distribution and on the cooling capacity of the evaporator. The model is built up by connecting one dimensional steady state models of multiport minichannel tubes in order to model the parallel channels. The single multiport minichannel model is successfully verified against commercial modelling software.

A test case evaporator consisting of two multiport minichannels in parallel is defined, which is used for the distribution study. The test case evaporator is based on a real evaporator, applied in an air-conditioning system using R134a as refrigerant. However, two different refrigerants, R134a and CO_2 are applied in the numerical experiments using the test case evaporator.

Two different distribution parameters, f_x and f_U are introduced. These parameters characterize the degree of non-uniformity of the liquid and vapour distribution and the airflow distribution, by relating the conditions in one of the channels to a mean condition. Both parameters hold values between

0 and 1, where 1 is uniform distribution and 0 is extreme maldistribution.

Non-uniform distribution of liquid and vapour

Considering the evaporator performance when imposing non-uniform distribution of the liquid and vapour in the inlet manifold, we find that the cooling capacity decreases by up to 20% at extreme maldistribution of the liquid and vapour in the inlet manifold when using R134a as refrigerant. On the other hand, the cooling capacity is not affected by the distribution of liquid and vapour when using CO_2 in the test case evaporator. This difference in behaviour between the two refrigerants is ascribed to the different pressure gradients along the channels for the two refrigerants. Using CO_2 in the test evaporator leads to very large contributions of the gravitational pressure drop contribution. In practice they may be unrealistically large but still very interesting for this study. Comparing the capacity reductions with reductions of the area covered by refrigerant in a two-phase condition shows that the reductions in capacity and in two-phase area are close to equal when imposing a non-uniform distribution of the liquid and vapour in the inlet manifold. The reductions in capacity are slightly smaller than the reduction of the two-phase area.

Non-uniform distribution of the airflow

Considering the impact of a non-uniform airflow distribution, the results show that the cooling capacity is strongly affected by the airflow non-uniformity for both refrigerants. However, the capacity reductions are more than twice as large for R134a than for CO_2. Comparing the relative reductions of the capacity to the relative reductions of the two phase area it is found that the decreases in the cooling capacity are significantly larger than decreases in the two-phase area.

Considering the two-phase area once more, we see that the two-phase area decreases at almost the same rate as the cooling capacity when imposing a non-uniform distribution of liquid and vapour. On the other hand the capacity decreases much more than the two-phase area in case of non-uniform airflow distribution. In a real system this could probably be used to identify whether non-uniform airflow or a non-uniform distribution of the liquid and vapour phases in the inlet manifold are causing capacity reductions.

Combined maldistribution

Combining non-uniform airflow and non-uniform distribution of liquid and vapour showed that a non-uniform airflow distribution to some degree can

be compensated by a suitable distribution of the liquid and vapour. It is shown that an optimum distribution of liquid and vapour at a given non-uniform airflow distribution can be obtained when the refrigerant out of both channels is fully evaporated and the superheat out of the individual channels is not exactly equal. However, if the system is controlled such that the superheat out of the individual channels is equal, the capacity is very close to the maximum. In reality this would probably be the easiest control strategy in order to recover most of the cooling capacity lost due to non-uniform airflow distribution.

Sensitivity study

A sensitivity study considering parameter changes shows that the course of the pressure gradient in the channel is significant, considering the magnitude of the capacity reductions due to non-uniform distribution of liquid and vapour and non-uniform airflow. Parameter variations that affect the ratio of the gravitational to the frictional pressure gradient, most significantly impact the capacity reductions. Furthermore, it is shown that the capacity is less sensitive to both non-uniform distribution of liquid and vapour and non-uniform airflow if the gravitational pressure gradient gives a significant contribution to the total pressure gradient. Presumably, the same benefits would be obtained if the frictional pressure drop in the first part of the channel was increased, which in practice may be a better solution than accepting a dominant contribution of the gravitational pressure gradient.

5.1 Outlook

The results presented in this thesis are based on a numerical study of the evaporator and therefore the most obvious issue for further work lies in a validation of the results against experimental data. Using an experimental set-up where both the airflow distribution and the distribution of liquid and vapour can be controlled would be ideal. However, controlling the distribution of liquid and vapour may be difficult in practice and a scenario, where the airflow distribution is controlled, while the distribution of liquid and vapour is either uniform or totally separated could be a solution to create experimental data for validation.

Furthermore, it would be interesting to extend the model such that not only two, but many parallel channels are considered. Considering the impact of a non-uniform airflow distribution, it is expected that the results obtained using two channels represent a worst case scenario. However, it would be interesting to study the impact of the distribution of liquid and vapour for

more than two parallel channels.

Another issue for further work would be to investigate the evaporator as part of the total refrigeration system. If the evaporator is part of a system, the saturation temperature at the evaporator inlet is not constant at different degrees of non-uniformity, as it was in the present study. Instead the volume flow out of the evaporator would be determined by the compressor. Non-uniform airflow distribution and non-uniform distribution of liquid and vapour would therefore not only impact the cooling capacity but also the evaporation pressure. Together these changes in capacity and evaporation pressure impact the system COP.

Non-uniform airflow and non-uniform distribution of liquid and vapour could also impact the dynamics of a system. The model used in the present study is a steady-state model, and the dynamics of the system has not been considered. With an extended, dynamic model of the evaporator, the impact of refrigerant maldistribution on the dynamics of the system could be investigated.

Bibliography

Bertsch, S. S., E. A. Groll, and S. V. Garimella (2009). A composite heat transfer correlation for saturated flow boiling in small channels. *International Journal of Heat and Mass Transfer 52*(7-8), 2110 – 2118.

Brix, W. and B. Elmegaard (2008). Distribution of evaporating CO_2 in parallel microchannels. In 8^{th} *IIR Gustav Lorentzen Conference on Natural Working Fluids*.

Brix, W. and B. Elmegaard (2009). Comparison of two different modelling tools for steady state simulation of an evaporator. In *SIMS50 - Modelling and Simulation of Energy Technology*.

Brix, W., A. Jakobsen, B. D. Rasmussen, and H. Carlsen (2007). Analysis of airflow distribution in refrigeration system. In *International Congress of Refrigeration*. ICR07-B2-581.

Brix, W., M. R. Kærn, and B. Elmegaard (2009). Modelling refrigerant distribution in microchannel evaporators. *International Journal of Refrigeration 32*(7), 1736–1743.

Brix, W., M. R. Kærn, and B. Elmegaard (2010). Modelling distribution of evaporating CO_2 in parallel minichannels. *International Journal of Refrigeration 33*(6), 1086–1094.

Caney, N., P. Marty, and J. Bigot (2007). Friction losses and heat transfer of single-phase flow in a mini-channel. *Applied Thermal Engineering 27*(10), 1715 – 1721.

Celata, G., M. Lorenzini, G. Morini, and G. Zummo (2009). Friction factor in micropipe gas flow under laminar, transition and turbulent flow regime. *International Journal of Heat and Fluid Flow 30*(5), 814 – 822.

Chen, J. C. (1966). Correlation for boiling heat transfer to saturated fluids in convective flow. *Industrial & Engineering Chemistry Process Design and Development 5*(3), 322 – 329.

Choi, K.-I., A. Pamitran, C.-Y. Oh, and J.-T. Oh (2007). Boiling heat transfer of R22, R134a, and CO_2 in horizontal smooth minichannels. *International Journal of Refrigeration 30*(8), 1336 – 1346.

Chung, P. M. Y. and M. Kawaji (2004). The effect of channel diameter on adiabatic two-phase flow characteristics in microchannels. *International Journal of Multiphase Flow 30*(7-8), 735 – 761.

Chwalowski, M., D. A. Didion, and P. A. Domanski (1989). Verification of evaporator computer models and analysis of performance of an evaporator coil. *ASHRAE Transactions 95*(1), 1229–1235.

Collier, J. G. and J. R. Thome (1994). *Convective Boiling and Condensation* (3rd ed.). Oxford Science Publications.

Danig, P. O. and H. V. Holm (1998). Fugtig luft. Technical Univesity of Denmark, Institut for Energiteknik.

Domanski, P. A. (1991). Simulation of an evaporator with nonuniform one-dimensional air distribution. *ASHRAE Transactions 97*, 793–802.

Dukler, A., M. Wicks III, and R. Cleveland (1964). Frictional pressure drop in two-phase flow. *A.I.Ch.E. Journal 10*(1), 38–51.

EES (2007). Engineering equation solver. Academic Professional V7.954-3D, F-Chart Software, Middleton, WI, USA.

Elbel, S. and P. Hrnjak (2004). Flash gas bypass for improving the performance of transcritical r744 systems that use microchannel evaporators. *International Journal of Refrigeration 27*(7), 724 – 735.

Fox, R. W. and A. T. McDonald (1998). *Introduction to fluid mechanics* (5th ed.). John Wiley & Sons.

Friedel, L. (1979). Improved friction pressure drop correlations for horizontal and vertical two-phase pipe flow. In *The European Two-Phase Flow Group Meeting*. ,Ispra, Italy, Paper No. E2.

Gnielinski, V. (1976). New equations for heat and mass-transfer in turbulent pipe and channel flow. *Iternational Chemical Engineering 16*(2), 359–368.

Hrnjak, P. (2004). Developing adiabatic two phase flow in headers - distribution issue in parallel flow microchannel heat exchangers. *Heat Transfer Engineering 25*(3), 61–68.

Hwang, Y., D.-H. Jin, and R. Radermacher (2007). Refrigerant distribution in minichannel evaporator manifolds. *HVAC&R Research 13*(4), 543–555.

Incropera, F. P. and D. P. DeWitt (2002). *Introduction to Heat Transfer* (4th ed.). John Wiley & Sons.

Jiang, H., V. Aute, and R. Radermacher (2006). Coildesigner: a general-purpose simulation and design tool for air-to-refrigerant heat exchangers. *International Journal of Refrigeration 29*, 601–610.

Kakac, S. and B. Bon (2008). A review of two-phase flow dynamic instabilities in tube boiling systems. *International Journal of Heat and Mass Transfer 51*(3-4), 399 – 433.

Kandlikar, S. G. (2007). A roadmap for implementing minichannels in refrigeration and air-conditioning systems - current status and future directions. *Heat Transfer Engineering 28*, 973–985.

Kandlikar, S. G. and W. J. Grande (2003). Flow passages—thermohydraulic performance and fabrication technology. *Heat Transfer Engineering 24*(1), 3–17.

Kew, P. A. and K. Cornwell (1997). Correlations for the prediction of boiling heat transfer in small-diameter channels. *Applied Thermal Engineering 27*, 705–715.

Kim, J.-H., J. E. Braun, and E. A. Groll (2009a). Evaluation of a hybrid method for refrigerant flow balancing in multi-circuit evaporators. *International Journal of Refrigeration 32*(6), 1283 – 1292.

Kim, J.-H., J. E. Braun, and E. A. Groll (2009b). A hybrid method for refrigerant flow balancing in multi-circuit evaporators: Upstream versus downstream flow control. *International Journal of Refrigeration 32*(6), 1271 – 1282.

Kim, M.-H. and C. W. Bullard (2002). Air-side thermal hydraulic performance of multi-louvred fin aluminium heat exchangers. *International Journal of Refrigeration 25*, 390–400.

Kim, M.-H., J. Pettersen, and C. W. Bullard (2004). Fundamental process and system design issues in CO_2 vapor compression systems. *Progress in Energy and Combustion Science 30*(2), 119 – 174.

Kirby, E. S., C. W. Bullard, and W. E. Dunn (1998). Effect of airflow nonuniformity on evaporator performance. *ASHRAE Transactions 104*(2), 755–762.

Kitto, J. B. J. and J. Robertson (1989). Effects of maldistribution of flow on heat transfer equipment performance. *Heat Transfer Engineering 10*(1), 18–25.

Knudsen, H. J. H. (2004). Refrigeration heat transfer, part ii: Cooling tower, evaporative condensers and air-coolers. Technical Univesity of Denmark, Department of Mechanical Engineering.

Kulkarni, T., C. W. Bullard, and K. Cho (2004). Header design tradeoffs in microchannel evaporators. *Applied Thermal Engineering 24*(5-6), 759 – 776.

Lombardi, C. and C. Carsana (1992). A dimensionless pressure drop correlation for two-phase mixtures flowing upflow in vertical ducts covering wide parameter ranges. *Heat and Technology 10*(1-2), 125–141.

McMullan, J. T. (2002). Refrigeration and the environment – issues and strategies for the future. *International Journal of Refrigeration 25*(1), 89 – 99.

Mueller, A. C. and J. P. Chiou (1988). Review of various types of flow maldistribution in heat exchangers. *Heat Transfer Engineering 9*, 36–50.

Müller-Steinhagen, H. and K. Heck (1986). A simple friction pressure drop correlation for two-phase flow in pipes. *Chem. Eng. Process. 20*, 291–308.

Palm, B. (2007). Refrigeration systems with minimum charge of refrigerant. *Applied Thermal Engineering 27*(10), 1693 – 1701.

Pamitran, A., K.-I. Choi, J.-T. Oh, and H.-K. Oh (2008). Two-phase pressure drop during co2 vaporization in horizontal smooth minichannels. *International Journal of Refrigeration 31*(8), 1375 – 1383.

Park, C. and P. Hrnjak (2007). CO_2 and R410a flow boiling heat transfer, pressure drop, and flow pattern at low temperatures in a horizontal smooth tube. *International Journal of Refrigeration 30*(1), 166 – 178.

Park, C. Y. and P. Hrnjak (2009). Flow boiling heat transfer, pressure drop, and flow pattern for CO_2 in a 3.5 mm horizontal smooth tube. *Journal of Heat Transfer 131*(9), 091501.

Payne, W. and P. Domanski (2003). Potential benefits of smart refrigerant distributors: Final report no. arti-21cr/610-20050-01. Technical report, Air-Conditioning and Refrigeration Technology Institute, Arlington, VA, USA.

Pettersen, J. (2004). Flow vaporization of CO_2 in microchannel tubes. *Experimental Thermal and Fluid Science 28*(2-3), 111 – 121. The International Symposium on Compact Heat Exchangers.

Revellin, R., V. Dupont, T. Ursenbacher, J. R. Thome, and I. Zun (2006). Characterization of diabatic two-phase flows in microchannels: Flow parameter results for r-134a in a 0.5 mm channel. *International Journal of Multiphase Flow 32*(7), 755 – 774.

Serizawa, A., Z. Feng, and Z. Kawara (2002). Two-phase flow in microchannels. *Experimental Thermal and Fluid Science 26*(6-7), 703 – 714.

Skovrup, M. J. (2005). Windali, v.3.34. Technical Univesity of Denmark, Department of Mechanical Engineering, http://www.et.web.mek.dtu.dk/WinDali/Index.html.

Thome, J. R. (2004-2007). *Engineering Data Book III.* Wolverine Tube, Inc. http://www.wlv.com/products/databook/db3/DataBookIII.pdf.

Thome, J. R. (2006). State-of-the-art overview of boiling and two-phase flows in microchannels. *Heat Transfer Engineering 27*(9), 4–19.

Thome, J. R. and G. Ribatski (2005). State-of-the-art of two-phase flow and flow boiling heat transfer and pressure drop of CO_2 in macro- and microchannels. *International Journal of Refrigeration 28*(8), 1149 – 1168.

Triplett, K. A., S. M. Ghiaasiaan, S. I. Abdel-Khalik, A. LeMouel, and B. N. McCord (1999). Gas-liquid two-phase flow in microchannels: Part ii: void fraction and pressure drop. *International Journal of Multiphase Flow 25*(3), 395 – 410.

Vestergaard, B. (2009). Product Marketing Manager, Micro Channel Heat Exchanger, Danfoss A/S. Personal Communication.

Vist, S. (2003). *Two-phase Flow Distribution in Heat Exchanger Manifolds.* Ph. D. thesis, Norwegian University of Science and Technology, NTNU, Norway.

Vist, S. and J. Pettersen (2003). Two-phase flow distribution in round tube manifolds. In *2nd International Conference on Heat Transfer, Fluid Mechanics and Thermodynamics*, Victoria Falls, Zambia. Paper number VS2.

Vist, S. and J. Pettersen (2004). Two-phase flow distribution in compact heat exchanger manifolds. *Experimental Thermal and Fluid Science 28*, 209–215.

Webb, R. L., K. Chung, and R. L. Webb (2005). Two-phase flow distribution to tubes of parallel flow air-cooled heat exchangers. *Heat Transfer Engineering 26*(4), 3–18.

Zhang, W., T. Hibiki, and K. Mishima (2004). Correlation for flow boiling heat transfer in mini-channels. *International Journal of Heat and Mass Transfer 47*, 5749–5763.

Appendix A

Additional graphs

A.1 Influence of neglecting pressure drop due to acceleration

When performing simulations using the evaporator model, the model turned out to have problems converging if considerable non-uniform airflow are imposed and refrigerant R134a was used. By neglecting the contribution to the pressure drop due to acceleration of the flow, the number of equations that need to be iterated could be reduced and the convergence problems disappeared. Therefore, in the calculations considering variation of the airflow distribution when using R134a this contribution to the pressure drop has been neglected in the calculations. The graphs in figures A.1 and A.2 show that the overall results are not affected by neglecting this term.

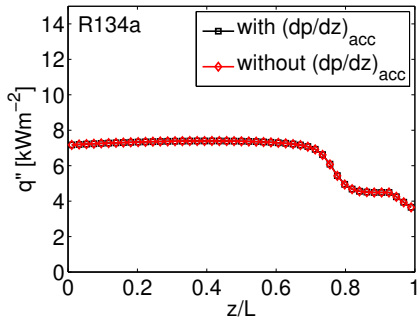

***Figure A.1**: Heat flux along the channel, calculated with and without including the pressure drop due to acceleration.*

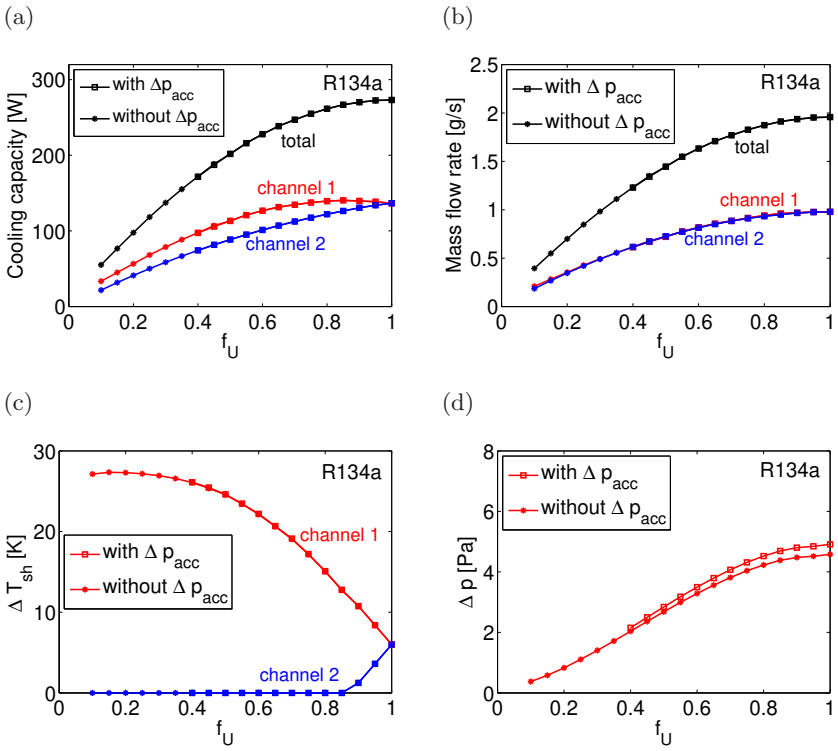

***Figure A.2**: The overall results are not affected by neglecting the pressure drop due to acceleration.*

A.2 Variable variations inside the channel

The following pages contain graphs showing different variables such as enthalpy, temperatures and heat transfer coefficients along the channel length inside the test case evaporator. Figure A.3 shows the variables using refrigerant R134a for three different distributions of the inlet qualities. Figure A.4 shows the same using CO_2 as refrigerant. Figures A.5 and A.6 show the variables using refrigerants R134a and CO_2, respectively, for three different airflow distributions.

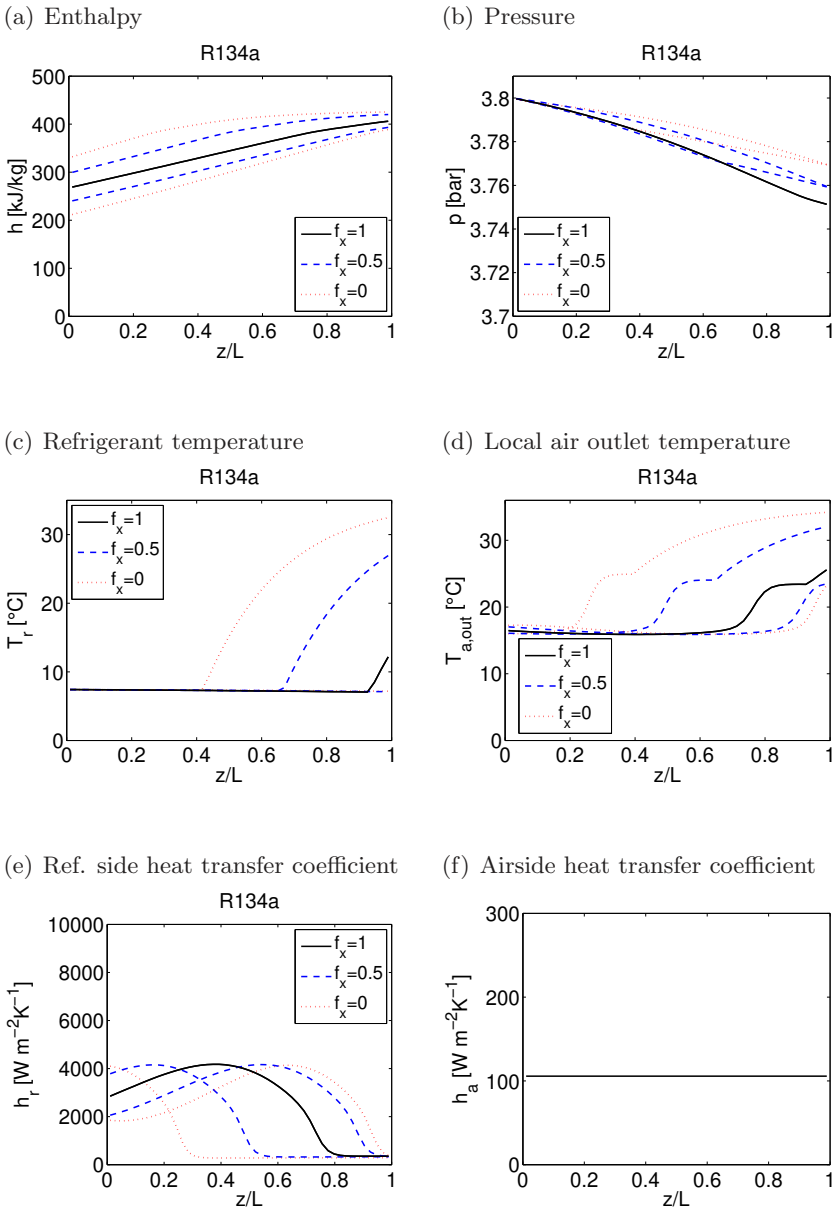

***Figure A.3**: Selected parameters shown along the channel length for three different inlet quality distributions using R134a as refrigerant.*

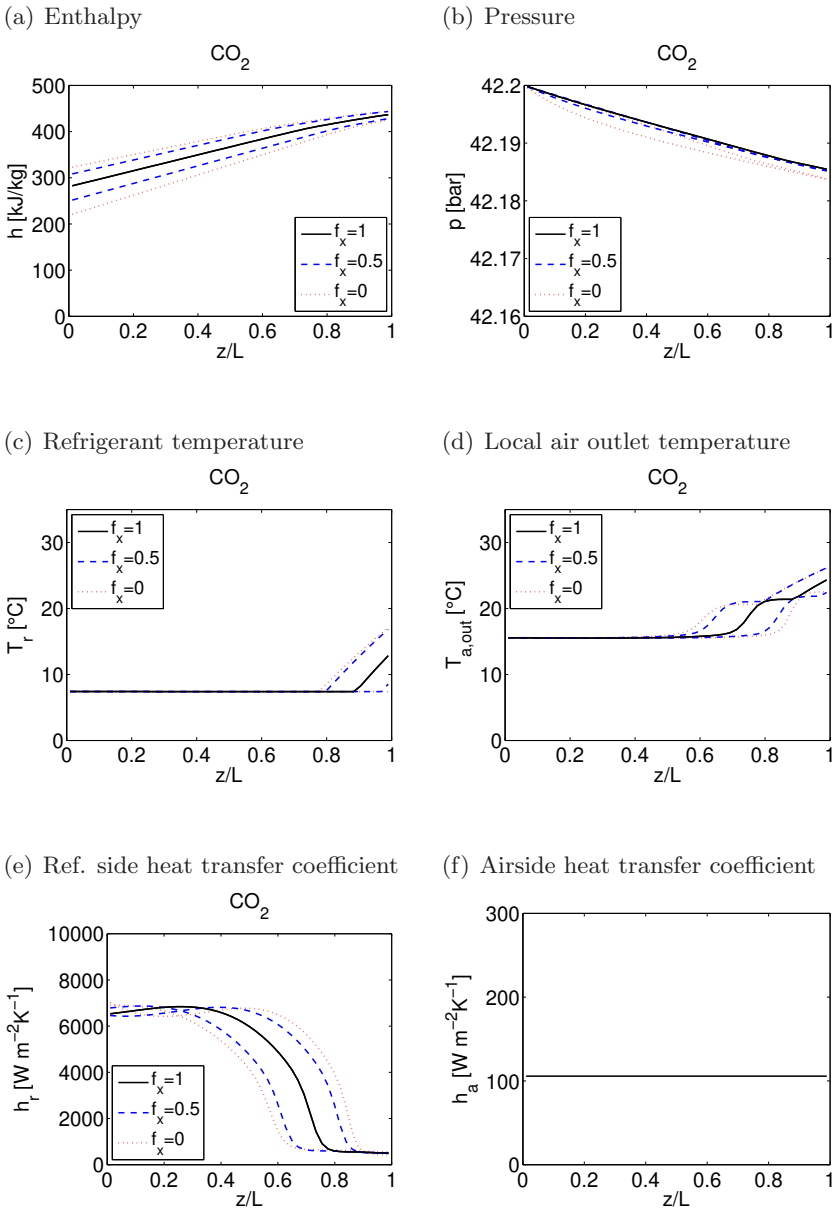

***Figure A.4**: Selected parameters shown along the channel length for three different inlet quality distributions using CO_2 as refrigerant.*

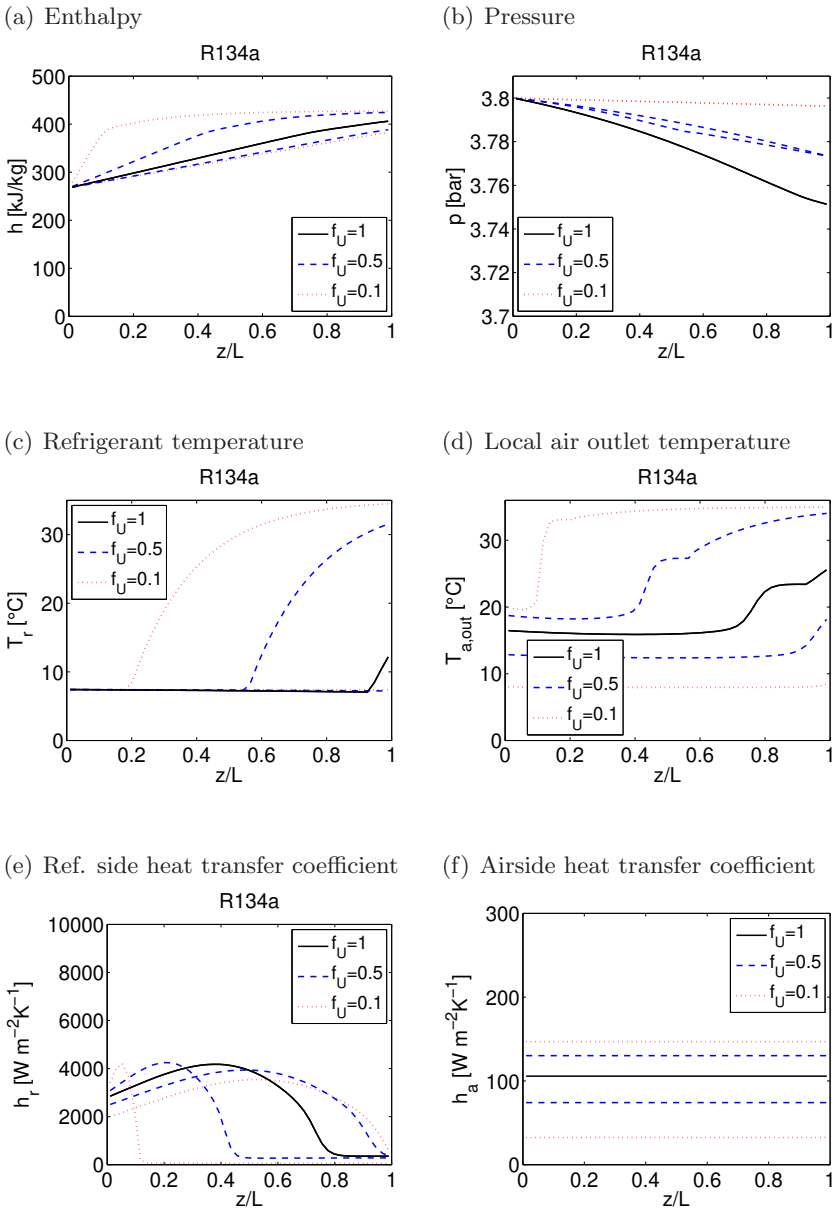

Figure A.5*: Selected parameters shown along the channel length for three different airflow distributions using R134a as refrigerant.*

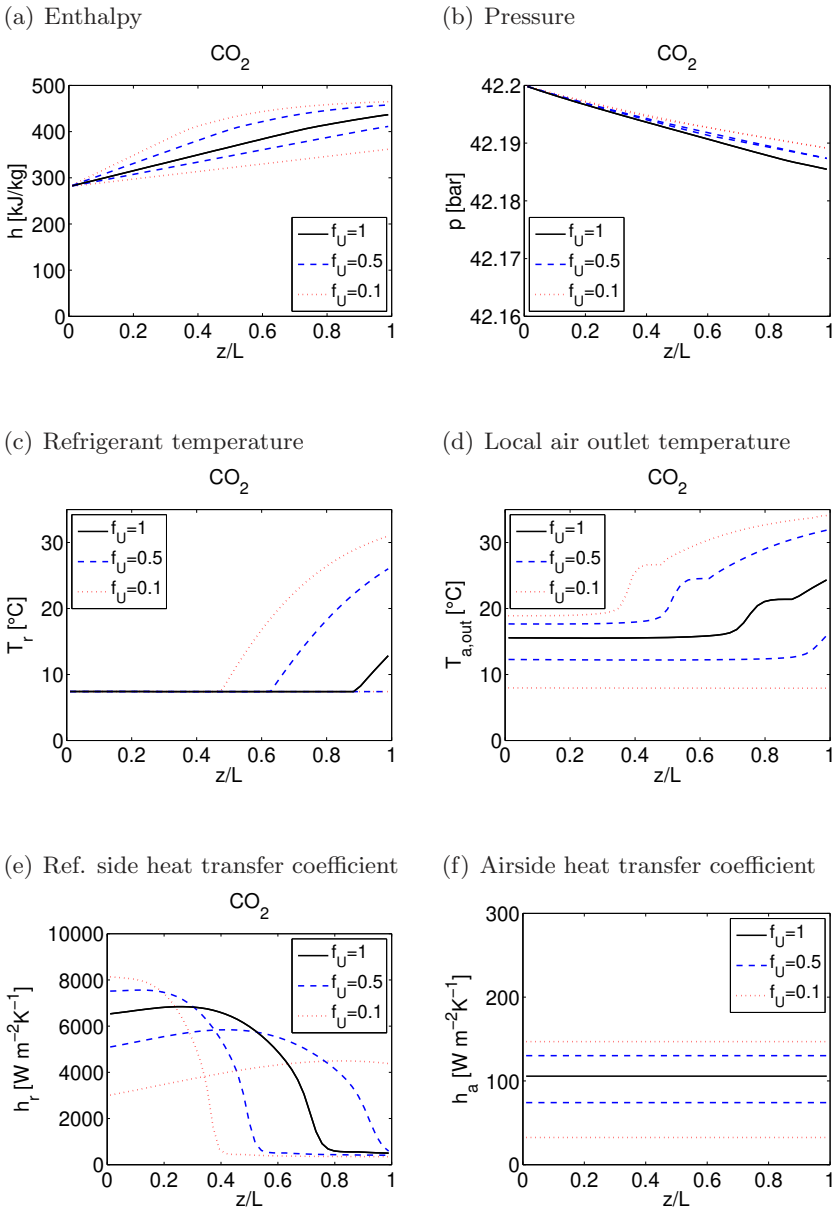

***Figure A.6**: Selected parameters shown along the channel length for three different airflow distributions using CO_2 as refrigerant.*

A.3 Mass flux vs. pressure drop

One of the instabilities that might occur in steady state flow evaporating in parallel channels is the Ledinegg instability. The Ledinegg instability has been extensively studied for more than fifty years and a review of studies on the Ledinegg instability has been performed by Kakac and Bon (2008). We will not go into great detail with this instability here, we will just explore whether the conditions for the instability to occur are present in the evaporator tested in this study.

An illustration of the conditions that determine the Ledinegg instability is shown in figure A.7. The instability occurs if the slope of the internal

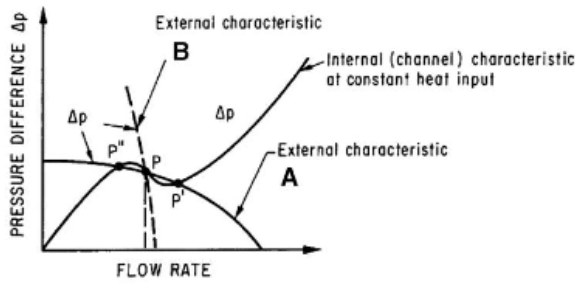

***Figure A.7**: Illustration of Ledinegg instability. Figure from Kakac and Bon (2008).*

characteristic curve, i.e. the pressure drop versus the mass flow rate in a given channel, is negative, and the external characteristic curve is less steep than the internal characteristic curve, such that the two curves have several intersections.

Usually the internal characteristic curve is shown for constant heat flux, which especially makes sense considering boilers in power plant systems. In an air cooled evaporator neither the heat flux nor the temperature is constant. Figure A.8 shows the internal characteristic curve for the evaporator defined in the present study for different values of the inlet quality and for the two refrigerants R134a and CO_2. Compared to the test case parameters defined in table 2.1 (page 25) the mass flow rate is given as an input when performing this study, such that the superheat out of the channel will vary. It is seen that the slope of the characteristic is positive in all cases for both refrigerants.

Figure A.9 shows the internal characteristic of an evaporator channel for different air velocities. In this case the inlet quality is 0.3, as defined for the test case. Also here the slopes are positive everywhere for all air velocities. It can thus be concluded that the Ledinegg instability is not expected to be a problem in the evaporator studied.

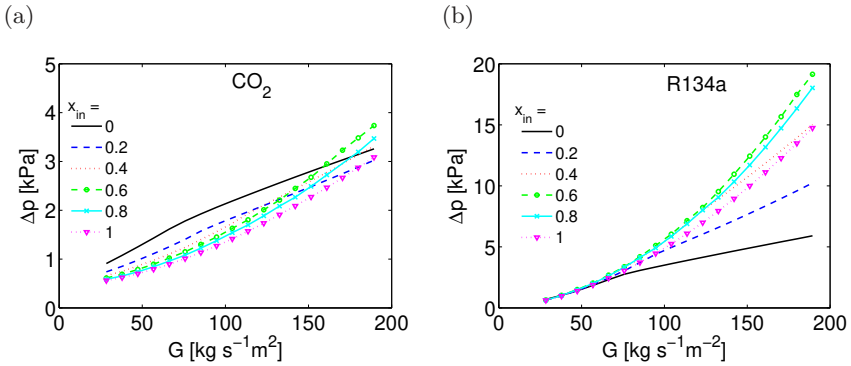

***Figure A.8**: Pressure drop in a single channel of the test case evaporator is shown as a function of the refrigerant mass flux for different inlet qualities and for refrigerants CO_2 and R134a.*

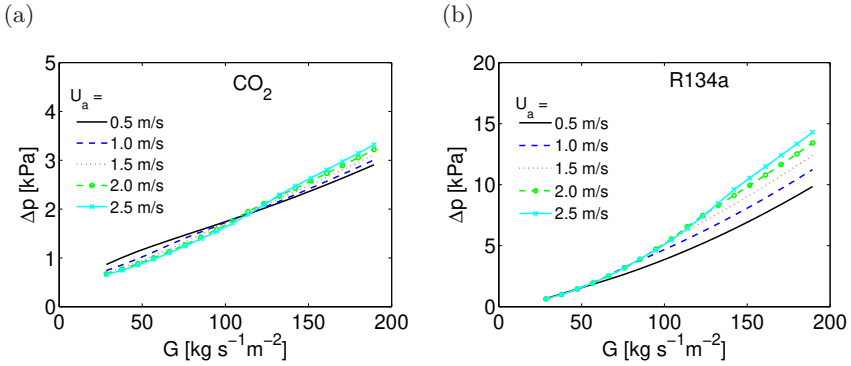

***Figure A.9**: Pressure drop in a single channel of the test case evaporator is shown as a function of the refrigerant mass flux for different air velocities and for refrigerants CO_2 and R134a.*

A.4 Changing the correlations for the two-phase heat transfer coefficent

Figures A.10 and A.11 show that the results of the mass flow rate, superheat out of the individual channels and the pressure drop are insignificantly dependent on the choice of correlation for the two-phase heat transfer correlation.

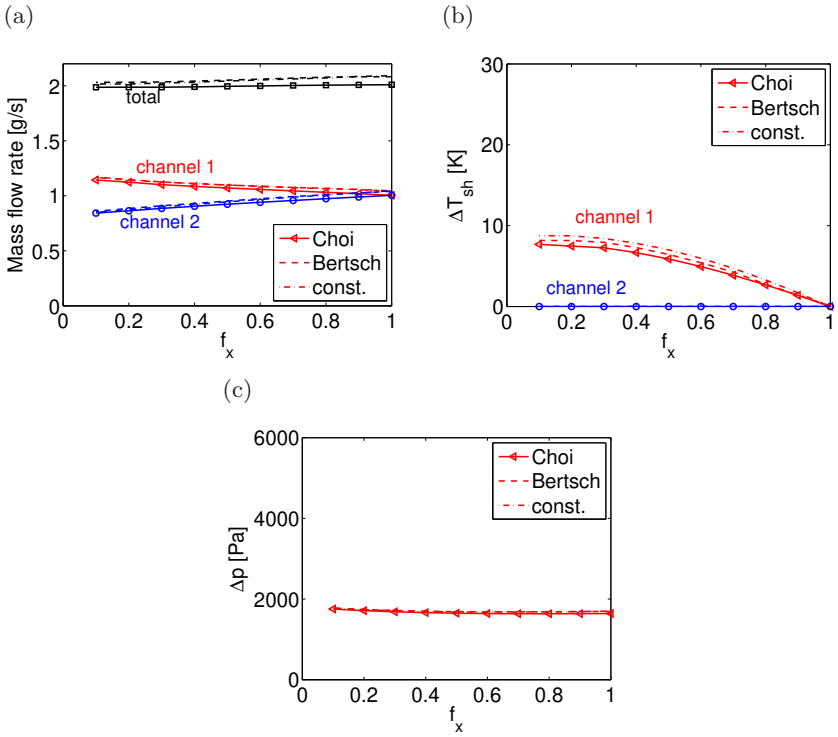

***Figure A.10**: Selected variables as a function of the gas-liquid distribution. Solutions found using three different correlations for the two-phase heat transfer coefficient.*

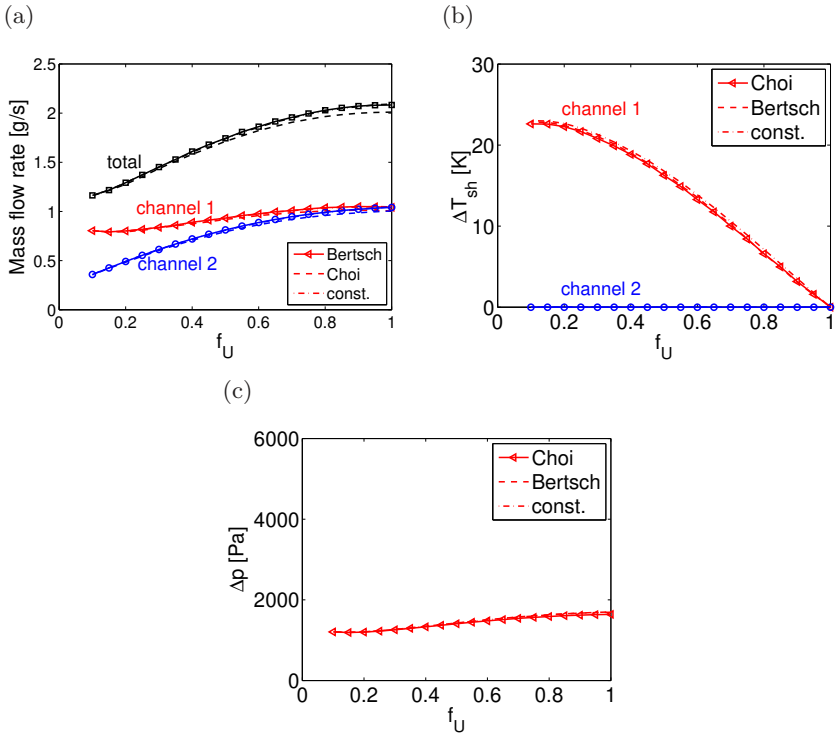

***Figure A.11**: Selected variables as a function of the airflow distribution. Solutions found using three different correlations for the two-phase heat tranfer coefficient.*

Appendix B

Publications

Paper I

Wiebke Brix, Martin Ryhl Kærn, Brian Elmegaard

Modelling refrigerant distribution in microchannel evaporators

International Journal of Refrigeration,
32(7), 1736–1743, (2009)

available at www.sciencedirect.com

ScienceDirect

journal homepage: www.elsevier.com/locate/ijrefrig

Modelling refrigerant distribution in microchannel evaporators

Wiebke Brix[a,*], Martin Ryhl Kærn[a,b], Brian Elmegaard[a]

[a]Department of Mechanical Engineering, Technical University of Denmark, Nils Koppels Allé Bygn. 402, DK-2800 Lyngby, Denmark
[b]Danfoss A/S, Refrigeration and Air Conditioning, Nordborgvej 81, DK-6430 Nordborg, Denmark

ARTICLE INFO

Article history:
Received 24 June 2008
Received in revised form
13 March 2009
Accepted 10 May 2009
Published online 20 May 2009

Keywords:
Heat exchanger
Evaporator
Microchannel
Review
Distribution
R134a
Modelling
Simulation
Heat transfer

ABSTRACT

The effects of refrigerant maldistribution in parallel evaporator channels on the heat exchanger performance are investigated numerically. For this purpose a 1D steady state model of refrigerant R134a evaporating in a microchannel tube is built and validated against other evaporator models. A study of the refrigerant distribution is carried out for two channels in parallel and for two different cases. In the first case maldistribution of the inlet quality into the channels is considered, and in the second case a non-uniform airflow on the secondary side is considered. In both cases the total mixed superheat out of the evaporator is kept constant. It is shown that the cooling capacity of the evaporator is reduced significantly, both in the case of unevenly distributed inlet quality and for the case of non-uniform airflow on the outside of the channels.

Modélisation de la distribution du frigorigène dans les évaporateurs à microcanaux

Mots clés : Échangeur de chaleur ; Évaporateur ; Microcanal ; Enquête ; Distribution ; R134a ; Modélisation ; Simulation ; Transfert de chaleur

1. Introduction

In many air conditioning and refrigeration systems a reduction of the overall system size is an important development goal. The use of compact heat exchangers helps achieving this target. Especially aluminum braced microchannel heat exchangers, with channel sizes in the 1 mm range are becoming more and more popular, since these heat exchangers not only aid

* *Corresponding author*. Tel.: +45 4525 4130; fax: +45 4593 5215.
E-mail address: wb@mek.dtu.dk (W. Brix).
0140-7007/$ – see front matter © 2009 Elsevier Ltd and IIR. All rights reserved.
doi:10.1016/j.ijrefrig.2009.05.006

reducing system sizes but also reduce the refrigerant charges needed in order to obtain a given cooling capacity.

Due to the small channel sizes a design with many parallel channels is required in order to keep the pressure drops at an acceptable level. For evaporators, where the entering fluid is usually in a two-phase state the use of many parallel channels induces problems of maldistribution of the refrigerant. This maldistribution of the refrigerant mass flow rates may appear due to maldistribution of the two phases in the dividing manifold or header, or due to maldistribution of the airflow or air temperatures on the secondary side of the heat exchanger.

The impact of a non-uniform airflow on the heat exchanger performances has been addressed in several studies. In a study by Chwalowski et al. (1989) it was shown experimentally that a capacity reduction of up to 30% could be found for a fin and tube evaporator in an air-conditioning duct that was exposed to a non-uniform airflow. However, it was not investigated how much of the capacity degradation appeared due to maldistribution of the airflow only, and how much originated from the resulting maldistribution of the refrigerant. In a numerical study performed by Domanski (1991) different airflow profiles were applied on a fin and tube evaporator, and the results showed reductions of the cooling capacity of up to 25%.

Choi et al. (2003) conducted experiments with R22 in a finned tube evaporator with 3 circuits to determine the capacity reduction due to non-uniform distribution of the refrigerant and airflow distribution. Results showed that for maldistributed refrigerant flow the capacity degradation could be as much as 30%, even when the superheat of the refrigerant was controlled to compensate for the degradation. Moreover, the study on a maldistributed airflow showed a maximum capacity degradation of 8.7%.

Considering the liquid/gas distribution in the manifold, several studies on two-phase flow distribution in manifolds or headers have been carried out for both conventional and microchannel evaporators. Vist and Pettersen (2004a) studied a manifold with 10 parallel evaporator channels and R134a as refrigerant experimentally. Both the liquid/gas distribution and the heat load on the different channels were investigated and a similar study was performed using CO_2 as refrigerant (Vist and Pettersen, 2004b). Hwang et al. (2007) investigated the distribution of the liquid phase in a manifold for a microchannel evaporator, considering different inlet locations. However, these studies focus primarily on the distribution in the header, and not on its effects on the heat exchanger performance.

The objective of the present study is to investigate the effects of maldistribution of refrigerants in parallel evaporator channels on the heat exchanger performance by numerical simulation. Both the maldistribution generated in the header, i.e. the distribution of liquid and vapour into the different channels, and the maldistribution of refrigerant occurring due to unevenly distributed air velocities are considered.

2. Method

In order to model the evaporator, a discretized 1D-model of a single microchannel tube is built using a finite volume method. A microchannel tube is here defined as one tube containing several flow ports for the refrigerant. On the air side louvered fins are assumed on each side of the tube, but only half of the fin length on each side is accounted to belong to the specific channel. The other half belongs to the neighbouring channel. In Fig. 1 a sketch of two microchannel tubes is shown.

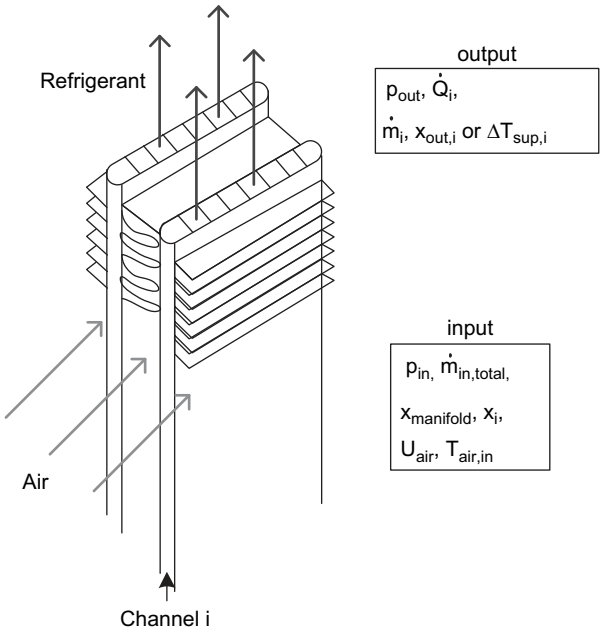

Fig. 1 – Sketch of two channels in parallel with input and output parameters to the model.

Each channel is discretized into an optional number of volumes, and each volume is treated as a small heat exchanger. For each volume the continuity equation, the momentum equation and the energy equation are solved under the assumption of steady state. No conduction is assumed between the different volumes. The mathematical modelling and solving of the final system of equations is performed using Engineering Equation Solver, EES (2007). The software solves the algebraic equations numerically using a Newton–Raphson method. The required accuracy of the solution is reached when the relative residuals are lower than 10^{-6}.

Table 1 – Summary of correlations used to calculate heat transfer coefficients and pressure drop.

Air side	
Heat transfer coefficient	Kim and Bullard (2002)
Two-phase region	
Heat transfer coefficient	Zhang et al. (2004) + smooth transition to single phase
Void fraction	Homogeneous model
Gravitational pressure drop	Homogeneous model
Accelerational pressure drop	Homogeneous model
Frictional pressure drop	Müller-Steinhagen and Heck (1986)
Single-phase region	
Heat transfer coefficient	Gnielinski (2002)
Frictional pressure drop	Blasius (2002)

In order to calculate the frictional pressure drop and heat transfer, coefficients validated correlations from the literature are applied, depending on the flow conditions. Table 1 summarizes the correlations that have been chosen.

The correlations used for calculating the frictional pressure drop for both two-phase and single-phase flow are correlations developed for conventional channels, but are here applied for microchannels. Revellin (2006) compared a wide range of pressure drop correlations, developed for both small channels and conventional channels, against experimental data of evaporating R134a in small channels. It was found that the (Müller-Steinhagen and Heck, 1986) correlation best predicted the data. For single-phase pressure drop, Caney et al. (2007) show that the conventional correlations predict pressure drop in a mini-channel well.

As mentioned in Table 1 a correlation presented by Zhang et al. (2004) is used to calculate the heat transfer coefficient on the refrigerant side in the two-phase region. However, this correlation is only valid for qualities <0.7, and does not take dryout into account. Therefore, the heat transfer coefficient for $0.7 < x < 1$ has to be found differently. This is done in a relatively simple, purely mathematical way. A smooth transition function, based on a tanh-function, is applied to connect the value of the heat transfer coefficient calculated by the Zhang et al. (2004) correlation and the single-phase heat transfer coefficient that is obtained at dry conditions.

Fig. 2 shows the development of the heat transfer coefficient as a function of quality under the conditions specified in the figure. Numerically this smooth transition between the different heat transfer coefficients is an advantage, since the equations are solved more stably when no large discontinuities are present.

A sensitivity analysis shows that the choice of correlations for calculation of the heat transfer coefficient only plays a minor role on the final results as long as the general trend is kept. For this reason it is assumed that the extended Zhang correlation is a reasonable choice in the two-phase flow. For single-phase heat transfer again a correlation developed for conventional channels is used. Since the heat transfer in single-phase flow is much lower than in the two-phase flow area, it is assumed that the choice of correlation does not affect the final results.

In order to investigate the influence of maldistribution of refrigerant in several parallel channels, the single channel models have to be connected. Although each microchannel tube contains a number of small parallel channels, it is assumed that there is no maldistribution of the refrigerant between the different ports in one microchannel tube, such that maldistribution can solely occur between the different tubes.

The different tubes are connected through, first of all, conservation of the total mass flow rate:

$$\dot{m}_{\mathrm{in,total}} = \sum_{i=1}^{N} \dot{m}_i, \tag{1}$$

where N is the total number of channels. Secondly, no pressure drop is assumed in the inlet or outlet manifolds, such that the total pressure drop over each tube has to be equal:

$$\Delta p_i = p_{\mathrm{in}} - p_{\mathrm{out}}. \tag{2}$$

Furthermore the manifolds are assumed to be adiabatic, and therefore the gas and liquid phases are conserved in the manifolds:

$$\dot{m}_{\mathrm{in,total}} x_{\mathrm{in,total}} = \sum_{i=1}^{N} \dot{m}_i x_i, \tag{3}$$

The pressure drop across any tube depends on the mass flow rate, inlet quality and heat load, and since the inlet quality is known and the heat load is calculated for each channel, the final distribution of mass flow rate between the channels is found.

3. Validation of the model

The microchannel evaporator model is validated against results obtained using the modelling software CoilDesigner (Jiang et al., 2006). A test case based on R134a evaporating in

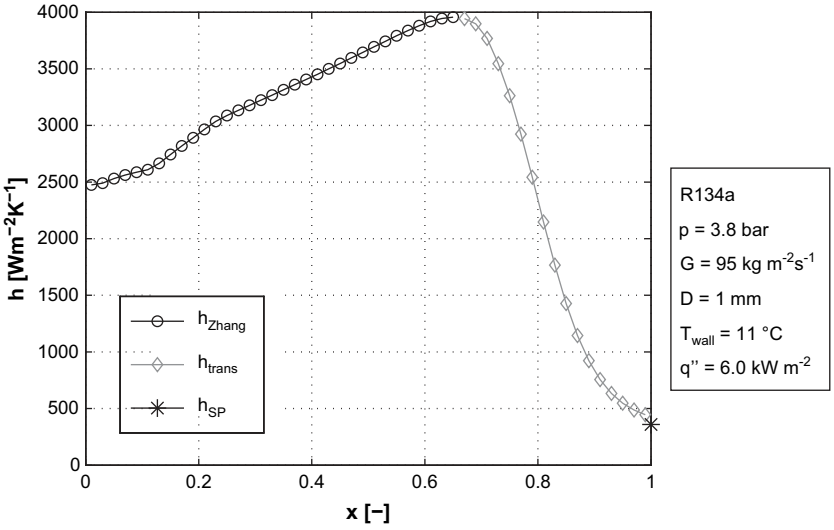

Fig. 2 – Development of the heat transfer coefficient in the two-phase region as a function of quality for the test conditions shown to the right.

Table 2 – Parameters defining the test case.

Evaporator geometry	
Tube length	0.47 m
# of ports in one tube	11
Cross-section of one port	0.8 × 1.2 mm
Flow depth	16 mm
Distance between two microchannels	8 mm
Fin pitch	727 m^{-1}
Flow parameters	
Air temperature	35 °C
Air velocity	1.6 m/s
Evaporation temperature	7.4 °C
Quality at manifold inlet	0.3
Total superheat	6 K

a microchannel tube is defined for validation and for the case study presented in the following. The parameters defining the heat exchanger geometry and the flow conditions are specified in Table 2.

In CoilDesigner a microchannel geometry is chosen and all geometry parameters are chosen to match the test case. Also correlations calculating the heat transfer and pressure drop need to be chosen. On the air side and for single-phase refrigerant, the same correlations are used for the CoilDesigner model and the present model. For two-phase heat transfer and frictional pressure drop this option was not available, therefore two different sets of available correlations are chosen. One case uses correlations presented by Jung and Radermacher (Jiang et al., 2006) for both the heat transfer coefficient and the frictional pressure drop. The other case uses a correlation presented by Shah (Jiang et al., 2006) for the heat transfer coefficient, and the homogeneous model for frictional pressure drop.

A model of one single channel is then compared to the results given by the CoilDesigner software and showed good agreement. In Table 3 some key parameters are summarized.

The best agreement is found between this model and the CoilDesigner 1 case. For CoilDesigner 1, the Jung and Radermacher correlations are used for two-phase heat transfer and pressure loss. Especially the pressure drop in the channel agrees very well, whereas the homogeneous pressure model predicts a considerably lower pressure drop. The overall heat transfer rate for the channel differs by only 4% between this model and the CoilDesigner 1 case, although there are significant differences in how the two-phase heat transfer coefficient is calculated. For both the Jung and Radermacher correlation and the Shah correlation the two-phase heat transfer coefficient is increasing or constant until the quality approaches $x = 1$, whereas the heat transfer coefficient used here, starts to decrease at a quality around $x = 0.7$, where it is assumed that dryout begins. Fig. 3 shows the temperatures of the refrigerant and the air outlet as calculated by the three models. It increases at a shorter distance from the inlet in the present model compared to the other models due to the decrease in the two-phase heat transfer coefficient. Otherwise both the refrigerant temperature and the air outlet temperature agree for the three models. We believe that the present model is more in accordance with reality as it accounts for dryout. We find that the model is verified.

Table 3 – Key parameters calculated by the different models. For CoilDesigner 1 the Jung and Radermacher correlations were applied, while for CoilDesigner 2 the Shah correlation and the homogeneous friction model were used.

	This model	CoilDesigner 1	CoilDesigner 2
Heat transfer rate, W	139.4	133.5	129.4
Mass flow rate, g/s	1.00	0.951	0.921
Total pressure drop, Pa	5000	4557	2493
Avg. $h_{r,TP}$, W m^{-2} K^{-1}	2850	3250	2389

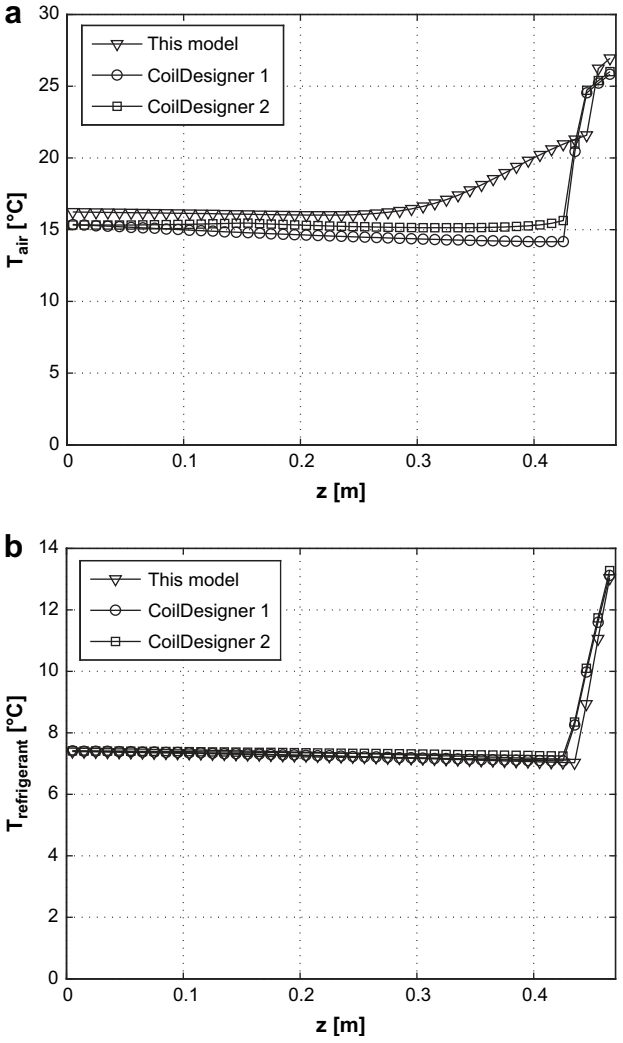

Fig. 3 – Comparison of the refrigerant temperature and the air outlet temperature along the channel. For CoilDesigner 1 the Jung and Radermacher correlations were applied, while for CoilDesigner 2 the Shah correlation and the homogeneous friction model were used.

4. Results and discussion

Using the model a case study is performed with two channels in parallel. The geometry and flow parameters were the same as specified in Table 2. The two channels are vertically oriented with the refrigerant flowing in the upwards direction. Two different cases are investigated. First, maldistribution of the inlet quality distribution into the two channels is considered, whereas the airflow is assumed to be uniformly distributed. Second, a non-uniform airflow is imposed, while the inlet quality is equal for both channels. For both cases the total superheat of refrigerant out of the exit manifold is kept constant as indicated in Table 2. The total mass flow rate of refrigerant in the two channels can thus vary depending on the distribution.

4.1. *Maldistribution of inlet quality*

The evaporator is usually fed by a mixture of liquid and vapour. How the two phases will distribute in the header depends on many parameters such as the header geometry, mass flow rates and refrigerant properties. The distribution of the two phases does influence the inlet quality into the different parallel channels. Since the flow in the header is not modelled in detail in the evaporator model used for this study, maldistribution of the inlet quality is studied by simply varying the inlet quality to the different channels.

In the first case considered, the inlet quality to each of the channels is varied, while the inlet quality to the header is kept constant at $x = 0.3$. The airflow is assumed to be uniformly distributed. The two microchannel tubes are numbered channel 1 and channel 2, and the inlet quality to the channels is varied such that the quality into channel 1 is increased and decreased in channel 2. Since the manifold is considered adiabatic, Eq. (3) has to be fulfilled at all times.

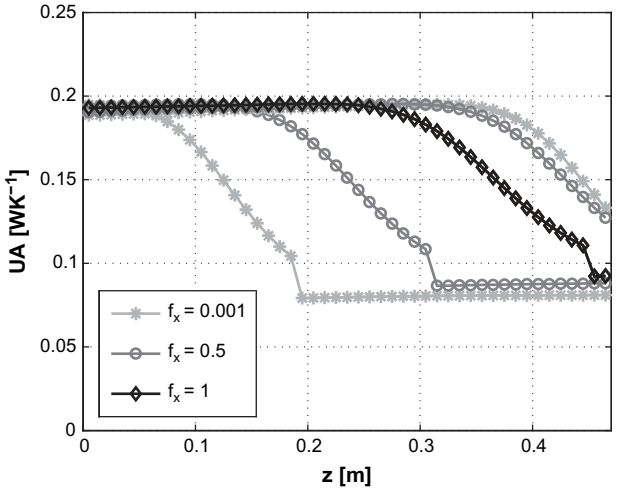

Fig. 4 – Local UA-values through the channel for three different inlet quality distributions. The two lines showing the UA-values in the case of equal distribution ($f_x = 1$) coincide, while for the two other cases each line shows the UA-value in one of the channels.

Table 4 – Mean UA-values for the two parallel channels together.

	$f_x = 1$	$f_x = 0.5$	$f_x = 0.001$
Mean UA-value, $W K^{-1}$	0.1741	0.1644	0.1501

A distribution parameter, f_x, is defined in order to quantify the distribution in a simple way:

$$f_x = \frac{x_2}{x_{manifold}}, \quad 0 \le f_x \le 1. \tag{4}$$

For equal distribution of the inlet quality $f_x = 1$, while for $f_x = 0$ only liquid is fed into channel 2 and a remaining mixture of liquid and gas goes into channel 1.

Fig. 4 shows the local UA-values, calculated along the channel, for three different distributions of the inlet quality. The local UA-values are calculated based on the local heat transfer coefficients and neglecting the conduction resistance in the channel wall:

$$\frac{1}{UA} = \frac{1}{h_r A_r} + \frac{1}{\eta_f h_a A_a}. \tag{5}$$

In the case of equal distribution, i.e. $f_x = 1$ the two lines coincide. At the channel inlet the local UA-values are more or

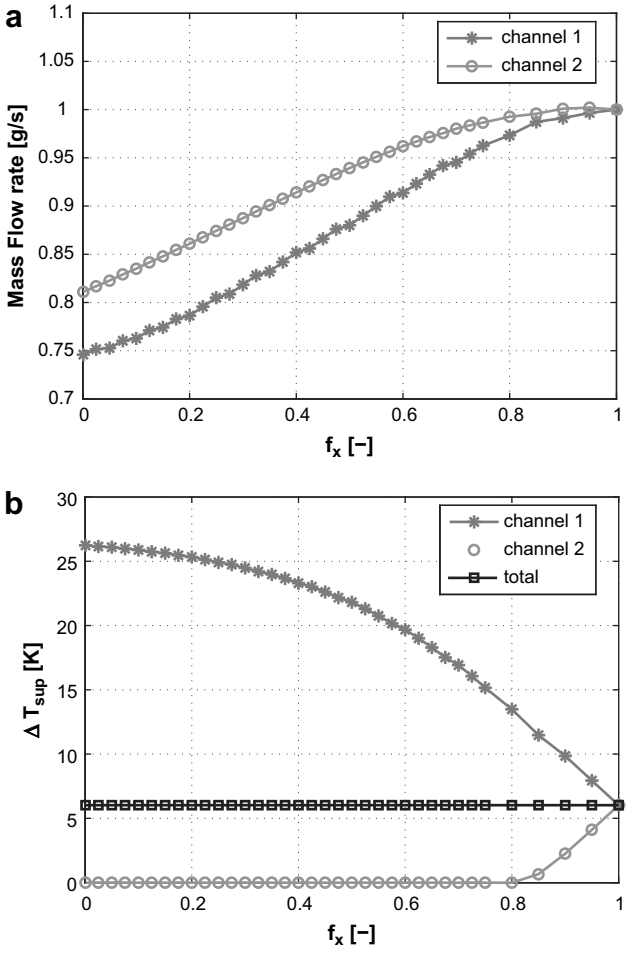

Fig. 5 – Influence of inlet quality distribution on the mass flow rate and on the outlet superheat.

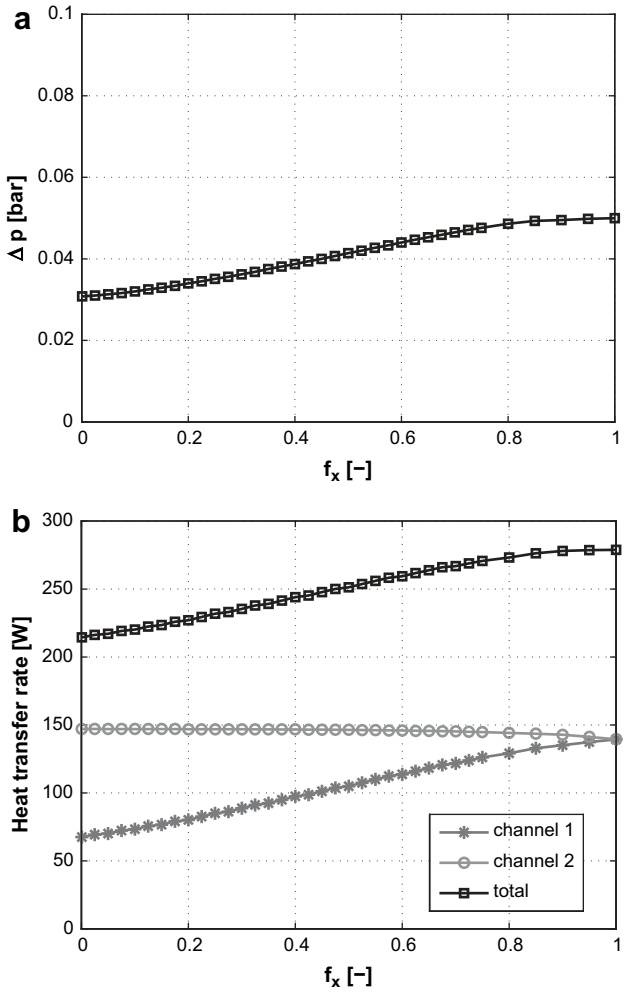

Fig. 6 – Influence of inlet quality distribution on the mass flow rate and on the outlet superheat.

less the same, independent of the inlet quality distribution. Following the flow in the channel, the UA-values stay constant at this level until dryout starts, and this position differs for the different inlet quality distributions. Shortly before only single-phase flow remains in the channel a jump in the curves can be seen. This jump occurs since the transition between the two-phase and single-phase heat transfer coefficients is not completely smooth in the model.

Comparing the two maldistributed cases to the equally distributed case, it is noticed that the beginning of dryout happens much earlier in channel 1, while it is delayed considerably less in channel 2. Integrating the UA-values of the two connected channels divided by the channel length gives a mean UA-value. In Table 4 these mean values are listed for the three distributions of the inlet quality. As expected the mean UA-value for the two channels together decreases with increasing maldistribution. As a consequence the heat transfer rate decreases for increased maldistribution of the inlet quality.

The distribution of the refrigerant mass flow rate in the two channels depends on the pressure gradients in the two channels. Since the pressure gradients along the channels are different, but the total pressure drop is the same for the two

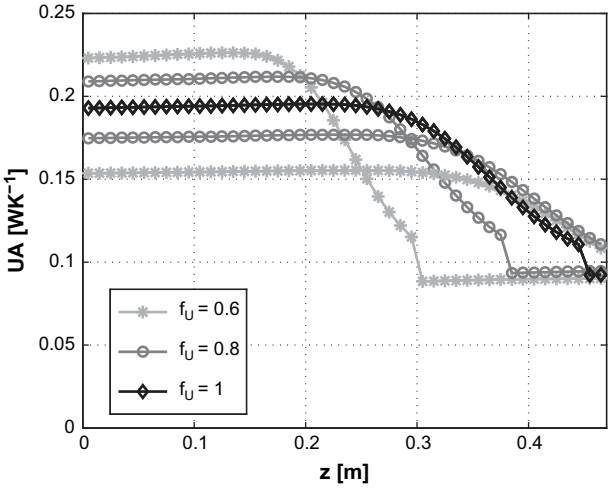

Fig. 7 – Local UA-values through the channel for different distributions of the airflow. The inlet quality on the refrigerant side is kept constant at $x = 0.3$ for all channels.

channels, the mass flow rate distributes according to these requirements. Fig. 5 shows the distribution of the refrigerant mass flow rate and the superheat out of each of the channels as a function of f_x. For increasing maldistribution of the inlet quality, the total mass flow rate decreases in order to keep a constant superheat. It is furthermore noticed that the mass flow decreases more in channel 1, which is the channel with a higher fraction of gas at the inlet. The superheat at the outlet of channel 1, shown in the lower graph of Fig. 5, approaches the air temperature for increased maldistribution, while not all of the liquid evaporates in channel 2 at inlet quality distributions of $f_x < 0.8$.

The reduction in the total mass flow rate together with the decreasing mean UA-value, results in a reduction of the cooling capacity of the two channels, which is shown in Fig. 6. It is seen that the cooling capacity of channel 2, which receives more and more liquid for increasing maldistribution, is more or less constant. The cooling capacity of channel 1 on the other hand decreases significantly. When only liquid enters into channel 2 and the remaining mixture enters channel 1, the total cooling capacity is reduced by 23%. This is thus the upper limit of the influence of maldistribution for the present case.

The upper graph in Fig. 6 shows the total pressure drop over the two channels. It is seen that the pressure drop over the evaporator channels decreases for increasing maldistribution. Future studies will investigate how this affects the total system performance.

Table 5 – Mean UA-values for the two parallel channels together.

	$f_U = 1$	$f_U = 0.8$	$f_U = 0.6$
Mean UA-value, W K^{-1}	0.1741	0.1690	0.1546

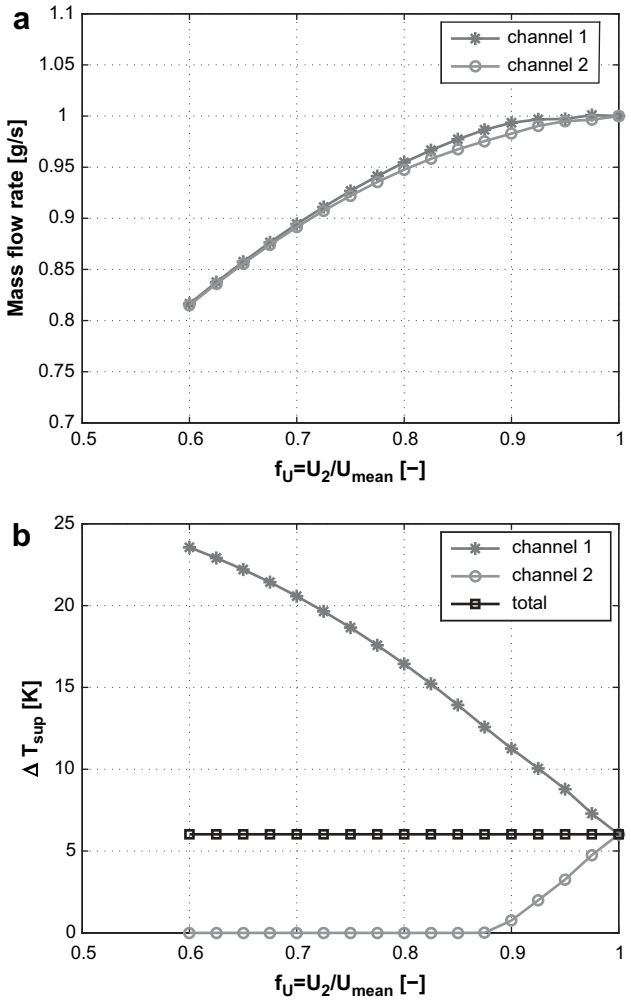

Fig. 8 – Influence of airflow maldistribution on the mass flow rate and on the outlet superheat.

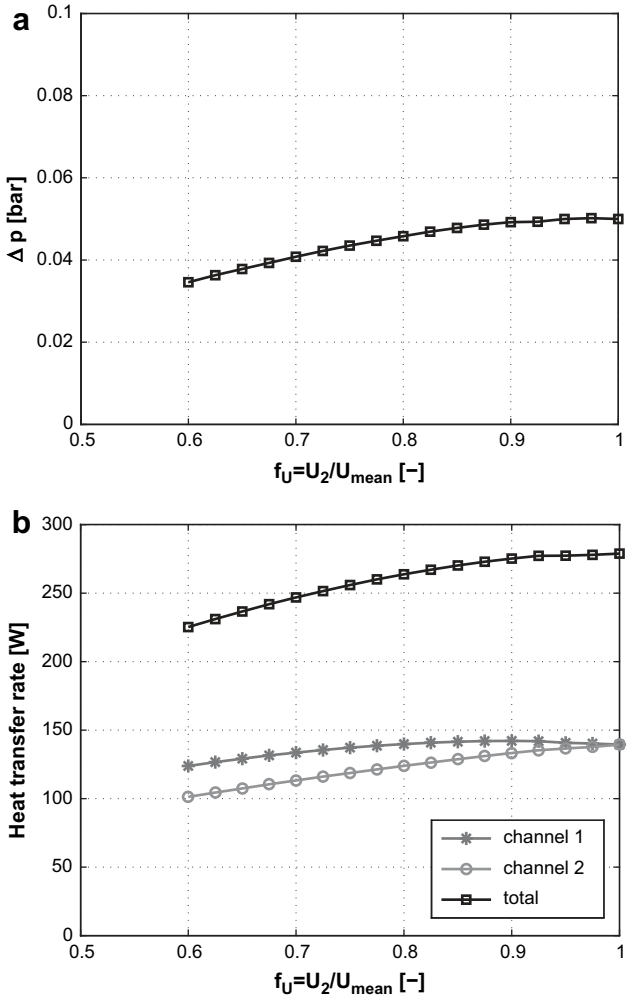

Fig. 9 – Influence of airflow maldistribution on the mass flow rate and on the outlet superheat.

4.2. *Maldistribution of airflow*

Maldistribution of the airflow also affects the distribution of refrigerant in the parallel channels. In this second case considered, the inlet quality is kept constant at 0.3 for both channels, while the airflow distribution is varied. The total volume flow rate of air is kept constant, and hence the mean velocity of the airflow. For simplicity the maldistribution of the airflow is imposed such that the air velocity is increased over the whole channel 1 and decreased over channel 2.

Again, a maldistribution parameter is defined in order to quantify the maldistribution:

$$f_U = \frac{U_2}{U_{mean}}, \quad 0 \le f_U \le 1, \tag{6}$$

where $f_U = 1$ for equal air velocities on both channels, while $f_U = 0$ when there is no airflow on channel 2, and all airflows by channel 1 only.

Fig. 7 shows the local UA-values along the two channels for three different distributions of the airflow. In this case the local UA-values at the channel inlet differ for the different distributions, because the air side heat transfer coefficient depends on the air velocity. However, the increase of the UA-value in the channel with the higher air velocity almost corresponds to the decrease in the other channel. Also in this case the position of the beginning dryout changes with the distribution. Mean UA-values are shown in Table 5. It is seen that the mean UA-value for the two channels decrease with increased maldistribution of the airflow rate.

Due to the lower average overall heat transfer coefficient for increased maldistribution, the total mass flow rate decreases in order to keep a constant superheat. For small degrees of maldistribution on the air side, i.e. $f_U > 0.9$ only very small changes in the total mass flow rate are found, which is shown in Fig. 8. For more non-uniform airflows the mass flow rate starts to decrease significantly. For a non-uniform distribution with $f_U = 0.6$, the total mass flow rate on the refrigerant side has decreased by almost 20%. It is noticeable that the mass flow rate decreases equally in both channels. If this is general or specific for the choice of geometry and flow parameters needs to be investigated further. The lower graph in Fig. 8 shows the superheat out of the two channels. For $f_U < 0.88$ not all of the refrigerant evaporates in channel 2, and a mixture of liquid and gas exits this channel.

Fig. 9 shows the cooling capacity and total pressure drop as a function of the maldistribution parameter. The cooling capacity of channel 1 increases slightly for small degrees of maldistribution on the air side, but starts to decrease for $f_U < 0.9$. In channel 2 the cooling capacity decreases steadily for increased maldistribution. As a result of this the total cooling capacity is almost constant for $0.9 < f_U < 1$ and then decreases for decreasing f_U. When $f_U = 0.6$, which corresponds to an air velocity of 2.24 m/s on channel 1 and 0.96 m/s on channel 2, the cooling capacity is decreased by 19%.

From the results it seems, that the maldistribution of the airflow mainly influences the heat exchanger performance as soon as one of the channels runs wet at the exit. For the case shown here it happened at $f_U = 0.88$.

5. Conclusions

A model of a microchannel evaporator was built in order to numerically investigate the effects of refrigerant maldistribution in the parallel channels on the heat exchanger performance. The model was validated against an evaporator modelled using the software CoilDesigner (Jiang et al., 2006). Good agreement was found between the two models. A case study for two channels in parallel was performed using a fixed heat exchanger geometry. It was studied how both the maldistribution generated in the header due to the two-phase flow distribution and the maldistribution that occurs due to an uneven airflow distribution influences the heat exchanger performance. It was shown that in both cases, the total cooling capacity was reduced for increased maldistribution.

REFERENCES

Blasius, P.R.H., 2002. VDI Wärmeatlas, ninth ed. Springer-Verlag. Ch. Lab.

Choi, J.M., Payne, W.V., Domanski, P.A., 2003. Effects of non-uniform refrigerant and air flow distribution of finned-tube evaporator performance. In: Proceedings of the International Congress of Refrigeration, Washington, DC, USA, ICR0040.

Chwalowski, M., Didion, D.A., Domanski, P.A., 1989. Verification of evaporator computer models and analysis of performance of an evaporator coil. ASHRAE Transactions 95 (1), 793–802.

Caney, N., Marty, P., Bigot, J., 2007. Friction losses and heat transfer of single-phase flow in a mini-channel. Applied Thermal Engineering 27, 1715–1721.

Domanski, P.A., 1991. Simulation of an evaporator with nonuniform one-dimensional air distribution. ASHRAE Transactions 97, 793–802.

EES, 2007. Engineering equation solver. Academic Professional V7. 954-3D, F-Chart Software, Middleton, WI, USA.

Gnielinski, V., 2002. VDI Wärmeatlas, ninth ed. Springer-Verlag. Ch. Ga.

Hwang, Y., Jin, D.-H., Radermacher, R., 2007. Refrigerant distribution in minichannel evaporator manifolds. HVAC&R Research 13 (4), 543–555.

Jiang, H., Aute, V., Radermacher, R., 2006. Coildesigner: a general-purpose simulation and design tool for air-to-refrigerant heat exchangers. International Journal of Refrigeration 29, 601–610.

Kim, M.-H., Bullard, C.W., 2002. Air-side thermal hydraulic performance of multi-louvred fin aluminium heat exchangers. International Journal of Refrigeration 25, 390–400.

Müller-Steinhagen, H., Heck, K., 1986. A simple friction pressure drop correlation for two-phase flow in pipes. Chemical Engineering and Processing 20, 291–308.

Revellin, R., 2006. Experimental two-phase fluid flow in microchannels. Ecole Polytechnique Fédérale de Lausanne, Switzerland, Thesis no. 3437, http://library.epfl.ch/en/theses/?nr=3437.

Vist, S., Pettersen, J., 2004a. Two-phase flow distribution in compact heat exchanger manifolds. Experimental Thermal and Fluid Science 28, 209–215.

Vist, S., Pettersen, J., 2004b. Two-phase flow distribution in round tube manifolds. ASHRAE Transactions 110 (1), 307–317.

Zhang, W., Hibiki, T., Mishima, K., 2004. Correlation for flow boiling heat transfer in mini-channels. International Journal of Heat and Mass Transfer 47, 5749–5763.

Paper II

Wiebke Brix, Martin Ryhl Kærn, Brian Elmegaard

Modelling distribution of evaporating CO_2 in parallel minichannels

International Journal of Refrigeration,
33(6), 1086–1094, (2010)

available at www.sciencedirect.com

ScienceDirect

journal homepage: www.elsevier.com/locate/ijrefrig

Modelling distribution of evaporating CO_2 in parallel minichannels

Wiebke Brix [a,*], *Martin Ryhl Kærn* [a,b], *Brian Elmegaard* [a]

[a] *Department of Mechanical Engineering, Technical University of Denmark, Nils Koppels Allé Bygn. 403, DK-2800 Lyngby, Denmark*
[b] *Danfoss A/S, Refrigeration and Air Conditioning, Nordborgvej 81, DK-6430 Nordborg, Denmark*

ARTICLE INFO

Article history:
Received 2 October 2009
Received in revised form
2 March 2010
Accepted 10 April 2010
Available online 18 April 2010

Keywords:
Heat exchanger
Microchannel
Modelling
Simulation
Carbon dioxide
Boiling
Two-phase flow
Distribution

ABSTRACT

The effects of airflow non-uniformity and uneven inlet qualities on the performance of a minichannel evaporator with parallel channels, using CO_2 as refrigerant, are investigated numerically. For this purpose a one-dimensional discretised steady-state model was developed, applying well-known empirical correlations for calculating frictional pressure drop and heat transfer coefficients. An investigation of different correlations for boiling two-phase flow shows that the choice of correlation is insignificant regarding the overall results. It is shown that non-uniform airflow leads to maldistribution of the refrigerant and considerable capacity reduction of the evaporator. Uneven inlet qualities to the different channels show only minor effects on the refrigerant distribution and evaporator capacity as long as the channels are vertically oriented with CO_2 flowing upwards. For horizontal channels capacity reductions are found for both non-uniform airflow and uneven inlet qualities. For horizontal minichannels the results are very similar to those obtained using R134a as refrigerant.

Modélisation de la distribution de CO_2 en évaporation dans les microcanaux parallèles

Mots clés : Échangeur de chaleur ; Micro-canal ; Modélisation ; Simulation ; Dioxyde de carbone ; Ébullition ; Écoulement diphasique ; Distribution

1. Introduction

Minichannel heat exchangers with extruded aluminium channels and folded, louvred fins are a popular choice for refrigeration systems using CO_2 as refrigerant. These heat exchangers are well suited for the high working pressures of CO_2 and provide good heat transfer. Especially for systems, where compactness and low refrigerant charge are desired, minichannel heat exchangers are favourable.

* *Corresponding author*. Tel.: +45 4525 4130; fax: +45 4593 5215.
E-mail addresses: wb@mek.dtu.dk (W. Brix), pmak@mek.dtu.dk (M.R. Kærn), be@mek.dtu.dk (B. Elmegaard).
0140-7007/$ – see front matter © 2010 Elsevier Ltd and IIR. All rights reserved.
doi:10.1016/j.ijrefrig.2010.04.012

Nomenclature

Roman

A	area (m^2)
f	maldistribution parameter (–)
h	heat transfer coefficient (W m^{-2} K^{-1})
$\dot{m}$	mass flow rate (kg s^{-1})
p	pressure (bar)
$\dot{Q}$	heat transfer rate (W)
T	temperature (°C)
U	air velocity (m s^{-1})
UA	overall heat transfer coefficient (W K^{-1})
x	quality (–)
z	channel length (m)

Greek

η_0	surface efficiency

Subscripts

a	air side
r	refrigerant side
sup	superheat
U	maldistribution of air velocity
x	maldistribution of inlet quality

However, maldistribution of the refrigerant is a challenge in this type of heat exchangers, especially for evaporators where the entering fluid is usually in two-phase condition (Kim et al., 2004; Kandlikar, 2007). The design of the distribution manifold plays an important role in how the gas and liquid phases distribute, as shown by Vist and Pettersen (2004) and Hwang et al. (2007). Furthermore, pressure drop in the manifolds may induce maldistribution of the refrigerant (Kulkarni et al., 2004). Another factor that may influence the distribution of the refrigerant in the parallel channels is the airflow distribution on the secondary side. Due to design constraints a uniform airflow is rarely attained across the evaporator. It is therefore interesting to study the effects of a non-uniform airflow distribution and a non-uniform gas–liquid distribution on the evaporator performance.

Several studies on conventional evaporators have shown that maldistribution of the refrigerant may cause a severe deterioration of the evaporator performance. In a study by Chwalowski et al. (1989) it was shown experimentally that a capacity reduction of up to 30% could be found for a finned tube evaporator in an air-conditioning duct that was exposed to a non-uniform airflow. It was not investigated how much of the capacity reduction appeared due to maldistribution of the airflow only, and how much originated from the resulting maldistribution of the refrigerant. Choi et al. (2003) conducted experiments with R22 in a finned tube evaporator with three circuits to determine the capacity reduction due to maldistribution of the refrigerant and airflow non-uniformity. Results showed that for maldistributed refrigerant flow the capacity reduction could be as much as 30%, while for the case of non-uniform airflow with evenly distributed refrigerant a capacity reduction of 6% was found. In a numerical study performed by Domanski (1991) different airflow profiles were applied on a three circuit finned tube evaporator. The gas–liquid distribution to the different circuits was uniform, but the mass flow rate into the circuits varied as a result of the non-uniform airflow. In the study the saturation temperature at the evaporator inlet and the outlet superheat were the same for all velocity profiles applied. The results showed reductions of the cooling capacity of up to 25% for non-uniform airflow profiles compared the capacity obtained for uniform airflow. Recently, Kim et al. (2009a,b) presented a numerical study of the effects of void fraction maldistribution, feeder tube blockages and airflow non-uniformity on the performance of a five circuit, finned tube evaporator using R410A as refrigerant. The non-uniformities were imposed such that the evaporator was divided into two sections. Two and three circuits thus worked under the same conditions, respectively. Significant reductions in cooling capacity and COP were found for airflow non-uniformity and refrigerant maldistribution due to both maldistribution of the inlet void fraction and feeder tube blockages.

Maldistribution caused by airflow non-uniformity and non-uniform gas–liquid distribution in two parallel multiport minichannel tubes have been studied numerically by Brix et al. (2009) using R134a as refrigerant. Non-uniform airflow or a non-uniform distribution of the gas and liquid at the inlet were imposed and the effects on the evaporator performance were studied. Initial results using CO_2 in a similar minichannel evaporator (Brix and Elmegaard, 2008) showed different behaviour when using CO_2 as refrigerant instead of R134a. A more detailed study of maldistribution of CO_2 in minichannel evaporators is therefore interesting.

The objective of the present study is to investigate the effects of maldistribution of CO_2 in parallel evaporator minichannels on the heat exchanger performance by numerical simulation. Maldistribution of refrigerant occurring due to a non-uniform airflow and maldistribution generated due to phase separation in the manifold, i.e. the distribution of liquid and vapour into the different channels, are considered.

2. Method

In order to model the evaporator, a discretised one-dimensional model of a single minichannel tube is built using the finite volume method. Each minichannel is discretized into an optional number of volumes, and each volume is treated as a small heat exchanger. For each volume the continuity equation, the momentum equation and the energy equation are solved under the following assumptions:

- The system is in steady state.
- The refrigerant flow is one-dimensional.
- The refrigerant flow is homogeneous and vapour and liquid are in thermodynamic equilibrium.
- Heat conduction in the flow direction of one tube and between different tubes is negligible.
- The air is dry.

The assumption of homogeneous flow, is applied only for calculating the void fractions as well as the gravitational and accelerational pressure gradients. The frictional pressure

Table 1 – Summary of correlations used to calculate heat transfer coefficients and pressure drop.

Air side	
Heat transfer coefficient	Kim and Bullard (2002)
Two-phase region	
Heat transfer coefficient	Bertsch et al. (2009)
Frictional pressure drop	Müller-Steinhagen and Heck (1986)
Single-phase region	
Heat transfer coefficient	Gnielinski (2002)
Frictional pressure drop	Blasius (2002)

gradients and the two-phase heat transfer coefficients are calculated using empirical correlations, depending on the flow conditions. Table 1 summarizes the correlations that are used in the model. The sensitivity of the model considering the choice of two-phase heat transfer and pressure drop correlations is investigated in Section 3.3. It is noted that the correlations applied for calculating single-phase heat transfer and pressure drop are correlations developed for conventional channels, not minichannels. However, several studies have shown that these classical correlations perform well when applied to small channels, both for pressure drop (Caney et al., 2007) and heat transfer (Owhaib and Palm, 2004; Rosa et al., 2009).

On the air side of the evaporator louvred fins are connecting two neighboring tubes. For the single tube model half of the fin of each side is accounted to belong to the specific channel. The surface efficiency of the air side heat transfer area is calculated assuming fins with an adiabatic tip (Incropera and DeWitt, 2002). In order to solve the energy balance the ϵ-NTU method for across flow heat exchanger is applied.

In the physical evaporator the different channels are connected through a dividing and a collecting manifold, i.e. the inlet and outlet manifold. The flow distribution in the manifold depends strongly on the design of the manifolds. Both flow conditions and the internal geometry, such as the shape of the inlet and the manufacturing details of connecting pipes

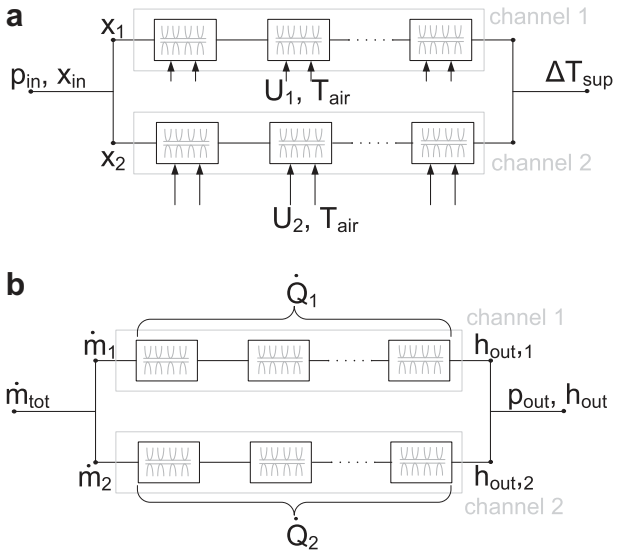

Fig. 1 – Schematic overview with (a) inputs and (b) outputs to the model.

to the manifold determine whether gas–liquid separation occurs and how the refrigerant will distribute between the different parallel channels (Hrnjak, 2004).

In the present evaporator model the flow in the manifolds is not considered in detail. The manifolds are assumed to be adiabatic and furthermore pressure drop in the manifolds is neglected. By neglecting the pressure drop in the manifold, also the maldistribution of refrigerant induced by pressure drop in the manifold is neglected. Depending on the manifold geometry, this might not be negligible in a real evaporator. This has to be kept in mind when considering the results.

The single channel models are hence simply connected through conservation of the total mass flow rate, conservation of energy within the manifolds and a requirement of equal pressure drop over the channels.

The distribution of gas and liquid flowing into the different channels has to be given as an input to the model. Further inputs required by the model are: air velocity and temperature, the thermodynamic state of the refrigerant into the dividing manifold, e.g. pressure and quality, and either the mixed superheat out of the evaporator or the refrigerant mass flow rate. An overview over the model and the inputs and outputs is shown in Fig. 1.

A non-uniform airflow may be imposed by defining different air velocities, and a non-equal distribution of the gas and liquid in the manifold is imposed by giving different qualities at the inlet of each channel.

The model was built and solved using the modelling and simulation software Windali (Skovrup, 2005b). The software solves the algebraic equations using a modified Newton iteration scheme. Thermodynamic and thermophysical properties were calculated using RefEqns (Skovrup, 2005a). The single channel model was validated using R134a as refrigerant in Brix et al. (2009).

2.1. *The test case*

In order to investigate the influence of maldistribution of the airflow and inlet qualities on the performance of a CO_2 evaporator, a test case is defined. For simplicity reasons the test case evaporator consists of only two multiport minichannel tubes in parallel. If nothing else is stated the channels are oriented vertically with the refrigerant flowing in the upward

Table 2 – Parameters defining the test case.

Evaporator geometry	
Tube length	0.47 m
Number of ports in one tube	11
Cross section of one port	0.8 × 1.2 mm
Flow depth	16 mm
Distance between two microchannels	8 mm
Fin pitch	727 m^{-1}
Flow parameters	
Air temperature	35 °C
Air velocity	1.6 m s^{-1}
Saturation temperature at evaporator inlet	7.4 °C
Quality at manifold inlet	0.3
Total superheat	0.05 K

direction. The parameters describing the modelled evaporator are summarized in Table 2. The total refrigerant flow through the evaporator channels is controlled by setting a constant mixed superheat out of the evaporator. This would be the case for refrigeration systems controlled by a thermostatic expansion valve, and is therefore the most obvious choice in the present case.

It should be noted that the evaporator in this study is considered alone, and not as a part of a system. As seen from Table 2, the saturation temperature at the evaporator inlet is kept constant. This would not be the case in a system, where load changes on the evaporator are responded by changing the mass flow rate through the expansion device in order to keep a constant superheat, while the volume flow into the compressor is constant for a compressor running at constant speed.

2.2. Definition of two maldistribution parameters

Two different sources of maldistribution are investigated, and for this purpose two different maldistribution parameters are defined. Firstly, maldistribution occurring due to non-uniform airflow is considered. The airflow is imposed such that each channel sees a constant air velocity. The total airflow rate is kept constant, while the velocity on each channel is varied. The two minichannel tubes are numbered channel 1 and channel 2, and for simplicity the velocities are always varied such that the velocity increases on channel 1 and decreases on channel 2. A non-dimensional parameter, f_U, which quantifies the degree of non-uniformity of the airflow, is defined as:

$$f_U = \frac{U_2}{U_{mean}}, \quad 0 \le f_U \le 1, \tag{1}$$

where $f_U = 1$ for equal air velocities on both channels, while $f_U = 0$ for no airflow across channel 2, and all airflows across channel 1.

Secondly, the maldistribution occurring due to non-equal inlet qualities to the channels is considered. Manifold design and flow conditions are determining how the gas and liquid phases distribute in the manifold. In this study focus is on the evaporation and not on the manifold, thus different inlet qualities are specified. The inlet quality to the manifold is kept constant, while the distribution of the two phases is varied. The qualities are varied such that the inlet quality of channel 1 is increased, while it is decreased in channel 2, according to the mass and energy balance in the manifold. Also for this cause of maldistribution a parameter, f_x, quantifying the degree of non-uniformity of the qualities is defined:

$$f_x = \frac{x_2}{x_{manifold}}, \quad 0 \le f_x \le 1. \tag{2}$$

For equal distribution of the inlet quality $f_x = 1$, while for $f_x = 0$ only liquid is fed into channel 2 and a remaining mixture of liquid and gas enters channel 1.

The two parameters f_U and f_x are varied only separately. In a real evaporator both the airflow and the inlet quality distribution will of course contribute to the resulting maldistribution of the refrigerant, but in order to gain a better understanding, the two contributions are kept separate when simulating the evaporator.

3. Results and discussion

3.1. Effects of non-uniform airflow

In Fig. 2 local overall heat transfer coefficients are shown along the channel direction for three different airflow distributions. The overall heat transfer coefficients are calculated as:

$$\frac{1}{UA} = \frac{1}{h_r A_r} + \frac{1}{\eta_0 h_a A_a}, \tag{3}$$

where conduction resistance in the channel walls is neglected. The areas A_r and A_a correspond to the heat transfer area on the refrigerant and air side of one volume in the discretised channel, respectively. The local UA values thus give the overall heat transfer coefficients of the small heat exchanger volumes. This means that the local UA values found depend on the discretisation.

For each of the three airflow distributions imposed, $f_U = 1$, $f_U = 0.5$ and $f_U = 0.1$, three curves are shown in Fig. 2. Two curves show the local UA values in each channel and the third, which is provided with markers shows the mean local UA values. The solid line with circular markers shows local UA values in the minichannels for a uniform airflow. In this case there is no maldistribution of the refrigerant and the three lines coincide. As long as the refrigerant flow in the channels is not approaching dryout, the local UA values are relatively constant. For $f_U = 1$ dryout of the channel walls starts to occur at around $z = 0.35$ m. This results in a decrease of the refrigerant side heat transfer coefficient, and hence in a decrease of the local UA value. At the outlet of the channel ($z = 0.47$ m) the refrigerant is fully evaporated and the refrigerant side heat transfer coefficient is calculated for single-phase conditions.

For $f_U = 0.5$ channel 1 is exposed to a higher air velocity than channel 2. In channel 1 the air side heat transfer coefficient will be higher than for the uniform airflow case, which results in a higher local UA value. However, in this channel single-phase gas flow is reached much earlier, at around $z = 0.32$ m. In the last part of the channel the local UA values are thus considerably lower since there is heat transfer to a single-phase gas. Channel 2, which is exposed to the low air velocity has lower UA values than in the uniform airflow case, due to the lower air side heat transfer coefficient. In this channel dryout is not reached in the channel length, and the UA values are therefore relatively constant

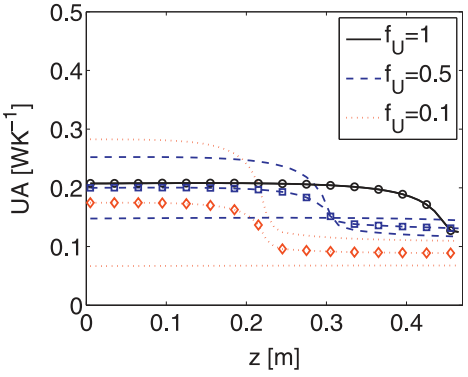

Fig. 2 – Local UA values in the channel for different airflow distributions. The lines with markers show local mean values of the two channels.

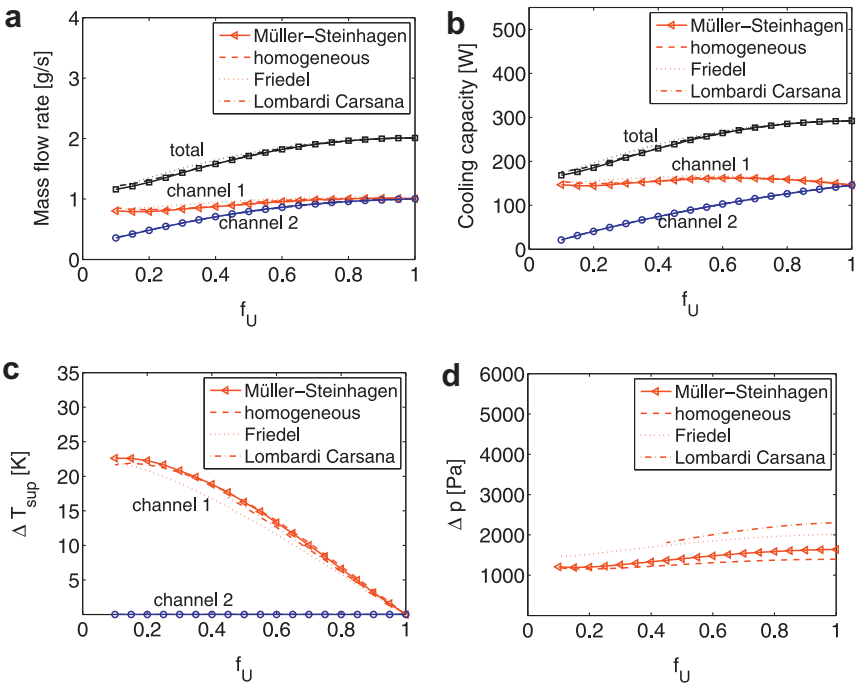

Fig. 3 – Selected parameters as a function of airflow distribution. CO_2 is used as refrigerant. For each channel results are found using four different pressure drop correlations.

throughout the channel. From the dashed line with square markers showing the mean local UA values of the two channels at $f_U = 0.5$, it is noted that as long as there is two-phase flow in both channels the mean local UA value is only slightly lower than for the uniform airflow case. However, for the part of the channel, where dryout has been reached in channel 1 the mean local UA values are considerable lower. From this a lower cooling capacity would be expected for $f_U = 0.5$. For $f_U = 0.1$, the same behaviour is seen as for $f_U = 0.5$, but it is even more pronounced.

Comparing the UA values gives an indication of the magnitude of the capacity degradation. However, the mass flow rate in the channels also has to be considered in order to understand the effects of non-uniform airflow. Changing the air velocity on the different channels, i.e. changing the heat load on the channel affects the pressure gradients along the channel. This may result in a maldistribution of the refrigerant mass flow rate, since the total pressure drop has to be equal for both channels. Fig. 3 shows mass flow rate, cooling capacity, outlet superheat and total pressure drop for both channels as a function of the airflow distribution. The total refrigerant mass flow rate decreases with increasing airflow maldistribution to keep the constant mixed outlet superheat. The refrigerant mass flow rate in channel 1, which receives the high air velocity, decreases less than in channel 2. Intuitively, the opposite might be expected, since frictional pressure drop is higher for gas flow than for liquid flow. However, the evaporator geometry and test conditions chosen for this numerical experiment are not typical, in that the channel diameters are larger and the mass flow rate is lower than what would typically be used in a CO_2 minichannel evaporator. Therefore the low viscosity and high density of CO_2 results in a very low frictional pressure gradient, while the gravitational contribution to the pressure drop is significant, especially at low qualities. The outlet superheat of channel 1 increases considerably for increasing non-uniformity of the airflow and approaches the air temperature, while the refrigerant at the outlet of channel 2 is not fully evaporated. The superheat from channel 1 is used to evaporate the liquid exiting channel 2. This is not expedient from a performance point of view. As can be seen the cooling capacity of the evaporator decreases considerably for increasing non-uniformity of the airflow.

If the evaporator were part of a system, the graphs in Fig. 3 would look differently. For increasing maldistribution of the airflow, and hence a decreasing overall heat transfer coefficient, the saturation temperature at the inlet of the evaporator would decrease. The temperature difference between air and refrigerant would thus increase, which increases the heat transfer. Therefore it would be expected, that the capacity

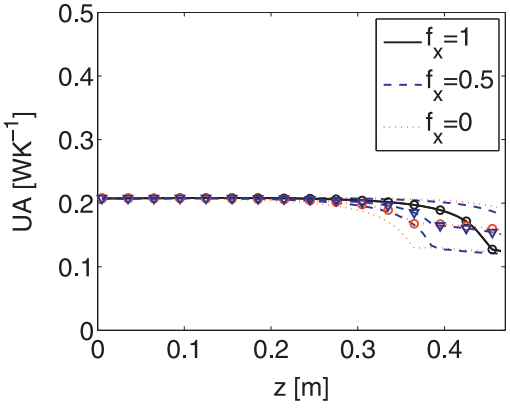

Fig. 4 – Local UA values in the channel for different distributions of the inlet qualities. The lines with markers show local mean values of the two channels.

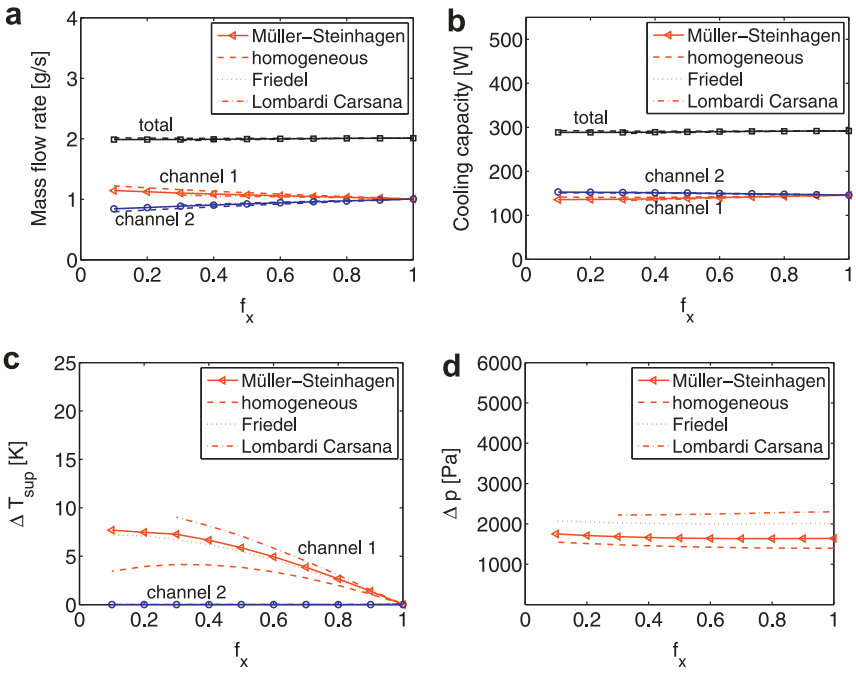

Fig. 5 – Selected parameters as a function of inlet quality distribution. For each channel results are found using four different pressure drop correlations.

reduction for an evaporator in a system would be smaller than reductions found in this study. On the other hand the decreasing saturation temperature would also induce a decrease of the system coefficient of performance (COP).

Another conclusion can be drawn considering Fig. 2. In the first part of the channel ($z < 0.15$ m), where the refrigerant is in a two-phase condition in all channels, it is seen that the mean local UA value decreases for increasing maldistribution. Comparing the mean local UA values for $f_U = 1$ and $f_U = 0.5$ in this region, only a small decrease is found. At severe airflow non-uniformity, $f_U = 0.1$, however, the mean local UA value is around 16% lower than for uniform flow. This indicates that only a severe non-uniformity of the airflow would impact on the cooling capacity of the evaporator if the refrigerant was in a two-phase condition throughout all channels.

3.2. *Effect of non-uniform gas–liquid distribution*

Varying the gas–liquid distribution by imposing different inlet qualities shows a different behaviour, as seen in Fig. 4. The figure shows the local UA values along the channel for three different inlet quality distributions. Again three curves are shown for each inlet distribution. Two curves show the local UA values in each channel and the third, which is provided with markers, shows the mean local UA values. For $f_x = 1$ the same three coinciding lines are shown as for $f_U = 1$ in Fig. 2. In the first part of the channel, before dryout occurs in any of the channels, the local UA values are not affected by changing the inlet quality distribution corresponding to a value of $f_x = 0.5$ or $f_x = 0$. However, the refrigerant flow in channel 1, which has a higher quality at the inlet, will reach dryout before the outlet of the channel, while the refrigerant in channel 2 is not fully evaporated at the outlet. The local UA value in channel 1 decreases, when single-phase flow is approached, while the local UA value stays higher in channel 2. The curve of mean local UA value decreases as dryout is approached in channel 1, but stays more or less constant after that. This means that a total mean UA value for the cases of $f_x = 0.5$ and $f_x = 0$ would actually not differ much from the uniform case of equal inlet qualities to the channels. From this it is expected that the inlet quality distribution does not influence

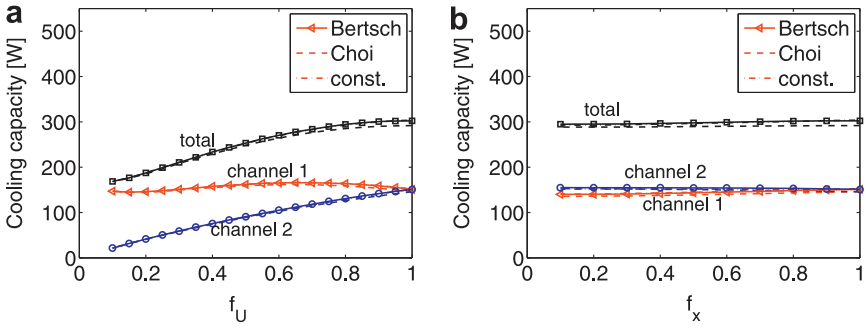

Fig. 6 – Cooling capacity as a function of f_U and f_x calculated using different correlation for two-phase heat transfer.

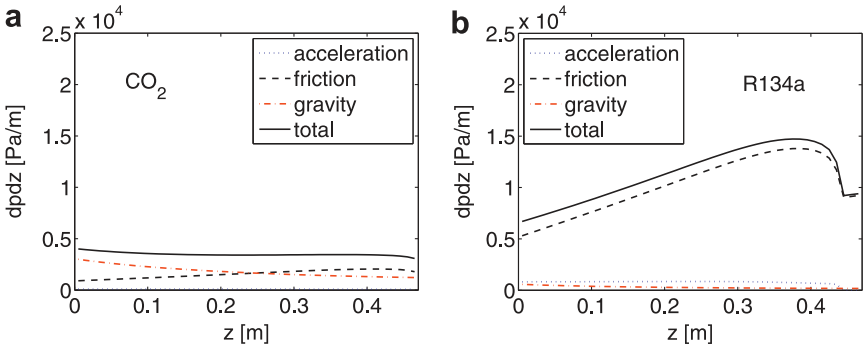

Fig. 7 – Pressure gradient contributions along the channel with $f_U = 1$ and $f_x = 1$ for (a) CO_2 and (b) R134a.

the cooling capacity significantly. Fig. 5 shows the refrigerant mass flow rate, cooling capacity, outlet superheat and total pressure drop for both channels as a function of the distribution of the inlet qualities. The results show that the total cooling capacity is not significantly affected by the change in inlet quality distribution. Also the cooling capacity of each channel does not change much, although the inlet quality to the channels is changed significantly. The reason why this is possible is that the mass flow rate into each channel varies. In channel 2, which receives more liquid for increasing maldistribution, the mass flow rate is reduced, while it increases in channel 1. Therefore, even with significant maldistribution most of the liquid will be evaporated at the channel outlet. The superheat out of channel 1 that is used for evaporating the remaining liquid from channel 2, is much lower than in the non-uniform airflow case. There is hence no significant capacity loss for evaporating excess liquid from channel 2, due to the favourable distribution of the mass flow rate.

3.3. *Significance of the choice of correlations*

Figs. 3 and 5 show results obtained using four different correlations for calculating the frictional pressure drop:

- Müller-Steinhagen and Heck (1986)
- Lombardi and Carsana (1992)
- Friedel (1979)
- Homogeneous flow with two-phase viscosity after Dukler et al. (1964)

A review of the literature on which pressure drop correlation should be applied for evaporating CO_2 in minichannels shows different recommendations. Pettersen (2004) was one of the first to study flow boiling of CO_2 in small channels, and the Lombardi and Carsana (1992) correlation was recommended to model frictional pressure drop. Park and Hrnjak (2007) recommended the Müller-Steinhagen and Heck (1986) correlation for evaporating CO_2 in a conventional channel. Thome and Ribatski (2005) also showed good results for this correlation for CO_2 in mini and microchannels. The Friedel correlation showed the best results in the study by Thome and Ribatski (2005) and is also recommended by Park and Hrnjak (2009). However, Pamitran et al. (2008) found no good results for this correlation, and recommend instead a homogeneous model using an expression for the two-phase viscosity proposed by Dukler et al. (1964).

The above mentioned recommendations are nearly all based on experimental data covering only higher mass fluxes than the mass fluxes in the present study. One exception is the study by Park and Hrnjak (2007) in a conventionally sized channel recommending the Müller-Steinhagen and Heck (1986) correlation. Therefore, the Müller-Steinhagen and Heck (1986) correlation was chosen in the baseline model. However, all of the mentioned correlations were developed covering low mass fluxes. Since no evident superior correlation could be found from the literature review, the three other correlations are applied for comparison, in order to see whether the choice of correlation is crucial for the modelling results. In Figs. 3d and 5d it is seen that the total pressure drop over the minichannel shows significant dependency on the choice of correlation. Using the Lombardi and Carsana (1992) correlation the pressure drop is found to be more than 60% higher than using the homogeneous model. However, the distribution of mass flow rate and the cooling capacities are insignificantly dependent on the choice of pressure drop correlation.

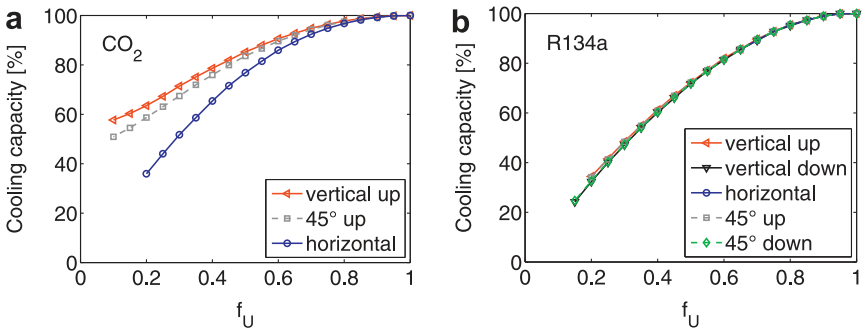

Fig. 8 – Cooling capacity vs. airflow distribution for (a) CO_2 and (b) R134a.

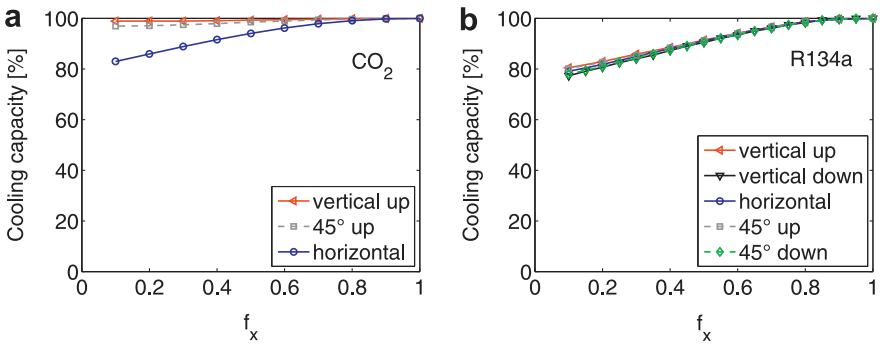

Fig. 9 – Cooling capacity vs. inlet quality distribution for (a) CO_2 and (b) R134a.

It could be argued, that the total pressure drop over the evaporator is relevant, if the whole refrigeration system was considered. For augmenting pressure drop in the evaporator the load on the compressor increases. However, the total pressure in the CO_2 system is very high, and the pressure ratio over the compressor will not change significantly, when using one correlation instead of the other. It would thus be expected that the isentropic efficiency is not significantly affected by the differences in pressure drop given by the different correlations. However, the compressor mass flow rate may also change due to differences in the inlet density, which could affect the system calculations. In future work it would be interesting to identify, which correlation actually gives the most correct results.

Considering two-phase heat transfer coefficients, the following correlations have been tested:

- Bertsch et al. (2009)
- Choi et al. (2007), with a smooth transition to the single-phase heat transfer coefficient for $x > 0.7$
- A constant two-phase heat transfer coefficient.

In the baseline model the Bertsch et al. (2009) correlation was applied for calculating the two-phase heat transfer coefficient. This correlation covers a wide range of refrigerants, including CO_2 and furthermore it covers mass fluxes down to 20 kg m^{-2} s^{-1} and vapour qualities from 0 to 1. The Choi et al. (2007) correlation, which has been applied for comparison, was developed for CO_2, but it does not cover the low mass fluxes used in this numerical experiment, and furthermore it only applies for qualities below 0.7.

As seen in Fig. 6 the calculated cooling capacity is almost independent on the choice of correlation. The same applies for the other outputs, which are not shown here.

3.4. *Effects of the channel orientation*

As mentioned, the evaporator used in this study is not typical in its design. A typical evaporator is designed such that the pressure drop in the channels is considerably higher than the pressure drop calculated for this evaporator, involving higher mass fluxes and/or smaller channels. From a system point of view the high pressure drop is not beneficial. However, the high pressure drop is necessary to ensure an equal mass flow rate distribution in the parallel channels, when taking the pressure drop in the manifolds into account and to avoid two-phase instabilities. Imagining a manifold that is designed specially to minimize the effects of manifold pressure drop on the mass flow distribution, the high pressure drop would not be necessary for CO_2, which is not as exposed to two-phase instabilities as conventional refrigerants, because the density differences between liquid and gas are smaller.

Based on the conditions given in the test case, the pressure gradients in the evaporator will develop differently for CO_2 than for a conventional refrigerant. Due to the low viscosity and the high density of CO_2 the ratio between frictional and gravitational pressure drop contributions is very different from that of a conventional refrigerant for the tested conditions. This is illustrated in Fig. 7. The figure shows the contributions to the pressure gradient along a minichannel tube for the equal distribution case (f_U and $f_x = 1$) for CO_2 and R134a. With these differences in mind, it is natural to study the effects of the channel orientation.

Fig. 8 shows the reduction of cooling capacity as a function of airflow maldistribution, for CO_2 and R134a having different channel orientations. When using R134a as refrigerant, the channel orientation does not affect the deterioration curve of the cooling capacity. This is different for CO_2. In the horizontal case, where no gravitational contribution enters into the pressure drop, a considerably larger reduction of the cooling capacity is found. In this case the frictional pressure gradient is dominating, just as in the R134a case. In this case the capacity reduction in the CO_2 evaporator corresponds more or less to the capacity reduction of the R134a evaporator. Exactly the same is seen for maldistribution of the inlet quality in Fig. 9. The large gravitational contribution to the pressure drop leads to a more expedient distribution of the mass flow rate when imposing non-uniform airflow or non-equal inlet qualities. Consequently, a smaller capacity reduction is found for the vertical channels.

4. Conclusions

A numerical model of a minichannel evaporator using CO_2 as working fluid has been developed in order to study the effects of airflow non-uniformity and uneven refrigerant inlet qualities on the evaporator performance. Two parallel channels were modelled and non-uniform airflow was imposed by keeping a constant airflow rate, but varying the velocities on each channel. Furthermore, the inlet qualities to each of the channels were varied keeping a constant inlet quality to the

manifold. The frictional pressure drop and heat transfer coefficients were modelled using correlations from the literature. A number of different correlations for both the two-phase frictional pressure drop and the two-phase heat transfer coefficient were tested. It was shown that the results for cooling capacity were not affected by the choice of the correlations.

Considering maldistribution, the results showed that airflow non-uniformity induces a significant maldistribution of the refrigerant and a considerable degradation of the cooling capacity of the evaporator. However, as long as both channels are containing two-phase refrigerant, only a severe non-uniformity of the airflow would impact the cooling capacity. In the case of unevenly distributed inlet qualities hardly any effect on the evaporator capacity was found, as long as both channels were oriented vertically with upward flow. However, these results only considered two channels in parallel, and the results for more channels may be different. Changing the orientation of the channels to horizontal, gave rise to a refrigerant maldistribution and capacity degradation. Also for the non-uniform airflow, the capacity degradation was increased when changing the channel orientation from vertical to horizontal. For the horizontal channels, where the gravitational forces did not contribute to the pressure drop, the results were very similar to results found for refrigerant R134a.

REFERENCES

Bertsch, S.S., Groll, E.A., Garimella, S.V., 2009. A composite heat transfer correlation for saturated flow boiling in small channels. International Journal of Heat and Mass Transfer 52 (7–8), 2110–2118.

Blasius, P.R.H., 2002. VDI Wärmeatlas, nineth ed. Springer-Verlag (Ch. Lab).

Brix, W., Elmegaard, B., 2008. Distribution of evaporating CO_2 in parallel microchannels. In: 8th IIR Gustav Lorentzen Conference on Natural Working Fluids, Copenhagen.

Brix, W., Kærn, M.R., Elmegaard, B., 2009. Modelling refrigerant distribution in microchannel evaporators. International Journal of Refrigeration 32, 1736–1743.

Caney, N., Marty, P., Bigot, J., 2007. Friction losses and heat transfer of single-phase flow in a mini-channel. Applied Thermal Engineering 27 (10), 1715–1721 (heat transfer and sustainable energy technologies).

Choi, J.M., Payne, W.V., Domanski, P.A., 2003. Effects of non-uniform refrigerant and airflow distribution of finned-tube evaporator performance. In: Proceedings of the International Congress of Refrigeration, Washington DC, USA, ICR0040.

Choi, K.-I., Pamitran, A., Oh, C.-Y., Oh, J.-T., 2007. Boiling heat transfer of R22, R134a, and CO_2 in horizontal smooth minichannels. International Journal of Refrigeration 30 (8), 1336–1346.

Chwalowski, M., Didion, D.A., Domanski, P.A., 1989. Verification of evaporator computer models and analysis of performance of an evaporator coil. ASHRAE Transactions 95 (1), 1229–1235.

Domanski, P.A., 1991. Simulation of an evaporator with nonuniform one-dimensional air distribution. ASHRAE Transactions 97, 793–802.

Dukler, A., Wicks III, M., Cleveland, R., 1964. Frictional pressure drop in two-phase flow. AIChE Journal 10 (1), 38–51.

Friedel, L., 1979. Improved friction pressure drop correlations for horizontal and vertical two-phase pipe flow. In: The European Two-Phase Flow Group Meeting, Ispra, Italy, Paper No. E2.

Gnielinski, V., 2002. VDI Wärmeatlas, nineth ed. Springer-Verlag (Ch. Ga).

Hwang, Y., Jin, D.-H., Radermacher, R., 2007. Refrigerant distribution in minichannel evaporator manifolds. HVAC&R Research 13 (4), 543–555.

Hrnjak, P., 2004. Developing adiabatic two phase flow in headers – distribution issue in parallel flow microchannel heat exchangers. Heat Transfer Engineering 25 (3), 61–68.

Incropera, F.P., DeWitt, D.P., 2002. Introduction to Heat Transfer, fourth ed. John Wiley & Sons.

Kandlikar, S.G., 2007. A roadmap for implementing minichannels in refrigeration and air-conditioning systems – current status and future directions. Heat Transfer Engineering 28, 973–985.

Kim, J.-H., Braun, J.E., Groll, E.A., 2009a. Evaluation of a hybrid method for refrigerant flow balancing in multi-circuit evaporators. International Journal of Refrigeration 32 (6), 1283–1292.

Kim, J.-H., Braun, J.E., Groll, E.A., 2009b. A hybrid method for refrigerant flow balancing in multi-circuit evaporators: upstream versus downstream flow control. International Journal of Refrigeration 32 (6), 1271–1282.

Kim, M.-H., Bullard, C.W., 2002. Air-side thermal hydraulic performance of multi-louvred fin aluminium heat exchangers. International Journal of Refrigeration 25, 390–400.

Kim, M.-H., Pettersen, J., Bullard, C.W., 2004. Fundamental process and system design issues in CO_2 vapor compression systems. Progress in Energy and Combustion Science 30 (2), 119–174.

Kulkarni, T., Bullard, C.W., Cho, K., 2004. Header design tradeoffs in microchannel evaporators. Applied Thermal Engineering 24 (5–6), 759–776.

Lombardi, C., Carsana, C., 1992. A dimensionless pressure drop correlation for two-phase mixtures flowing upflow in vertical ducts covering wide parameter ranges. Heat and Technology 10 (1–2), 125–141.

Müller-Steinhagen, H., Heck, K., 1986. A simple friction pressure drop correlation for two-phase flow in pipes. Chemical Engineering and Processing 20, 291–308.

Owhaib, W., Palm, B., 2004. Experimental investigation of single-phase convective heat transfer in circular microchannels. Experimental Thermal and Fluid Science 28 (2–3), 105–110 (The International Symposium on Compact Heat Exchangers).

Pamitran, A., Choi, K.-I., Oh, J.-T., Oh, H.-K., 2008. Two-phase pressure drop during CO_2 vaporization in horizontal smooth minichannels. International Journal of Refrigeration 31 (8), 1375–1383.

Park, C., Hrnjak, P., 2007. CO_2 and R410a flow boiling heat transfer, pressure drop, and flow pattern at low temperatures in a horizontal smooth tube. International Journal of Refrigeration 30 (1), 166–178.

Park, C.Y., Hrnjak, P., 2009. Flow boiling heat transfer, pressure drop, and flow pattern for CO_2 in a 3.5 mm horizontal smooth tube. Journal of Heat Transfer 131 (9), 091501.

Pettersen, J., 2004. Flow vaporization of CO_2 in microchannel tubes. Experimental Thermal and Fluid Science 28 (2–3), 111–121 (The International Symposium on Compact Heat Exchangers).

Rosa, P., Karayiannis, T., Collins, M., 2009. Single-phase heat transfer in microchannels: the importance of scaling effects. Applied Thermal Engineering 29 (17–18), 3447–3468.

Skovrup, M.J., 2005a. Refeqns, v.3.10. Technical Univesity of Denmark, Department of Mechanical Engineering. http://www.et.web.mek.dtu.dk/WinDali/Index.html.

Skovrup, M.J., 2005b. Windali, v.3.34. Technical Univesity of Denmark, Department of Mechanical Engineering. http://www.et.web.mek.dtu.dk/WinDali/Index.html.

Thome, J.R., Ribatski, G., 2005. State-of-the-art of two-phase flow and flow boiling heat transfer and pressure drop of CO_2 in macro- and micro-channels. International Journal of Refrigeration 28 (8), 1149–1168.

Vist, S., Pettersen, J., 2004. Two-phase flow distribution in round tube manifolds. ASHRAE Transactions 110 (1), 307–317.

Paper III

Wiebke Brix, Arne Jakobsen, Bjarne D. Rasmussen
Henrik Carlsen

Analysis of airflow distribution in refrigeration system

International Congress of Refrigeration,
ICR07-B2-581, (2007)

ANALYSIS OF AIR FLOW DISTRIBUTION IN REFRIGERATION SYSTEM

W. BRIX[(a)], A. JAKOBSEN[(a)], B.D. RASMUSSEN[(b)], H. CARLSEN[(a)]
[(a)] Technical University of Denmark,
Department of Mechanical Engineering,
DK-2800 Lyngby, Denmark
Fax: +45 45935215, e-mail: wb@mek.dtu.dk
[(b)] Danfoss A/S
Refrigeration and Air Conditioning,
DK-6430 Nordborg, Denmark

ABSTRACT

A simulation model with heat transfer and pressure drop properties based on existing correlations was built to investigate the influence of unevenly distributed air flows on a microchannel evaporator. On the refrigerant side liquid overfeed is used in the evaporator and on the air side only dry air is considered to flow through the evaporator. The simulation model was used to analyze the capacity degradation caused by the airflow non-uniformity. It was found that the cooling capacity of the heat exchanger was decreased by 20% for extreme maldistributions of the airflow. However, for not so severe airflow maldistributions, the degradation of the overall heat transfer coefficient was limited. Finally, the evaporator model was built into a relatively simple refrigeration system model in order to analyse influence of the airflow maldistribution on the total system performance. It was found that the degradation of the COP was only 4% in the extreme case and negligible for all air flow distributions that were not severely non-uniform.

INTRODUCTION

When dimensioning refrigeration systems it is normally assumed that the flows of the working fluids are evenly distributed when the performance of the respective heat exchangers is calculated. Sometimes actual measurements in a running system reveal performance degradation compared to the dimensioning data. It is very complicated to measure possible uneven distribution of say air and refrigerant flow across an evaporator. Therefore a simulation model that can tell the consequences of non-uniform flows would be helpful both in design situations and in order to understand existing systems behaviour.
Previous studies of air cooled evaporators exposed to a non-uniform airflow have been carried out for different types of heat exchangers and with various conclusions.
Chwalowski *et al.* (1989) performed experiments on the evaporator of an air conditioning system. The airflow maldistribution was induced by tilting the heat exchanger relative to the main airflow direction. In the extreme case, a capacity reduction of 30% was found relative to the case, where the airflow is perpendicular to the evaporator inlet. Kirby *et al.* (1998) experimentally investigated the effect of airflow non-uniformity on the performance of a 5.3 kW window air conditioner, and their results showed only very small degradations of the performance, when a maldistribution of the airflow was generated by a disc, covering 16% of the face inlet area. Choi *et al.* (2003) conducted an experimental investigation to determine the capacity degradation due to non-uniform refrigerant and airflow distributions. The experiments were carried out on a R22 finned-tube evaporator. Results showed that for mal-distributed refrigerant flow the capacity degradation could be as much as 30%, even when the superheat of the refrigerant was controlled in order to compensate for the degradation. Moreover the study on a mal-distributed airflow showed a maximum capacity degradation of 8.7%. Numerical investigations of airflow maldistributions on finned tube evaporators have been performed by Aganda *et al.* (2000) and Chen *et al.* (2004) and in both papers a maximum capacity degradation of more than 20% was found.

In this paper we focus on a microchannel evaporator working in a CO_2 refrigeration system. Using a relatively simple model to calculate the heat transfer properties of the evaporator, the impact of a non-uniform airflow distribution on both the evaporator performance and on the total system performance is investigated. The distribution of the inlet velocity is an input to the model. The following main assumptions have been made: liquid overfeed is used in the evaporator and the air flow is dry, i.e. frost formation on the surfaces is not included.

MODELLING THE EVAPORATOR

The modelled evaporator is a 280x240mm aluminium microchannel heat exchanger with louvered fins as shown in figure 1. As mentioned liquid overfeed is used in the evaporator and since the pressure drop for CO_2 is small, any temperature glide will be neglected, such that a constant surface temperature of the microchannel tubes can be assumed. The fins are treated as perpendicular, rectangular fins with an adiabatic tip when calculating the fin efficiency, as in Incropera (2002). An estimate of the temperature difference between the base and the adiabatic symmetry point yields $\Delta T \approx 1$ K, and we thus make the assumption that the total air side surface area has a constant temperature and is equal to the evaporation temperature of the refrigerant.
The evaporator is modelled statically, which is reasonable since only dry air is considered through the evaporator so that the otherwise important transient phenomena, frosting and defrosting, are not taken into account.

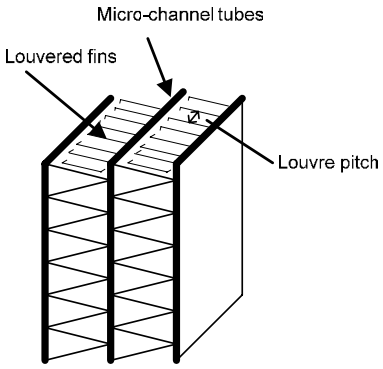

Figure 1: A small section of the heat exchanger.

The face inlet area is discretized into an optional number of rectangles, and each cell is treated as a small heat exchanger. For each cell an inlet velocity is specified such that it is possible to apply non-uniform airflow distribution to the heat exchanger model.

An overall heat transfer coefficient is calculated for each cell as shown in equation (1), where fouling has been neglected. It is assumed that the conduction resistance, R_w, and the refrigerant side contributions are negligible.

$$\frac{1}{UA} = \frac{1}{\eta_0 h_a A_a} + R_w + \frac{1}{h_r A_r} \approx \frac{1}{\eta_0 h_a A_a} \tag{1}$$

In order to decide whether it is reasonable to neglect the refrigerant side contributions, an estimate of the products $h_r A_r$ and $\eta_0 h_a A_a$ is made. The airside contribution is calculated by the model, while the refrigerant side heat transfer coefficient needs to be estimated. Based on experimental results from Pettersen (2004), who found heat transfer coefficients for CO_2 in flat multiport microchannel tubes, an estimate of $h_r = 10$ kW/(m^{2}K) seems reasonable. Based on this the two contributions are:

$$\frac{1}{\eta_0 h_a A_a} = 5.4 \quad \text{and} \quad \frac{1}{h_r A_r} \approx 0.6$$

Neglecting the refrigerant side contribution will thus result in a *UA*-value that is around 10% higher than the *UA*-value calculated using both term. However, it will be assumed that the refrigerant side contributions can be neglected.

Calculation of the air side convective heat transfer coefficient and of the pressure loss is based on a correlation presented by Kim and Bullard (2002). Kim and Bullard (2002) base their correlation on an experimental study of 45 different multi-louvered fin and flat tube heat exchangers. The correlation giving the dimensionless Colburn *j*-factor is developed from results for $100 < Re_{Lp} < 600$. The Reynolds number, Re_{Lp}, is based on the louvre pitch (shown in figure 1) in stead of the hydraulic diameter, which is usually used.

In order to validate the model, simulation results are compared to measurement results from a test stand, where the evaporator is part of a CO_2 refrigeration system. The calculated cooling capacity was found 17% higher than the measured, and the calculated air temperature out of the heat exchanger was found to be 1.0 K lower than the measured temperature.

RESULTS

The influence of a mal-distributed airflow into the evaporator is investigated using the evaporator model. For this purpose the evaporator is split vertically in two halves. The maldistribution is modelled by giving a different inlet velocity for each of the two parts. A parameter, f_U, defining the skewness of the airflow is then introduced. This parameter takes a value between 0 and 1 and is defined as:

$$f_U = \frac{U_1}{U_m}, \tag{2}$$

where U_1 is the face inlet velocity of section 1, and U_m is the mean face inlet velocity of the total face area, $U_m = (U_1 + U_2)/2$, where $U_1 < U_m < U_2$. For a uniform inlet distribution, $f_U = 1$, while if section 1 is totally blocked, but the same mean velocity over the total area is kept, $f_U = 0$. The advantage of this very simple maldistribution of the flow is that it is easy to quantify the degree of maldistribution.

Constant evaporation temperature

The evaporator model is run for two different cases: one, where the evaporation temperature is kept constant, and another, where the refrigeration capacity is kept constant. Furthermore, the mean face velocity and the parameter f_U are given. The input for case 1 is:

Mean face velocity: 2 m/s
Surface temperature: -8 °C
Air inlet temperature: 2 °C
Air inlet pressure: 1.013 bar

Keeping the evaporation temperature constant while increasing the degree of maldistribution, i.e. decreasing the parameter f_U, results in a reduction of the total *UA*-value, and thus in a reduction of the cooling capacity.

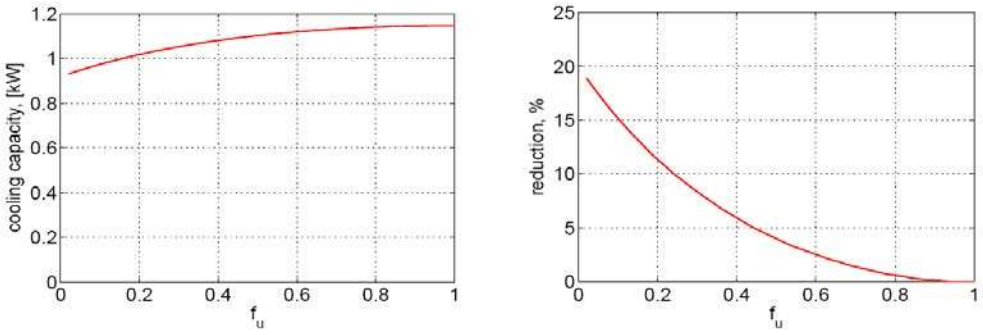

Figure 2: *Left*: The cooling capacity, as a function of f_U. For $f_U = 1$ the velocity is uniformly distributed. *Right*: Relative reduction of the cooling capacity compared to the uniform case.

In figure 2 the cooling capacity is shown as a function of f_U, and it is seen that the reduction of the cooling capacity is small for $f_U > 0.8$, but the reduction increases for stronger maldistributions. However, it must be noted, that whenever $f_U < 0.35$ the inlet velocity of section 1 gets lower than 0.7 m/s, which results in a Re_{Lp} lower than 100 and thus gets below the range, for which the correlation for h_a is developed.

Constant cooling capacity

The second simulation is made for constant cooling capacity. Also in this case the *UA*-value will decrease for increasing maldistribution of the flow, and in order to be able to keep constant cooling capacity, the logarithmic mean temperature difference will increase by decreasing the evaporation temperature. For case 1 a cooling capacity of 1.148 kW was found for the uniform distributed flow, and in order to obtain the same surface temperature for $f_U = 1$, the fixed cooling capacity is chosen to be 1.148 kW. All other input parameters are kept the same as for case 1.

In figure 3 the evaporation temperature is shown as a function of f_U. The nature of the development of the surface temperature is very similar to the results seen in the previous section. For $f_U > 0.8$ hardly any influence is seen, while for $f_U < 0.3$ the temperature decreases by more than 1 K.

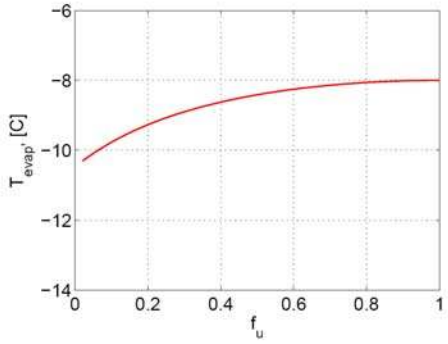

Figure 3: Evaporation temperature as a function of f_U at constant cooling capacity.

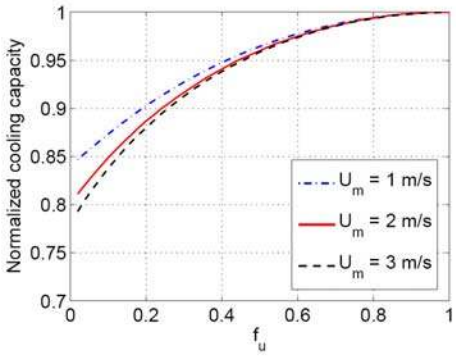

Figure 4: The cooling capacity normalized by the maximum value, shown as a function of f_U for different mean velocities.

Varying mean velocity

For both cases considered above, the mean velocity is kept constant at $U_m = 2$ m/s. The influence of the mean velocity has been investigated. For this purpose the simulations are repeated using different mean velocities. In figure 4 the cooling capacities normalized by the maximum values are plotted as a function of f_U for different mean velocities. From the figure it is seen that the cooling capacity decreases relatively more for higher mean velocities. For the tested velocities the relative difference is very small, especially for the values of f_U close to 1. For $f_U > 0.5$ hardly any difference can be seen for different mean face velocities. Again, it is noticeable to mention that the heat transfer correlation was developed for $100 < Re_{Lp} < 600$, which corresponds to a face inlet velocity between 0.7 and 4.4 m/s. For $U_m = 3$ m/s the inlet velocity of section 2 thus already exceeds the range for $f_U < 0.5$ and for $U_m = 1$ m/s the inlet velocity of section 1 is lower than 0.7 m/s for $f_U < 0.3$. However, the tendency having a relatively larger reduction in the capacity for higher mean velocities is seen from the points in the valid range.

Influence on the refrigeration system

A simple model of the refrigeration system outlined in figure 5 is built in order to investigate the influence of the maldistribution on the total system. The previously investigated evaporator model is built into this system model,

whereas the other components are modelled in a simple way by energy and mass balances. The investigation is done in the same way as for the evaporator alone, by splitting the evaporator in two halves and introducing the parameter f_U. The total volume flow rate of air through the evaporator is again kept constant, corresponding to a mean face inlet velocity of 1.65 m/s.

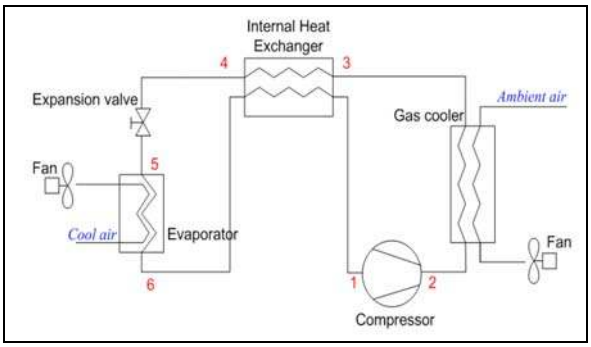

Figure 5: Component outline of the modelled refrigeration system.

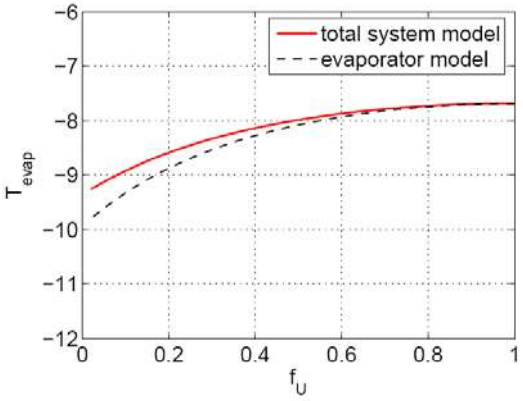

Figure 6: The evaporation temperature as a function of f_U. The dashed line is found from the evaporator model alone, with fixed cooling capacity.

For a specific compressor, the volume flow rate of refrigerant that can be circulated is fixed, depending on the inlet and outlet states of the refrigerant and on the volumetric efficiency. The refrigerant mass flow rate is hence calculated inside the compressor part of the model. This means that the cooling capacity is calculated outside the evaporator, and thus the simulation most of all resembles case 2, where the cooling capacity is fixed. It is thus expected that the evaporation temperature decreases for decreasing f_U. In figure 6 the evaporation temperature is shown as a function f_U, and as expected the evaporation temperature decreases for decreasing f_U. The figure also shows the evaporation temperature found using only the evaporator part of the model, with constant cooling capacity as input. It is seen that the temperature decrease for the total model is lower than the decrease calculated using the evaporator model with fixed cooling capacity as input.

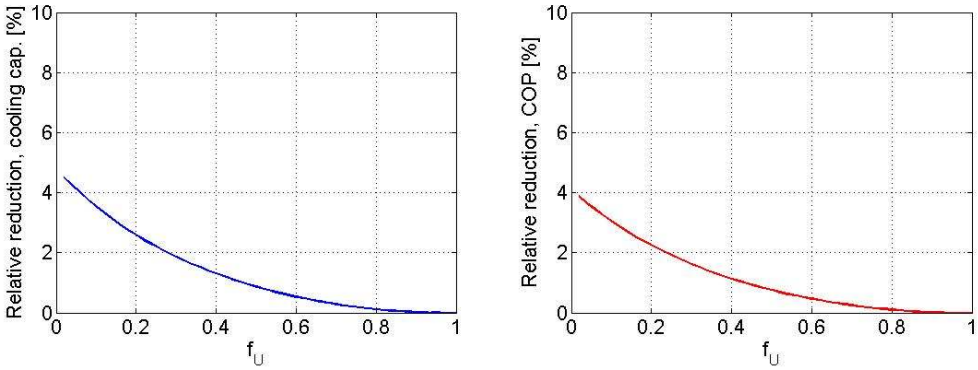

Figure 7: *Left*: Relative reduction in cooling capacity depending on f_U. *Right*: Relative reduction of the coefficient of performance (COP), shown as a function of f_U.

The reason why the temperature decrease is lower for the system model is that as a result of the decreasing evaporation temperature, also the suction pressure into the compressor decreases, this then results in a decrease of the refrigerant density at the compressor inlet and hence in a reduced refrigerant mass flow rate. This again, gives a reduced cooling capacity, so in this case actually both the evaporation temperature and the cooling capacity will decrease for increasing maldistribution. In figure 7 the reduction in cooling capacity (left) and in the coefficient of performance (right) is shown as functions of f_U. It is seen that although a reduction in both

cooling capacity and COP is found for maldistributed airflow into the evaporator, the reductions are small. For f_U > 0.5 the reduction in cooling capacity is < 1% and the reduction in COP is < 0.75%.

DISCUSSION

The relatively simple models, used in order to analyse the evaporator performance and the general system performance when the evaporator is exposed to a maldistributed air flow build on the assumption that the air side properties are dominating the contribution to the overall heat transfer properties. However, this assumption might be too crude.
As long as the assumption of evenly distributed refrigerant holds, and we know that we have liquid overfeed inside the evaporator, the air side properties will indeed be dominating the total heat transfer. However, a maldistribution of the air flow might induce dryout in some channels although the total evaporator outlet quality is still less than one. This would change the situation considerably, since the heat transfer coefficient in a dry channel is not necessarily much higher than the air side.
Also the pressure drop would rise significantly in the microchannel with a dryout and this again would reduce the mass flow rate in this channel. Finally the maldistributed airflow could induce a maldistributed refrigerant flow, which has not been taken into consideration in this work.

Furthermore, frost formation and defrosting, which has not been taken into account by the model, probably also has an impact on the flow distributions and on the heat transfer properties. Including these effects would most likely also change the results and conclusions.

It seems that the working conditions or assumptions play an important role on the results, and this is probably also one of the reasons why so many different conclusions can be found in the literature.

CONCLUSION

In this paper the influence of a non-uniform airflow distribution on the performance of an evaporator and on the total refrigeration system has been studied. For this purpose a simulation model of the evaporator, which focuses on the airside, has been built. The model allows a non-uniform inlet airflow distribution as an input variable, so it could be used to simulate the influence of a mal-distributed airflow on the heat transfer properties of the heat exchanger. A general investigation was made by splitting the heat exchanger in two halves and letting the mean velocity stay constant, while the velocity was increased in one half and simultaneously decreased in the other half. It was found that for maldistributions, where the lower velocity is higher than 50% of the mean velocity, the consequences on the capacity and on the evaporating temperature were small. In the extreme case, where one half was totally blocked, the capacity degradation was around 20% in the case of a constant evaporating temperature. In the case of constant cooling capacity, the evaporation temperature was decreased by 2 K for the extreme case.

Furthermore the evaporator model was built into a relatively simple model of a total refrigeration system. The simulation results show that the influences of a non-uniformly distributed inlet airflow on the cooling capacity and the system coefficient of performance were limited. Comparing the simulation results with the results obtained from the evaporator model alone, the maximum decrease of the evaporation temperature is even lower for the total system than for the evaporator model, modelled with constant capacity. In return for this, the cooling capacity is also reduced, but both the reduction of the cooling capacity and the reduction of the COP are very small, with a maximum reduction of around 5% and 4%, respectively for extreme maldistributed airflow.

To conclude, the simulation results show that under the assumptions of liquid overfeed in the evaporator and dry airflow though the heat exchanger the influence of a non-uniform airflow distribution on the system performance is very small. However, for an evaporator with superheated sections and frost formation on the fins the results would probably look different. An investigation of this is the subject for further work.

NOMENCLATURE

Roman			Subscripts	
A	area	(m^2)	a	air side
f_U	distribution parameter	(-)	evap	evaporation
h	convection heat transfer coefficient	($W/(m^2K)$)	i	inlet
p	pressure	(bar)	Lp	louvre pitch
$\dot{Q}$	heat transfer rate	(kW)	m	mean
R	conduction resistance	(K/W)	r	refrigerant side
Re	Reynolds number	(-)	w	wall
T	temperature	(°C)		
UA	overall heat transfer coefficient	(W/K)		
U	face air velocity	(m/s)		

Greek

η_0	Fin temperature effectiveness	(-)

REFERENCES

1. Aganda A.A., Coney J.E.R., and Sheppard C.G.W., 2000, airflow maldistribution and the performance of a packaged air conditioning unit evaporator, *Applied Thermal Engineering*, 20:515-528.
2. Chen N., Xu L., Feng d.H., Yang g.C., 2005, Performance of a finned tube evaporator under the oblique frontal air velocity distribution, *Applied Thermal Engineering*, 25:113-125.
3. Choi J.M., Payne W.V., and Domanski P.A., 2003, Effects of Non-Uniform Refrigerant and Air Flow distribution of Finned-Tube Evaporator Performance. *International Congress of Refrigeration,* ICR0040.
4. Chwalowski M., Didion D.A., and Domanski P.A., 1989, Verification of Evaporator computer Models and Analysis of Performance of an Evaporator Coil. *ASHRAE Transactions*, 95(1):793-802.
5. Incropera F.P., and DeWitt D.P., 2002, *Introduction to Heat Transfer*. John Wiley & Sons, 4th edition, 892p.
6. Kim M.-H., and Bullard C.W, 2002, Air-side thermal hydraulic performance of multi-louvered fin aluminium heat exchangers. *International Journal of Refrigeration*, 25:390-400.
7. Kirby E.S., Bullard C.W., and Dunn W.E., 1998, Effect of airflow non-uniformity on evaporator performance. *ASHRAE Transactions*, 104(2):755-762.
8. Pettersen J., 2004, Flow Vaporization of CO_2 in Microchannel Tubes. *Experimental Thermal and Fluid Scienc,.*28:111-121

Paper IV

Wiebke Brix, Brian Elmegaard

Distribution of evaporating CO_2 in parallel microchannels

8^{th} IIR Gustav Lorentzen Conference on Natural Working Fluids, (2008)

DISTRIBUTION OF EVAPORATING CO_2 IN PARALLEL MICROCHANNELS

W. BRIX, B. ELMEGAARD
Technical University of Denmark, Department of Mechanical Engineering,
Nils Koppels Allé, Bygn. 402, DK-2800 Lyngby, Denmark
Fax: +45 45935215, e-mail: wb@mek.dtu.dk

ABSTRACT

The impact on the heat exchanger performance due to maldistribution of evaporating CO_2 in parallel channels is investigated numerically. A 1D steady state simulation model of a microchannel evaporator is built using correlations from the literature to calculate frictional pressure drop and heat transfer coefficients. For two channels in parallel two different cases of maldistribution are studied. Firstly, the impact of a non-uniform air flow is considered, and secondly the impact of maldistribution of the two phases in the inlet manifold is investigated. The results for both cases are compared to results obtained using R134a as refrigerant, and it is found that the performance of the evaporator using CO_2 is less affected by the maldistribution than the evaporator using R134a as refrigerant. For both cases studied, the impact of the maldistribution was very small for CO_2.

1. INTRODUCTION

Microchannel heat exchangers are a popular choice for refrigeration systems using CO_2 as refrigerant. One of the reasons why these heat exchangers are especially attractive for CO_2 systems is that the small channels can handle the high working pressures of CO_2 very well. Furthermore microchannel heat exchangers are very compact, which helps reducing system sizes and helps reducing the refrigerant charge needed in order to obtain a given cooling capacity. In order to keep pressure drops at acceptable levels, microchannel heat exchangers are designed with many parallel channels. The refrigerant has to be distributed into these parallel channels, and there are many factors that play a role in how the refrigerant will be distributed during operation.
Especially for evaporators a uniform distribution of the refrigerant is a challenge, since the refrigerant enters the evaporator in two phase condition, and thus each of the two phases has to be distributed equally in order to guarantee an even distribution of the total mass flow rate. The design of the distribution manifold or header plays an important role in how the flow will be distributed. Furthermore the distribution of the air flow on the secondary side may influence the distribution of the refrigerant in the parallel channels.
Several studies have shown that the distribution of the refrigerant is important considering the performance of the evaporator. In a study by Chwalowski et al. (1989) it was shown experimentally that a capacity reduction of up to 30% could be found for a fin and tube evaporator in an air-conditioning duct that was exposed to a non-uniform air flow. It was not investigated how much of the capacity degradation appeared due to maldistribution of the air flow only, and how much originated from the resulting maldistribution of the refrigerant. Choi et al. (2003) conducted experiments with R22 in a finned tube evaporator with 3 circuits to determine the capacity reduction due to non-uniform distribution of the refrigerant and air flow distribution. Results showed that for maldistributed refrigerant flow the capacity degradation could be as much as 30%, even when the superheat of the refrigerant was controlled to compensate for the degradation. Moreover, the study on a maldistributed air flow showed a maximum capacity degradation of 8.7%.
Vist and Pettersen (2004a) studied a manifold with 10 parallel evaporator channels and CO_2 as refrigerant experimentally. Both the liquid/gas distribution and the heat load on the different channels were investigated and a similar study was performed using R134a as refrigerant (Vist and Pettersen, 2004b).
The objective of the present study is to investigate the effects of maldistribution of CO_2 in parallel evaporator channels on the heat exchanger performance by numerical simulation, and to compare the results to results obtained for refrigerant R134a. Both the maldistribution of refrigerant occurring due to unevenly distributed air

velocities and the maldistribution generated in the header, i.e. the distribution of liquid and vapour into the different channels are considered.

2. MODELLING THE EVAPORATOR

In order to model the evaporator, a discretized 1D-model of a single microchannel tube is built using a finite volume method. Each volume is considered as a small individual heat exchanger. Conductive heat transfer between the different volumes is neglected. For each volume the continuity equation, the momentum balance and the energy balance are applied. To calculate frictional pressure drop and heat transfer coefficients, different correlations are applied depending on the flow conditions. The correlations chosen are summarized in Table 1. The heat transfer coefficient on the refrigerant side in the two-phase region is calculated by a correlation presented by Choi et al. (2007) for qualities up to 0.7. For qualities between $0.7 < x < 1$, a smooth transition function between the value of the heat transfer coefficient at $x = 0.7$ and the single phase heat transfer coefficient is applied to simulate dryout. The modelling and solving of the final system of equations is performed using Engineering Equation Solver, (EES, 2007).

Table 1: Summary of correlations used to calculate heat transfer coefficients and pressure drop.

Air side	
Heat transfer coefficient	Kim and Bullard (2002)
Two-phase region	
Heat transfer coefficient	Choi et al. (2007)
	+ smooth transition to single phase
Void fraction	Homogeneous model
Gravitational pressure drop	Homogeneous model
Acceleration pressure drop	Homogeneous model
Frictional pressure drop	Müller-Steinhagen and Heck (1986)
Single phase refrigerant	
Heat transfer coefficient	Gnielinski (2002)
Frictional pressure drop	Blasius (2002)

In order to investigate the influence of non-uniform air flow and maldistributed inlet quality in parallel channels, the single channel models have to be connected. It is assumed, that there is no maldistribution of the refrigerant between the different ports in one microchannel tube, such that maldistribution of the refrigerant is only considered between the different tubes.

A sketch of two channels in parallel is shown in Figure 1. Furthermore input and output from the model are shown. Three equations connect the two channels. The first equation ensures conservation of mass:

$$\dot{m}_{in,total} = \sum_{i=1}^{N} \dot{m}_i \tag{1}$$

Pressure drops in the headers are neglected, such that the pressure drop over each of the channels will be equal:

$$\Delta p_i = p_{in} - p_{out} \tag{2}$$

Furthermore the manifolds are assumed to be adiabatic and therefore the gas and liquid phases are conserved in the manifolds:

$$\dot{m}_{in,total} x_{header,in} = \sum_{i=1}^{N} \dot{m}_i x_i \tag{3}$$

The pressure drop of each tube depends on the mass flow rate, inlet quality and heat load, and since the inlet quality is known and the heat load is calculated for each channel, the final distribution of mass flow rate between the channels can be found.

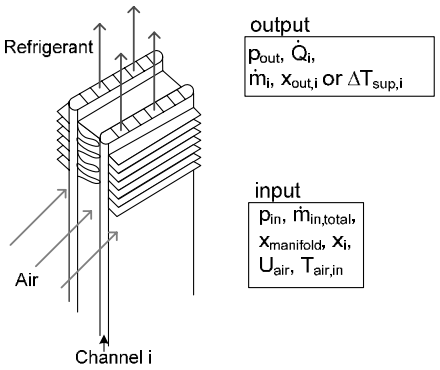

Figure 1: Two channels in parallel with model input and output.

3. RESULTS

A model of two channels in parallel is used for a case study with a fixed heat exchanger geometry, working under fixed flow conditions. The parameters chosen for the case study are summarized in Table 2. The channels are vertically oriented and CO_2 is evaporating in upwards flow direction. Two different cases are considered: first, it is studied how a non-uniform air flow affects the refrigerant distribution and the cooling capacity of the evaporator. Second, it is studied how maldistribution of the liquid and gas phases in the manifold resulting in a non-uniform inlet quality to the channels, affects the mass flow rate distribution of the refrigerant and the heat exchanger capacity. As specified in Table 2, the total superheat is kept constant, so that the total mass flow rate through the channels may change.

Table 2: Parameters defining the test case.

Evaporator geometry	
Tube length	0.47 m
# of ports in one tube	11
Cross section of one port	0.8 x 1.2 mm
Flow depth	16 mm
Distance between two microchannels	8 mm
Fin pitch	727 m^{-1}
Flow parameters	
Air temperature	35°C
Air velocity	1.6 m/s
Evaporation temperature	7.4°C
Quality at manifold inlet	0.3
Quality at manifold outlet	1
Total superheat	0 K

3.1 Maldistribution of the air flow rate

A non-uniform air flow over the channels affects the heat load on the channels, which again determines how fast the refrigerant inside the channels evaporates. The pressure gradient at a certain point in the tube depends on the quality of the refrigerant, and in order to keep the same total pressure drop over each of the two channels, the mass flow rate will distribute accordingly. In this first case, the inlet quality is assumed to be constant at $x = 0.3$ for both channels. Maldistribution of the air flow is imposed such that the air velocity is increased on one channel and decreased on the other channel, while the total volume flow rate of air passing the evaporator is kept constant. In order to quantify the degree of maldistribution in a simple way a distribution parameter is defined as:

$$f_U = \frac{U_2}{U_{\text{mean}}}, \quad 0 < f_U < 1, \tag{4}$$

Where U_{mean} is the mean velocity over the two channels, which is kept constant, and U_2 is the air velocity over channel 2, which is decreased for increased maldistribution. The parameter f_U thus takes a value between 0 and 1, where $f_U = 1$ for a uniform air flow distribution, and $f_U = 0$, when there is no air flow on channel 2 and all air flows by channel 1. In this study simulations are run for $0.6 < f_U < 1$. The extreme case where $f_U = 0.6$ corresponds to a velocity of 2.24 m/s on channel 1 and 0.96 m/s on channel 2.

Figure 2 shows the influence of non-uniform air flow on the distribution of the refrigerant mass flow rate and on the total pressure drop. The total refrigerant mass flow rate is not affected by small degrees of non-uniformity on the air side, but for $f_U < 0.9$ the total refrigerant mass flow decreases with up to 8% in the extreme case in order to keep constant outlet conditions.

For small degrees of non-uniform air flow also the refrigerant stays almost equally distributed between the two channels. For larger maldistribution on the air side also a maldistribution on the refrigerant side starts to occur. Whereas the refrigerant mass flow rate stays almost constant or is slightly decreasing in channel 1, it decreases more in channel 2. The channel with the higher heat load thus gets more refrigerant mass flow rate.

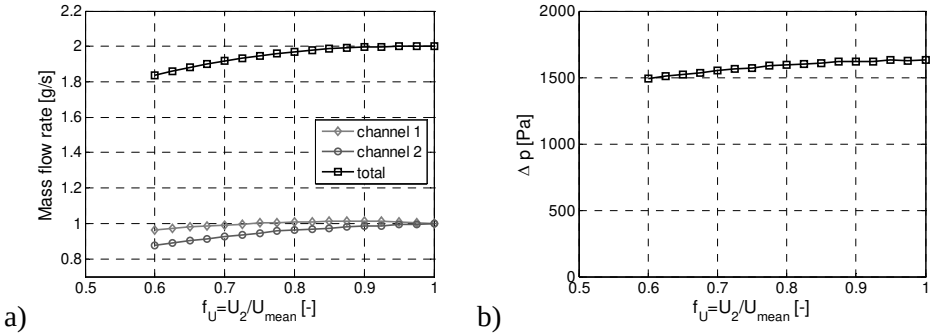

a) b)

Figure 2: (a) Influence of non-uniform air flow on the mass flow rate in the channels and (b) on the total pressure drop.

Since frictional pressure drop is higher for gas than for liquid, it could intuitively be expected that the channel with the high heat load and therefore faster evaporation would receive less mass flow rate of refrigerant. The reason why this is not the case here, is because the low viscosity and high density of CO_2, results in a very low frictional pressure gradient, while the contribution of the gravitational pressure gradient is large compared to conventional refrigerants. For the present case study, the contribution of the gravitational pressure drop actually exceeds the frictional pressure drop contribution at low qualities. Graph b in Figure 2 shows that the total pressure drop decreases for increasing maldistribution of the air flow. How this affects the performance of a full system will be studied in future investigations.

In Figure 3 it is shown how the heat transfer is affected by the maldistribution. It is seen that the total heat transfer rate is constant for small degrees of maldistribution ($f_U > 0.9$) and decreases slightly for larger maldistribution of the air flow. In the most extreme case, the total cooling capacity is decreased by 10%. Although the air side heat transfer coefficient increases with the increased air velocity, the heat transfer rate of channel 1 increases only slightly, whereas it decreases considerably for channel 2.

The local *UA*-values are calculated based on the air and refrigerant side heat transfer coefficients, neglecting the heat transfer resistance of the tube:

$$UA = \left(\frac{1}{h_r A_r} + \frac{1}{\eta_f h_a A_a} \right)^{-1} \tag{5}$$

Looking at the local *UA*-values for three different distributions of the air flow, shown in graph b of Figure 3, it is seen that the local *UA*-value does increase for increased air velocity in channel 1. However, dryout is reached at

much lower values of z, and this is accompanied by a significant drop in the refrigerant side heat transfer coefficient, which is also seen as a decrease of the local UA-value. For the other channel, in which the air velocity is reduced, dryout occurs later than for the case of uniform air flow. Graph c in Figure 3 shows the mean local UA-value for the two channels together. It is seen that the total mean UA-value decreases with increasing maldistribution of the air flow. This decrease occurs mainly due to the changed dryout positions and not due to the changes in the air side heat transfer coefficients alone.

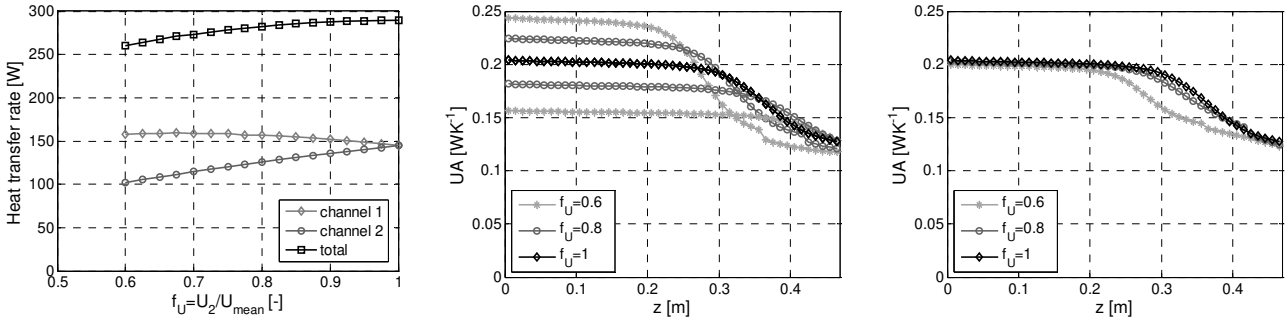

a) b) c)

Figure 3: (a) Influence of non-uniform air flow on the cooling capacity. (b) The local UA-values in the channels for different distributions of the air flow. (c) The mean local UA-value for the two channels together.

3.2 Maldistribution of the inlet quality

Apart from the air flow, also the distribution of the liquid and gas phase in the distributing header influences on the distribution of the refrigerant in the parallel channels. The refrigerant entering the distribution manifold is usually partly evaporated, and in order to guarantee an equal distribution of the mass flow rate, the liquid and gas phases have to be distributed evenly.

Since no detailed model of refrigerant flow in the manifold is considered in the model, the impact of the distribution of the gas and liquid phases on the cooling capacity is studied by varying the inlet quality to the different channels. The inlet quality to the manifold is kept constant at x = 0.3, while the inlet quality to the parallel channels is varied by letting more and more liquid go into channel 2. The air flow distribution is uniform for this study. Again a distribution parameter is defined in order to quantify the maldistribution in a simple manner:

$$f_x = \frac{x_2}{x_{\text{manifold,in}}}, \quad 0 < f_x < 1, \tag{6}$$

It is assumed that more and more liquid enters channel 2, while more and more gas enters channel 1. The parameter takes a value between 0 and 1, where f_x = 1 for uniform distribution of the inlet quality, and f_x = 0 when only liquid enters channel 2 and the remaining mixture of liquid and gas enters channel 1. In Figure 4 the distribution of the mass flow rate in the two channels is shown for increasing maldistribution of the inlet quality. It is seen that the total mass flow rate stays more or less constant, while the mass flow rate in channel 1 increases, and decreases in channel 2 for increasing maldistribution of the inlet quality.

As mentioned above, the contribution of the gravitational pressure drop is dominating the total pressure gradient at low qualities. This is also the reason why the refrigerant mass flow rate decreases in the channel, where the inlet quality is decreased (channel 1). From graph b in Figure 4 it is seen that the total pressure drop increases with increased maldistribution of the inlet quality.

Figure 5 shows how the heat transfer is affected by the maldistribution of the inlet quality. Although maldistribution of the refrigerant mass flow rate was found, graph a shows that the total cooling capacity stays more or less constant for increasing maldistribution of the inlet quality. Looking at the two channels individually it is seen that the heat transfer rate increases slightly for channel 2 and decreases slightly for channel 1, but these changes are insignificant.

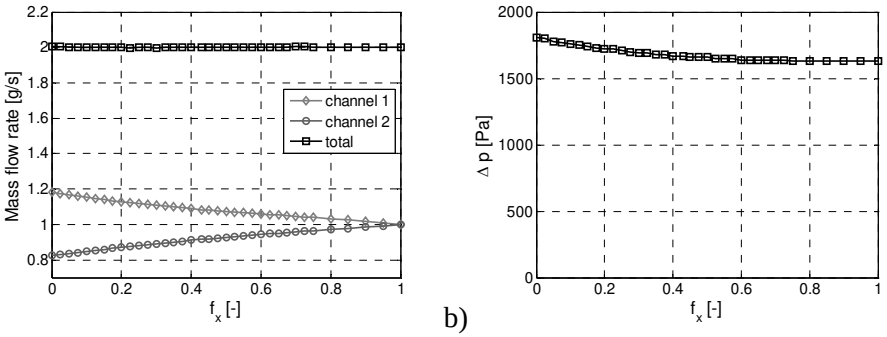

a) b)

Figure 4: (a) Influence of maldistributed inlet quality on the mass flow rate in the channels and (b) on the total pressure drop.

Figure 5b shows the local *UA*-values for three different distributions of the inlet quality. As long as the refrigerant is in two-phase conditions, the heat transfer coefficients are not affected by the maldistribution. However, the dryout positions are affected. Average local *UA*-values of two connected channels are shown in Figure 5c. Here it is seen, that while the overall heat transfer coefficient decreases for increased maldistribution in some regions the average local *UA*-values actually increase with increasing maldistribution in other regions. The total average *UA*-value is thus almost constant, in spite of the maldistribution.

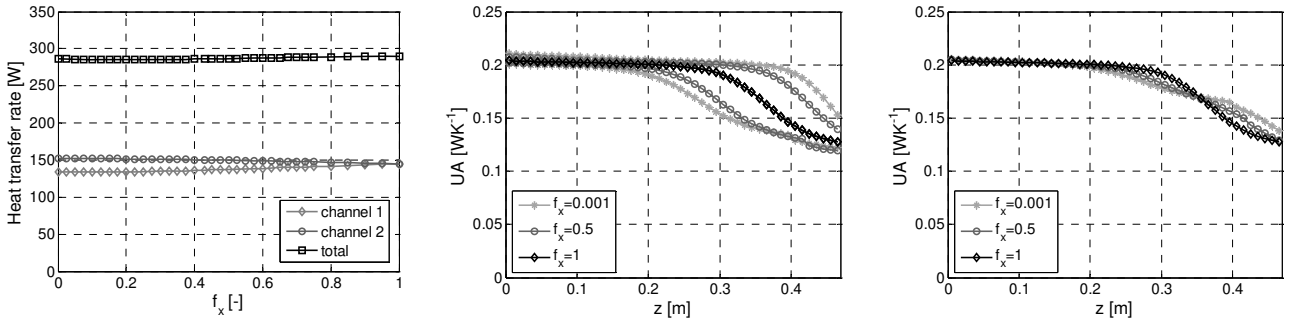

a) b) c)

Figure 5: (a) Influence of non-uniform inlet quality on the cooling capacity. (b) The local UA-values in the channels for different distributions of the inlet quality. (c) The mean local UA-value for the two channels together.

3.3 Comparison with results obtained for refrigerant R134a

Simulations similar to the ones presented above are performed using R134a as the refrigerant (Brix et al., 2008). Geometry and flow parameters are kept the same as for the simulations using CO_2. Figure 6 shows the reduction of the total mass flow rate and the reduction of the cooling capacity for increased maldistribution of the air flow. For both refrigerants the reduction in cooling capacity corresponds almost to the reduction of the cooling capacity. The results obtained for R134a show a significantly larger reduction in mass flow rate and cooling capacity with increased maldistribution than the results for CO_2. The reduction is a factor two larger for R134a than for CO_2.

Considering a maldistribution of the inlet quality instead, even bigger differences between the two refrigerants are found, which is shown in Figure 7. Whereas the results for CO_2 show no change in the total mass flow rate with increased maldistribution of the inlet quality, the total mass flow rate is decreased by more than 20% if only liquid R134a enters channel 2 and the remaining refrigerant enters channel 1. A similar picture is seen when looking at the reduction in cooling capacity. Here a reduction in cooling capacity of 23% is found for R134a.

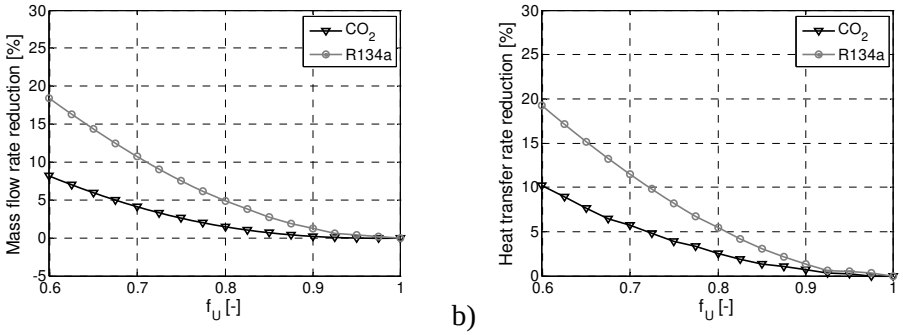

a) b)

Figure 6: Reduction in total mass flow rate and cooling capacity for increased maldistribution of the air velocity, for refrigerants CO_2 and R134a.

There is more than one reason that can explain these differences between the different refrigerants. One of the reasons, regarding the different pressure drop contributions, has already been mentioned above. For R134a the frictional pressure gradient is clearly dominating the accelerational and the gravitational contributions, thus both maldistribution of the air flow rate and maldistribution of the inlet quality affects the distribution of the refrigerant mass flow rate differently. Another reason is that the heat transfer coefficient of single phase CO_2 is higher than the heat transfer coefficient of single phase R134a.

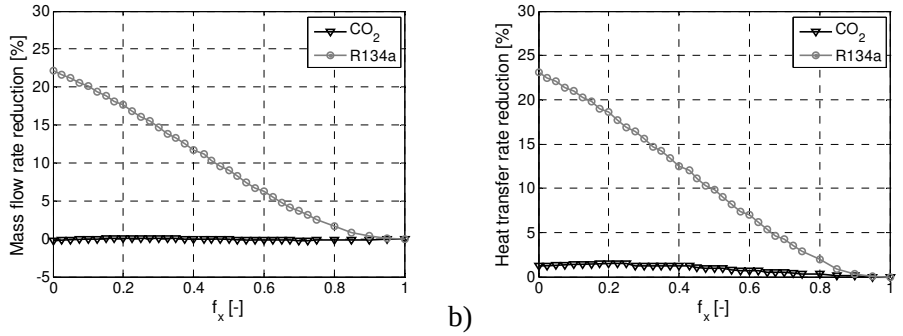

a) b)

Figure 7: Reduction in total mass flow rate and cooling capacity for increased maldistribution of the air velocity, for refrigerants CO_2 and R134a.

4. DISCUSSION

The presented results based on two different case studies show that the effects of maldistribution on the heat exchanger performance clearly depends on the choise of refrigerant. Also other factors, which have not been considered in this study could play an important role on the significance of the maldistribution. The type and geometry of the heat exchanger, temperatures and flow conditions as well as the control strategy of the refrigeration system. In this study the superheat out of the evaporator was controlled as in a direct expansion system. If a flooded evaporator system or other control systems were applied, preliminary studies show that performance decrease should be expected. However, the exact figures will vary. In order to obtain a complete understanding of maldistribution of airflow or inlet quality on evaporator performance, and the influence on overall system performance, further studies are carried out.

5. CONCLUSION

A numerical study of CO_2 flow in parallel evaporator channels has been performed. A 1D steady state simulation model was built, using correlations from the literature to calculate frictional pressure drop and heat transfer coefficients. A test heat exchanger was defined with two parallel channels, using CO_2 as refrigerant and air on the secondary side. For the test case the effects of a non-uniform air flow and the effects maldistribution of the inlet

quality on the heat exchanger performance were studied. The results for CO_2 were furthermore compared to results for a similar heat exchanger working with R134a as refrigerant. For a non-uniform airflow imposed, a reduction of the cooling capacity of up to 10% was found. However, the impact of the airflow maldistribution was considerably larger, when R134a was used as refrigerant. For maldistribution of the inlet quality the impact on the cooling capacity was found to be diminishingly small for CO_2 used as refrigerant, whereas a much larger impact was found for R134a. It could be concluded that for the heat exchanger geometry and flow conditions chosen in this study CO_2 as refrigerant was much less affected by maldistribution of the airflow or inlet quality than R134a.

NOMENCLATURE

Roman			Subscripts	
A	area	(m^2)	a	air side
f_U	distribution parameter	(-)	evap	evaporation
f_x	distribution parameter	(-)	f	fin
h	convection heat transfer coefficient	($W/(m^2K)$)	i	channel i
$\dot{m}$	mass flow rate	(kg/s)	in	into inlet manifold
p	pressure	(bar)	out	out of exit manifold
$\dot{Q}$	heat transfer rate	(kW)	r	refrigerant side
T	temperature	(°C)	sup	superheat
UA	overall heat transfer coefficient	(W/K)	w	wall
U	face air velocity	(m/s)		

Greek		
η	Fin temperature effectiveness	(-)

REFERENCES

1. Blasuis, P. R. H., 2002. VDI Wärmeatlas, 9th Edition. Springer-Verlag, Ch. Lab.
2. Brix, W., Elmegaard B., Kærn, M.R., 2008, Modelling refrigerant distribution in microchannel evaporators, *submitted to: International Journal of Refrigeration*.
3. Choi J.M., Payne W.V., and Domanski P.A., 2003, Effects of Non-Uniform Refrigerant and Air Flow distribution of Finned-Tube Evaporator Performance. *International Congress of Refrigeration,* ICR0040.
4. Choi, K.-I., Pamitran, A.S., Oh, C.-Y., Oh, J.-T., 2007, Boiling heat transfer of R-22, R-134a, and CO_2 in horizontal smooth minichannels. *International Journal of Refrigeration*, 30:1336-1346.
5. Chwalowski M., Didion D.A., and Domanski P.A., 1989, Verification of Evaporator computer Models and Analysis of Performance of an Evaporator Coil. *ASHRAE Transactions*, 95(1):793-802.
6. EES 2007. Engineering equation solver. Academic Professional V7.954-3D, F-Chart Software, Middleton, WI, USA.
7. Gnielinski, V., 2002. VDI Wärmeatlas, 9th Edition. Springer-Verlag, Ch. Ga
8. Kim M.-H., and Bullard C.W, 2002, Air-side thermal hydraulic performance of multi-louvered fin aluminium heat exchangers. *International Journal of Refrigeration*, 25:390-400.
9. Müller-Steinhagen, H., Heck, K., 1986. A simple friction pressure drop correlation for two-phase ow in pipes. Chem. Eng. Process. 20, 291-308.
10. Pettersen J., 2004, Flow Vaporization of CO_2 in Microchannel Tubes. *Experimental Thermal and Fluid Scienc,.*28:111-121
11. Vist, S., Pettersen, J., 2004a. Two-phase flow distribution in round tube manifolds. ASHRAE Transactions 110 (1), 307-317.
12. Vist, S., Pettersen, J., 2004b. Two-phase flow distribution in compact heat exchanger manifolds. Experimental Thermal and Fluid Science 28, 209-215.

Paper V

Wiebke Brix, Brian Elmegaard

Comparison of two different modelling tools for steady state simulation of an evaporator

SIMS50 - Modelling and Simulation of Energy Technology, (2009)

Proceedings of SIMS 50
Fredericia, Denmark
October 7–8, 2009

COMPARISON OF TWO DIFFERENT MODELLING TOOLS FOR STEADY STATE SIMULATION OF AN EVAPORATOR

Wiebke Brix *and Brian Elmegaard
Technical University of Denmark
Department of Mechanical Engineering
2800 Lyngby
Denmark

ABSTRACT

In this paper a test case is solved using two different modelling tools, Engineering Equation Solver (EES) and WinDali, in order to compare the tools. The system of equations solved, is a static model of an evaporator used for refrigeration. The evaporator consists of two parallel channels, and it is investigated how a non-uniform airflow influences the refrigerant mass flow rate distribution and the total cooling capacity of the heat exchanger. It is shown that the cooling capacity decreases significantly with increasing maldistribution of the airflow. Comparing the two simulation tools it is found that the solutions differ only slightly depending on which software is used for solving due to differences in the thermophysical property functions. Considering the solution time, WinDali solves the equations more than 100 times faster than EES.
Keywords: Evaporator, Maldistribution, Engineering Equation Solver, WinDali

NOMENCLATURE

h	Enthalpy [kJ/kg]
f_U	Distribution parameter [-]
$\dot{m}$	Mass flow rate [kg/s]
p	Pressure [bar]
$\dot{Q}$	Heat transfer rate [W]
R	Relative residual
T	Temperature [°C]
U	Velocity [m/s]
x	Quality [-]
Subscipts	
i	channel i
in	inlet
out	outlet
sup	superheat

INTRODUCTION

Modelling and simulation of energy systems is widely used as an alternative to experimental investigations for both design and optimization of a system. The general scheme is always the same, first the relevant equations describing the system in the level of details desired are found. Next, the question arises: Which tool will be suitable to help solving this set of equations? Many different modelling tools exist, which are specifically minded for solving equations describing energy systems. Each tool has its advantages, some tools are suitable for dynamic systems, while others have their strength in solving algebraic equations describing a steady state solution. It is difficult to find any guidelines in the literature of which tool to choose, mostly the choice is based on which tool is previously used, and often in-house codes are developed. In this paper a steady state model of an evaporator is developed and solved as a test case using two different modelling tools in order to compare the two tools and point out advantages and disadvantages of these two tools. The tools applied are: Engineering Equation Solver (EES) [1], and WinDali, [2].

The test case

Flow distribution of a fluid evaporating in parallel channels is interesting for applications of very dif-

*Corresponding author: Phone: +45 4525 4130 Fax: +45 4593 5215 E-mail:wb@mek.dtu.dk

ferent scales. In a steam generator of a power plant water evaporates in many parallel channels along the boiler walls. On a much smaller scale the evaporator in a refrigeration system may consist of many parallel mini- or microchannels.
Within the field of refrigeration, especially aluminum braced microchannel evaporators, with channel sizes in the 1 mm range have become very popular, since these heat exchangers both reduce the system sizes and reduce the refrigerant charge needed in order to obtain a given cooling capacity. Due to the small channel sizes a design with many parallel channels is required in order to keep the pressure drop at an acceptable level. However, parallel channels also induce the possibility of a maldistribution of the evaporating fluid. Maldistribution of the mass flow rate of refrigerant may occur due to different reasons, of which one could be an uneven heat load on the channels.
As a test case for this study, the impact of a non-uniform air velocity on the refrigerant mass flow distribution and on the cooling capacity of a microchannel evaporator is investigated. In order to keep the model relatively simple, only two, vertical microchannel tubes in parallel are considered. A microchannel tube is a flat tube with a number of small, rectangular or circular channels or ports. Two different refrigerants, R134a and CO_2, are considered, while air is flowing on the secondary side of the heat exchanger. In order to enhance the air side heat transfer, the parallel tubes are connected by louvered fins. Figure 1 shows a sketch of the two channels, and table 1 summarizes the parameters, which define the geometry of the test case evaporator as well as the flow conditions.

Evaporator geometry	
Tube length	0.47 m
# of ports in one tube	11
Cross section of one port	0.8 x 1.2 mm
Flow depth	16 mm
Distance between two microchannels	8 mm
Fin pitch	$727\,\mathrm{m}^{-1}$
Flow parameters	
Air temperature	35°C
Air velocity	1.6 m/s
Evaporation temperature	7.4°C
Quality at manifold inlet	0.3
Total superheat (R134a)	6 K
Total superheat (CO_2)	0 K
Quality at outlet (CO_2)	1

Table 1: Parameters defining the test case.

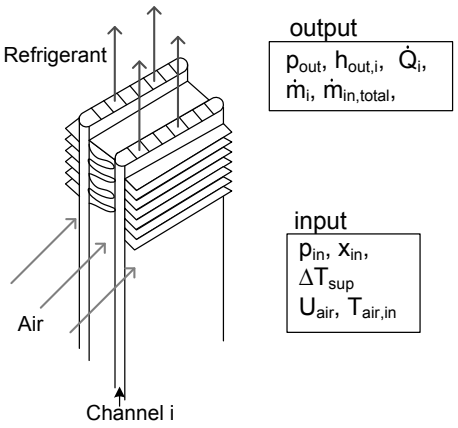

Figure 1: Sketch of two channels in parallel with input and output parameters to the model.

MODELLING THE EVAPORATOR

Besides showing a sketch of the geometry, figure 1 also shows the desired model inputs and outputs. It is assumed that the thermodynamic conditions at the inlet, the total mixed outlet superheat and the airside velocity and temperature distribution are measureable and therefore used as input to the model. Output are the total mass flow rate as well as the mass flow rate distribution, the thermodynamic conditions of the refrigerant at the outlet of each channel and the cooling capacity of each tube.
In order to model the evaporator, a discretized model of a single microchannel tube is built using a finite volume method. In the evaporator fins are connecting two neighboring tubes. For the single tube model half of the fin length is assumed to belong to the channel on each side. Each microchannel tube is discretized into an optional number of volumes, and each volume is treated as a small heat exchanger.
For each volume the continuity equation, the momentum equation and the energy equation are solved under the following assumptions:

- The system is in steady state.
- The refrigerant flow is one-dimensional.
- The refrigerant flow is homogeneous and vapor and liquid are in thermodynamic equilibrium.
- Axial heat conduction in the tube walls and between different tubes is negligible.

- The air is dry.

The frictional pressure drop and heat transfer coefficients are calculated using correlations from the literature, depending on the flow conditions. Table 2 summarizes the correlations that have been chosen. The different tubes are connected through, first of all, conservation of the total mass flow rate:

$$\dot{m}_{\text{in,total}} = \sum_{i=1}^{N} \dot{m}_i, \tag{1}$$

where N is the total number of channels. Secondly, no pressure drop is assumed in the inlet or outlet manifolds, such that the total pressure drop over each tube has to be equal:

$$\Delta p_i = p_{\text{in}} - p_{\text{out}}. \tag{2}$$

Since the total superheat out of the evaporator often is used as a control parameter in refrigeration systems, this parameter is given as an input to the model instead of the mass flow rate. Both the total mass flow rate and the distribution of the mass flow rate are thus calculated from the model. The pressure drop across any tube depends on the mass flow rate, inlet quality and heat load, why almost all model equations depend on each other. This is illustrated in the model flowchart shown in figure 2. The flowchart shows the top layer of the model, while most of the calculations are performed in the box indicated as procedure HX_volume. In this procedure the pressure drop and energy balance is calculated for each volume.

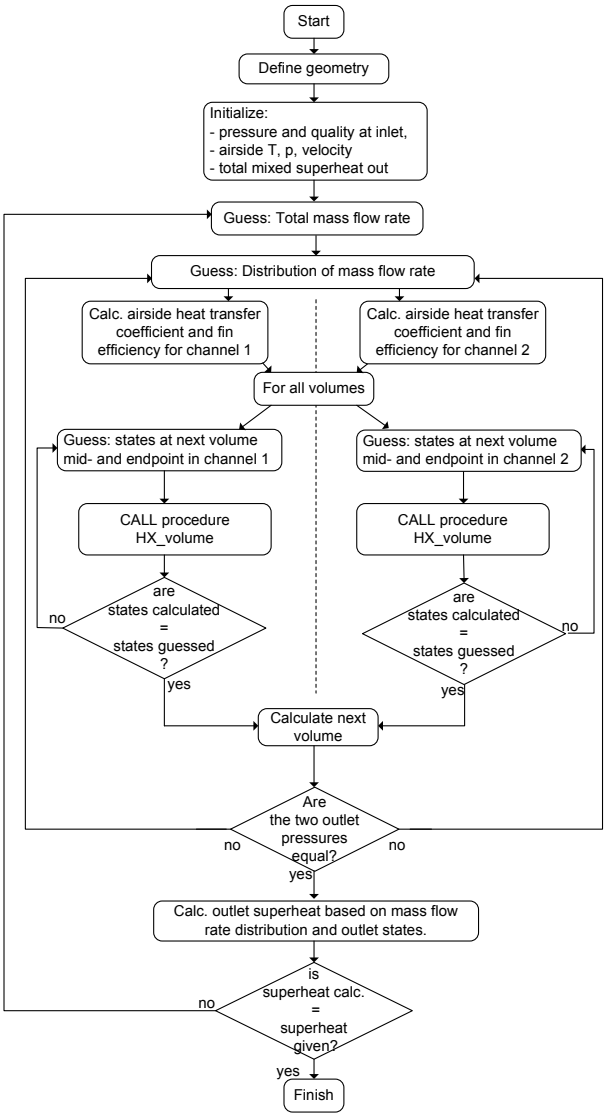

Figure 2: Flowchart of the model equations. The pressure drop and heat transfer calculations are performed inside the procedure HX_volume.

MODELLING TOOLS

In order to solve the model equations, the model is implemented using two different modelling tools. Both modelling tools are implemented in equation solvers, and both tools are designed for solving models of thermodynamic processes.

Engineering Equation Solver

Engineering Equation Solver (EES) [1], is developed for numerically solving systems of algebraic equations, but it is also possible to solve differential equations. Using EES the model is written as mathematical equation in a very free form where equations are implemented in arbitrary order. The equations may be arranged in according to the user's preferences. Pascal-like functions and procedures may be implemented. For the numerical solution the equations are blocked, and each block is solved using a Newton-Raphson method. Convergence of the solution is reached as soon as the relative residuals are smaller than a specified value. Thermophysical properties of a large number of fluids can be found using the built in thermodynamic functions that call an equation of state in order to calculate the wanted properties.

Air side	
Heat transfer coefficient	Kim and Bullard [3]
Two-phase region	
Heat transfer coefficient (R134a)	Zhang et al. [4]
	+ smooth transition to single phase
Heat transfer coefficient (CO_2)	Choi et al. [5]
	+ smooth transition to single phase
Frictional pressure drop	Müller-Steinhagen and Heck [6]
Single phase region	
Heat transfer coefficient	Gnielinski [7]
Frictional pressure drop	Blasius [8]

Table 2: Summary of correlations used to calculate heat transfer coefficients and pressure drop.

WinDali

WinDali [2] is a modelling and simulation software that solves systems of ordinary differential equations (ODE's) or algebraic equations (AE's). The software comprises of two parts, a model editor, which is a Free Pascal Editor, and a simulation program that reads the compiled model and solves the equations. All static equations that are part of the iterations need to be formulated as residual equations. The algebraic equations are solved using a modified Newton iteration scheme, which includes convergence and divergence control [2]. Otherwise, the software has the same main properties as EES, i.e. functions with thermodynamic properties are a built-in part, and it is possible to include procedures and functions.

Accuracy of the solution

For both modelling tools a stop criterion for the Newton-Raphson iterations needs to be given. For both EES and WinDali this criterion is given by setting the maximum allowable relative residual. The relative residual is defined as the relative difference between the solutions of two successive iteration steps:

$$R = \frac{y^k - y^{(k-1)}}{y^{(k-1)}}, \tag{3}$$

where y^k is the solution found for iteration number k. The accuracy of the solution increases with decreased residuals, but so does the solution time, therefore a suitable stop criterion is found.

A relative error of the solution at a given stopping criterion is found by comparing the solutions to a more accurate solution:

$$\text{Error} = \max\left(\left|\frac{y - y_{acc}}{y_{acc}}\right|\right), \tag{4}$$

where y is a solution vector containing all static variables found by iteration, and y_{acc} is assumed to be the accurate solution. Since no analytical solution is availiable, y_{acc} is a numerical solution with a very small relative residual requirement.

In table 3 errors are summarized for the solution of the uniformly distributed case. For the Newton method quadratic convergence would be expected, such that for each iteration step, the number of correct digits is roughly doubled. This behavior is seen for the WinDali solutions. An extra iteration is performed when setting the maximum relative residual from 10^{-3} to 10^{-4}, while for the following solutions no extra iteration is needed to fulfill the residual requirement. Using EES the behavior is different, here the solution converges more slow. A stop criterion of 10^{-4} is chosen for both modelling tools.

R	10^{-3}	10^{-4}	10^{-5}	10^{-6}
Error, EES	9.1e-3	2.7e-4	6.4e-5	6.8e-6
Error, WinDali	2.1e-3	3.9e-7	3.9e-7	3.9e-7

Table 3: Error for different stop criteria.

Comparison of solutions obtained using EES and WinDali

The evaporator model is solved using both EES and WinDali. For the comparison of the solutions uniform airflow is considered, there is hence no maldistribution of the refrigerant in these cases. Two different refrigerants, R134a and CO_2, are applied using the test case parameters listed above. Figures

3 and 4 show the local heat flux and the pressure along the channel for R134a and CO_2, respectively. It is seen, that the solutions using EES and Windali do not totally coincide for neither of the refrigerants. The largest difference in the heat flux is 309 W/m^2 for R134a, which corresponds to 4.6%, while for CO_2 it is 68 W/m^2 or a little less than 1%. The differences in the solution of the pressure are smaller, < 0.1% for R134a and < 0.01% for CO_2. These discrepancies occur because of differencies in the thermophysical property functions. However, the solutions are considered sufficiently identical to compare the two tools.

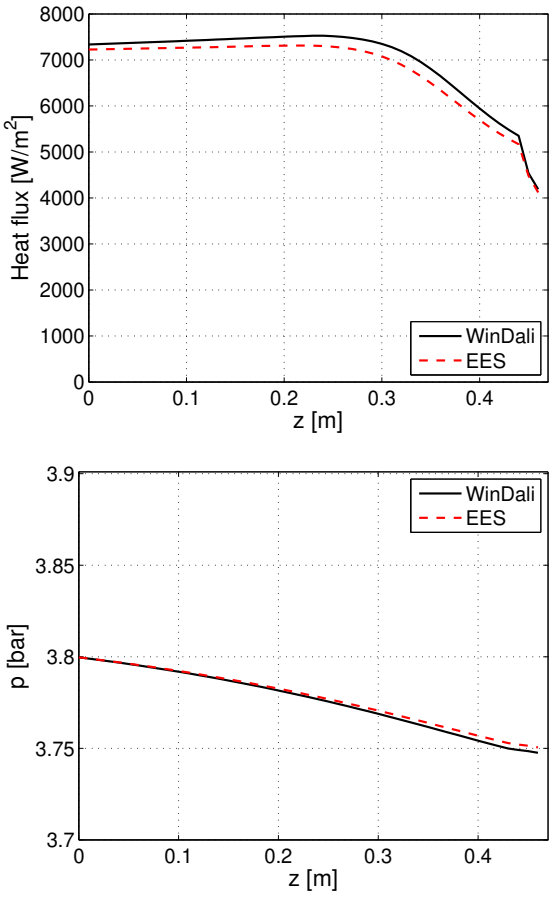

Figure 3: Comparison of the local heat flux and pressure in the channel for refrigerant R134a with uniform distribution of the airflow.

RESULTS AND DISCUSSION

The aim of modelling the parallel channel evaporator was to investigate the impact of a non-uniform

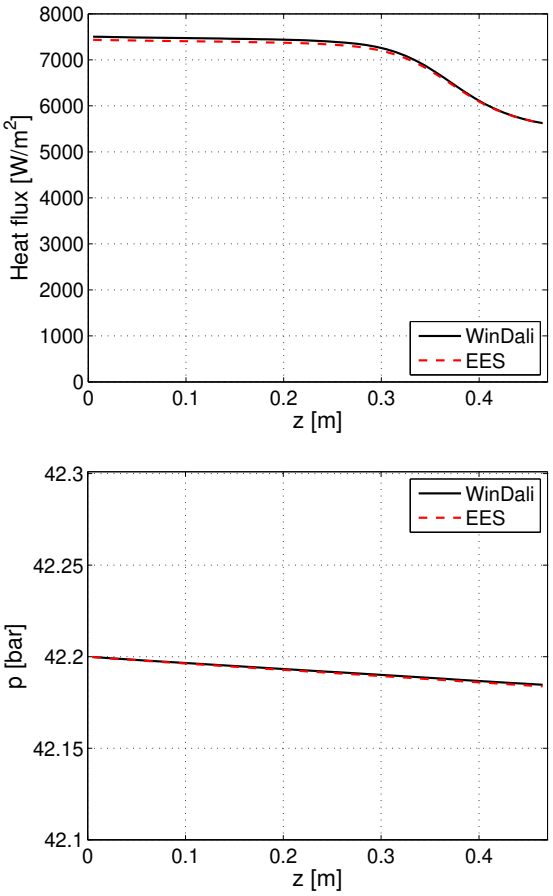

Figure 4: Comparison of the local heat flux and pressure in the channel for refrigerant CO_2 with uniform distribution of the airflow.

airflow on the cooling capacity of the heat exchanger. The airflow over the channels affects the heat load on each, which again determines how fast the refrigerant inside the channels evaporates. In order to keep the same total pressure drop over each of the channels, the mass flow rate will distribute accordingly. In order to perform the investigation, a simple airflow distribution is used, where the air velocity is increased over one channel and decreased over the other, while the mean velocity is kept constant. In order to quantify the degree of maldistribution in a simple way, a distribution parameter is defined as:

$$f_U = \frac{U_2}{U_{\text{mean}}}, \quad 0 < f_U < 1, \tag{5}$$

where U_{mean} is the mean velocity and U_2 is the air velocity on channel 2, which is decreased for increased maldistribution. The parameter f_U thus takes a value

between 0 and 1, where $f_U = 1$ for a uniform air flow and $f_U = 0$, when there is no airflow on channel 2 and all air flows by channel 1.

Figure 5 shows how the mass flow rate and cooling capacity are influenced by maldistribution of the airflow for refrigerant R134a for both modelling tools. For an increasing maldistribution of the airflow. i.e. decreasing f_U, the mass flow rate decreases in both channels. In channel 1, where the air velocity is increased, the airside heat transfer coefficient will increase, which again increases the UA-value of this channel. In this channel the refrigerant therefore evaporates faster. However, since the frictional pressure gradient is higher for gas than liquid, the mass flow rate of refrigerant has to decrease in order to keep the pressure drop equal on both channels.

The lower graph in figure 5 shows how the cooling capacity is affected by maldistribution of the airflow. As it is expected, the cooling capacity decreases in the channel 2, due to the lower air velocity. Since the air side heat transfer coefficient does not change linearly, such that it increases less with higher air velocity than it decreases with lower air velocity, the UA-value of the total evaporator will decrease with increased maldistribution of the airflow. A decrease in the UA-value results in a decreased cooling capacity. Meanwhile, in order to keep the total mixed superheat out of the evaporator constant the total mass flow rate decreases, as seen in the upper graph in 5. This decrease of the mass flow rate is responsible for the decrease of the cooling capacity in channel 1, and hence for the decrease of the total cooling capacity.

The dashed lines in figure 5 show results obtained using EES, while the solid lines show WinDali results. It is seen that EES consistently predicts a slightly lower mass flow rate and heat transfer rate, but the shape of the curves are the same. For $f_U < 0.55$ EES fails to converge. WinDali does the same for $f_U < 0.525$. Since both solvers fail to converge at almost the same values, it can be assumed that this limit is given by something in the system of equations rather than the solver.

At the largest maldistribution modelled here, $f_U = 0.525$, which corresponds to a velocity of 2.36 m/s in channel 1 and 0.84 m/s in channel 2, the cooling capacity is decreased by 27%.

In figure 6 similar graphs are shown using CO_2 as refrigerant. Although the thermodynamic properties

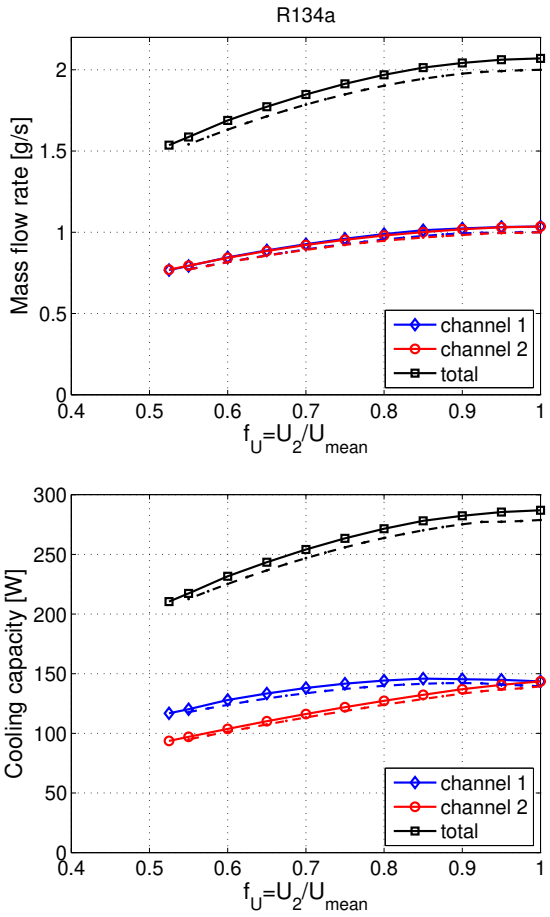

Figure 5: Influence of airflow maldistribution on the mass flow rate and cooling capacity of the two channels using R134a as refrigerant. The solid lines with markers shows the results obtained using WinDali, and the dashed lines show the results using EES.

of CO_2 are quite different from R134a, the general behavior is very similar, at least for this case. Also for CO_2 the mass flow rate decreases in both channels. The total cooling capacity stays almost constant for $0.9 < f_U < 1$, but decreases for smaller values of f_U. In channel 1, which recieves the higher air velocity, the cooling capacity increases slightly until $f_U = 0.7$. However, for smaller values of f_U the cooling capacity of this channel decreases due to the reduced mass flow rate in the channel.

Again, the solid lines show the results obtained from WinDali, while the dashed lines show the EES results. The results obtained from EES and WinDali agree very well, only for very small values of f_U small discrepancies are seen. Also for CO_2 both software fail to converge at some point. For Win-

Dali, the solver cannot converge to a solution for $f_U < 0.25$, while EES fails to converge at f_U smaller than 0.2.

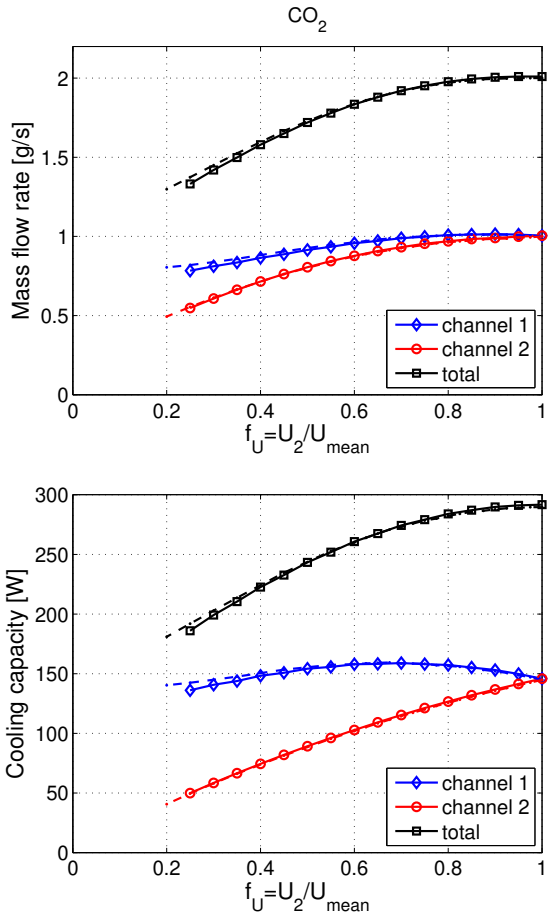

Figure 6: Influence of airflow maldistribution on the mass flow rate and cooling capacity of the two channels using CO_2 as refrigerant. The solid lines with markers shows the results obtained using WinDali, and the dashed lines show the results using EES.

Figure 7 compares the reduction of the cooling capacities due to maldistribution of the airflow. For R134a the percentwise reduction of the cooling capacity is independent of the modelling tool, despite the differences that were seen in figure 5. For the worst cases the reduction in cooling capacity for R134a is more than 20%. For CO_2 the cooling capacity is less affected by airflow maldistribution than R134a. At $f_U = 0.6$, the cooling capacity down to 80% for R134a, while it is only down to 90% for CO_2.

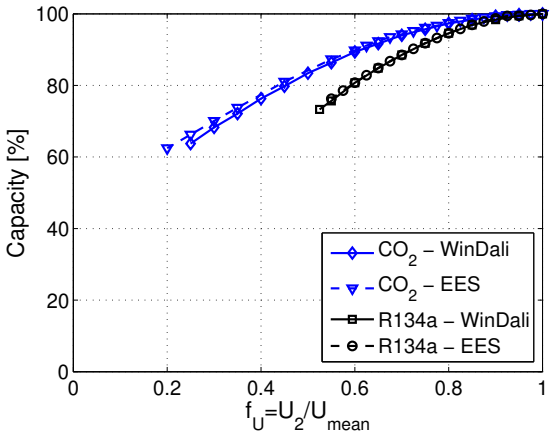

Figure 7: Comparison of the reduction of cooling capacity due to maldistribution of the airflow for R134a and CO_2 using both EES and WinDali.

General experiences with the different tools

The most significant difference between the two modelling tools when modelling the test case, is the solution time. Figure 8 shows the time used for solutions. All calculations were performed on the same personal computer, an Intel(R) Core(TM) 2 CPU, U7600@1.2 GHz and 2 GB of RAM. It was furthermore tested that the solution times were repeatable. For all points shown in the figure the same initial guesses - the solution of the uniformly distributed case - were used. This means that for the points at $f_U = 1$, the solution of the problem is used as initial guess. In this case WinDali is 25 times faster than EES for R134a and 40 times faster for CO_2. Changing the parameter f_U with increasing steps results in longer solution times. In general, if not the solution is used as initial guess, WinDali solves the equations more than 100 times faster than EES.

It is furthermore interesting to know, how dependent the solver is on accurate initial guesses when performing parameter variations. The largest parameter change (in f_U) where WinDali is still able to converge is $f_U = 0.6$ for R134a and $f_U = 0.55$ for CO_2. For EES it is also $f_U = 0.6$ when using R134a as refrigerant, while EES can go down to $f_U = 0.2$ when using CO_2. There is hence no unambiguous answer, on which tools is most stable considering parameter changes.

When running the model, WinDali thus has some considerable advantages to EES, since it is much

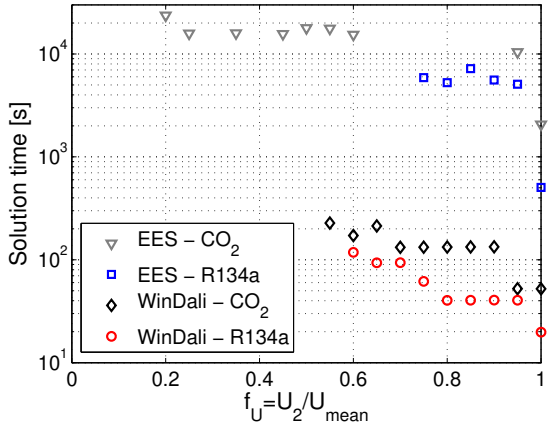

Figure 8: Time used to reach the solution when the solution of the uniform distribution case ($f_U = 1$) is used as guess values.

faster. However, on the implementation side EES has advantages. Implementation of small models in EES is extremely easy and fast and it is also straightforward to build up a larger model gradually, extending the model bit by bit. Using WinDali the model structure is more locked.
When implementing the evaporator model discussed above, EES was used for prototyping. For this purpose EES is an excellent tool. The final model was then transferred to WinDali.

CONCLUSION

In this paper a model of two parallel evaporator channels was built in order to investigate how non-uniform airflow influences on the cooling capacity of the evaporator. Furthermore the model was used as a test case in order to compare and evaluate two different modelling tools: EES [1] and WinDali [2]. Two different refrigerants, R134a and CO_2 were used in the evaporator, and it was shown, that the cooling capacity decreased considerably with increasing maldistribution of the airflow for both refrigerants. However, the cooling capacity of the evaporator using refrigerant R134a was considerably more affected by the airflow maldistribution than the evaporator using CO_2 as refrigerant.
It was furthermore found that the two modelling tools do not give identical results since the functions used for to calculate thermophysical data are not identical. Especially for CO_2 in the superheated region significant discrepancies occur.
Comparing the two modelling tools showed that the solutions agreed very well. Only small discrepancies were found, which occured since the functions used for calculating the thermophysical data were not identical. Considering solution times WinDali was in general more than 100 times faster than EES. However, the implementation of a model in EES is much more straightforward than WinDali.

REFERENCES

[1] EES. Engineering equation solver, 2007. Academic Professional V7.954-3D, F-Chart Software, Middleton, WI, USA.

[2] Morten Juel Skovrup. Windali, 2008. Technical Univesity of Denmark, Department of Mechanical Engineering, http://www.et.web.mek.dtu.dk/WinDali/Index.html.

[3] M.-H. Kim and C. W. Bullard. Air-side thermal hydraulic performance of multi-louvred fin aluminium heat exchangers. *International Journal of Refrigeration*, 25:390–400, 2002.

[4] W. Zhang, T. Hibiki, and K. Mishima. Correlation for flow boiling heat transfer in mini-channels. *International Journal of Heat and Mass Transfer*, 47:5749–5763, 2004.

[5] J. M. Choi, W. V. Payne, and P. A. Domanski. Effects of non-uniform refrigerant and air flow distribution of finned-tube evaporator performance. *Proceedings of the International Congress of Refrigeration*, 2003. . Washington D.C., USA, ICR0040.

[6] H. Müller-Steinhagen and K. Heck. A simple friction pressure drop correlation for two-phase flow in pipes. *Chem. Eng. Process.*, 20:291–308, 1986.

[7] V. Gnielinski. *VDI Wärmeatlas*, chapter Ga. Springer-Verlag, 9th edition, 2002.

[8] P. R. H. Blasius. *VDI Wärmeatlas*, chapter Lab. Springer-Verlag, 9th edition, 2002.

Paper VI

Wiebke Brix

Modelling of refrigerant distribution in microchannel evaporators

Danske Køledage 2008

Modelling of refrigerant distribution in microchannel evaporators

Wiebke Brix,
Department of Mechanical Engineering, Technical University of Denmark, email: wb@mek.dtu.dk

Abstract

The effects of refrigerant distribution in parallel evaporator channels on the heat exchanger performance are investigated numerically. For this purpose a 1D steady state model of refrigerant R134a evaporating in a microchannel tube is built. A study of the refrigerant distribution is carried out for two channels in parallel. It is shown that the cooling capacity is reduced, both if the inlet quality is unevenly distributed and if the airflow on the outside of the channels is not equally distributed.

Introduction

Microchannel evaporators are getting more and more popular because these heat exchangers are very effective considering their volume. They help reducing system sizes and reducing the refrigerant charge needed in order to obtain a given cooling capacity.
The use of channels with a small diameter has thus great advantages on the heat transfer. However, the pressure drop in the heat exchanger would increase significantly if traditional designs were used. This problem is solved by using many parallel channels. However, this introduces another problem, on which we will focus in this work: maldistribution of the refrigerant in the parallel channels.

Maldistribution of the refrigerant may result in unevenly distributed superheated regions of an evaporator, maybe even so much that the refrigerant in some channels is not fully evaporated, while in other channels the superheat is so high that the heat transfer is extremely low in the dry end of the channel. This may lead to a reduced cooling capacity and system performance (COP).

Since the refrigerant flow is usually in a two-phase state at the inlet manifold, the distribution of the liquid and gas phase depends on the manifold design. This is one of the reasons why maldistribution occurs. Another reason for maldistribution of the refrigerant could be an uneven heat load on the air side.

A number of experimental studies have been performed on two-phase refrigerant distribution in parallel channels, both for conventional and microchannels. Vist and Pettersen conducted experiments on horizontal manifolds with 10 parallel, vertical channels with refrigerants R134a [1] and CO_2 [2]. Both the liquid/gas distribution in the header as well as the heat load on the different channels have been investigated. Hwang *et al.* [3] have investigated distribution of the liquid phase in a manifold for a microchannel evaporator. However, these studies focus primarily on the distribution in the header and not on the effects of the distribution on the heat exchanger performance.

We here present a numerical study of the effects of maldistribution of refrigerant into parallel microchannel tubes. Both the maldistribution generated in the header, i.e. the distribution of liquid and vapour into the different channels, and the maldistribution of refrigerant occurring due to unevenly distributed air velocities are considered. The main objective is to quantify effects of the maldistribution on the heat exchanger performance.

Method

An evaporator model is built as a 1D steady state model of the channels using a finite volume method. Each channel is thus discretized into a number of volumes. Each volume can hold either single phase flow or two-phase flow. For each volume the continuity equation, the momentum equation and the energy

equation are applied. In order to calculate frictional pressure drop and heat transfer coefficients different correlations are applied depending on the flow conditions. The correlations chosen are summarized in Table 1.

	Model
Air-side:	
Heat transfer coefficient	Kim and Bullard [4]
Two-phase:	
Heat transfer coefficient	Zhang *et al.* [5] Smooth transition to single phase HT
Void fraction	Homogenous
Frictional pressure drop	Müller-Steinhagen and Heck [6]
Single phase:	
Heat transfer coefficient	Gnielinski [7]
Frictional pressure drop	Fanning friction factor

Table 1: Summary of empirical correlations used to calculate heat transfer coefficients and frictional pressure drop.

General assumptions that have been made are: dry air on the airside, no pressure drop in the manifolds and furthermore it is assumed that there is no maldistribution of the refrigerant between the ports of one multiport microchannel tube. The model handles the multiport channels such that pressure drop and heat transfer coefficients are calculated for a single port, while the total heat transfer area of the multiport tube is considered when calculating the heat transfer rate for the tube.

A sketch of the evaporator with model inputs and outputs is shown in Figure 1. The single microchannel tube models are linked together as parallel channels assuming that the pressure drop is equal for all tubes:

$$\Delta p_i = p_{in} - p_{out}, \quad (1)$$

conservation of the total mass flow rate:

$$\dot{m}_{in,total} = \sum_{i=1}^{N} \dot{m}_i \quad (2)$$

and conservation of the liquid and gas mass flow rates in the header:

$$\dot{m}_{in,total} x_{header,in} = \sum_{i=1}^{N} \dot{m}_i x_i \quad (3)$$

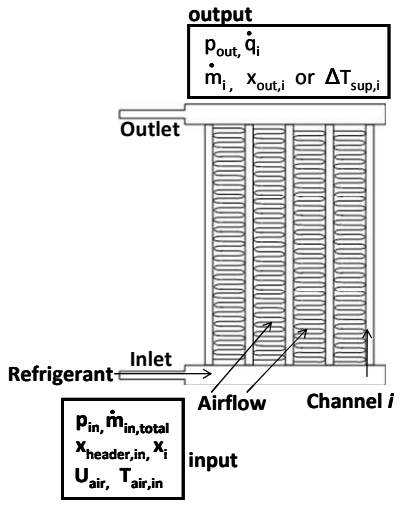

Figure 1: Input and output of the model are shown.

Modelling results and discussion

A fixed heat exchanger geometry is chosen in order to perform investigations on two microchannel tubes in parallel. The two channels are vertically oriented with upwards flow direction, and each of the channels has six ports with a dimension of 1.2x1.5 mm. R134a is chosen as the refrigerant. The most important input parameters are listed in Table 2.

Four different cases are studied: Two cases where the effects of the inlet quality distribution are considered and two cases where the effects of maldistributed airflow on the outside of the tubes are considered. In each of these groups, the effect of maldistribution is investigated for constant mass flow rate and constant superheat.

Mean air velocity	2 m/s
Air temperature	2°C
Refrigerant inlet pressure	2 bar (-10°C)
Refrigerant mass flow rate	2 g/s
Channel length	1.2 m
Inlet quality to manifold	0.2

Table 2: Input parameters.

Maldistribution of inlet quality

Usually a mixture of liquid and vapour is fed into the evaporator. How the two phases will distribute in the header depends on many parameters such as the header geometry, mass flow rates and refrigerant properties. The distribution of the two phases does then influence on the distribution of the inlet quality to the different parallel channels. Since we have no detailed model of the flow in the header, maldistribution of the inlet quality is studied by simply varying the inlet quality to the different channels.

In this first case the inlet quality to each of the channels is varied, while the inlet quality to the header is kept constant at 0.2. The total mass flow rate of refrigerant in the channels is also kept constant at 2 g/s. The airflow is assumed to be evenly distributed. The two tubes are numbered as channel 1 and channel 2, and the inlet quality to the channels is varied such that the quality into channel 1 is increased and decreased in channel 2. Since the manifold is considered adiabatic, equation (3) has to be fulfilled at all times.

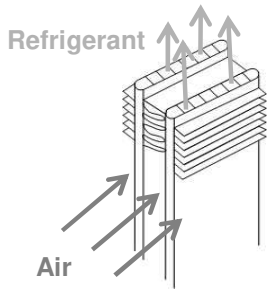

Figure 2: Sketch of the two microchannel tubes.

A distribution parameter, f_x, is defined in order to quantify the distribution in a simple way:

$$f_x = \frac{x_2}{x_{header,in}}$$

This parameter will take a value between 0 and 1. For equal distribution of the inlet quality $f_x = 1$, while when $f_x = 0$ only liquid is fed into channel 2 and a remaining mixture of liquid and gas goes into channel 1.

In Figure 3 the influence of the inlet quality on the mass flow rates and superheat is shown. As expected the mass flow rate decreases in channel 1 when the inlet quality into this channel is increased. In the right graph it is seen that the superheat in channel 1 increases and approaches the air temperature.

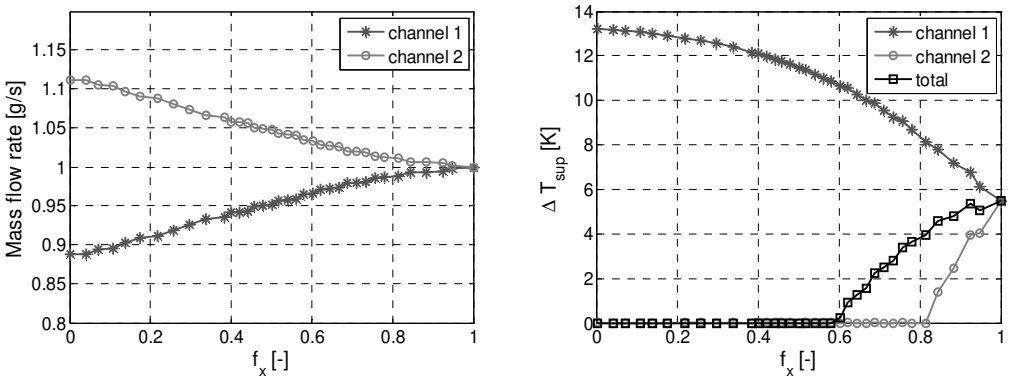

Figure 3: Influence of inlet quality distribution on the mass flow rate and on the outlet superheat.

With increasing maldistribution of the inlet quality, a larger part of channel 1 will be dry, and thus a larger part of the channel will have low heat transfer. Meanwhile, for $f_x < 0.8$ the refrigerant in channel 2, where we have a higher mass flow rate and lower inlet quality, not all of the refrigerant will evaporate. How this affects the total heat transfer rate is shown in Figure 4. In the figure it is seen that the total heat transfer rate decreases slowly with increasing maldistribution of the inlet quality. For a small degree of maldistribution no reduction in heat transfer rate is found, and when only liquid enters channel 2, the heat transfer rate of both channels together is reduced by 13%.

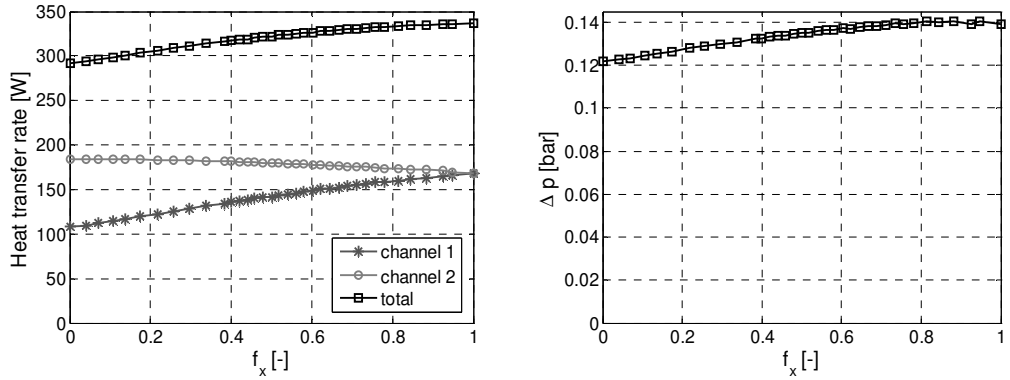

Figure 4: Influence of inlet quality distribution on the heat transfer rate and total pressure drop.

In the right graph of Figure 4 the pressure drop over the two channels is shown. Interestingly the total pressure drop decreases for increased maldistribution, so as a first thought it could look as if it is more favourable for the flow to be maldistributed. However, as mentioned different mechanisms in the manifold are responsible for the distribution of the inlet quality, so nothing can really be concluded from this graph alone.

In the second case considered, the total superheat is kept constant at $\Delta T_{sup} = 5.5K$ instead of the total mass flow rate. In this case the total mass flow rate is reduced with increasing maldistribution on the inlet quality, as can be seen in Figure 5.

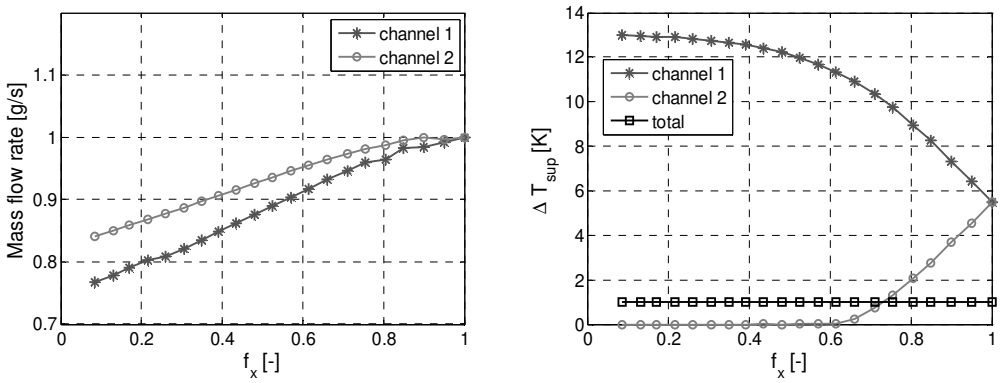

Figure 5: Mass flow rate and superheat as a function of inlet quality distribution for constant suberheat.

Although the mass flow rate decreases in both channels, channel 2 does again have a higher mass flow rate than channel 1. From the right graph in Figure 5, which shows the superheat of the single channels as well as the mixed superheat, it can be seen that even though the total superheat is constant, the refrigerant in channel 2 does not fully evaporate at $f_x < 0.6$.

The decrease in total mass flow rate also influences the cooling capacity of the channels, which is shown in Figure 6. The heat transfer rate from channel 2 is almost constant, where it in the previous case was slightly increased. Therefore also the total heat transfer rate is decreased slightly more than in the previous case. At $f_x = 0.1$ the heat transfer rate is reduced by 20% compared to the base case with equal inlet quality distribution.

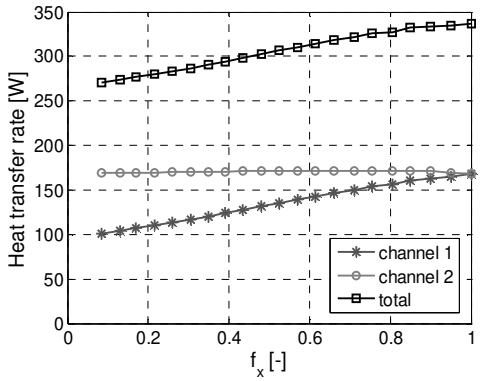

Figure 6: Influence of inlet quality distribution on the heat transfer load, when the mixed superheat is kept constant.

Finally, the two cases show that the distribution of the inlet quality clearly does have an impact on the heat exchanger capacity. It also shows that the cooling capacity in the case of constant mixed superheat is more affected than in the case of constant mass flow rate. Often, the superheat out of the evaporator is used as a control parameter of the total refrigeration system, and therefore this case is especially interesting.

Airflow maldistribution

If the heat transfer coefficients are higher for some channels than others, e.g. due to a higher air velocity on these channels, evaporation will happen faster in these channels. This affects the pressure gradient in the channels and because the total pressure drop over all channels is held constant, this also affects the

mass flow rate in the channels. Therefore a maldistribution of the airflow can have an effect on the distribution of refrigerant inside the channels.

In the next two cases considered, the inlet quality is kept constant at 0.2 for both channels, and the airflow distribution is varied. The total volume flow of air is kept constant, and hence the mean velocity of the airflow. To keep it relatively simple, it is assumed that when introducing a maldistribution of airflow, it will happen such that the air velocity is increased over the whole channel 1 and decreased over channel 2. Again, a maldistribution parameter is defined in order to quantify the maldistribution.

$$f_U = \frac{U_2}{U_{mean}}$$

This parameter will take a value between 0 and 1, where $f_U = 1$ for equal air velocities on both channels, while $f_U = 0$ when there is no airflow on channel 2, and all air passes channel 1.

The same input parameters are used as in the previous cases, and again the total mass flow rate is kept constant for the first results. In Figure 7 the effect of airflow maldistribution on the refrigerant mass flow distribution is shown, as well as the superheat in the channels. It is seen that as long as the mixture superheat is above zero, the refrigerant mass flow rates are not affected significantly. However, as soon as the evaporator runs wet, the mass flow rate decreases in channel 1 and increases in channel 2.

The fact that the mass flow rate will decrease in channel 1, which gets the higher air velocity, certainly influences the heat transfer rate, as can be seen in Figure 8. Channel 2 for which the heat transfer coefficient on the airside will be lower, thus furthermore holds more refrigerant inside, so that relatively more refrigerant will see the lower overall heat transfer coefficient. At $f_U = 0.6$, i.e. $U_1 = 2.8$ m/s and $U_2 = 1.2$ m/s the heat transfer rate is reduced by 11% compared to the uniform airflow case.

This reduction in cooling capacity cannot be directly compared to the previous case with varying inlet quality directly, since f_x and f_U are not comparable.

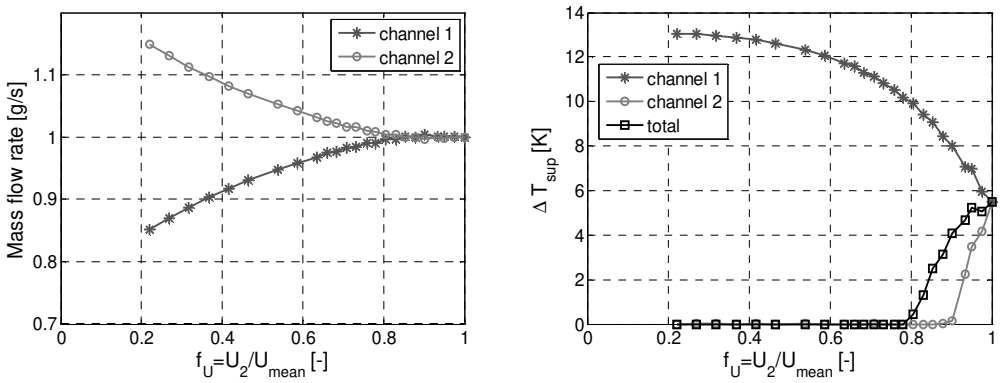

Figure 7: Influence of airflow distribution on the distribution of refrigerant mass flow rate and superheat in the channels.

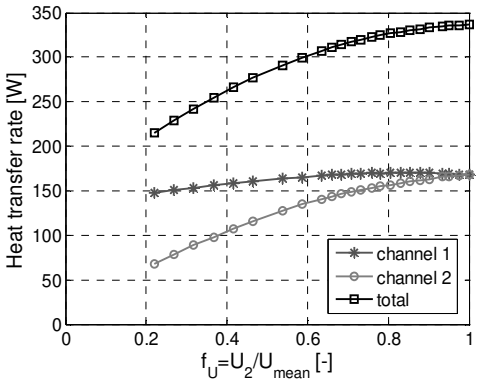

Figure 8: Influence of airflow distribution on the heat transfer rate.

Next, the superheat is kept constant, again at ΔT_{sup} = 5.5K. In Figure 9 it is seen that in this case the mass flow rate decreases significantly in both channels for increasing airflow maldistribution. Interestingly, the mass flow rate stays more or less equally distributed between the two channels. The reduction in heat transfer rate is in this case mainly induced by the reduction in total mass flow rate.

Figure 10 shows the heat transfer rate of the channels, and it is seen that the heat transfer rate is reduced almost equally for the two channels. The total heat transfer rate is affected at relatively small discrepancies in the airflow velocities, and at f_U = 0.6 a reduction of 23% on the capacity is found compared to a case of uniform air flow. This is twice as much as in the case of constant mass flow rate.

Although the heat transfer rates and mass flow rates show very similar behaviour in this case, the evaporation processes inside the channels are different, which is seen from the right graph in Figure 9. This can be seen from the right graph in Figure 9, which shows the outlet superheat of the channels. The evaporation of the refrigerant in channel 1 with the high air velocity happens fast, which means that for increasing airflow maldistribution a larger part of the channel is occupied by fully evaporated gas, resulting in low heat transfer coefficients in this part of the channel. On the other hand, not the entire refrigerant is evaporated in channel 2, such that not the full potential of the high heat transfer coefficients during evaporation is utilised. Whether it is a coincidence that the curves of mass flow rates and heat transfer rates follow each other that closely, needs to be investigated in future work, by considering different geometry and flow inputs.

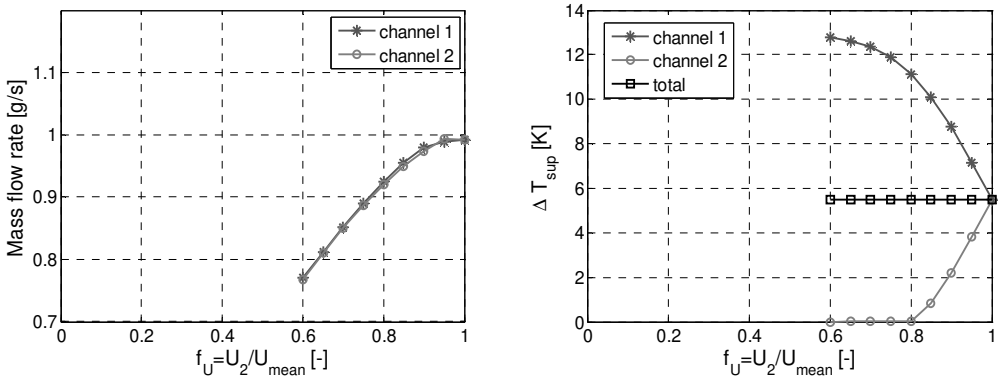

Figure 9: Influence of airflow distribution on refrigerant mass flow distribution and superheat.

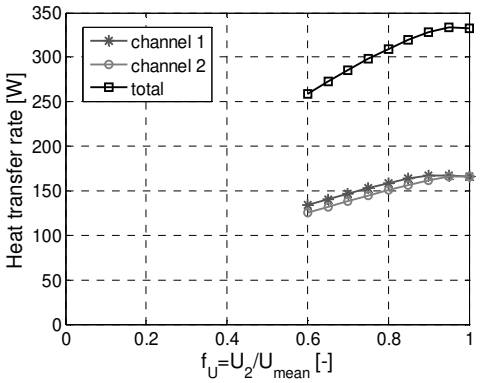

Figure 10: Influence of airflow distribution on heat transfer rate at constant superheat.

In reality it would probably be impossible to separate the effects of inlet quality distribution and airflow distribution. Most likely a combination of these two will influence on the heat exchanger performance. However, to get an image of the importance of the different mechanisms it makes sense to split the two sources and investigate each maldistribution by itself, as it has been done here.

Conclusions

A model of a microchannel evaporator has been built in order to numerically investigate the effects of refrigerant maldistribution in the parallel channels on the heat exchanger performance. A fixed heat exchanger geometry was chosen and results have been found for two channels in parallel. It was studied how both the maldistribution generated in the header due to the two-phase flow distribution and the maldistribution that occurs due to an uneven airflow distribution influences on the heat exchanger performance. It was shown that in all cases considered, the total cooling capacity was reduced for increased maldistribution. The reductions in performance were larger in the case of constant superheat at the outlet of the evaporator, than for constant refrigerant mass flow rate.

References

[1] Vist, S., Pettersen, J., Two-phase flow distribution in compact heat exchanger manifolds. *Experimental Thermal and Fluid Science*, 28:209-215, 2004.

[2] Vist, S., Two-phase flow distribution in round tube manifolds. *ASHRAE Transactions,* 110(1):307-17, 2004.

[3] Hwang, Y., Jin, D.-H., Radermacher, R., Refrigerant Distribution in Minichannel Evaporator Manifolds. *HVAC&R Research*, 13(4):543-555, 2007.

[4] Kim, M.-H., Bullard C. W., Air-side thermal hydraulic performance of multi-louvered fin aluminum heat exchangers. *International Journal of Refrigeration*, 25:390-400, 2002.

[5] Zhang, W., Hibiki, T., Mishima, K., Correlation for flow boiling heat transfer in mini-channels. *International Journal of Heat and Mass Transfer*, 47:5749-5763, 2004.

[6] Müller-Steinhagen, H., Heck, K., A Simple Friction Pressure Drop Correlation for Two-Phase Flow in Pipes. *Chem. Eng. Process*., 20:291-308, 1986.

[7] VDI Wärmeatlas, Chapter Ga, Springer, 9th edition, 2002

Paper VII

Wiebke Brix

Modelling refrigerant distribution in a minichannel evaporator using CO_2 and R134a

Danske Køledage 2010

MODELLING REFRIGERANT DISTRIBUTION IN A MINICHANNEL EVAPORATOR USING CO_2 AND R134A

Wiebke Brix
DTU Mechanical Engineering
wb@mek.dtu.dk

ABSTRACT

Both non-uniform airflow and non-uniform distribution of the inlet quality affect the refrigerant distribution in parallel evaporator channels. In this paper the impact of a non-uniform airflow and non-uniform inlet quality distribution on the evaporator performance is investigated numerically. The evaporator considered is an aluminium braced minichannel heat exchanger with parallel channels. Both CO_2 and R134a are used as refrigerants. It is shown that capacity reductions due to refrigerant maldistribution are smaller for CO_2 than for R134a. R134a on the other hand has a larger potential for capacity recovery by controlling the superheat in the individual channels.

INTRODUCTION

In recent years compact refrigeration systems with low refrigerant charges have become more and more popular. For many applications, especially for mobile or unitary applications compactness and weight is an important design issue. Increasing compactness is usually accompanied by material savings that lead to cost reductions. Low refrigerant charges help reducing the system weight, and are furthermore interesting due to safety and legislative issues. One solution in the design of compact, minimum charge systems is to use aluminium braced minichannel heat exchangers.

One of the main challenges in minichannel heat exchangers is to ensure a uniform refrigerant distribution. Especially for the evaporator the distribution of the flow into the parallel channels is a challenge [1, 2], since the refrigerant is usually in a two-phase condition at the inlet to the evaporator. The design of the distribution manifold plays an important role in how the flow will be distributed. Furthermore the distribution of the airflow on the outside may influence the distribution of the refrigerant in the parallel channels.

Several studies have shown that the distribution of the refrigerant is important considering the performance of conventional, finned tube evaporators [3, 4, 5]. The objective of the present study is to investigate the effects of refrigerant maldistribution in a minichannel evaporator on the heat exchanger performance by numerical simulation. Both the maldistribution of refrigerant occurring due to unevenly distributed air velocities and the maldistribution generated in the header, i.e. the distribution of liquid and vapour into the different channels are considered.

MODELLING THE EVAPORATOR

In order to model the evaporator, a discretised one-dimensional model of a single minichannel tube is built using the finite volume method. Each minichannel is discretized into an optional number of volumes, and each volume is treated as a small heat exchanger. For each volume the continuity equation, the momentum equation and the energy equation are solved under the assumption of steady state. Furthermore the two-phase refrigerant flow is assumed homogeneous, heat conduction
in the tube walls and between different tubes is neglected and only dry air is considered.
The frictional pressure gradients and the two-phase heat transfer coefficients are calculated using correlations from the literature, depending on the flow conditions. Table 1 summarizes the correlations that are used in the model. In order to solve the energy balance the ε-NTU method for a cross flow heat ex-

changer is applied.

Air side	
Heat transfer coefficient	Kim and Bullard [6]
Two-phase region	
Heat transfer coefficient	Bertsch [7]
Frictional pressure drop	Müller-Steinhagen and Heck [8]
Single phase region	
Heat transfer coefficient	Gnielinski [9]
Frictional pressure drop	Blasius [10]

Table 1: Summary of correlations used to calculate heat transfer coefficients and pressure drop.

In the physical evaporator the different channels are connected through a dividing and a collecting manifold, i.e. the inlet and outlet manifold. In the present evaporator model the flow in the manifolds is not considered in detail. The manifolds are assumed to be adiabatic and pressure drop in the manifolds is neglected. The single channel models are hence simply connected through conservation of mass and energy within the manifold and a requirement of equal pressure drop over the channels.
The distribution of gas and liquid flowing into the different channels has to be given as an input to the model. An overview over the model and the inputs and outputs is shown in figure 1. By imposing either a non-uniform airflow or non-equal qualities at the inlets of the parallel channels maldistribution of the refrigerant may be induced.

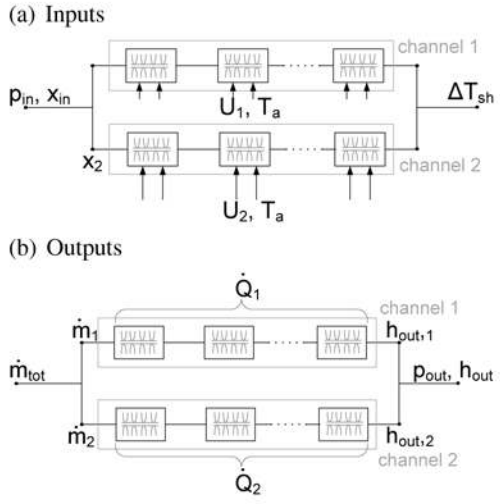

Figure 1: Schematic overview with (a) inputs and (b) outputs to the model.

The model was built and solved using the modelling and simulation software Windali [11], and the single channel model was verified using R134a as refrigerant in Brix *et al.* [12].

The test case

In order to investigate the influence of non-uniform airflow and non-uniform inlet qualities on the performance of a mini-channel evaporator, a test case is defined. For simplicity reasons the test case evaporator consists of only two minichannels in parallel. The channels are oriented vertically with the refrigerant flowing in the upwards direction. The parameters describing the modelled evaporator are summarized in table 2. The total refrigerant flow through the evaporator channels is controlled by setting a constant mixed superheat out of the evaporator. This would be the case for refrigeration systems controlled by a thermostatic expansion valve, and is therefore the most obvious choice in the present case. Two different refrigerants, R134a and CO_2, are used in the evaporator.

Evaporator geometry	
Tube length	0.47 m
Number of ports in one tube	11
Cross section of one port	0.8 x 1.2 mm
Flow depth	16 mm
Distance between two microchannels	8 mm
Fin pitch	$727\,m^{-1}$
Flow parameters	
Air temperature	35°C
Air velocity	1.6 m/s
Evaporation temperature	7.4°C
Quality at manifold inlet	0.3
Total superheat	6 K

Table 2: Parameters defining the test case.

RESULTS
Non-uniform gas/liquid distribution

When entering the evaporator the mixture of liquid and gas coming from the expansion valve has to be distributed into the parallel minichannels of the evaporator. A uniform distribution of especially the liquid is preferable, since the heat exchanger area is not utilized ideally if some channels receive only gas.
As mentioned, the manifold is not modelled in detail, and the liquid distribution is thus simply given as an input. In order to quantify the degree of maldistribution a distribution parameter, f_x, is defined

as

$$f_x = \frac{x_2}{x_{\mathrm{mf}}}, \quad 0 \leq f_x \leq 1. \tag{1}$$

Here x_2 is the quality into channel 2. For increased maldistribution the quality into channel 2 is decreased, while the manifold inlet quality, x_{mf} is kept constant. For equal distribution of the inlet quality $f_x = 1$, while for $f_x = 0$ only liquid is fed into channel 2 and the remaining mixture of liquid and gas enters channel 1.

In figure 2 the local heat flux along the channels is shown for CO_2 and R134a. For each of the three liquid distributions imposed, $f_x = 1$, $f_x = 0.5$ and $f_x = 0$, three curves are shown. Two curves show the heat flux in each channel. The third, which is provided with markers, shows the mean local heat flux. The solid line with circular markers shows the heat flux for a uniform liquid distribution. In this case there is no maldistribution of the refrigerant and the three lines coincide.

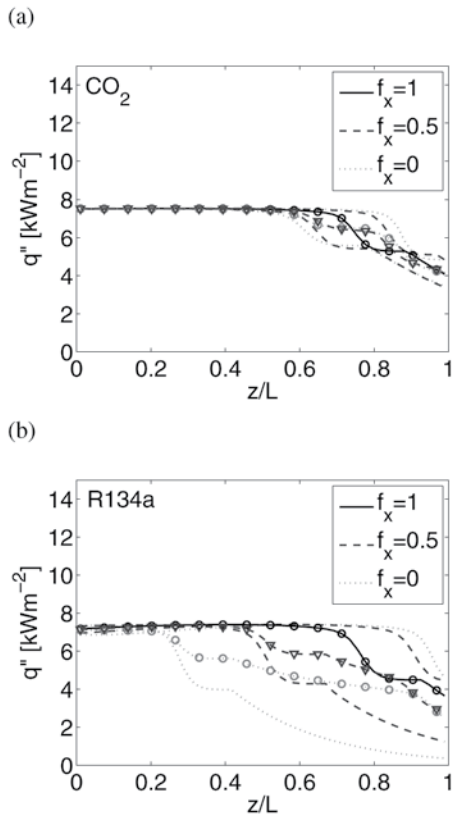

Figure 2: Local heat flux in the channel for CO_2 and R134a for different inlet quality distributions. The curves without markers show the local values in each channel, while the curves equipped with markers show a local mean of the two channels.

As long as the refrigerant flow in the channels is not approaching dryout, the local heat flux is constant. When approaching fully evaporated flow, the refrigerant side heat transfer coefficient begins to decrease until it reaches the single phase heat transfer coefficient. This results in a decrease of the overall heat transfer coefficient, and thus the heat flux. When all liquid is evaporated the temperature difference between the refrigerant and the air decreases, which results in the continued decrease of the heat flux in the superheated zone.

Imposing liquid maldistribution corresponding to a value of $f_x = 0.5$ or $f_x = 0$, does not change the heat flux significantly as long as the refrigerant is in a two-phase condition. However, the refrigerant flow in channel 1, which has a higher quality at the inlet, will reach dryout earlier than in the evenly distributed case, while the refrigerant in channel 2 stays in two-phase condition further down the channel.

A comparison of the graphs for CO_2 and R134a shows some significant differences. For CO_2 the total area of the evaporator containing two-phase flow is more or less constant when imposing liquid maldistribution. For R134a the refrigerant in channel 1, receiving less liquid, evaporates very fast such that the area with two-phase flow decreases for increased liquid maldistribution. Consequently, the mean heat flux is lower for increased maldistribution of the liquid, when using R134a, and a capacity reduction is expected.

The different behaviour of CO_2 and R134a seen in figure 2 can be explained by a different distribution of the mass flow rate into the two channels when imposing liquid maldistribution. Figure 3 shows the mass flow rate in each of the channels as well as the total mass flow rate as a function of f_x for the two refrigerants.

For CO_2 the mass flow rate in channel 1 increases and the mass flow rate in channel 2 decreases for increased liquid maldistribution, while the total mass flow rate stays more or less constant. For R134a the total mass flow rate decreases in order to keep the superheat out of the evaporator at the specified value. The distribution of the mass flow rate is such that channel 2 actually receives slightly more refrigerant than channel 1.

The reason for the different mass flow distribution of the two refrigerants can be explained by the dominance of different contributions to the pressure drop.

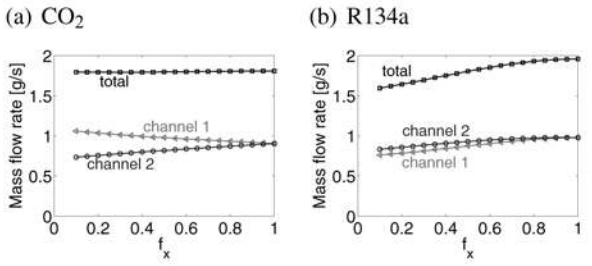

Figure 3: Distribution of the mass flow rate into the two channels as a function of the liquid distribution.

For R134a the frictional contribution to the pressure drop is clearly the most dominant, while the gravitational contribution is almost negligible. CO_2 has a higher density and a lower viscosity, and therefore the gravitational contribution to the pressure drop is significant, while the frictional contribution is much smaller than for R134a.

Figure 4 shows the cooling capacity of each of the parallel channels and the total cooling capacity as a function of the liquid distribution. As expected, the cooling capacity of the evaporator using CO_2 does not change significantly when imposing a nonuniform liquid distribution. Using R134a the cooling capacity of the channel receiving mostly gas decreases significantly, while the extra liquid in channel 2 only increases the cooling capacity of this channel moderately, such that the total cooling capacity decreases considerably.

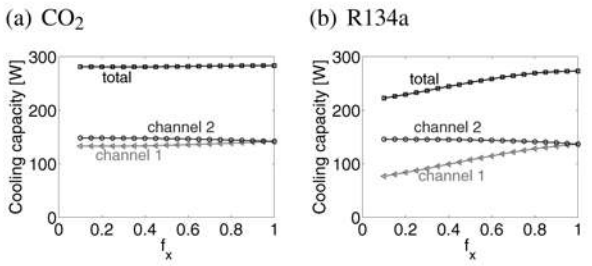

Figure 4: Cooling capacity as a function of the liquid distribution.

Figure 5 compares the reduction of the mass flow rate, the cooling capacity and the area of the evaporator that is in contact with two-phase flow (the two-phase area) as a function of the liquid distribution. For both refrigerants the curves showing the cooling capacity and the mass flow rate coincide. It is furthermore noticed that the capacity decreases at the same rate as the two-phase area.

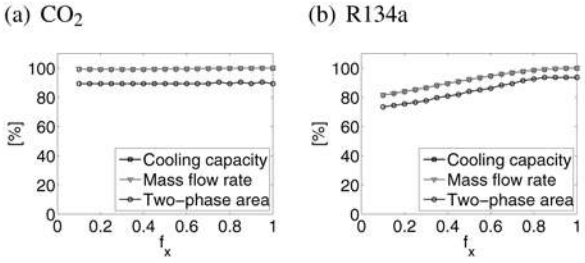

Figure 5: Comparison of the reduction in cooling capacity, mass flow rate and two-phase area as a function of the liquid distribution. The curves for cooling capacity and mass flow rate coincide.

Non-uniform airflow

Apart from the liquid distribution, also the distribution of the air velocity on the outside of the channels influence the refrigerant distribution in the parallel channels. Keeping the air flow rate constant and varying the velocities over the different channels, changes the heat load on the channels, which results in different pressure gradients inside the channel, and hence influences the mass flow rate distribution and the capacity.

When investigating the impact of the airflow distribution on the cooling capacity of the evaporator, the airflow is imposed such that each channel receives a constant air velocity. The total airflow rate is kept constant, while the velocity on each channel is varied. The velocities are varied such that the velocity increases for channel 1 and decreases for channel 2. A non-dimensional parameter, f_U, which quantifies the degree of non-uniformity of the airflow, is defined as:

$$f_U = \frac{U_2}{U_{\text{mean}}},\ 0 \leq f_U \leq 1, \tag{2}$$

where $f_U = 1$ for equal air velocities on both channels, while for $f_U = 0$ there is no airflow on channel 2, and all air passes by channel 1. While performing the investigations on the impact of the airflow distribution, the liquid distribution is considered uniform. In figure 6 the local heat flux is shown along the channel direction for three different airflow distributions.

For each of the three airflow distributions imposed, $f_U = 1$, $f_U = 0.5$ and $f_U = 0.1$, three curves are

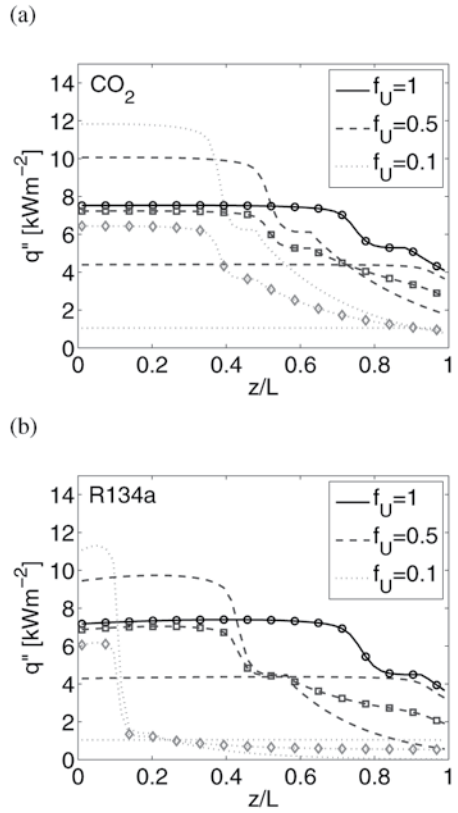

Figure 6: Local heat flux in the channel for CO_2 and R134a for different airflow distributions. The curves without markers show the local values in each channel, while the curves with markers show a local mean of the two channels.

shown for each graph in figure 6. Two curves show the local values in each channel and the third, which is provided with markers shows the mean local heat flux. The solid curve with circular markers shows local values in the minichannels for a uniform airflow. In this case there is no maldistribution of the refrigerant and the three curves coincide.

For $f_U = 0.5$ channel 1 receives a higher air velocity than channel 2. In channel 1 the air side heat transfer coefficient will be higher than for the uniform airflow case, which results in a higher heat flux. However, in this channel the refrigerant is fully evaporated much earlier than in the uniform airflow case. In the part of the channel containing single phase gas, the overall heat transfer coefficient is considerably lower, which results in a lower heat flux. As the temperature difference between the air and refrigerant decreases in the superheated part of the channel, the heat flux continues to decrease. Channel 2, which receives the low air velocity has lower heat flux than in the uniform airflow case, due to the lower air side heat transfer coefficient. In this channel dryout is not reached before the very end of the channel, and the heat flux is thus relatively constant throughout this channel.

From the dashed curve with square markers showing the mean heat flux of the two channels at $f_U = 0.5$, it is noted that as long as there is two-phase flow in both channels the mean heat flux is only slightly lower than for the uniform airflow case. However, for the part of the channel, where dryout has been reached in channel 1 the mean heat flux is considerably lower. For $f_U = 0.1$, the same behaviour is seen as for $f_U = 0.5$, but it is even more pronounced. In this case the mean heat flux is lower than in the uniform airflow case also when there is two-phase refrigerant flow in both channels. This indicates that as long as all channels are wet inside only a severe non-uniformity of the airflow will impact the cooling capacity of the evaporator.

Figure 7 shows the distribution of the mass flow rate in each of the two channels as well as the total mass flow rate as a function of airflow distribution. For both refrigerants the total mass flow rate decreases with increasing airflow non-uniformity.

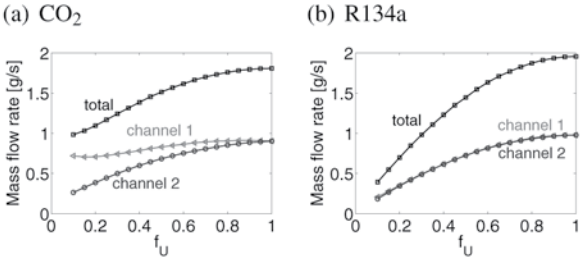

Figure 7: Distribution of the refrigerant mass flow rate as a function of the airflow distribution.

Looking at the impact of the airflow distribution on the cooling capacity for CO_2, shown in figure 8(a), it is seen that the cooling capacity of channel 1 is slightly increasing for f_U decreasing to 0.65 and decreasing slightly for lower values of f_U, although the airside heat transfer coefficient increases for increasing air velocity on this channel. Nevertheless, the reduced mass flow rate and the increasing single phase zone prevents the cooling capacity to increase. In channel 2 the cooling capacity decreases steadily as the air velocity on this channel is decreased.

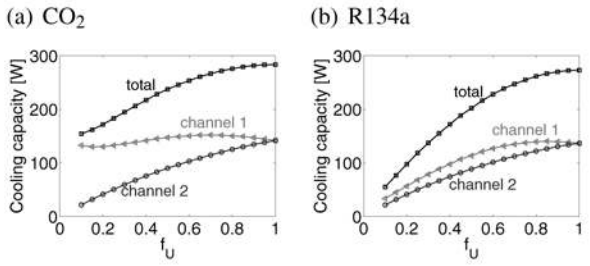

Figure 8: Cooling capacity of the individual channels and the total cooling capacity of the evaporator as a function of the airflow distribution.

Using R134a as refrigerant the cooling capacity of channel 1 is slightly increasing for f_U decreasing to 0.8 and decreasing for lower values of f_U, due to the reduced mass flow rate. In channel 2 the cooling capacity decreases as for CO_2. For small degrees of non-uniformity of the airflow, the total cooling capacity is not affected much. However, for larger degrees of maldistributed airflow, the cooling capacity of the evaporator decreases significantly. It is furthermore worth noting, that in the extreme case ($f_U = 0.1$), the capacity of the evaporator with R134a is reduced more than twice as much as the evaporator with CO_2 compared to the case with uniform airflow.

Figure 9 compares the reduction of the cooling capacity, the total mass flow rate and the area of the evaporator containing two phase flow. The curves showing the cooling capacity and the mass flow rate coincide, and these actually decrease faster than the two-phase area.

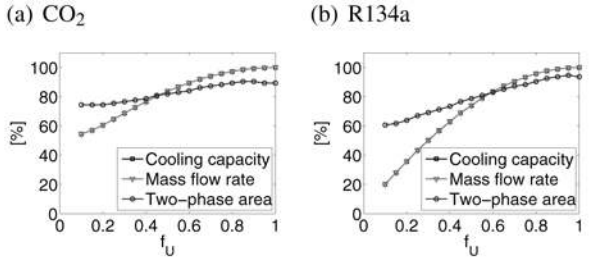

Figure 9: Comparison of the reductions in mass flow rate, cooling capacity and the area of the evaporator containing two-phase flow.

Although the two distribution parameters f_U and f_x cannot be compared directly, it is interesting to compare the findings of the liquid distribution and the distribution of the airflow. First of all, the capacity was affected much more by the airflow distribution than by the liquid distribution in the extreme cases. Furthermore, it was found that where the capacity decreased at the same rate as the two-phase area for varying liquid distribution, the capacity decreased more than twice as much as the two-phase area for varying airflow distribution.

Combining non-uniform liquid distribution and non-uniform airflow

One thing is to vary the liquid distribution and the airflow distribution only separately, but in a real system most likely both of the sources of a maldistribution of the refrigerant will be present at the same time. Therefore, an investigation of combined non-uniform distribution of the liquid in the manifold and the airflow is performed.

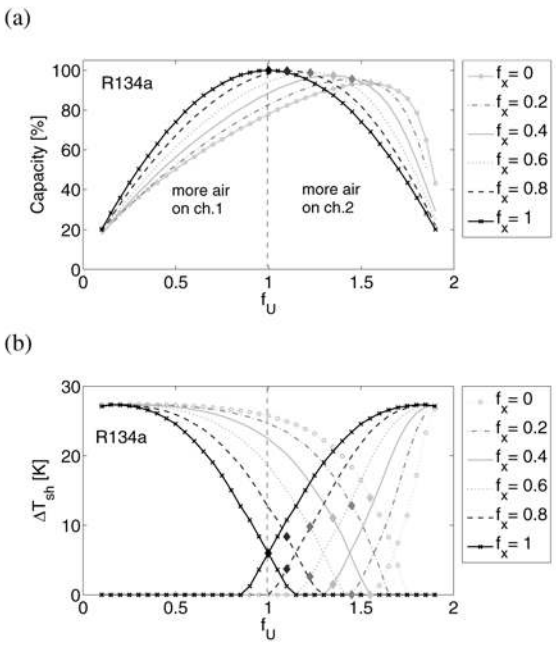

Figure 10: (a) The cooling capacity for simultaneous variation of the airflow and liquid distribution using R134a as refrigerant. At uniform distribution of both liquid and airflow the capacity is 100%. (b) The superheat out of the individual evaporator channels.

For this purpose the airflow distribution parameter, f_U, is varied between 0 and 2, such that both of the channels are exposed to both increased and decreased air velocities. Figures 10(a) and 11(a) show the relative total cooling capacity as a function of the

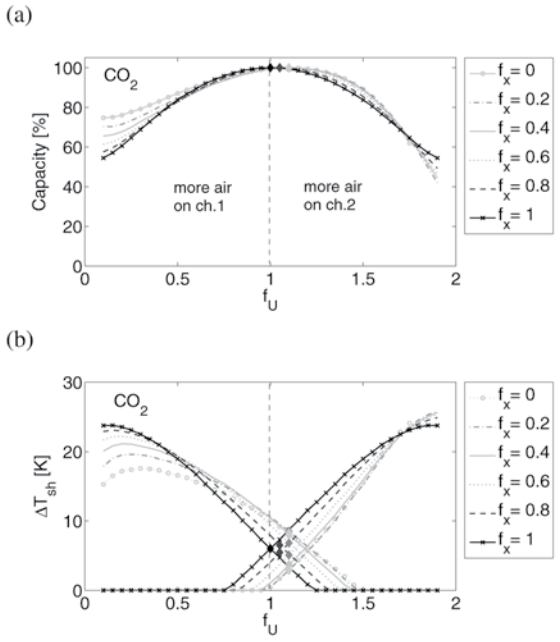

Figure 11: (a) The cooling capacity for simultaneous variation of the airflow and liquid distribution using CO_2 as refrigerant. At uniform distribution of both liquid and airflow the capacity is 100%. (b) The superheat out of the individual evaporator channels.

airflow distribution for different liquid distributions, for R134a and CO_2, respectively. The capacity is set to 100% for uniform distribution of both the airflow and the liquid in the manifold. Furthermore the superheat out of the individual channels is shown in figures 10(b) and 11(b).

Considering the evaporator using R134a, it clearly seen that for a given liquid distribution an optimum airflow distribution exists and vice versa. For each curve the optimum cooling capacity is marked with a diamond shaped marker in the figure. Having uniform airflow the optimum liquid distribution is also uniform. However, for a non-uniform airflow distribution an optimum capacity can be obtained at a certain, non-uniform, liquid distribution. As it could be expected it is desirable to have a larger fraction of the liquid going into the channel, that is exposed to a higher air velocity. The optimum cooling capacity is slightly decreasing with increasing airflow non-uniformity, which means that most, but not all of the capacity can be recovered by distributing the liquid suitably.

Comparing graphs (a) and (b) in figure 10 it is seen that the optimum cooling capacity is attained in the region where the refrigerant is fully evaporated out of both channels, but where the superheat out of channel 2 is lower than in channel 1. In practice it would probably be difficult to control the system to reach the exact optimum. It could, however, be possible to control the liquid distribution such that the superheat out of the channels is equal. At this point the capacity is still very close to the optimum, since the curve is very flat in the region around the optimum.

Considering CO_2 as refrigerant, for which the liquid distribution has only minor influence on the capacity, the graphs look slightly different, shown in figure 11. Also in this case an optimum cooling capacity can be reached by a suitable liquid distribution. However, the optimum is not far from the curve having uniform liquid distribution. For CO_2 the largest airflow maldistribution that can be compensated to the optimum by controlling liquid distribution is $f_U = 1.1$. At this point only liquid enters channel 2. For larger degrees of airflow non-uniformity, the capacity decreases regardless the liquid distribution. For R134 this point of a maximum airflow distribution that can be compensated to the optimum capacity by controlling the liquid distribution is found at a considerably higher degree of airflow non-uniformity up to $f_U = 1.55$.

CONCLUSION

Distribution studies with two parallel channels were presented. First the impact of the liquid distribution in the inlet manifold on the evaporator performance were investigated. We could conclude that the cooling capacity was not affected by the liquid distribution when using CO_2 as refrigerant, but decreased by up to 20% for R134a at extreme maldistribution of the liquid. The decreases in the cooling capacity were equal to decreases in the two-phase area.

Next the impact of the airflow distribution on the evaporator performance was considered. We found that the cooling capacity is strongly affected by airflow non-uniformity and that the capacity reductions were more than twice as large for R134a than for CO_2. In this case the decreases in the cooling capacity are larger than decreases in the two-phase area.

Furthermore, combining the non-uniform airflow and liquid distribution showed that a non-uniform airflow distribution could be compensated by a suitable liquid distribution. When controlling the super-

heat out of the individual channels to be equal, the optimum capacity is almost reached. Comparing the two refrigerants showed that R134a had a higher potential for capacity recovery than CO_2.

REFERENCES

[1] M.-H. Kim, J. Pettersen, and C. W. Bullard, "Fundamental process and system design issues in CO_2 vapor compression systems," *Progress in Energy and Combustion Science*, vol. 30, no. 2, pp. 119 – 174, 2004.

[2] S. G. Kandlikar, "A roadmap for implementing minichannels in refrigeration and air-conditioning systems - current status and future directions," *Heat Transfer Engineering*, vol. 28, pp. 973–985, 2007.

[3] M. Chwalowski, D. A. Didion, and P. A. Domanski, "Verification of evaporator computer models and analysis of performance of an evaporator coil," *ASHRAE Transactions*, vol. 95, no. 1, pp. 1229–1235, 1989.

[4] J. M. Choi, W. V. Payne, and P. A. Domanski, "Effects of non-uniform refrigerant and air flow distribution of finned-tube evaporator performance," *Proceedings of the International Congress of Refrigeration*, 2003. Washington D.C., USA, ICR0040.

[5] J.-H. Kim, J. E. Braun, and E. A. Groll, "Evaluation of a hybrid method for refrigerant flow balancing in multi-circuit evaporators," *International Journal of Refrigeration*, vol. 32, no. 6, pp. 1283 – 1292, 2009.

[6] M.-H. Kim and C. W. Bullard, "Air-side thermal hydraulic performance of multi-louvred fin aluminium heat exchangers," *International Journal of Refrigeration*, vol. 25, pp. 390–400, 2002.

[7] S. S. Bertsch, E. A. Groll, and S. V. Garimella, "A composite heat transfer correlation for saturated flow boiling in small channels," *International Journal of Heat and Mass Transfer*, vol. 52, no. 7-8, pp. 2110 – 2118, 2009.

[8] H. Müller-Steinhagen and K. Heck, "A simple friction pressure drop correlation for two-phase flow in pipes," *Chem. Eng. Process.*, vol. 20, pp. 291–308, 1986.

[9] V. Gnielinski, "New equations for heat and mass-transfer in turbulent pipe and channel flow," *Iternational Chemical Engineering*, vol. 16, no. 2, pp. 359–368, 1976.

[10] R. W. Fox and A. T. McDonald, *Introduction to fluid mechanics*. John Wiley & Sons, 5th ed., 1998.

[11] M. J. Skovrup, "Windali, v.3.34," 2005. Technical Univesity of Denmark, Department of Mechanical Engineering, http://www.et.web.mek.dtu.dk/WinDali/Index.html.

[12] W. Brix, M. R. Kærn, and B. Elmegaard, "Modelling refrigerant distribution in microchannel evaporators," *International Journal of Refrigeration*, vol. 32, pp. 1736–1743, 2009.

DTU Mechanical Engineering
Section of Thermal Energy Systems
Technical University of Denmark

Nils Koppels Allé, Bld. 403
DK- 2800 Kgs. Lyngby
Denmark
Phone (+45) 45 88 41 31
Fax (+45) 45 88 43 25
www.mek.dtu.dk
ISBN: 978-87-90416-27-0

DCAMM
Danish Center for Applied Mathematics and Mechanics

Nils Koppels Allé, Bld. 404
DK-2800 Kgs. Lyngby
Denmark
Phone (+45) 4525 4250
Fax (+45) 4593 1475
www.dcamm.dk
ISSN: 0903-1685